UNIVERSITY OF OKLAHOMA

GRADUATE COLLEGE

# INTEGRATING SEQUENCE STRATIGRAPHY AND SEISMIC ATTRIBUTES FOR QUANTITATIVE RESERVOIR CHARACTERIZATION: A CASE STUDY OF A PLIOCENE RESERVOIR, CAMPECHE SOUND, MEXICO

A DISSERTATION

SUBMITTED TO THE GRADUATE FACULTY

in partial fulfillment of the requirements for the

Degree of

DOCTOR OF PHILOSOPHY

By

EFRAIN MENDEZ-HERNANDEZ
Norman, Oklahoma
2008

INTEGRATING SEQUENCE STRATIGRAPHY AND SEISMIC ATTRIBUTES FOR QUANTITATIVE RESERVOIR CHARACTERIZATION: A CASE STUDY OF A PLIOCENE RESERVOIR, CAMPECHE SOUND, MEXICO

A DISSERTATION APPROVED FOR THE
CONOCOPHILLIPS SCHOOL OF GEOLOGY AND GEOPHYSICS

BY

_____
Dr. Roger Slatt, Chair

_____
Dr. Shankar Mitra

_____
Dr. Roger Young

_____
Dr. James Forgotson

_____
Dr. Chandra Rai

_____
Dr. Arcangelo Sena

# TABLE OF CONTENTS

**Page**

**Page**

**Page**

# ACKNOWLEDGEMENTS

I wish to express my deepest appreciation to Dr. Roger Slatt for his invaluable advice and direction as my advisor in this dissertation and for his constant encouragement to reach my goals at The University of Oklahoma.

I thank the other members of my committee, Dr. Roger Young, Dr. James Forgotson, Dr. Shankar Mitra, Dr. Chandra Rai and Dr. Arcangelo Sena for their important suggestions to accomplish the objectives of this dissertation.

I thank Dr. John Castagna for giving me the confidence and support to start this PhD program while he was Director of the Institute for Exploration and Development Geosciences (EDGE), housed in the School of Geology and Geophysics at The University of Oklahoma, and for his important contribution to my PhD education.

I am grateful to PEMEX Exploration and Production for allowing me to lead the Utan project, the subject of this dissertation, particularly to PEMEX managers Jesus García, Adan Oviedo, Arturo Pérez-Aldana and Francisco Sánchez de Tagle.

Thanks to my friends Carlos Bahamon and Natalia León for their friendship, the good times and their invaluable technical work associated with this dissertation. My sincere gratitude to Juan Mitterhofer, Carlos Moreno, María Pérez, Raúl Cabrera and Catalina Acuña for the help provided to reach the goals of this work.

Thanks to my family, Isabel, Graciela and Efrain Jr. for their kind motivation and patience during every moment of this extraordinary experience.

# LIST OF FIGURES

**Page**

**Page**

**Page**

# LIST OF TABLES

# ABSTRACT

An integrated workflow including analysis of seismic, core, well log and biostratigraphic data was developed and conducted to both construct a reliable geologic model and characterize a Pliocene gas reservoir which overlies the Cantarell field in the Campeche Sound, southern Gulf of Mexico.

In 2003, the offshore exploratory Utan #1 well was drilled to investigate the gas potential of the Pliocene sequence. The well provided successful results from facies characterized by thin mixed siliciclastic-carbonate beds contained within a faulted rollover anticline.

Campeche Sound is the most prolific Mexican oil producing province where the best fields are Mesozoic-Paleocene carbonates in structural traps. Therefore, little exploration has been focused on the overlying late Tertiary and more siliciclastic section, representing a gap in the knowledge of this part of the basin where new expectations arise for non-associated gas entrapments in a traditionally oil-producing province.

Based upon development of a sequence stratigraphic framework, a new play analysis is developed where the reservoirs are identified as retrogradational shoreface parasequences sitting atop third-order sequence boundaries. Basic and advanced seismic attributes contribute to the stratigraphic interpretation and gas detection. Seismic inversion for reflectivity allowed better identification of key stratigraphic

surfaces. Modeled Type-I AVO and a dimmed spectral decomposition response following structural contours provide reliability to gas discrimination and reservoir delineation. The seismic attributes will require additional support to be valuable as reservoir quality predictors.

Because biogenic methane and thin sheet reservoirs define the rock-fluid system, development may be uneconomic. However, the trapped gas could be reinjected at deeper depths to improve recovery efficiency of oil in the Cantarell field.

The knowledge gained from this research is an important contribution to the petroleum geology of Mexico and the Gulf of Mexico basin. It confirms the petroleum system for this Pliocene play, proposes a new play concept and provides the basis for further research in the study area.

Future work is recommended to extend the regional geological mapping using the integrated methodology and play analysis developed from this dissertation. New well and seismic data focused on Neogene levels should also be obtained to improve the knowledge and assure expectations for future exploration and development strategies in these and other subtle stratigraphic gas traps of this traditional oil province.

# Chapter 1

# INTRODUCTION

Natural gas is playing an important role in the energy industry and is widely expected to be the fastest growing primary energy source in the world over the next 20 years. Particularly, in the Mexican industry the demand has been increasing as new combined cycle power plants are built and existing power plants are converted to natural gas. Mexico's government expects the natural gas demand will double over the next ten years, and that half of this gas will be used to generate electricity. While the country is still a net gas importer, most gas production in Mexico is associated and is decreasing dramatically. The additional resource has to come from boosting internal gas production, discovering new non-associated gas provinces, or by developing non-conventional reservoirs.

Main non-associated gas provinces of Mexico include the onshore Burgos, Veracruz and Macuspana basins. Beyond onshore prospecting for gas, Campeche Sound, which is the most prolific oil producing province of Mexico, has recently shown new opportunities for gas in this typical oil province.

Campeche Sound is a Mesozoic offshore province in the Gulf of Mexico that belongs to the petroleum Southeast Basins (Cuencas del Sureste) of Mexico (figure 1.1). Fractured Mesozoic-Paleocene carbonate rocks and structural traps form the main oil reservoirs in Campeche Sound including Abkatun Field, Ku-Maloob-Zaap

Complex, and the super giant Cantarell Field, the latter of which has produced approximately 7000 million barrels of oil during almost 20 years of production and development.

On the other hand, little exploration has been focused on the late Tertiary section of Campeche Sound, representing a gap in the knowledge of this part of the basin. The lack of a comprehensive understanding of these units can be attributed to:

- Most of the wells have been drilled for Mesozoic-Paleocene targets, causing a lack of well log and core information for the late Tertiary.
- Seismic data which have been acquired and processed for deeper structural objectives have limited use for interpreting these shallower and mostly stratigraphic targets.
- The first wells drilled to test the gas potential of Tertiary targets were not successful, being either non-producers or commercially non-producers. However, some wells drilled for deeper targets reported important Tertiary gas shows in the Campeche Sound.

**Dissertation problem statement**

As a result of recent Mexican gas exploration strategies for late Tertiary targets in Campeche Sound, the exploratory Utan-1 well, located 67km offshore northwestward of Ciudad del Carmen, Campeche State (figure 1.2), was drilled in 2003. It provided successful results in a Pliocene mixed siliciclastic-carbonate section overlying Cantarell field. The well provided new expectations for non-associated gas developments in this traditionally oil producing province.

Geologically, Utan field is located in a minibasin formed by growth and antithetic faulting. The field has two reservoirs comprised of thin Pliocene mixed sandstone-carbonate sediments. The trap mechanism is a rollover closure against a single major fault (figure 1.3). A depositional model, including an understanding of spatial and temporal variations as well as controls on these mixed sequences, had not yet been well stated at the beginning of this dissertation in 2005. At that time they were interpreted as deep water depositional environments (Pemex´s internal reports). This confusion, coupled with the sparse biostratigraphic and well log data at these Pliocene intervals, and the lack of seismostratigraphic studies, are the basis for some of the problems. The new proposed model, based on Bahamon (2006) and Mendez et al. (2006), supports shallower depositional environments.

The study of mixed sequences has a variety of distinctive petroleum reservoir characteristics for both exploration and development programs. These include paleogeographic settings and records of sea level, tectonics, climate and sediment supply, which have received less attention than carbonate or siliciclastic end members. Thus, conventional reservoir quality analysis, characterization and delineation are difficult in this mixed setting. Even, the use of seismic attributes developed for siliciclastic sequences are not fully applicable for thin gas reservoirs in mixed sequences.

On the other hand, drilling activities and infrastructure to develop a field are expensive in offshore areas. Consequently, a promising show of hydrocarbons should not be considered an outstanding discovery until some ideas of the geological model, as well as the size of the field and its potential productivity are obtained.

In consequence, new concepts and thinking that have not been previously used in the study area have to be employed to understand the geological record of the Pliocene in Campeche Sound, and an integrated and quantitative methodology has to be developed to provide an understanding of the geological model and gas distribution in the mixed section of Utan field, opening an unexplored line of research in the study area. This is the framework of this dissertation.

Based on the above statements, the purpose of this dissertation is to develop an integrated and quantitative analysis of the Pliocene mixed siliciclastic-carbonate section at Utan field to provide a geological understanding and characterization of the spatial distribution of the reservoir properties and gas distribution within a sequence stratigraphic framework. In addition, an integrated and quantitative approach has to be developed to test the applicability of advanced and conventional seismic attributes to reduce the uncertainty in both constructing a realistic reservoir model and understanding the spatial distribution of reservoir rock properties in this kind of mixed sequence. A key implication of this research is to develop a standard characterization methodology to recommend feasible solutions if analogous projects are undertaken in the future.

**Approach/methods**

To accomplish the objective of this dissertation, seismic, core, well log and biostratigraphic data were integrated to establish in the study area a sequence stratigraphic framework. Sequence stratigraphy combines well logs with biostratigraphy and seismic patterns to understand the relationships among rock layers,

their seismic expression and depositional environments for a more accurate prediction of reservoir settings, source rocks and seals. This framework is mostly needed to decipher relationships in terms of relative age and depositional setting for litostratigraphic units when it is needed to predict the position of analogous stratigraphic traps in different parts of the basin.

Additionally, sequence stratigraphy provides the framework needed to properly interpret seismic attributes in terms of stratigraphic analysis, reservoir property distribution and hydrocarbon anomalies in the study area. Modern analysis of seismic attributes plays a key role in reservoir characterization by combining amplitude and frequency properties of a seismic signal to estimate both static and dynamic reservoir properties in a three-dimensional scheme. The accuracy of predicting a reservoir property from seismic data improves when those attributes that are statistically different, but present a significant correlation to certain physical properties, are properly combined for the interpretation.

Unfortunately, most of the seismic attributes developed by the industry are based on amplitudes and only applicable to siliciclastic sequences with more predictable depositional behaviors than carbonate settings. Methodologies such as Spectral Decomposition, Seismic Inversion for Reflectivity, and Amplitude versus Offset analysis were evaluated in this study in order to validate how much they can enhance some stratigraphic features, or how sensitive they can be to quantify rock/pore fluid properties in this mixed setting.

Some other considerations and additional potential benefits are placed in this same Chapter as "Implications of this research".

**Location of the study area and available data**

The study area covered in this dissertation is defined by the limits of seismic and well data provided by PEP (PEMEX E&P), the Mexican government oil company, and encompasses an area of approximately 300 $km^2$, surrounding Utan field in the Cantarell area of the Campeche Sound (figure 1.4).

Seismic data provided for this research involved 3D seismic PSTM (pre-stacked time migrated) CDP gathers and stacked data from an Ocean Bottom Cable survey acquired and processed in 1996-1997.

Cantarell is a giant operating field, thus providing a huge accumulation of log and core data for dozens of drilled wells in this province. Unfortunately, most of the wells have been drilled for Mesozoic-Paleocene targets, causing a lack of enough well log, core and biostratigraphic information for the late Tertiary. Out of these dozens of wells available, over 45 wells were screened under the criteria of having a suitable suite of well logs for correlation and application of sequence stratigraphic concepts, as well as biostratigraphic analysis, core and engineering data. After the screening process, only a smaller group of wells met the requirements needed to create the stratigraphic framework and perform the seismic analysis for this research:

- 7 Wells with partial or full well log information at reservoir levels (including the discovery well): C-3068, Utan-1, C-283, C-2295, C-2275A , C-219, C-429/418D
- 3 wells with biostratigraphic data (including the discovery well)

- 1 well with core data (the discovery well) and 7 wells with core data from outside the study area
- Engineering data for available wells (two wells with pressure tests): Utan 1, C-283
- 4 wells used for multimineral analyses, fluid substitution and synthetic seismic modeling: UTAN-1, C-3068, C-429 y C-468.

Additional data for use in this study included formation tops, as well as petrophysical analyses and Pemex confidential internal reports. These data were reviewed and integrated into the various analyses.

The discovery well was the main control well because it contained a comprehensive geological data set including paleontology reports, three cored intervals, petrographic studies, cuttings descriptions and engineering reports.

Details of the database used in this work are provided in the following Chapters of this research.

**Methodology**

Figure 1.5 shows a workflow developed to accomplish the objectives addressed for this dissertation. The workflow relies on a combination of sequence stratigraphic interpretation from well and seismic data, coupled with structural, biostratigraphic, petrophysical, and geochemical analyses. The workflow includes single geological and geophysical activities undertaken in a synergistic approach along separate tracks

followed by merging of the sequence stratigraphic framework and seismic analysis to develop the G&G integrated interpretation.

As a first step, seismic, core, well log and biostratigraphic data were integrated in the study area to establish a geological model. Previous interpretations in Pemex´s internal reports considered the reservoir facies as associated with deepwater deposits. The new proposed model, based on Bahamon (2006) and Mendez et al. (2006), supports a shallower depositional environment.

After that, the sequence stratigraphic framework was established for the Utan-1 well, based on the core analysis, well log data, biostratigraphy and tied to the eustasy curve published for the Gulf of Mexico (Wornardt et al., 2002). Once the key surfaces for stratigraphic correlation were identified, they were transferred to the seismic data to extrapolate them to nearby wells. Several loops between seismic and well log data were performed to assure agreement of interpretations.

Engineering information was also integrated within this framework. Pressure tests from two wells were analyzed to test connectivity between some intervals and verify the stratigraphic correlation.

According to the workflow, during the course of this research the following tasks were undertaken in a synergistic approach:

⇒ Review of previous works and the related technical literature

⇒ Database compilation, screening and validation (quality control)

⇒ Core descriptions and comprehensive review of cuttings descriptions and detailed core analyses

⇒ Review and synthesis of the geological framework

⇒ Formation evaluation and petrophysical analysis of key wells

⇒ Reservoir quality analysis

⇒ Definition of the geological environment for the study area

⇒ Definition of the sequence stratigraphic framework for the Utan-1 well

⇒ Seismic data conditioning, phase rotation, frequency content and seismic resolution analysis, wavelet extraction, synthetic seismograms, well tie to stacked data, time-depth conversion

⇒ Basic seismic interpretation

⇒ Extension of the sequence stratigraphic framework in the Utan-1 well to nearby key wells and seismic data

⇒ Extraction of seismic attributes for stratigraphic interpretation (instantaneous attributes, spectral decomposition, inversion for reflectivity)

⇒ Extraction of seismic attributes for hydrocarbon detection (AVO, spectral decomposition)

⇒ Evaluation of petroleum engineering information (Drill Stem Tests (DST) and drilling reports)

⇒ Integrated interpretation based on facies distribution and reservoir physical properties.

Each step in the workflow will be detailed further in the corresponding section of this dissertation.

This approach was applied to understand the geological record of the Pliocene in Campeche Sound, where the gas reservoir in Utan field was discovered. Beyond this achievement, a key implication of this research was to develop a standard characterization methodology to recommend feasible solutions if analogous projects are undertaken in the future. Therefore, this workflow is presented here as a possible template for use in other areas when the appropriate data set is available.

**Organization**

This dissertation has been divided into the following parts:

1. A first Chapter with a general introduction, objectives, main contributions, database, resources, methodology and organization of this research;
2. A second Chapter describes the general background of the study area, covering general issues of the Gulf of Mexico basin and the Mexican portion of this basin, as well as the regional geologic framework and petroleum systems of the Campeche Sound. It concludes with a brief summary and general characteristics of Utan field;
3. A general overview on sequence stratigraphy as an exploration tool is provided in Chapter 3;

4. Chapter 4 contains well log analysis, formation evaluation and petrophysics, whereas Chapter 5 is involved with seismic data analysis, conditioning and modeling of the data available for this dissertation;
5. Following that, two Chapters (labeled as 6 and 7) describe the integrated analysis of geological-geophysical-engineering data to construct a geological model under a seismic sequence stratigraphic framework. The nature and applicability of seismic attributes applied in this work are used to define the spatial distribution of reservoir rocks, taking into account reservoir quality conditions for future exploration and development strategies in the study area;
6. A final Chapter establishes the conclusions of this dissertation as well as several recommendations for future analogous works.

Most of the chapters of this dissertation are not meant to be complete in themselves; they complement each other to provide an overall knowledge to accomplish the objectives of this dissertation.

**Implications of this research**

The main contributions of this work are:

- To develop new concepts, skills and a workflow to explore for gas in this traditional oil province. This work will generate knowledge promoting the use of new concepts and technology to draw reliable conclusions about cause-and-effect relationships

conducted in an integrated manner for these new, potential gas accumulations overlying Cantarell Field.

- This work will contribute to define further E&P strategies to determine whether Campeche Sound could be a potential source of undiscovered gas reserves in Mexico in this kind of mixed setting.

**Support and resources**

The author of this dissertation was granted permission by Pemex E&P (PEP, the Mexican Oil and Gas Government Company) to develop this research after an author's requirement for a PhD dissertation project which could add value and generate knowledge in a novel and little explored Mexican petroleum basin.

Once the subject of this research was determined by PEP, a joint PEP-The University of Oklahoma project titled "Study of Evaluation of Pliocene Gas Plays of the Utan Area, Campeche Sound, Mexico", was established between both institutions to be led by the author of this dissertation under the direction of Dr. Roger Slatt.

Oil and Gas exploration in Cantarell Asset is currently the responsibility of both *Región Marina NE (RMNE)***,** and *Subdirección de la Coordinación de Estrategias de Exploración (SCTER)* with offices at the Mexican cities of Ciudad del Carmen, and Villahermosa, respectively. These PEP organizations sponsored this research.

As a part of this collaborative project, there were activities developed and led by the author of this dissertation carried out at:

- The University of Oklahoma at Norman, Oklahoma, with active collaborative participation from Carlos Bahamon, who completed his Master´s thesis on the

Neogene sequence stratigraphy of the study area, developed in the School of Geology and Geophysics at OU under the direction of Dr. Roger Slatt.

- PEP´s offices at Ciudad del Carmen, México, with continuous feedback from geoscientists of this PEP´s Asset.
- PEP´s offices at Villahermosa, and Poza Rica, México.
- Fusion Geophysical offices in Norman, Oklahoma, and Houston, Texas, USA, with participation from geoscientists of this company in the early stages of this research.

Table 1.1 shows itemized tasks, locations and people involved during development of this Dissertation:

| Task | Location | Who |
|---|---|---|
| Early planning of the Dissertation. | The University of Oklahoma at Norman | Mendez & Slatt |
| Final planning of the Dissertation | The University of Oklahoma at Norman | Mendez & Dissertation Committee |
| Database compilation and validation. | PEMEX offices at Cd. Carmen and Villahermosa, MEXICO | Mendez |
| Review of the related technical literature and geological framework | PEMEX offices at Cd. Carmen; The University of Oklahoma at Norman | Mendez |
| Editing of well logs and petrophysical work | The University of Oklahoma at Norman; Fusion offices at Norman, OK and Houston, Tx | Fusion´s geoscientists under Mendez´s supervision |

| | | |
|---|---|---|
| Reservoir quality analysis of key wells | The University of Oklahoma at Norman; Fusion offices at Norman, OK and Houston, Tx | Mendez, Bahamon and Slatt, |
| Core descriptions | PEMEX offices at Cd. Carmen and Villahermosa | Slatt, Mendez and Bahamon |
| Sequence stratigraphy analysis including biostratigraphic and well log correlation, seismic pattern analysis and correlation, and EMI interpretation | PEMEX offices at Cd. Carmen and Villahermosa; The University of Oklahoma at Norman | Mendez, Bahamon and Slatt, |
| Seismic conditioning, seismic-well tie, seismic attribute extraction | Fusion offices at Houston, Tx. | Fusion´s geoscientists under Mendez´s supervision |
| Seismic attribute interpretation, integrated interpretation, risk analysis and proposal of new drilling locations | The University of Oklahoma at Norman; Fusion offices at Norman, OK and Houston, Tx.; PEMEX offices at Cd. Carmen and Villahermosa | Mendez and Slatt |
| Writing of the Drafts and Final Dissertation | The University of Oklahoma at Norman; PEMEX offices at Poza Rica, Veracruz | Mendez |

**Table 1.1: Itemized tasks during the development of this dissertation**

## Stratigraphic Nomenclature and Semantics

Even though there is an established and accepted lithostratigraphic column with formational names for the onshore Southeast Basins, lithostratigraphic names for Campeche Sound are informal. This research has been concerned primarily with defining a geologic model through identifying sequence boundaries and ranking third and higher order sequences from a chrono- and lithostratigraphic point of view to characterize reservoir distribution and quality in the study area. In this sense, during development of this dissertation, there was no attempt to provide formal names to the

Neogene stratigraphic units analyzed. Therefore, they are classified as units from their chrono- and lithostratigraphic point of view and not referred to as formations. In addition, some of the technical documents from which several observations and concepts were derived as a source of reference for this research are unpublished or classified as confidential by PEP.

For the purpose of consistency and to avoid arguments over semantics, Mexican names and terms have been anglicized where appropriate; e.g., the *Sonda de Campeche* becomes the Campeche Sound and the *Cuencas del Sureste* becomes the Southeast Basins.

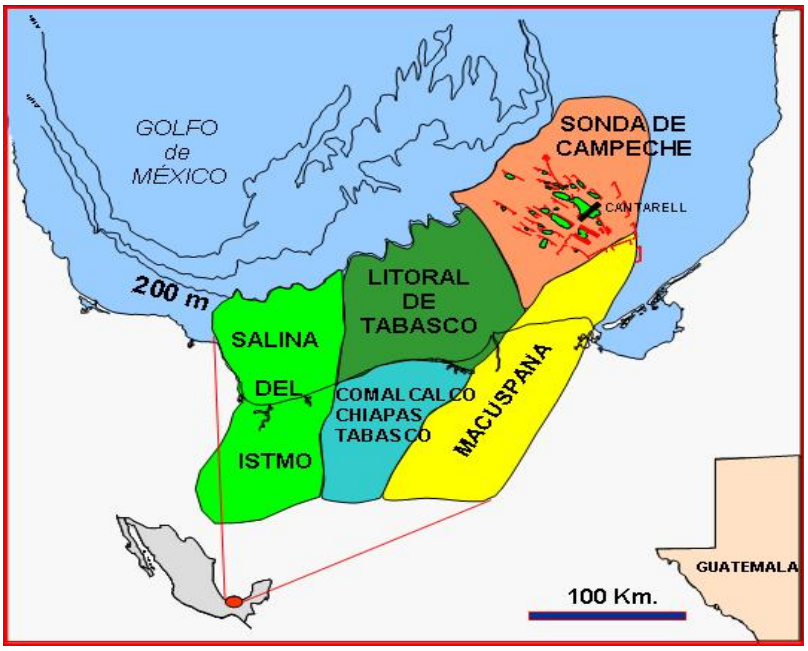


**Figure 1.1: Location of Southeast Basins, Campeche Sound (Sonda de Campeche) Province, and Cantarell Field, MEXICO.**

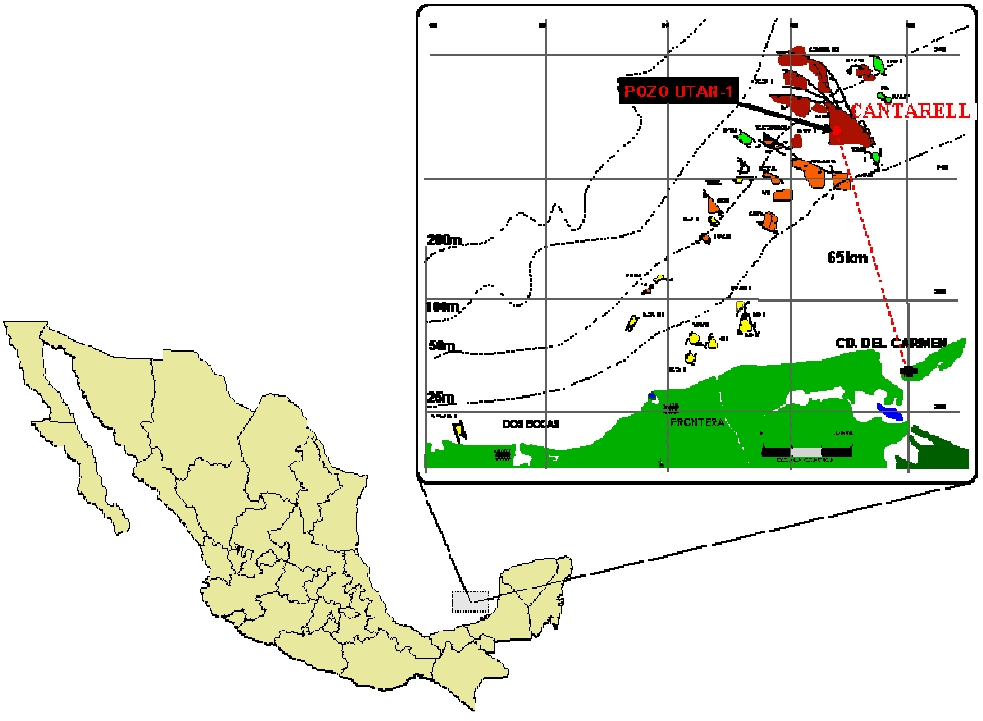


**Figure 1.2: Utan-1 well location.**

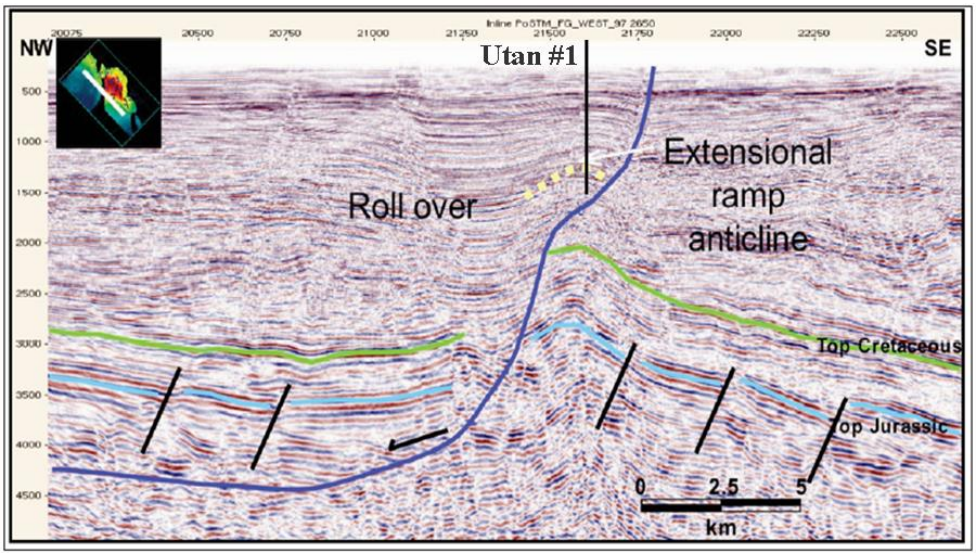


**Figure 1.3: Structural setting and trap mechanism at the Utan-1 well location.**

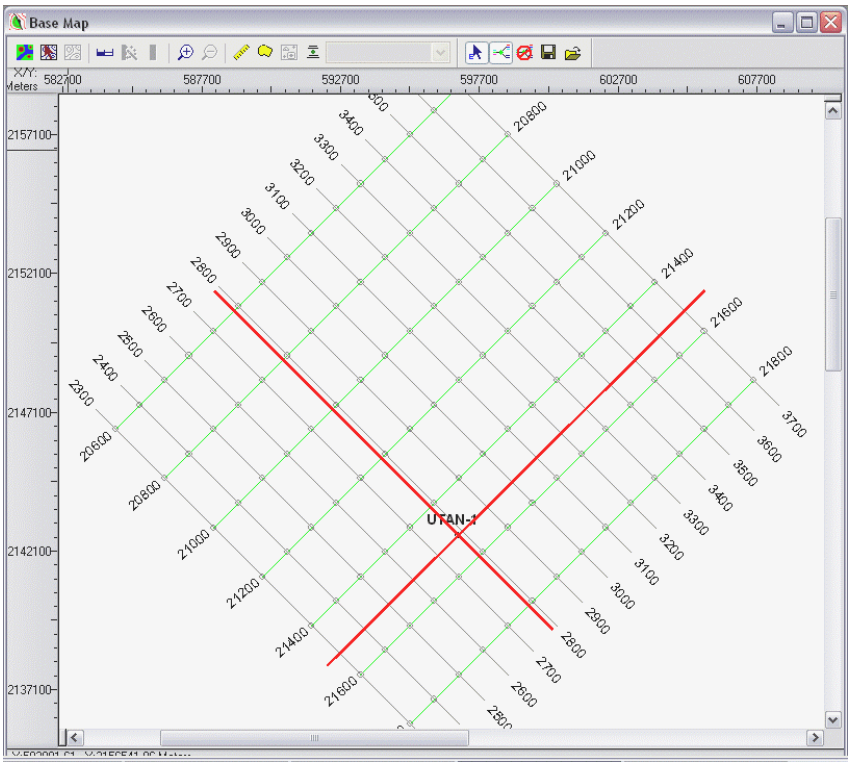


**Figure 1.4: Location of the study area defined by an area of approximately 300 km$^2$ of seismic data surrounding Utan field.**

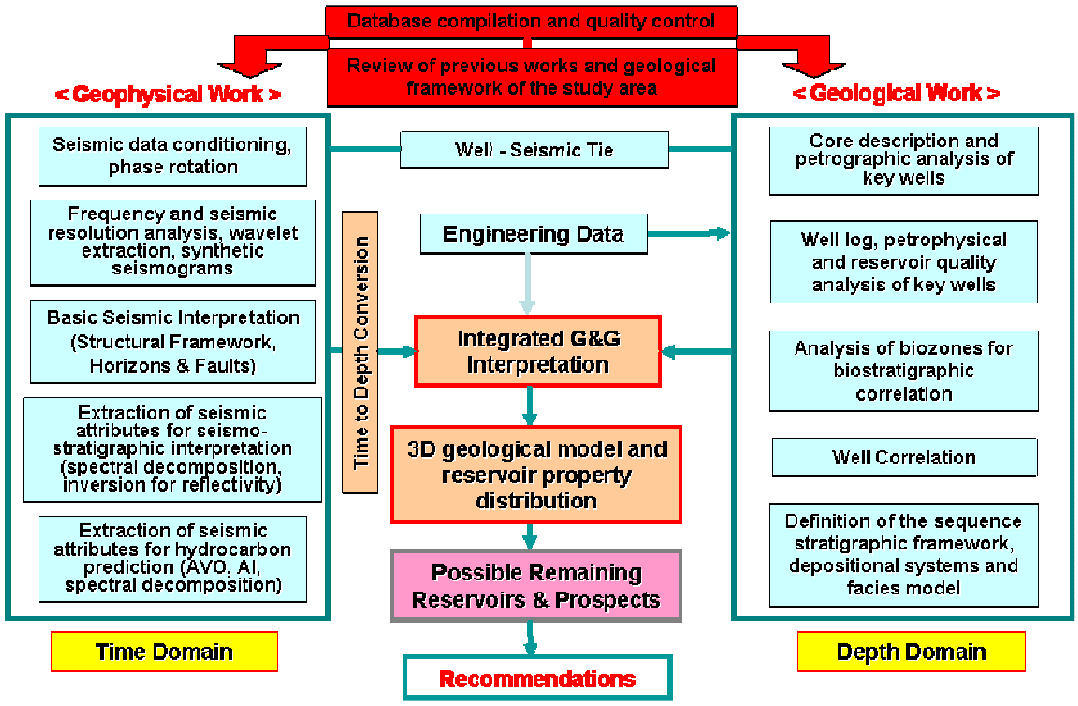


**Figure 1.5: Workflow for the integrated reservoir characterization developed in this dissertation.**

# Chapter 2

# GENERAL BACKGROUND

## 2.1 Introduction

The Gulf of Mexico basin has been studied more extensively than most basins in the world. The current knowledge of the basin has been the result of decades of cumulative geological and geophysical work developed not only by the petroleum industry, but also by academic institutions, government agencies and consortia. From the petroleum E&P point of view, the smaller U.S. northern portion has been highly explored in comparison with the larger and less explored part of the basin that lies in Mexico.

Campeche Sound is located in the southern part of the Mexican Gulf of Mexico. It represents the most prolific Mexican oil producing province where the best reservoir conditions for oil entrapment occur in Mesozoic-Paleocene carbonate structural traps. Most of the geological knowledge has been concentrated in this carbonate-prone section and less exploration has been focused on the late Tertiary siliciclastic section of this province. Therefore, not much is known of the younger Cenozoic environmental nature and reservoir potential, representing a gap in knowledge of this part of the basin where recent Pliocene, non-associated gas discoveries, have provided big expectations in this traditionally oil producing area.

Utan Field, discovered in 2003, is one of these Pliocene gas fields in the Campeche Sound. The Utan-1 discovery well provided successful results in two of three tested intervals. Geologically, a listric growth fault defines the structural framework of this reservoir and a faulted rollover anticline forms the trap. Reservoir rocks comprise mixed siliciclastic-carbonate facies.

This chapter attempts to provide a general overview on several items needed to understand the geologic framework of the study area on which this dissertation will be developed. From the general to particular, a brief description of the Gulf of Mexico basin and the portion of the basin which lies in Mexico is provided. Then, a more detailed structural, stratigraphic and tectonic analysis, including the description of petroleum systems, is developed for the Campeche Sound province and the giant Cantarell field where the Utan field is located. Finally, general aspects on the Utan-1 discovery well are provided.

## 2.2 The Gulf of Mexico Basin. A brief overview

The Gulf of Mexico basin is a roughly circular structural basin approximately 1,500 km in diameter, locally modified by a number of second-order structural elements including uplifts, archs, platforms, sub-basins, and salt diapirs. The topographic relief and bathymetry of the Gulf of Mexico basin closely reflect the geologic structure of the basin which extends onshore (fig. 2.1). Therefore, the limits of the Gulf of Mexico basin correspond, for the most part, with structural features (fig. 2.2). Parts of the structural rims along the northern, northwestern, and western flanks of the basin are marked by mountain ranges and highlands whereas the Florida

carbonate platform and the Yucatan carbonate platform represent the very gentle eastern and southern flanks of the basin, respectively.

Particularly, and according to Salvador (1991a), the southern and western limits of the basin have been placed roughly at the foot of the Chiapas massif and the Sierra Madre Oriental of Mexico, and along the eastern edge of the Coahuila platform. To the north, the structural limits of the basin correspond, from west to east, with the basinward flanks of the Marathon uplift, the Ouachita Mountains, the Central Mississippi deformed belt, and the southern reaches of the Appalachian Mountains. From the Appalachians to the shores of the Atlantic Ocean, the limit of the basin is arbitrary because no distinct structural feature clearly separates it from the Atlantic Coastal Plain (figure 2.2).

The central part of the basin is occupied by the waters of the Gulf of Mexico, which cover an area of more than 1,500,000 $km^2$, with maximum water depths of 3,750m on its abyssal plain. From the deepest part, the floor of the Gulf of Mexico rises steeply to the east and south along the Florida and Campeche escarpments which form the gulfward limits of the Florida and Yucatan platforms. Elsewhere, the floor of the Gulf rises toward the coast through generally well-defined rise, slope, and continental shelf physiographic provinces. The Gulf of Mexico is surrounded in the continental part by a low coastal plain which ranges in width from a narrow zone in eastern and central Mexico to more than 550 km in the central part of the U.S. Gulf Coastal Plain (figures 2.1 and 2.2).

Salvador (1991a, b, and c), Sawyer et al. (1991), and Ewing (1991), provide precise descriptions of the evolution of understanding of the geologic and geophysical

composition and geologic history of the Gulf of Mexico basin. The geological and geophysical information now available provide a reasonably good understanding of the stratigraphy and structure of the Gulf of Mexico basin, the types of crust that underlie it and their general distribution, the main structural features of the basin and the location and pattern of its many second-order structural features, as well as the nature of the thick sedimentary section filling the basin.

Nowadays, it is known that the crust under the Gulf of Mexico basin can be divided into oceanic, transitional, and continental types according to the manner in which crust was either created or modified by Mesozoic rifting. Sawyer et al. (1991) state that the terms "crust" and "basement" are used as synonyms in studies related to the Gulf of Mexico basin and point out that:

A) Continental crust, is interpreted as crust that predated the formation of the Gulf of Mexico basin and was not significantly modified (i.e., extended, thinned, or intruded) by the Middle to Late Jurassic rifting, the main stage of rifting that led to the formation of the Gulf of Mexico basin. Continental crust is observed around the periphery of the basin. The continental crust is typically 35 to 40 km thick,

B) "Transitional" crust occurs between continental and oceanic crust. Transitional crust was originally continental and after that "rifted" or "stretched", being significantly extended and thinned, and probably intruded with magma, during Middle and Late Jurassic rifting and, in some places, there is evidence of Late Triassic through Early Jurassic rifting. Transitional crust is also divided into thick transitional crust, which was somewhat thinned during rifting, and thin transitional crust, which was dramatically thinned during rifting. The boundary between oceanic and thin transitional crust is reasonably well defined by seismic refraction and reflection data by assuming that salt was originally deposited over continental crust which became transitional crust after rifting. Therefore, the edge of transitional crust is often marked by the edge of salt deposition. The continental crust and the transitional crust consist of a variety of igneous, metamorphic, and older sedimentary rocks.

C) Oceanic crust was formed under the deep Gulf of Mexico basin during the Late Jurassic.sea-floor spreading and continued for about 5 to 10 m.y. It is not known whether this oceanic crust was like that forming today at sea-floor spreading centers. The transition from rifting to sea-floor spreading is not well understood at any passive

margin. The oceanic crust in the Gulf of Mexico basin is generally 5 to 6 km thick and is believed to be composed of basalt pillows, dikes, and massive gabbro or serpentinite.
.

Geophysical studies indicate that the "basement" in the central, deepest part of the basin can be estimated to be about 12 to 16 km below sea level. This deep central part of the basin is underlain by an oceanic-type crust, whereas most of the U.S. Gulf Coastal Plain, the Florida and Yucatan platforms, and the remainder of Mexico are underlain by continental or thick transitional crust. Transitional crust also occurs between the continental and oceanic crust under the northern and southern parts of the Gulf of Mexico whereas along the western and eastern limits the boundary between oceanic and continental crust is represented by a narrower belt of transitional crust. (figure 2.3).

This crust-type distribution has strongly suggested a model of the evolution of the crust under the Gulf of Mexico basin that includes (Sawyer et al., 1991): (1) a Late Triassic-Early Jurassic phase of early rifting; (2) a Middle Jurassic phase of rifting, crustal attenuation, and formation of a broad area of transitional crust; (3) a Late Jurassic period of oceanic crust formation in the deep central Gulf of Mexico; and (4) subsequent crustal subsidence modified by sediment deposition.

Sawyer et al. (1991), also suggest that a widespread unconformity at the base of the marine Mesozoic section more accurately represents the overall configuration of the modern Gulf of Mexico basin. This surface represents the boundary between the crust, basement and pre-rift sequences beneath which are overlain and onlapped by Middle Jurassic salt (or equivalent rocks) as well as younger sedimentary rocks.

It is assumed that from the cessation of sea-floor spreading, the transitional and oceanic crust cooled and subsided, allowing deposition of thick sedimentary sequences in the Gulf of Mexico basin being filled with up to 15 km of sedimentary rocks that range in age from Late Triassic to Holocene (Ewing, 1991). Three main stratigraphic-structural provinces in existence during the Mesozoic that were preserved during the Cenozoic around the center of the Gulf of Mexico basin are now clearly recognized (Salvador, 1991; Galloway, et al., 1991):

a) A carbonate-evaporite province of the Florida and Yucatan platforms to the east and southeast;

b) A province to the west and southwest predominantly composed of carbonates and fine-grained clastic sediments, i.e. a "Laramide-modified" province;

c) A province to the north and northwest characterized by dominantly terrigenous clastic sedimentation and basinward progradation.

Major regional unconformities or hiatuses have also been identified which have been related to worldwide sea-level changes in the preparation of composite charts outlining the chronostratigraphy and eustatic cycles of the Mesozoic and Cenozoic (Haq, et al., 1988). The central part of the Gulf of Mexico remaining under deep waters, is usually considered as a fourth stratigraphic-structural province

From the tectonic point of view, three distinct types of margins can be regionally distinguished in the basin: a stable margin to the east and southeast, corresponding to the carbonate-evaporite province of the Florida and Yucatan platforms; a compressional margin to the west extending the length of the Sierra Madre Oriental of Mexico (the "Laramide-modified" province); and a northwestern

and northern margin characterized by sustained subsidence and sedimentary progradation.

Regarding the hypothesis on the origin and development of the Gulf of Mexico basin, Salvador (1991b), details how for more than 100 years scientists speculated about the initial steps of the formation of the present basin. Nowadays, reasonable interpretations of the origin and development of the basin have been developed based largely on oil industry exploratory drilling and geophysical surveys.

The plate tectonics framework together with new and more precise information on the distribution and tectonic behavior of the salt deposits supports the notion that the Gulf of Mexico basin originated with rifting during the Triassic-Jurassic as North America began to separate from Africa-South America. The salt may have been formed during Middle-Late Jurassic time either in: a) a single evaporitic basin, which was later spread apart by the formation of new oceanic crust in the central part of the Gulf of Mexico, together with the southward movement of the Yucatan block to its present position, or b) by the break-up of the Gulf area into a series of separate subsiding basins, some of which contained thick salt deposited in shallow marine environments. A drift and subsidence phase began in Late Jurassic time, with major rifting of the central Gulf and formation of new ocean crust (Xue and Galloway, 1990). This concept has been incorporated in one way or another into all modem interpretations of the origin of the Gulf of Mexico basin.

There are, however, still many unanswered questions and poorly understood stratigraphic, structural and tectonic problems regarding development of the Gulf of Mexico basin. One of these localities in Mexico is the subject of this dissertation.

## 2.3 The Mexican portion of The Gulf of Mexico Basin

The Gulf of Mexico is considered one of the largest and successful petroleum basins in the world. As shown in Figure 2.4, the northernmost part of the basin is located in the U.S., whereas its southern part lies in Mexico. From the petroleum E&P point of view, the smaller U.S. northern portion has been highly explored compared to the larger and less explored part of the basin that lies in Mexico.

The Mexican part of the Gulf of Mexico (MGOM) is limited on the north by the maritime United States–Mexico border (roughly following the 26º parallel); on the west and south by the states of Tamaulipas, Veracruz, and Tabasco; and on the east by the states of Campeche and Yucatán as well as by the maritime Cuba–Mexico border.

Geologically, the MGOM extends onshore into several producing basins. Guzman and Marquez (2001) describe how the area onshore, and offshore in < 200m water depths, has been subdivided into several basins and provinces in order to improve the geological knowledge and to evaluate the hydrocarbon potential (counterclockwise from north to south): Burgos on the northwest; Tampico-Misantla on the west; and Veracruz and Southeast Basins on the south (figure 2.5).

The Southeast Basins include three Tertiary provinces (the so called –Cuencas del Sureste-) formed within the Mesozoic basin as Tertiary depocenters: a) Salina del Istmo; b) Comalcalco (which includes the Mesozoic Chiapas-Tabasco light-oil province), and c) Macuspana. To the north, the Southeast Basins have two offshore Mesozoic provinces: Litoral de Tabasco and Campeche Sound (Sonda de Campeche). On the east, the MGOM includes the non-producing Yucatán Platform, limited by the Caribbean (Figure 2.6).

The Mexican deep-water Gulf of Mexico (>200m in depth) covers an area of approximately 530,000km$^2$. It has been subdivided into eight petroleum provinces based mostly on their tectonic characteristics: Franja Distensiva, Delta del Río Bravo, Franja de Sal Alóctona, Cinturón Plegado de Perdido, Cordilleras Mexicanas, Cañon de Veracruz, Salina del Golfo Profundo, and Planicie Abisal (Guzman and Marquez-Dominguez, 2001).

The MGOM has been producing oil and gas since the beginning of the twentieth century. All these hydrocarbons have been extracted from the onshore and shallow offshore parts of the basin (<200m water depth). Actually, almost the entire Mexican oil and gas production comes from the onshore and shallow offshore Gulf of Mexico.

Southeast Basins including Campeche Sound has been the most prolific Mexican oil producing province since the middle 1970´s when the Mesozoic onshore light oil from the Chiapas-Tabasco subprovince was discovered (Guzman and Marquez-Dominguez, 2001). The main oil reservoirs in Campeche Sound include Abkatun Field, Ku-Maloob-Zaap Complex, and the super giant Cantarell Field, the latter of which has produced approximately 7000 million barrels of oil during almost 20 years of production and development. However, the oil production from the giant Cantarell is nowadays declining and the strategies for future oil production have to focus on deep-water provinces (holding what seems to be large undiscovered reserves that, although not yet tested, are likely to be a future profitable petroleum province based on recent exploration campaigns in the MGOM and the wildcats in the US

portion), non-traditional provinces including Chicontepec, the shallow offshore areas outside Campeche, and others).

On the other hand, most gas production in Mexico is associated and even though the country is one of the biggest oil exporters worldwide, it is still a net gas importer. Main non-associated gas provinces in the MGOM include the onshore Burgos, Veracruz and Macuspana basins (figure 2.5). The additional resource has to come from boosting internal gas production, discovering new non-associated gas provinces, and/or by developing non-conventional reservoirs. Beyond onshore prospecting for gas, recent discoveries in the Mexican part of the Gulf of Mexico platform have shown new opportunities for gas in this typical oil province. One of these recent discoveries is the subject of this dissertation.

## 2.4 Regional Geological Framework of Campeche Sound

Campeche Sound is a Mesozoic offshore province located on the Mexican continental platform of the Gulf of Mexico that belongs to the petroleum Southeast Basins of Mexico. The province covers approximately 15,000km$^2$ (from the approximately 60,000 km$^2$ which are covered by the Southeast Basins), offshore the states of Yucatán, Campeche and Tabasco, in a strip encompassing isobaths from 20m to 200m deep (figure 2.7).

The Chiapas-Tabasco (onshore) and Campeche Sound (offshore) areas are adjacent to each other and are similar both geologically and in reservoir behavior (Santiago and Baro, 1992; Angeles-Aquino, 2004). Actually, the offshore extension of the Mesozoic Chiapas-Tabasco province is the Litoral de Tabasco area and the

Campeche Sound. For this reason, these provinces are sometimes considered analogous from both geologic and petroleum points of view, even though there are local important differences between them.

The Mesozoic section in Campeche Sound includes Callovian salt deposits, Upper Jurassic sandstones, anhydrites, limestones and shales. The Cretaceous comprises limestones, dolomites, shales and carbonate breccias, whereas the Cenozoic section includes calcarenites and interlayered clastic, carbonate and mixed clastic-carbonate units.

Campeche Sound has been affected by at least three episodes of deformation which produced the trap-forming structures: first, extensional tectonism related to the opening of the Gulf of Mexico, then Miocen compressional mechanisms, and finally Pliocene to Recent extensional tectonism.

Tithonian shales and shaly limestones are the source rocks in Campeche Sound. Oolite bars, slope and shelf carbonates and breccias, calcarenites and Tertiary clastics are the main reservoirs. Evaporites and shales are the regional seals.

### 2.4.1 Stratigraphy

The stratigraphic column of the Southeast Basins, which includes the Campeche Sound, comprises a thick sedimentary section ranging in age from the Middle Jurassic to the Holocene (figure 2.8). Even though there is an established and accepted lithostratigraphic column with formational names for the onshore Southeast basins, lithostratigraphic names for Campeche Sound are informal. Francisco Angeles-Aquino, a highly respected Mexican petroleum explorer, has carried out extensive and

intensive work describing the tectonic and stratigraphic evolution of Campeche Sound. Some of his works have been published by the Mexican Association of Petroleum Engineers (Angeles-Aquino, 2003 and 2004).

Particularly, magnetic interpretations (Angeles-Aquino et al., 1994) indicate that magnetic basement in central Campeche Sound reaches depths of 12,000m. Even though no well has cut the basement rocks in this province, the sedimentary column studied in Campeche Sound is thought to rest on basement rocks which could be granitic and metamorphic, similar in composition to the igneous metamorphic complex drilled by Pemex at the bottom of three exploratory wells in the Yucatan platform and to rocks exposed in the Chiapas and Mixtequita Massifs whose isotopic age has been dated as Late Silurian to Permian (Santiago and Baro, 1992; Angeles-Aquino et al., 1994). Recent studies reported by Padilla y Sanchez (2007), refer more precise isotopic ages of ~ 250 My for rocks sampled from the Chiapas Massif, which has been dated as Pennsylvanian (Upper Carboniferous) (figure 2.9).

This investigated igneous-metamorphic composition of the basement in Campeche Sound has been interpreted by Sawyer et al. (1991), as corresponding to thin transitional crust formed during the opening of the Gulf of Mexico. The basement dips in this area from the northeast to southwest and forms an arc which is deepest in the southwest. The same authors establish that the boundary between thin transitional crust and thick transitional crust is located toward the northeast boundary of Cantarell Complex, while the boundary between transitional crust and continental crust lies toward the southwest where granites are exposed in the Mixtequita Massif.

The most important red-bed and salt sequences in Mexico are Jurassic and are located in eastern Mexico in or around the Gulf of Mexico (Rueda-Gaxiola, 2003). In the study area, the basal units include evaporites, carbonates, and terrigenous sandstones and siltstones of Callovian–Oxfordian age.

During the Late Triassic–Lower Jurassic (the rift phase associated with the opening of the Gulf of Mexico), deposition of these Callovian salt bodies, identified as Isthmian salt, covered the entire Campeche Sound with thicknesses ranging from 3,000m in the southwest to 160m in the northeast (Salvador, 1991; Angeles-Aquino et al., 1994). Salt tectonics resulted in the later formation of structural and stratigraphic traps both in the Chiapas-Tabasco and Campeche areas for the Cretaceous and the Miocene.

Early Jurassic salt is overlain almost always by evaporitic sequences that mark the beginning of the Middle Jurassic transgressive sequence. During the Callovian and the beginning of the Upper Jurassic, marine conditions extended over all of the Southeast basins. In particular, the Oxfordian in the Campeche area is a sedimentary sequence of shallow-marine clastics, evaporites, and shallow organic-rich carbonates (Guzman-Vega and Mello, 1999). One of the best oil reservoirs in the Campeche shelf, the Ek-Balam Field, produces from the sandy member of this group (Angeles-Aquino and Cantu-Chapa, 2001).

The marine transgression increased in the Southeast Basins during the Kimmeridgian. The Kimmeridgian units consist of a lower section of shaly sediments and an upper section of oolites and partially dolomitized limestones. These

Kimmeridgian oolitic bank deposits constitute important petroleum reservoirs in this province.

Maximum flooding occurred during the Tithonian. As a consequence, organic-rich shaly limestones and black shales containing mainly type II kerogen were deposited. These rocks are considered the most likely important source rock in the Southeast Basins (Guzman-Vega and Mello, 1999).

The Lower and middle Cretaceous in Campeche area consist of dolomites and shaly limestones whereas this section in the Chiapas-Tabasco area is occupied by carbonate-evaporitic deposits. Oil accumulations are associated with these sections in both areas.

Upper Cretaceous deposits are represented in the Campeche area by dolomites, shaly limestones, and chert. Paleogeographic conditions at the Upper Cretaceous locally overlapped the beginning of the Paleocene (Santiago and Baro, 1992) and there was a predominance of dolomitized limestone breccia covering the Upper Cretaceous/early Paleocene section which extends southward to part of the states of Chiapas and Tabasco. Dolomitized breccias are the main reservoir play in the Campeche area. The origin of these breccia deposits is still a matter of discussion; they are variously attributed to the Chicxulub meteoritic impact, flows of calcareous detritus coming from the Yucatan shelf (Santiago and Baro, 1992), or they may have been of an uplift/karstic nature. The breccia forms part of a series of unusual stratigraphic, structural, sedimentological and diagenetic events along the western margin of the Gulf of Mexico (Horbury et al., 2003).

The breccia is transitionally covered by argillaceous limestones and marls, which, in turn, grade upward to fine-grained terrigenous sediments—shales and bentonitic shales of middle and late Paleocene age which provide the sealing conditions for the breccia reservoirs.

The overlying Eocene is composed of bentonitic, greenish-gray pyritic shales. In the northeastern part of the Gulf of Campeche the presence of calcarenite facies deposited as turbidity currents flowing from the western margin of the Yucatan platform have been reported in the middle Eocene (Pemex internal reports). These Eocene calcarenites constitute a secondary reservoir in the Campeche Sound.

In a general sense, the beginning of the Cenozoic, in both the Sonda de Campeche and Chiapas-Tabasco areas, is generally characterized by the contrast in sedimentation between carbonate rocks from the Upper Cretaceous-Early Paleocene period and the siliciclastic rock formations from the middle and late Paleocene-Pleistocene. Seismically, the Mesozoic-Paleocene section is characterized by a high-seismic velocity, carbonate-prone interval, that underlies a lower-velocity siliciclastic interval.

The Oligocene is predominantly composed of shales, some of which are bentonitic (Galloway et al., 1991). During the Oligocene, there were marked periods of erosion that formed a regional unconformity in some areas; allochthonous salt also has been observed as sills between the upper Oligocene and lower Miocene and between different stratigraphic levels (Santiago and Baro, 1992).

The Miocene and younger units consist of interlayered clastic and carbonate rocks. In the Southeast Basins, Miocene sediments mainly include shales and

bentonitic shales, with sandstones and limestone inclusions close to the Yucatan shelf. Middle Miocene sediments comprise outer-middle-shelf sediments; by the late Miocene the deposition was of delta front/lagoonal or inner-middle-shelf mixed carbonate/clastic facies sourced from the Yucatan margin and continental rivers. Several wells drilled at Cantarell, Abkatun and Pol fields have reported numerous gas shows in Miocene sediments of Campeche Sound. They have been traditionally good oil and gas reservoirs in Chiapas-Tabasco area (Santiago and Baro, 1992).

At the end of the Miocene the sea began to withdraw, increasing sand deposition during the Pliocene and Pleistocene. From the early Pliocene to the Holocene, inner-shelf and fluvial environments became established. As such, coarse siliciclastic slope to deltaic and coastal plain systems entered the Reforma-Akal subbasin for the first time (Angeles et al., 1994). Deposition was accompanied by continued development of listric normal faults; in the Southeast Basins, these are middle–late Miocene in age (Angeles et al., 1994) and flatten above ductile middle Miocene shales. Pliocene facies will be the topic of a more detailed analysis for the study area in the following chapters.

Throughout the late Cenozoic the basin filled with a thick prograding sequence of shale and sandstone, building the shelf edge out to its present position.

### 2.4.2 Regional Tectonic and Structural Framework

The current regional tectonic configuration in which Mexico is placed is a consequence of the interaction of the North American, Cocos, Eastern Pacific and the Caribbean plates (figure 2.10). In particular, crustal deformation in southeast Mexico

and Central America is due to the relative motion of the Cocos, Caribbean and North American plates (Lyon-Caen et al., 2006) (figures 2.10 and 2.11). The boundary between Caribean and North American plates is marked by the complex left-lateral Polochic-Motagua Fault System (figure 2.12).

The Gulf of Mexico Basin has been largely considered a passive margin basin in which most of the basement subsidence related to plate tectonics had ceased by Tertiary times (Horbury et al., 2003), leaving a deep marine environment over much of the area. Much of the rapidly deposited late Cenozoic fill occurs in an overall progradational pattern, which was accommodated in this bathymetric deep.

On the other hand, recent studies (Horbury et al., 2003), show that this margin could not be strictly considered a passive margin, as most models have traditionally implied. Actually, the structural and stratigraphic history in the southeast part of Mexico has been enormously influenced by the Pacific active-plate margin realm. The Middle Eocene compression which resulted in formation of the Sierra Madre Oriental fold and thrust belt, and the Early Miocene compression which resulted in formation of the Chiapas-Campeche fold and thrust belt, where both a result of this Pacific active-plate margin realm. Nowadays, compression continues with the effects of the active Motagua-Polochic plate boundary to the south. These Pacific tectonic influences, combined with the passive margin salt and shale tectonics and gravity systems such as the Perdido and Mexican Ridges fold belts, have made the western Gulf of Mexico Basin a very complex passive margin.

Locally, the tectonic framework in the Southeast Basins is defined by the Chiapas Massif to the south-southeast, the Comalcalco Basin, the Macuspana Basin,

the named Reforma-Akal folded strip where the main fields of Campeche Sound are located, and the Yucatán platform (figures 2.6 and 2.13). According to Murillo & Figueroa (2004), the Yucatán Platform, which is a stable tectonic element since Triassic times and the Miocene compressive stress direction are the elements that gave rise to the tectonic structure of the study area and explain how the main regional tectonic elements as the Macuspana and Comalcalco basins, as well as the Reforma-Akal high, were formed.

Another important piece of the Southeast Basins local tectonic framework is the Motagua-Polochic strike-slip fault system that crosses the Republic of Guatemala and the Chiapas state of Mexico, which marks the on-land plate boundary between the North American and the Caribbean plates (figures 2.3, 2.11, 2.12 and 2.13). Most of the North America-Caribbean plate boundary is a left-lateral transform boundary. The Motagua-Polochic fault system extends along ~ 400 km from the Caribbean Sea to the Pacific Coast (Lyon-Caen, 2006). Relative motion between the two plates takes place along several faults of this system and range from 9 to 34 mm/yr (Guzman-Speziale, 2001).

The complex nature of the plate boundary is particularly noticeable along its western end in northern Central America, where it approaches a still speculative triple junction with the Cocos Plate. The plate boundary offshore, the Swan Islands fault zone, becomes the Motagua and Polochic faults inland, but their trace is lost in western Guatemala and Chiapas where the system becomes a broad zone of deformation. To

the north of Motagua-Polochic, the deformation zone includes the strike-slip faults of Southeastern Mexico tectonic province (Guzman-Speziale, 2001).

Just south of the Motagua-Polochic fault system and north of the volcanic arc associated with the Cocos-Caribean subduction, a broad zone of essentially east-west extension is expressed along a series of north-south trending grabens (Guzman-Speziale, 2001; Lyon-Caen, 2006). On the other hand, the fault system also constitutes the southwestern border of the Chiapas Granitic Massif where basement rocks are exposed. These basement rocks are thought to be similar to the ones over which the sedimentary column of Campeche Sound rests. The Motagua-Polochic Fault System and the Chortis Block (figure 2.12) interacted in the most important deformation event that led to the trap-forming mechanisms of the Chiapas-Tabasco and Campeche Sound provinces during Miocene times.

In fact, the structural framework of the Cenozoic southeastern basins of Mexico, east of the Isthmus of Tehuantepec, contrasts markedly with that of the Tampico-Misantla and Veracruz basins northward (figures 2.2 and 2.5). While these two basins are bounded to the west by the compressive eastern front of the Sierra Madre Oriental, which reflects the effects of the Laramide orogeny during Late Cretaceous, this compressive front was not prolonged across the Isthmus, and the tectonic activity of the Laramide orogeny in southeastern Mexico is not clearly recognized (Salvador, 1991(b)).

Santiago and Baro (1992), explain that there were at least five different deformation episodes recorded in the stratigraphic column which affected the Chiapas-

Tabasco and Sonda de Campeche areas. Shankar Mitra and collegues (Mitra and Duran, 2005; Mitra et al., 2005; Garcia et al., 2005, Mitra et al., 2006), who have extensively worked in the three-dimensional restoration of key Mesozoic and Cenozoic units of some producing fields in the Campeche Sound, explain that from the five episodes cited by Santiago and Baro, the three most important tectonic events that controlled the formation of the trap-forming structures in the region, are: (1) Jurassic to Early Cretaceous extension, resulting in the formation of normal faults that displaced Tithonian, Kimmeridgian, and Lower Cretaceous units; (2) Miocene compression, during which the Cantarell–Sihil thrust system was formed; and (3) Pliocene to Holocene extension, during which several of the preexisting Jurassic normal faults were reactivated (figure 2.14).

The Early Jurassic to Early Cretaceous extension took place in a generally E-W direction which resulted in the N-S orientation of the Mesozoic fault system although, due to the kinematics of the plates, some faults rotated during later periods of deformation to more NW-SE trends. Some of these faults exhibit listric geometries and detach in Oxfordian units with possible reactivation during the Tertiary (Mitra et al, 2005). Recent studies (Chernikoff et al., 2006) confirm that the Mesozoic extensional fault systems exhibit low-angle, listric geometry, with growth from Oxfordian to Lower Cretaceous time in contrast to older interpretations with high-angle planar geometry. This Mesozoic normal faulting has generally not been detected in areas of high structural complexity due to low frequency seismic data.

Regional tectonic stability characterized the period between the remainder of the Cretaceous and the Lower Miocene. Laramide orogeny affected eastern Mexico

during Late Mesozoic-Early Cenozoic time, but its effects are not clearly recognized in Campeche Sound (Salvador, 1991(b)). In fact, Murillo and Figueroa (2004), point out that the Laramidic effects were not relevant in the sedimentary patterns of the Campeche oil entrapments which were deformed by a later tectonic event.

The second and most important stage of deformation occurred during the Middle to Late Miocene compressive episode resulting in the formation of most of the major thrust-related structural traps in Campeche Sound. According to Padilla-Sanchez (2007), this major event started in the Middle Miocene, during the Serravalian, when both compressive stresses resulting from the lateral movement of the Chortis Block, and the subduction of the Cocos Plate against the southern end of the North American Plate, took place together (figure 2.12). Offset of the Chortis block had occurred along the Motagua-Polochic strike-slip fault system that is considered the present-day northern boundary of this tectonic block (Mann and Rogers, 2005; Marshall, 2007). The compressional component of the movement had formed the folds and faults of the Chiapas-Reforma-Akal belt over a detachment zone localized in the Jurassic salt layer (Garcia et al., 2005). Padilla-Sanchez (2007) also points out that later, these structures were tilted to the north-northwest when the salt was mobilized northward. The change of location of this mass of salt caused new depocenters and minibasins, controlled by faults with a vergence toward the deepest parts of the Gulf of Mexico, and by regional antithetic faults, which limit the Southeast Basins. The gravitational movement of the Cenozoic deposits finally caused tectonic inversion in the Neogene basins, from which the most evident is the Macuspana Basin. As a result of the compressional tectonics, large structures were created in the easternmost part of the so called Akal horst, where

the Campeche Sound is located. Very prolific fields such as the giant Cantarell, Sihil, Ku-Maloob-Zaap, Abkatun, Taratunich, and Bacab are among those structures (figures 2.6, 2.7 and 2.15). In particular, the Sihil fault originates in an Oxfordian-Callovian detachment, ramps up through the Jurassic-Cretaceous units, and flattens in an upper detachment in the lower Tertiary section (Mitra et al., 2005). Movement of the allochthonous block over this ramp resulted in the formation of the Cantarell structure which was additionally folded by the Sihil structure related to the sub-Sihil thrust fault.

The last episode of deformation is the Pliocene to Holocene extensional phase, which immediately followed the compressive deformation, resulting in: a) formation of listric normal faults in the Neogene section that have a Middle Miocene shaly interval as the main detachment surface, and b) reactivation of some pre-existing Jurassic–Cretaceous normal faults. Since the Jurassic salt level also worked as a detachment zone during the Miocene compressional phase, the whole mechanism can be considered to be a “negative tectonic inversion” (García et al., 2005).

### 2.4.3 Petroleum Geology

The Southeast Basins, which covers approximately 60,000 $km^2$ onshore and offshore southeast Mexico (Figure 2.6), have been traditionally the main producing area of Mexico. Exploration for hydrocarbons in the Southeast Basins began in the late 1920´s, but the main discoveries were made in the 1950s for the Salina basin, the mid-1970´s, when the Mesozoic Chiapas-Tabasco onshore light-oil province was discovered, and in the late 1970´s for the extremely prolific Mesozoic Campeche Sound province (Acevedo and Mejia-Dautt, 1980; Guzman and Marquez, 2001). With

the exception of the Macuspana basin, which is mainly gas prone, all the basins are oil prone. The petroleum resources of these basins are concentrated in the Campeche Sound area, which has more than 95% of the total Mexican reserves and production.

The Campeche Sound, producer of heavy oil in its northeastern sector, covers 15,000km$^2$ in waters less than 100m deep. Since its discovery in 1976, 24 fields from which 18 are still producing -including the prolific giant Cantarell, the subthrust Sihil structure, Ku-Maloob-Zaap Complex, Abkatun, Taratunich, and Bacab- have been discovered (figures 2.7 and 2.15) with a cumulative production of ~12,000 million bbl of oil and ~7 tcf of associated gas. Reserves are estimated in ~20,000 million bbl of oil and ~11 tcf of associated gas.

Particularly, Cantarell field, over which the study area for this dissertation was defined, was discovered in 1976 and constitutes one of the giants in the oil industry worldwide. Until 2005, average production in Cantarell field exceeded 2 million b/d with cumulative production above 10 billion (10 thousand million) barrels of oil for over 25 years of production and exploitation (Garcia et al., 2005). Production comes from more than 200 wells using primary and secondary recovery methods. Oil produced from this field has an API of 20-24°. Cantarell field is located 80 km northwest of Ciudad del Carmen in the Campeche Sound and consists of a broad nortwest-southeast trending, faulted anticline, which is made up of four blocks: Akal, Nohoch, Chac, and Kutz (Figures 2.16 and 2.17). The main field is located in Akal structure, containing more than 90% of the oil reserves.

During the exploitation of Cantarell field, evidence from some of the wells implied the presence of thrusted structures in this area. During the late 1990´s, and

after integration of new seismic information with reprocessing of older seismic, new detailed geologic studies, and application of advanced deviated well drilling and well termination techniques, the repeated section below Cantarell field was confirmed. The hypothesis for a subthrust Sihil structure was finally supported for a new, totally independent reservoir with lighter oil (28° versus 24° API in the upthrown block), and total reserves of 1300 million bbl of oil (figure 2.14) (Aquino et al., 2001). The Cantarell-Sihil complex contains the largest producing hydrocarbon reserves in Mexico at the present time (Guzman and Marquez-Dominguez, 2001).

Structurally, Cantarell (Figure 2.14) is limited in its eastern portion by what was interpreted as a right lateral strike slip fault (Aquino 2001) and in the north and east directions by a reverse fault. Both the hanging-wall fold known as Akal, and the footwall fold known as Sihil, have a regional west/northwest-east/southeast orientation, the last one following the overhanging block trend.

Mitra and colleagues (Mitra and Duran, 2005; Mitra et al., (2005), developed three-dimensional models for Cantarell and Sihil structures by integrating 3-D seismic interpretation, well markers and dipmeter data. They conclude that the geometry of the Cantarell–Sihil structure varies considerably along trend from a simple fault-related structure in the south to a duplex, consisting of the Cantarell and Sihil structures in the central part, to a more complex system consisting of compressive blocks separated by Tertiary normal faults in the north (figure 2.14). As a part of this complexity northward, the western Kutz block is separated from the main Akal block by a major Tertiary normal fault against which the Utan structure, subject of this dissertation, was formed. The main field in the allochthonous block is the Akal field which has been

faulted by numerous Jurassic and Tertiary normal faults. Secondary fields include Kutz and Nohoch.

The elements of the petroleum system of Campeche Sound are briefly summarized as follows (figure 2.8):

- The main source rocks in Campeche Sound are the Tithonian marine black shales and shaly limestones which are rich in type II organic matter. According to Guzman-Vega et al., (2001), the Tithonian generative subsystem has produced more than 80% of all oil reserves from the Mexican Gulf Coast Basin. Oxfordian shaly limestones represent another minor source of oils in the Campeche area. Specific oil gravity for oils in Campeche Sound ranges from 20° API in the northeast to 35° API in the southeast.
- Reservoir rocks are widely distributed through the Mesozoic and Cenozoic column. Oolite bars, slope and shelf carbonates and breccias, calcarenites and Tertiary clastics are the main reservoir rocks. According to Angeles-Aquino (1994), the high reservoir quality present in Campeche Sound reflect not only reservoir-quality depositional facies (e.g. oolite bars in the Kimmeridgian) but also dolomitization and fracturing of the carbonate section. The most prolific reservoir rocks are the Upper Cretaceous-Paleocene dolomitized breccia deposited in a slope environment. The reservoirs in the middle and Lower Cretaceous consist of dolomitized and fractured shaly limestones. Other secondary potential reservoirs in this petroleum system include Oxfordian sandstones, Kimmeridgian

oolite bars, Upper Paleocene- Eocene calcarenites, as well as Tertiary siliciclastics and mixed siliciclastic-carbonate rocks.

- The Tertiary shaly section is the regional seal. Locally, interbedded Cretaceous and Jurassic shales, as well as Jurassic evaporites provide sealing conditions.
- Angeles-Aquino (1994), explains that the tectonism in Campeche Sound produced three types of traps: a) faulted blocks during the drifting stage; b) diapirs during the phase of crustal cooling; c) faulted anticlines during the Middle Miocene compressive stage. The main overthrust and subthrust Cantarell –Sihil structures constitute the largest traps in this petroleum system and produce primarily out of carbonate reservoirs in the Upper Cretaceous to Paleocene breccia and carbonates and the middle and Lower Cretaceous (Acevedo, 1980). Even though there has been little exploration focused on the Tertiary, stratigraphic traps and rollover anticlines are currently being tested to prove their capacity as traps from the middle Miocene until the Recent. One of these systems is the Pliocene Utan section, the subject of this dissertation.
- Expulsion and migration of oil and gas occurred during Tertiary burial and culminated in the Miocene. The presence of multiple, vertically stacked petroleum reservoirs from Kimmeridgian to Pleistocene in marine-siliciclastic and carbonate reservoirs containing the same genetic type of oil suggest that vertical pathways are an important secondary migration mechanism including a main Tithonian, vertically-drained petroleum system (Guzman et al. (1991), and Guzman-Vega and Melo (1999)).

## 2.5 Utan Field

In 2002, the exploratory drilling location Utan #1, located 67km offshore northwestward of Ciudad del Carmen, Campeche, MEXICO, in waters 60m deep, was proposed to investigate the gas production potential of the late Tertiary sequence at the west side of the Akal block overlying Cantarell field (figure 2.18, same as figure 1.1 and repeated for reference purposes). The well was drilled and completed in a rollover anticline structure in 2003, providing successful results in a Pliocene mixed siliciclastic-carbonate section for two of the three tested intervals as well as good expectations for a probable future gas development of this traditionally oil producing province.

Geologically, Utan field is located in a minibasin formed by growth and antithetic faulting. The field has two reservoirs comprising thin Pliocene mixed sandstone-carbonate sediments. The producing facies in Utan field have not been studied in detail by integrated approaches and a comprehensive understanding of the spatial and temporal variations as well as controls on these mixed sequences has not been well established, thus providing a favorable environment for systematic research, one of the goals of this dissertation.

The trap mechanism is a rollover closure against a single major fault, namely the Kutz fault. This listric growth fault defines the structural framework of the reservoir where a derived hanging-wall, rollover anticline is present; the hanging wall rotates into the growth fault at the west side of the fault (figure 2.19). The fault separation decreases from north to south. The faulted rollover anticline, rather than the fault itself, forms the trap. An antithetic fault forms the mini-basin in which the

reservoir structure is located and a number of secondary faults compartmentalize the structure and reservoir intervals. The reservoir is essentially a three-way closure against the major fault.

Three Pliocene intervals were tested at the Utan-1 discovery well:

• **INTERVAL III (Upper):** 1075 – 1085 m. **– RESERVOIR 2**

• **INTERVAL II (Middle):** 1220 - 1228 m

• **INTERVAL I: (Lower):** 1317 – 1322 m **- RESERVOIR 1**

Gas presence was proven for two of the three tested intervals. The shallower and the deeper intervals tested flow rates of 7.46MMcfd (1075 – 1085m) and 4.13MMcfd (1317 – 1322m) respectively. The middle interval (1220 – 1228m) tested as non producer (figure 2.20).

Three intervals were cored in Utan well. Unfortunately, not all of them were properly recovered nor did they sample more than one meter of the tested intervals:

- **CORE 1:** 1084-1093m, recovery: 9m (100%), only the lowermost meter of Reservoir II was cored
- **CORE 2:** 1225-1232m, recovery: 7.2m (80%)
- **CORE 3:** 1321-1324m, recovery: 3.75m (42%), only the lowermost meter of Reservoir I was cored

Several conventional core analyses were completed on these cores by CoreLab™ and provided for this dissertation, including: measurement of spectral gamma radiation, X-ray diffraction, porosity, gas permeability (Ka) and Klinkenberg-corrected permeability at various confining stresses, relative permeability, minipermeameter measurements, grain density, petrographic and sedimentologic analyses, capillary pressure and others. Accurate placement of each cored section within the well bore was possible with the spectral gamma ray log measured in the laboratory.

Figure 2.21 shows the location of the study area and the position of the discovery well and some of the nearby wells and drilling locations on the seismic dataset which were used for the analysis. In the same figure, locations of inline 2781 and cross-line 21516 are shown. These two lines intersect at the UTAN #1 location and, therefore, they are repeatedly used in the discussion in this dissertation.

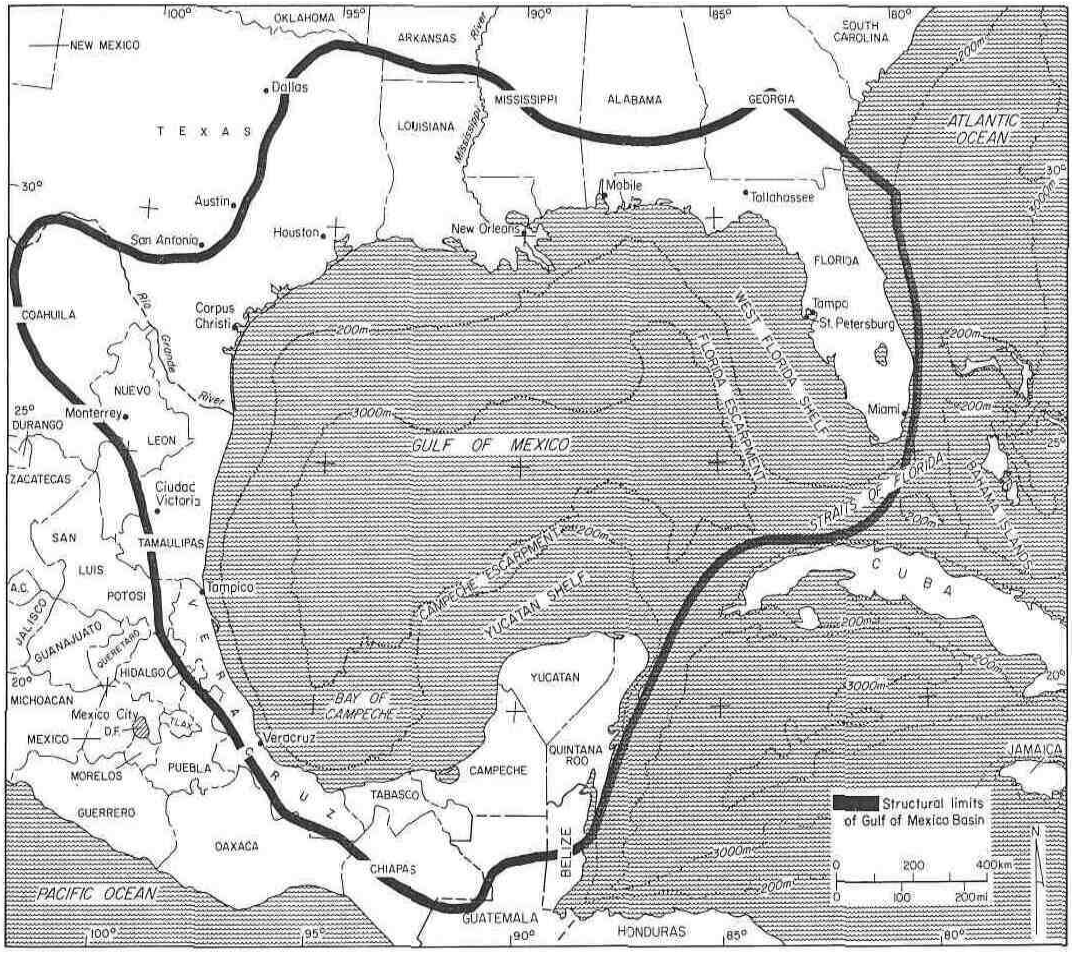


**Figure 2.1: Location of most important geographic features of Gulf of Mexico Basin, which structurally extends onshore (Salvador, 1991a).**

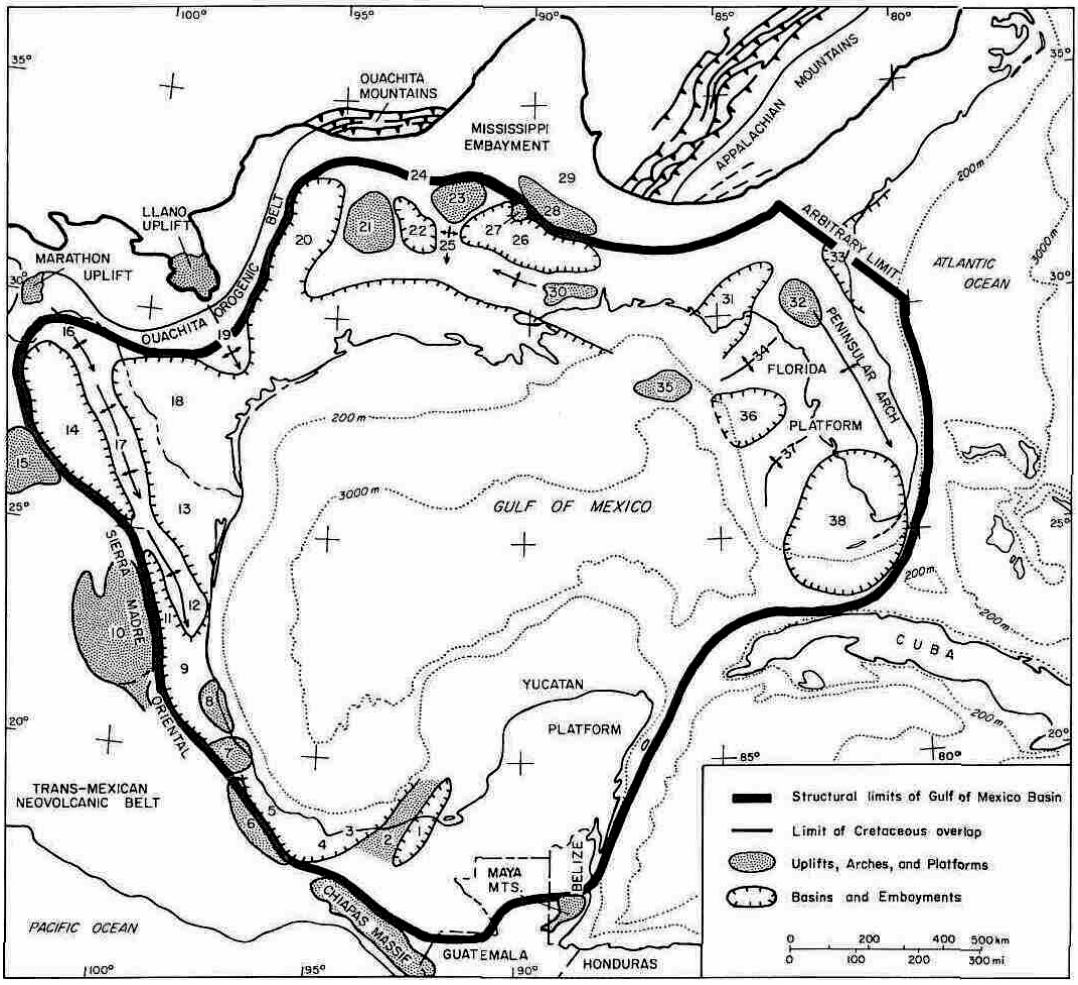


**Figure 2.2: Second-order structural features within the Gulf of Mexico Basin: 1, Macuspana basin; 2, Villahermosa uplift; 3, Comalcalco basin; 4, Isthmus Saline basin; 5, Veracruz basin; 6, Cordoba platform; 7, Santa Ana massif; 8, Tuxpan platform; 9, Tampico-Misantla basin; 10, Valles-San Luis Potosi platform; 11, Magiscatzin basin; 12, Tamaulipas arch; 13, Burgos basin; 14, Sabinas basin; 15, Coahuila platform; 16, El Burro uplift; 17, Peyotes-Picachos arches; 18, Rio Grande embayment; 19, San Marcos arch; 20, East Texas basin; 21, Sabine uplift; 22, North Louisiana salt basin; 23, Monroe uplift; 24, Desha basin; 25, La Salle arch; 26, Mississippi salt basin; 27, Jackson dome; 28, Central Mississippi deformed belt; 29, Black Warrior basin; 30, Wiggins uplift; 31, Apalachicola embayment; 32, Ocala uplift; 33, Southeast Georgia embayment; 34, Middle Ground arch; 35, Southern platform; 36, Tampa embayment; 37, Sarasota arch; 38, South Florida basin, (Salvador, 1991a).**

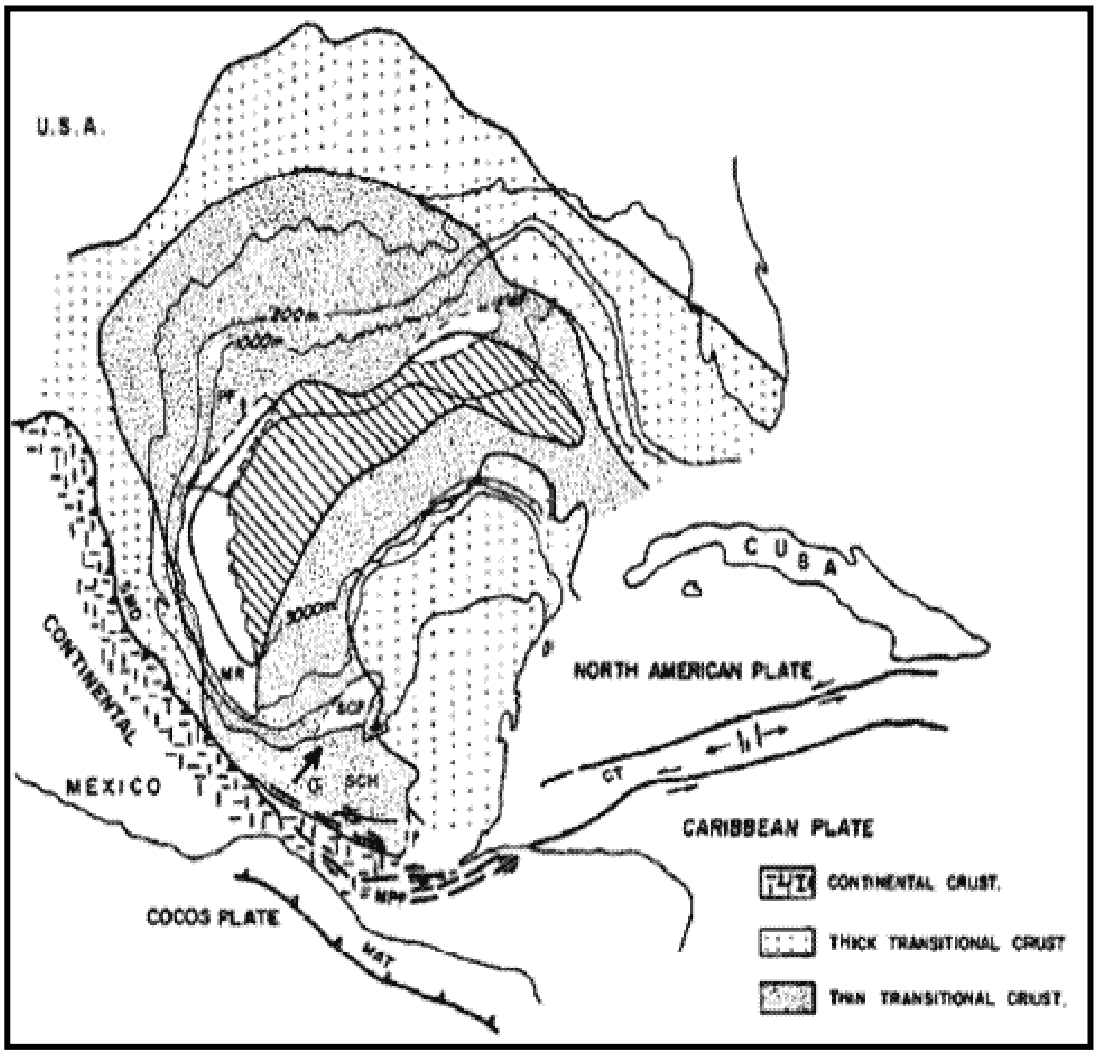


**Figure 2.3: Distribution of four crust types for the Gulf of Mexico basin: continental, thick transitional, thin transitional, and oceanic crust. Some regional tectonic features are also shown: SCF: Campeche Sound; SCH: Sierra de Chiapas; MR: Mexican Ridges; PF: Perdido fold belt; MF: Mississippi fold belt; MPF: Motagua-Polochic fault system; SMO: Sierra Madre Oriental; CT: Cayman Trough; MAT: Middle America Trench (after Angeles-Aquino, 1994).**

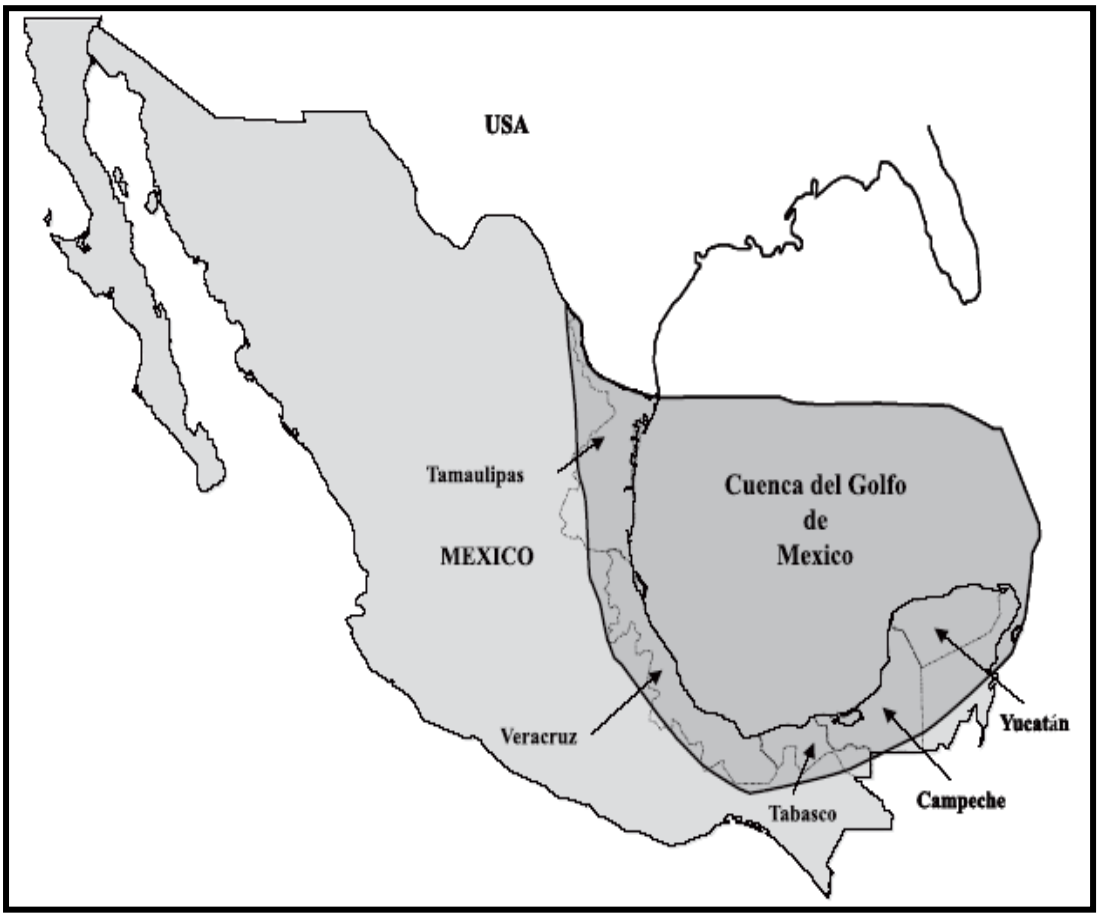


**Figure 2.4: The Mexican portion of the Gulf of Mexico (Guzman and Marquez-Dominguez, 2001).**

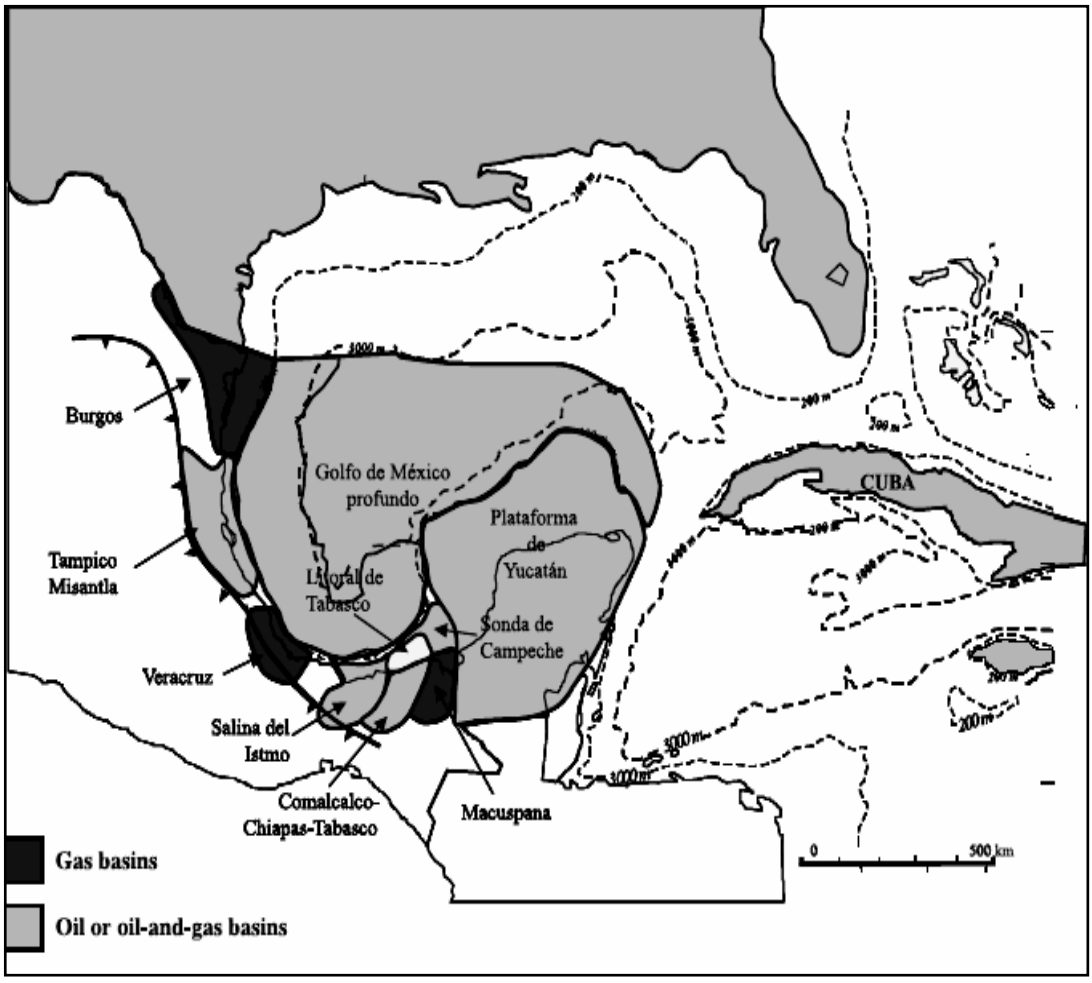


**Figure 2.5: Provinces of the Mexican portion of the Gulf of Mexico Basin (MGOM) (Guzman and Marquez-Dominguez, 2001).**

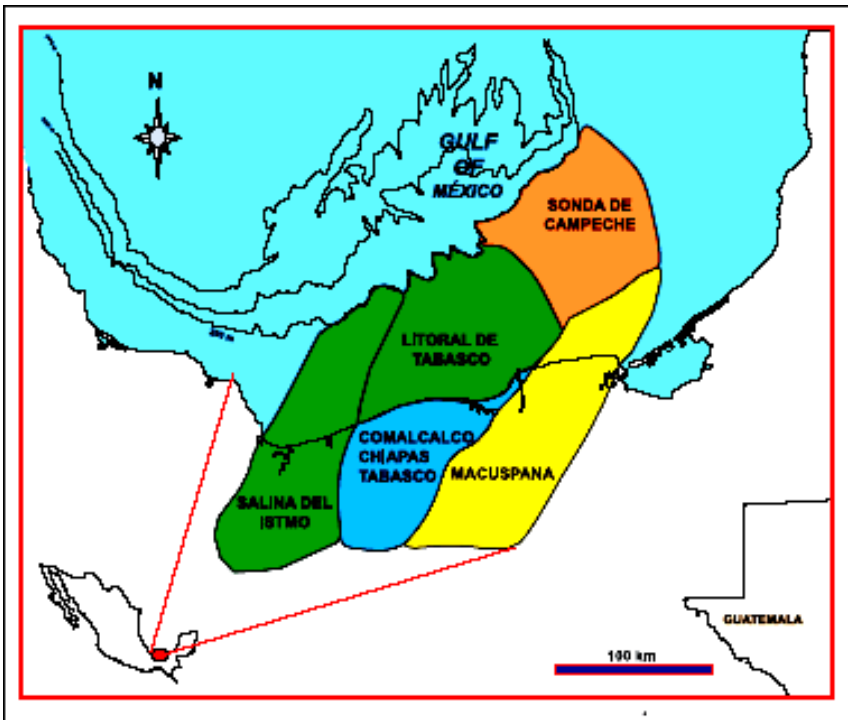


**Figure 2.6: Southeast Basin provinces (Guzman and Marquez-Dominguez, 2001).**

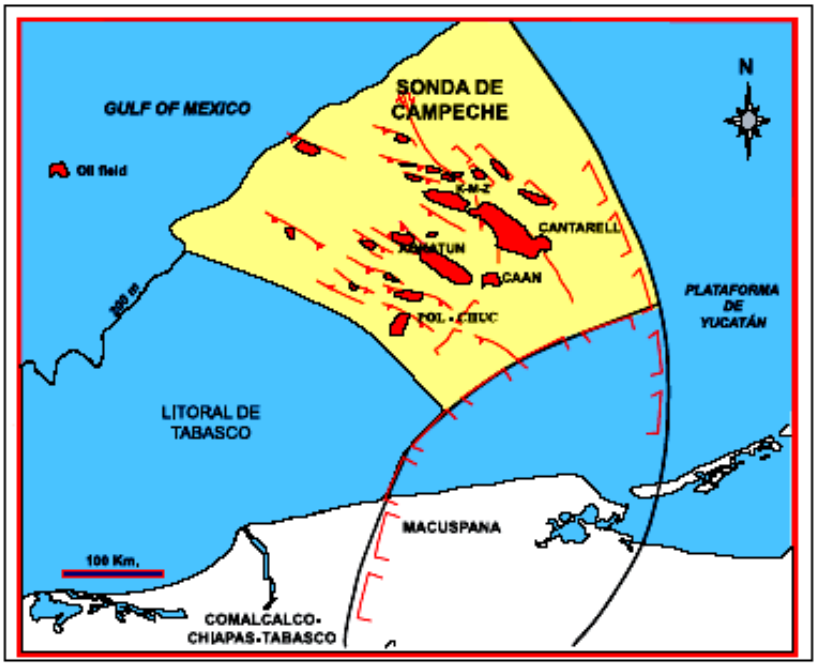


**Figure 2.7: Campeche Sound province and some of the main oil fields (Guzman and Marquez-Dominguez, 2001).**

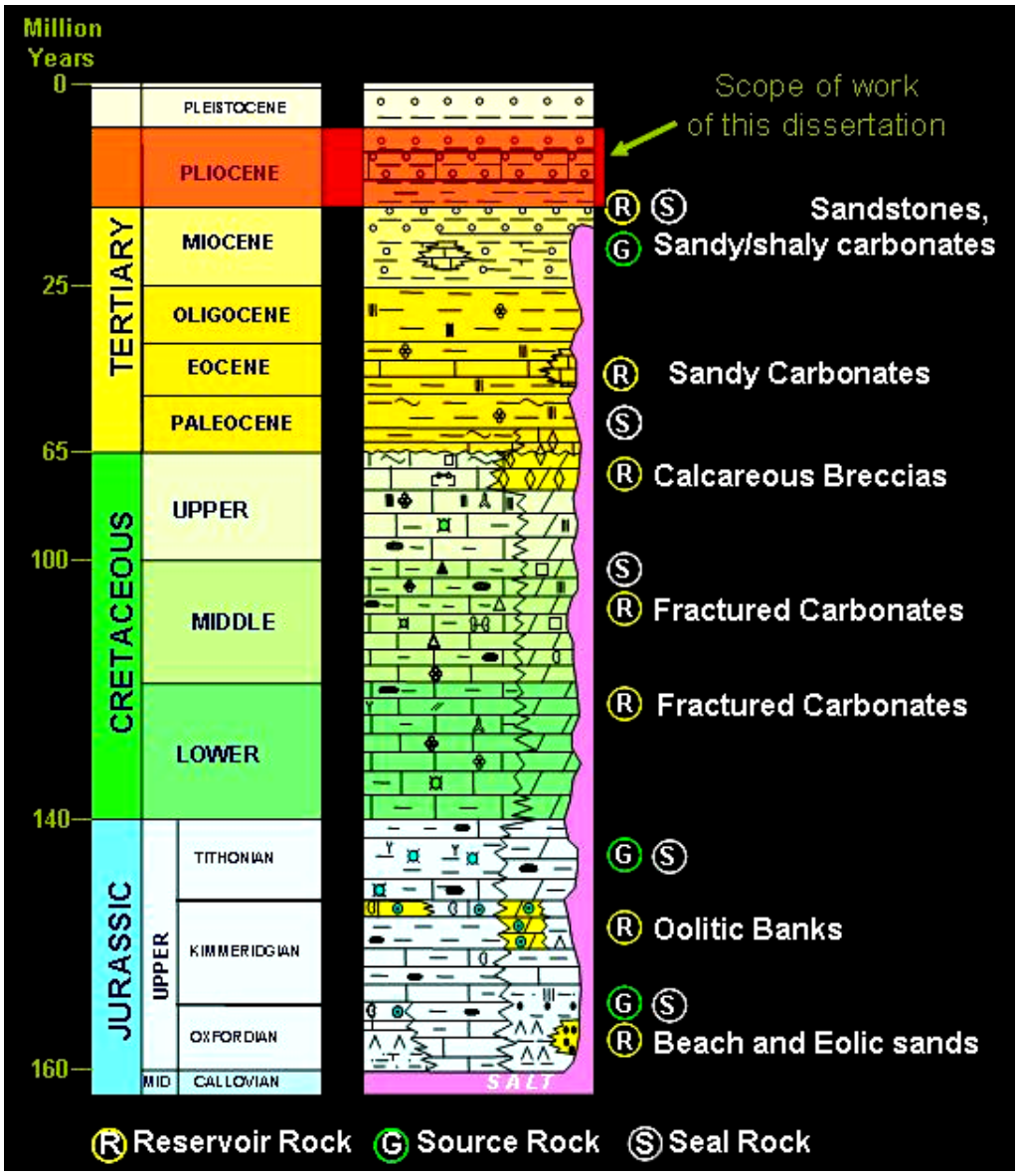


**Figure 2.8: Simplified stratigraphic section and main producing plays for the Campeche Sound area (adapted from non-published Pemex internal reports).**

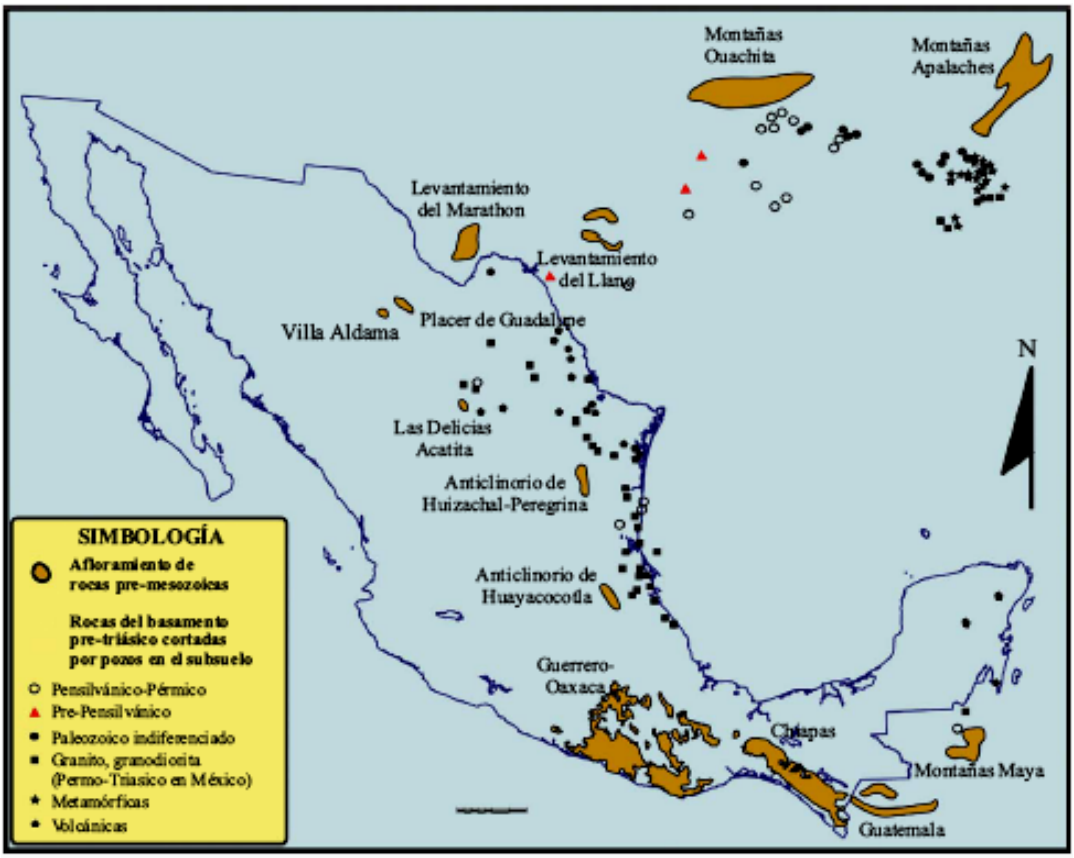


**Figure 2.9: Localities in Mexico and surrounding areas where pre-Mesozoic basement rocks are either exposed (brown areas) or have been drilled (small symbols) (Padilla y Sanchez, 2007).**

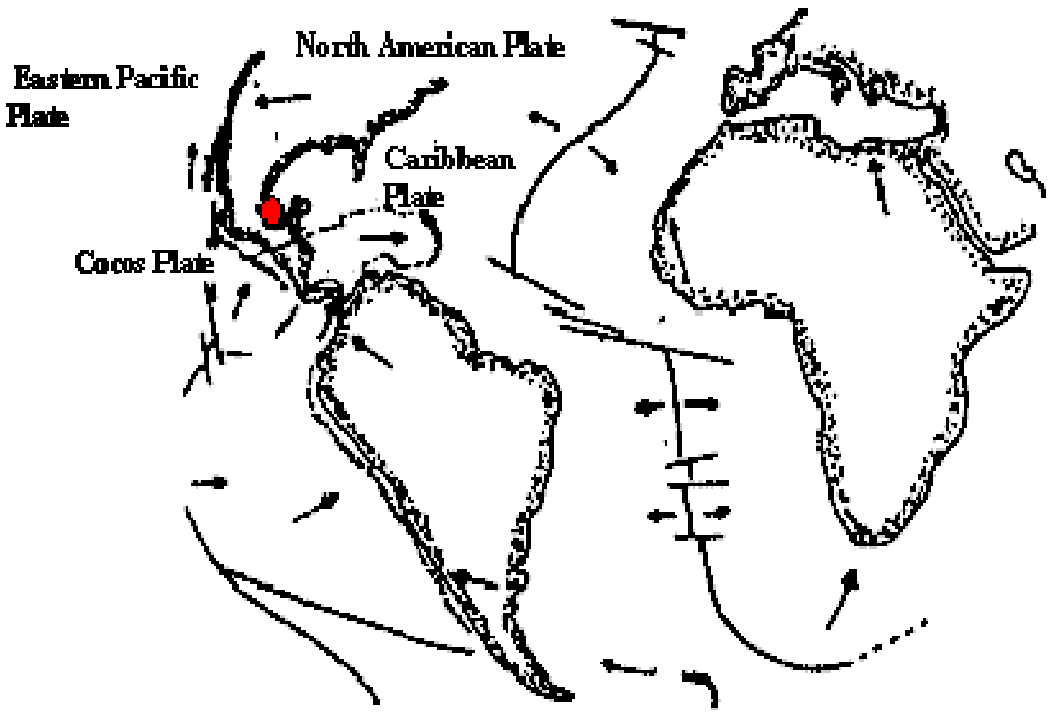


**Figure 2.10: Regional tectonic framework affecting the current southern Mexican Gulf. North American plate with south-west displacement, Eastern Pacific plate with north displacement, Cocos plate with north-east displacement and Caribbean plate with east displacement. Small red dot represents the study area (after Bahamon, 2006).**

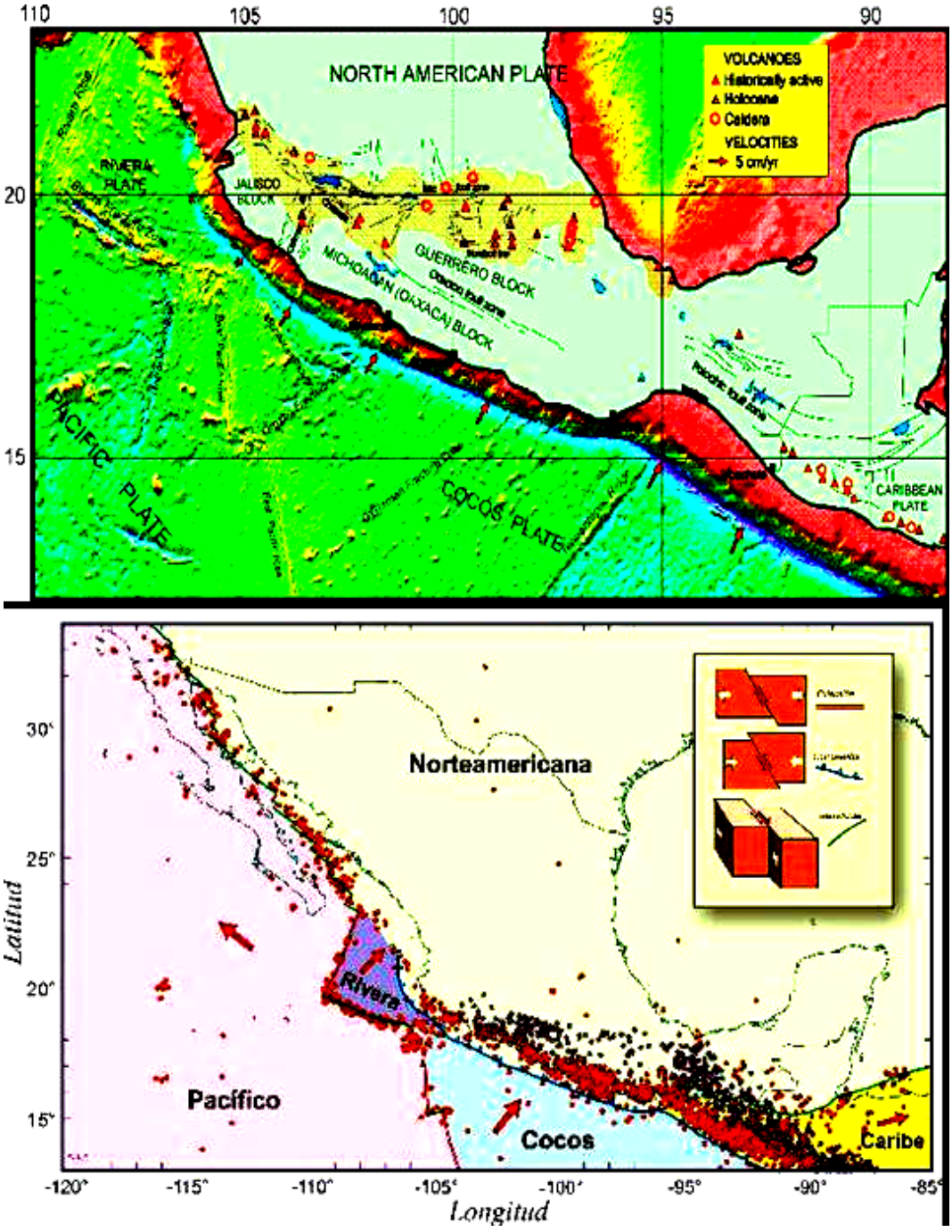


**Figure 2.11: Composite figure showing tectonic configuration and seismicity of Mexico. Red and black dots represent earthquake epicenters (websites: http://www.ssn.unam.mx/website/jsp/tectonica.jsp and www.tlacaelel.igeofcu.unam.mx).**

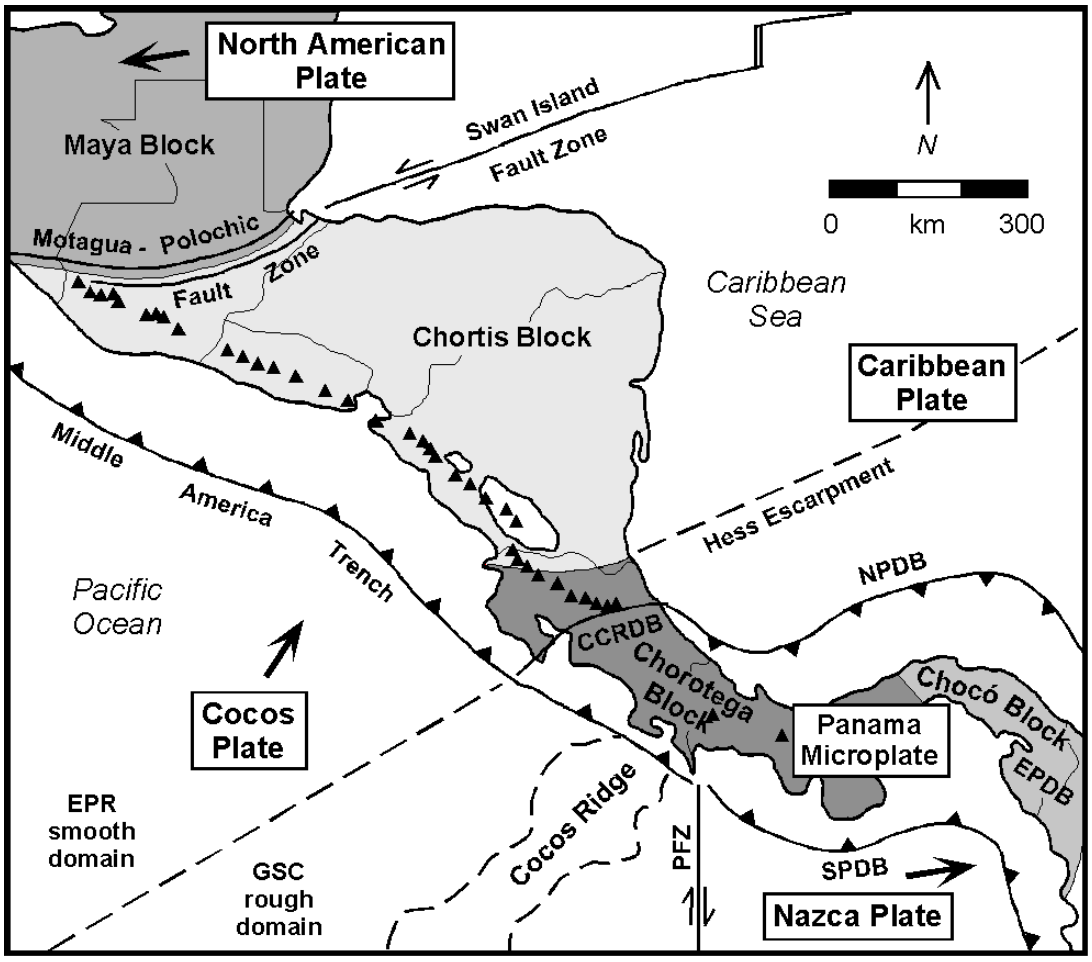


**Figure 2.12: Tectonic map of Central America, showing the regional geometry of tectonic plates and basement blocks. Plate names are in white boxes (North American, Caribbean, Cocos, Nazca, and Panama). Large arrows show plate motions relative to Caribbean plate. Active plate boundaries are shown as solid lines (with teeth on upper plate of convergent margins, and opposing arrows indicating transform motion). Shaded areas show basement blocks (Maya, Chortis, Chorotega, and Chocó). Dashed lines mark major bathymetric features. EPR: East Pacific Rise; GSC: Galapagos Spreading Center; PFZ: Panama Fracture Zone; CCRDB: Central Costa Rica deformed belt; NPDB: North Panama deformed belt; SPDB: South Panama deformed belt; EPDB: East Panama deformed belt. The figure shows the Motagua-Polochic Fault System as the boundary between the Caribbean and North American plates (Marshall, 2007).**

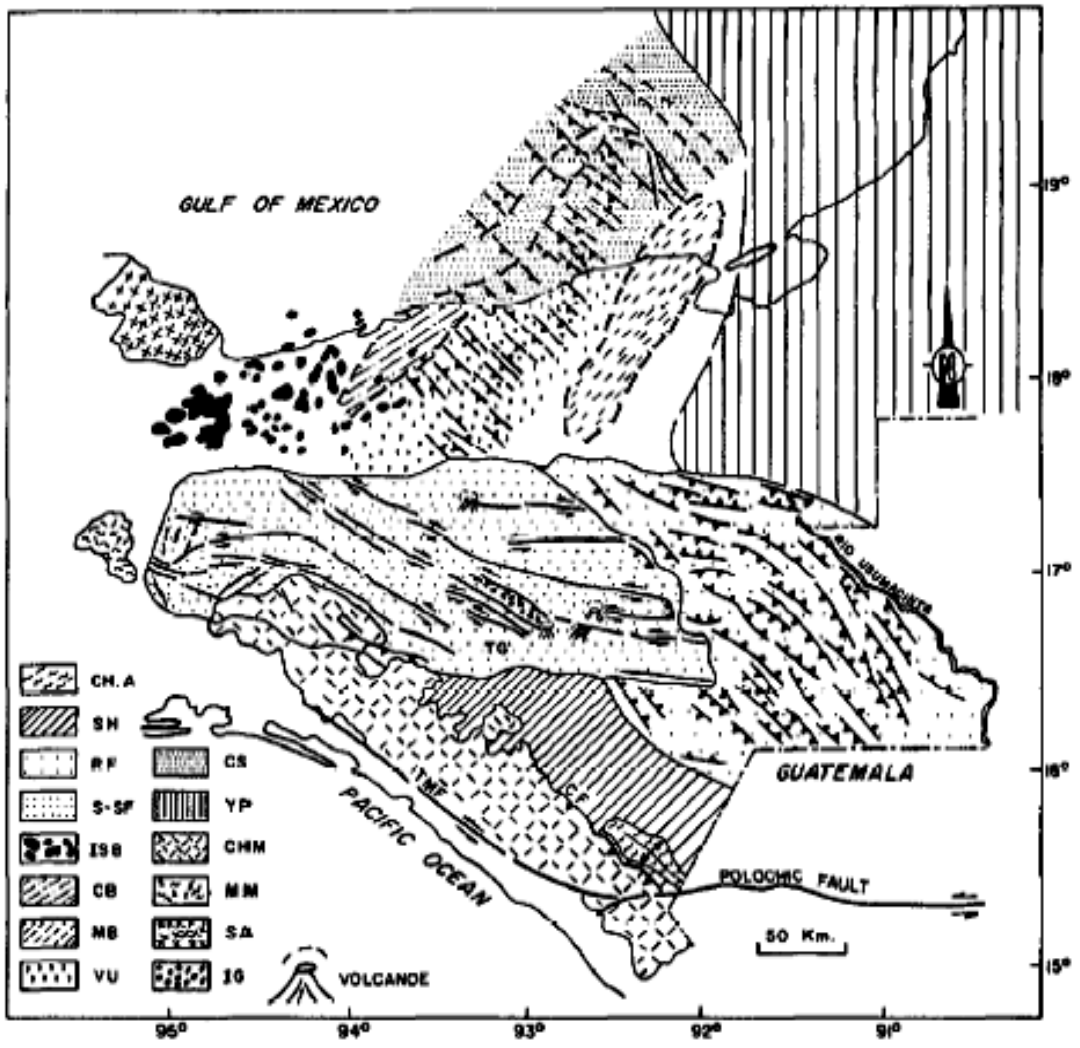


**Figure 2.13: Local tectonic map of southeast Mexico. CHA: Chicomuelo Anticlinoreum; SH: Sierra Homocline; RF: Reverse Fault Province; S-SF: Strike-Slip Fault Province; ISB: Isthmian Saline Basin; CB: Comalcalco Basin; MB: Macuspana basin; VU: Villahermosa Uplift; CS: Campeche Sound; YP: Yucatán Platform; CHM: Chiapas Massif; MM: Mixtequita Massif; SA: San Andres Tuxtla Massif; IG: Ixtapa Graben (Angeles-Aquino, 1994).**

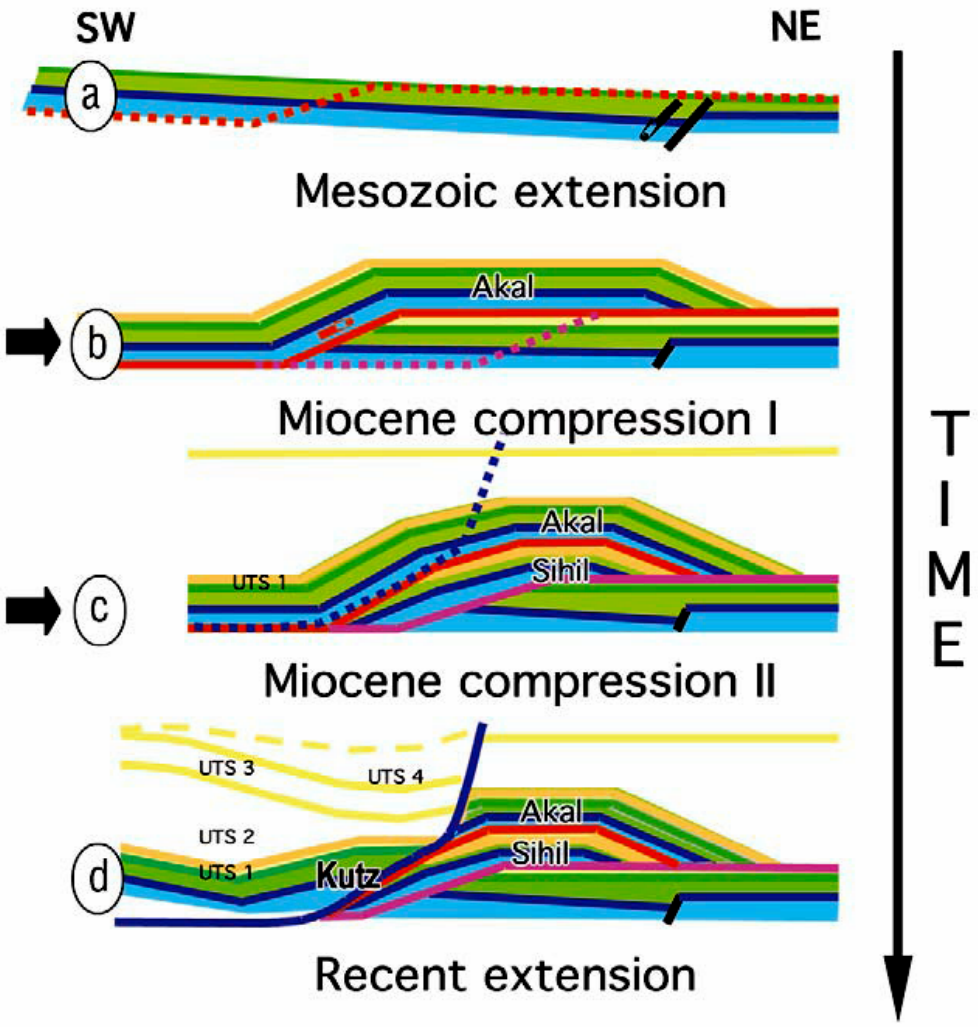


**Figure 2.14a: Main tectonic episodes that played an important role in the current deformation styles and the development of the basin structures in the Campeche Sound, shown through the structural evolution of the Cantarell-Sihil complex: (a) Jurassic-Cretaceous extension, (b) and (c) represent the Chiapaneca episode in two phases, corresponding the first one to the initial compression during the Lower-Middle Miocene to produce a verging overthrust, and a second phase which produces the duplex overriding; d) Plio-Pleistocene listric negative inversion; such a extension produced the rollover anticline where the Utan well is located (Garcia et al., 2005).**

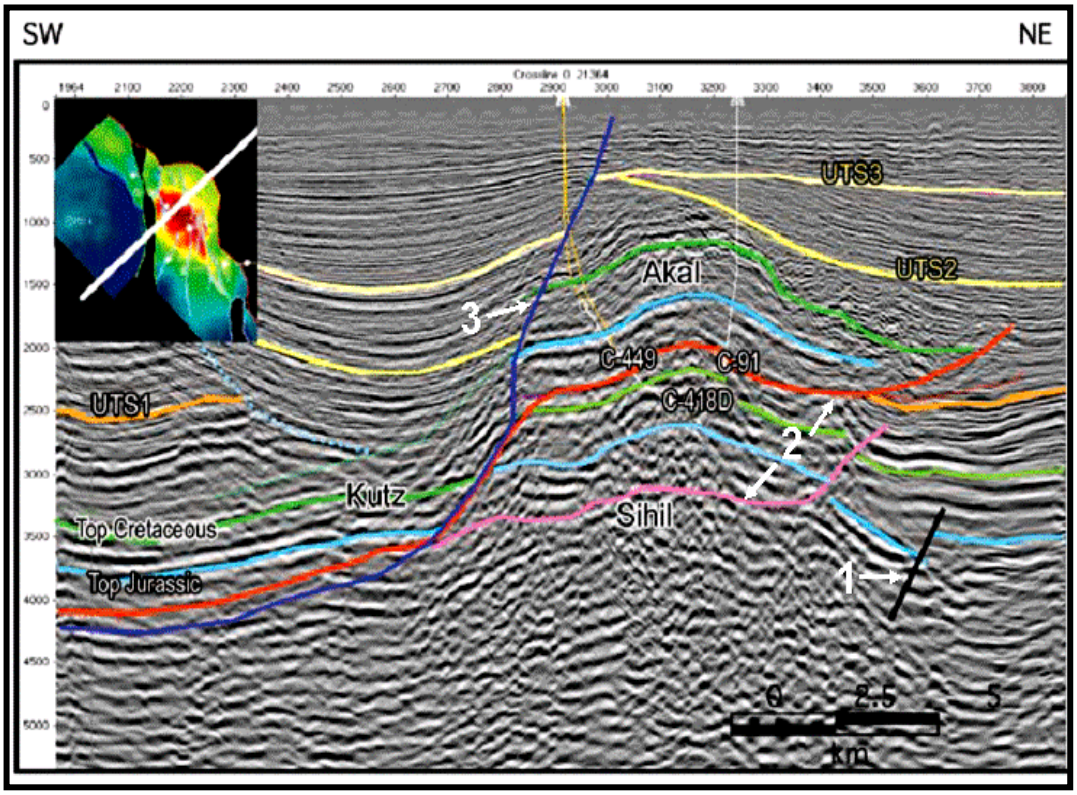


**Figure 2.14b: Cross-section showing the three main structural events in Cantarell: (1) Mesozoic extension represented by the normal "half graben" type features (black fault); (2) Miocene compression represented by low angle thrusts (red and purple faults); and (3) the Plio-Pleistocene extension (blue fault) (after García et al., 2005).**

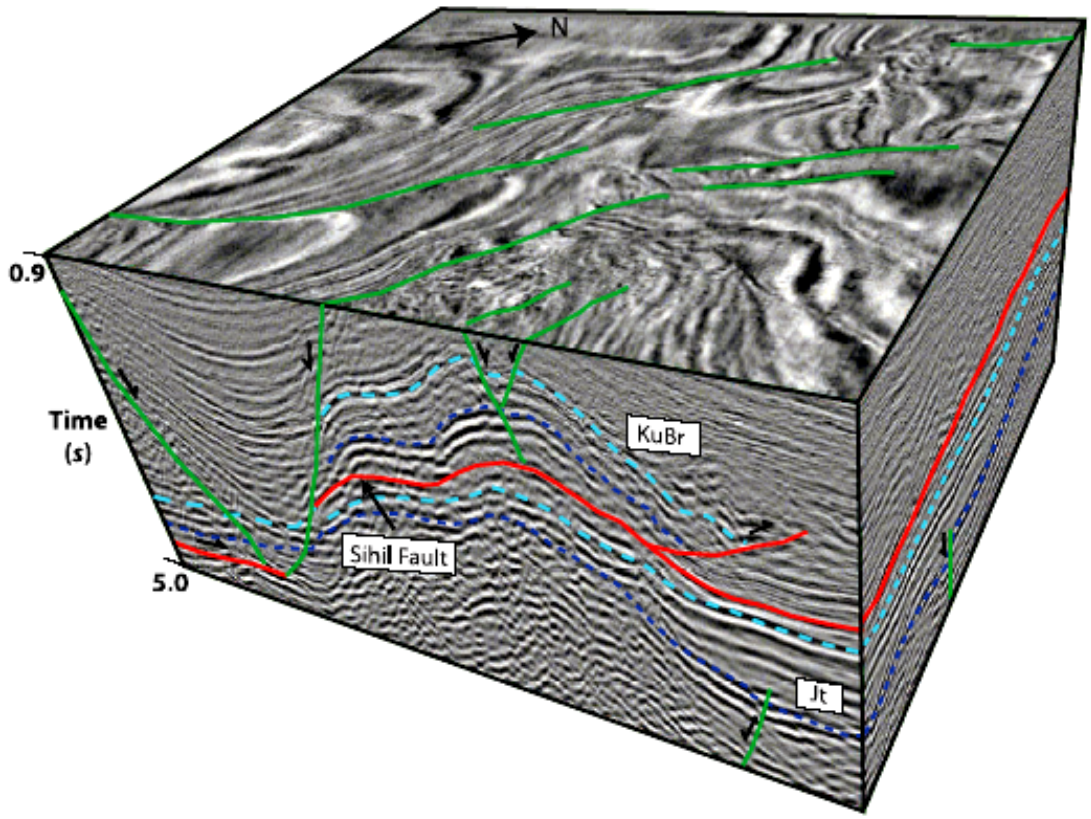


**Figure 2.14c: Three-dimensional seismic cube showing the seismic expression of the structural geometry in the northern part of the Cantarell–Sihil structures. Normal faults are shown in green, and thrust faults are shown in red. The Tertiary normal faults have an approximate north-south trend, whereas the compressive structures trend approximately northwest-southeast or parallel to the sides of the cube. KuBr = top of Upper Cretaceous breccia; Jt = top of Jurassic Tithonian (Mitra et al., 2005).**

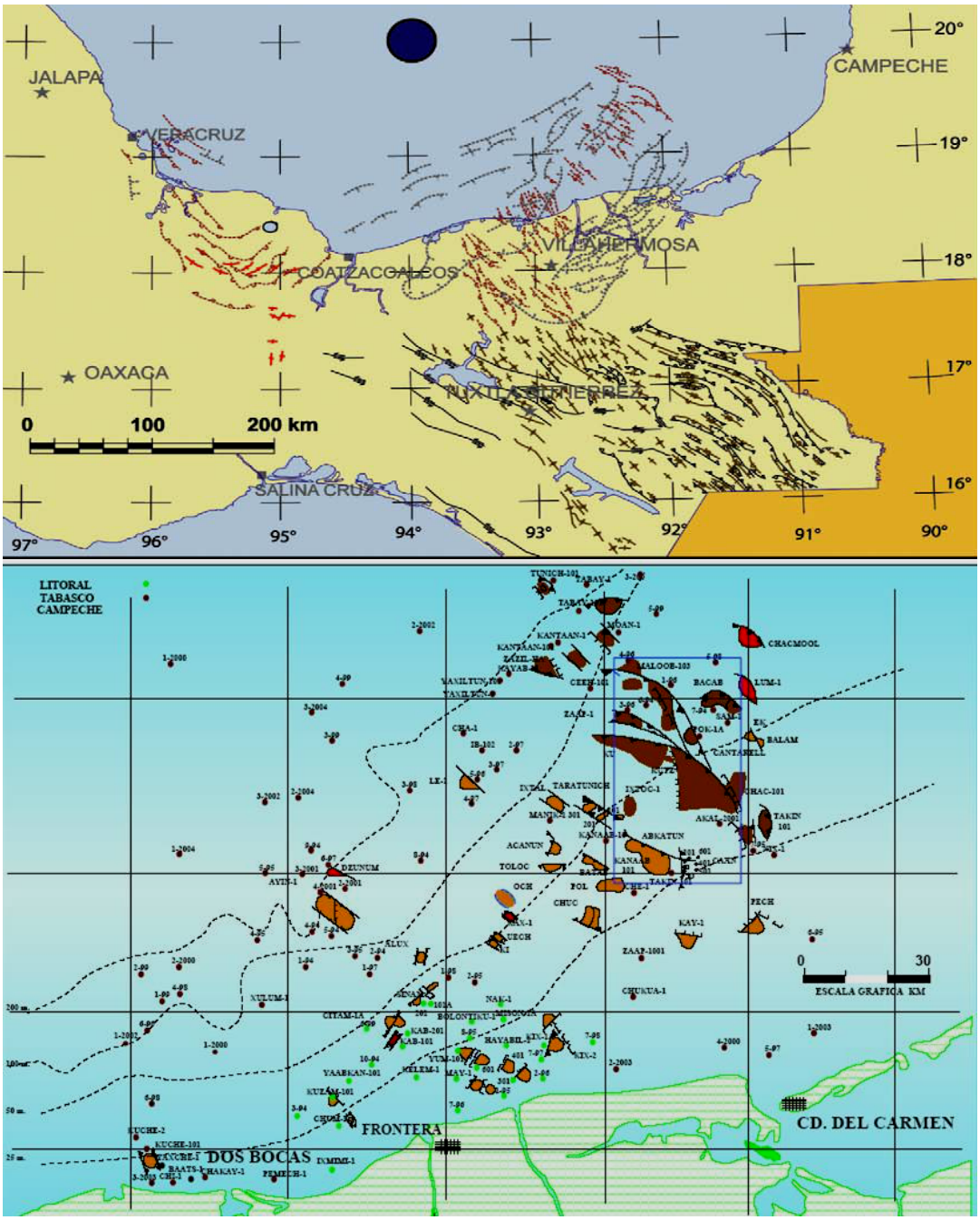


**Figure 2.15: Composite figure: (upper) Cenozoic structures in the southeastern Mexico showing Miocenic compressive folding and faulting alignments and Plio-Pleistocenic transversal extensional faulting, and (lower) corresponding main oil fields of the Campeche Sound province (after Padilla y Sanchez, 2007; Pacheco, 2002).**

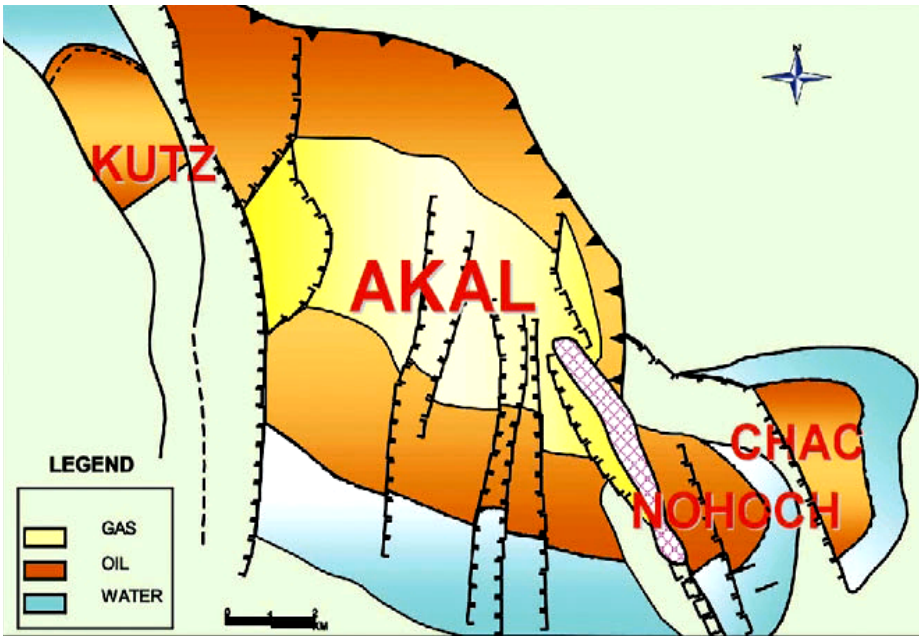


**Figure 2.16: The Cantarell complex consists of a broad NW-SE trending, faulted anticline. The structure has been divided into several blocks. Note the NS-trending normal faults, on the broad anticline.**

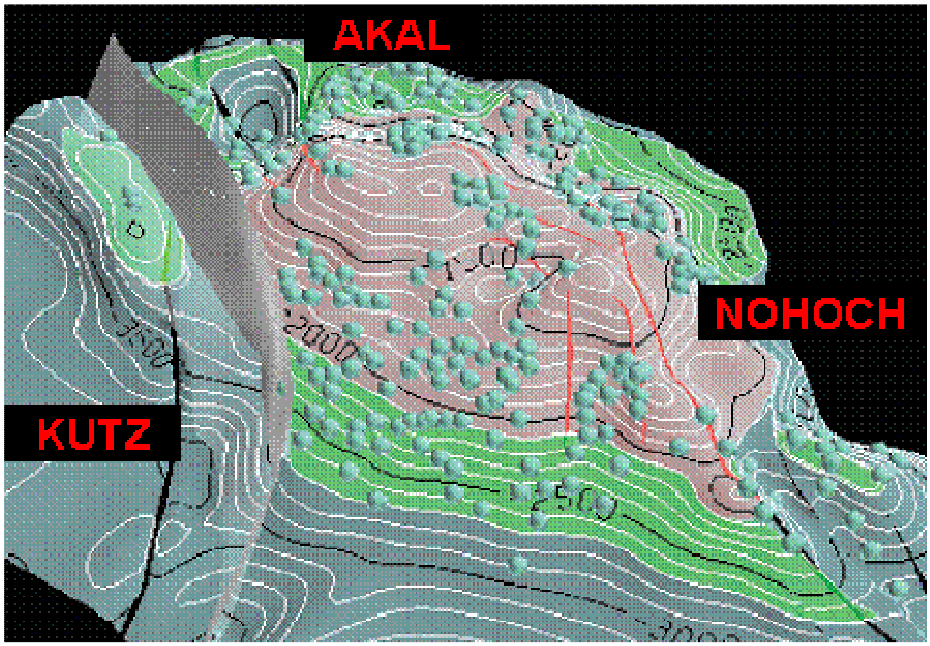


**Figure 2.17: Three-dimensional depth model for the top of the Cretaceous breccia showing the Akal, Kutz, and Nohoch fields (after Mitra et al., 2005).**

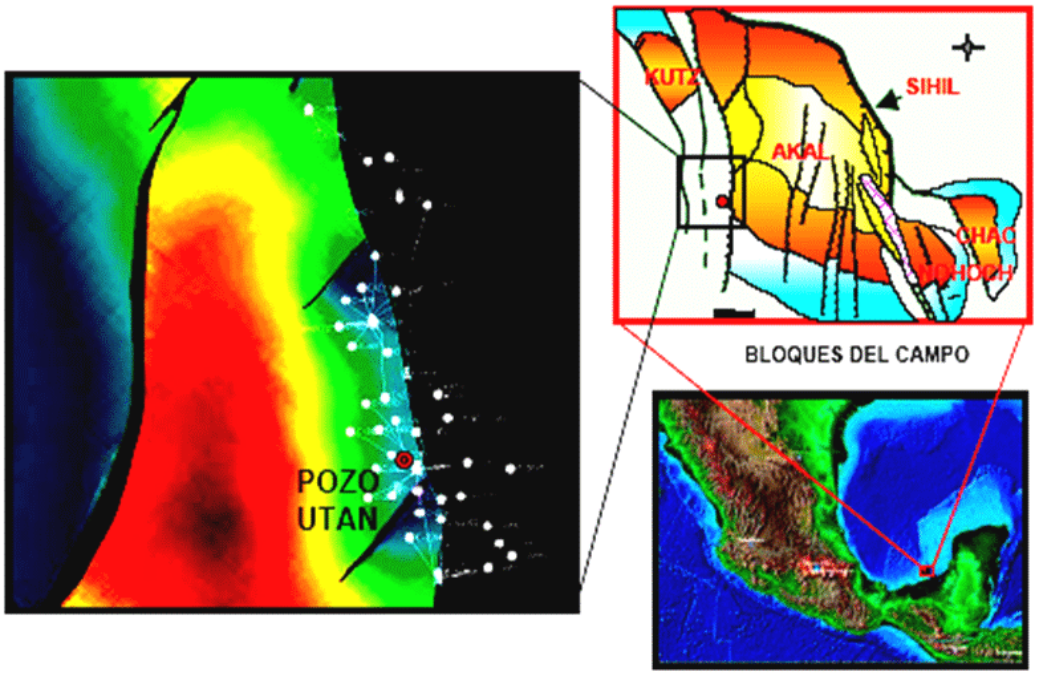


**Figure 2.18: Blocks of the Cantarell Complex and the Utan-1 well location (non-published Pemex internal reports).**

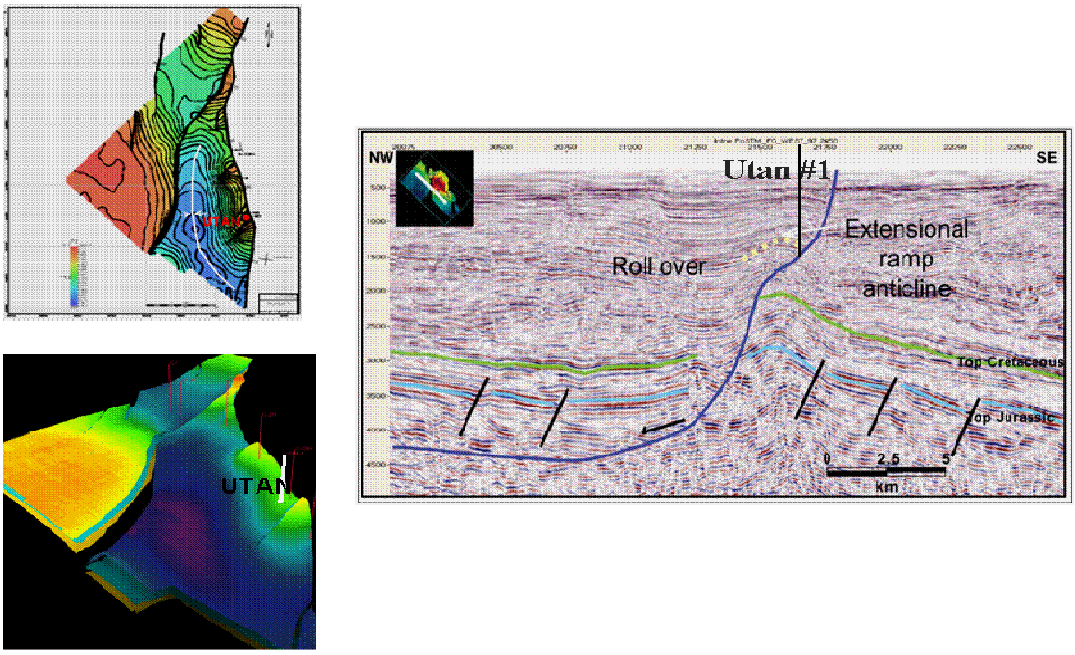


**Figure 2.19: Composite figure showing structural framework for Utan well locality (Garcia-Hernández et al., 2005 and non-published Pemex internal reports).**

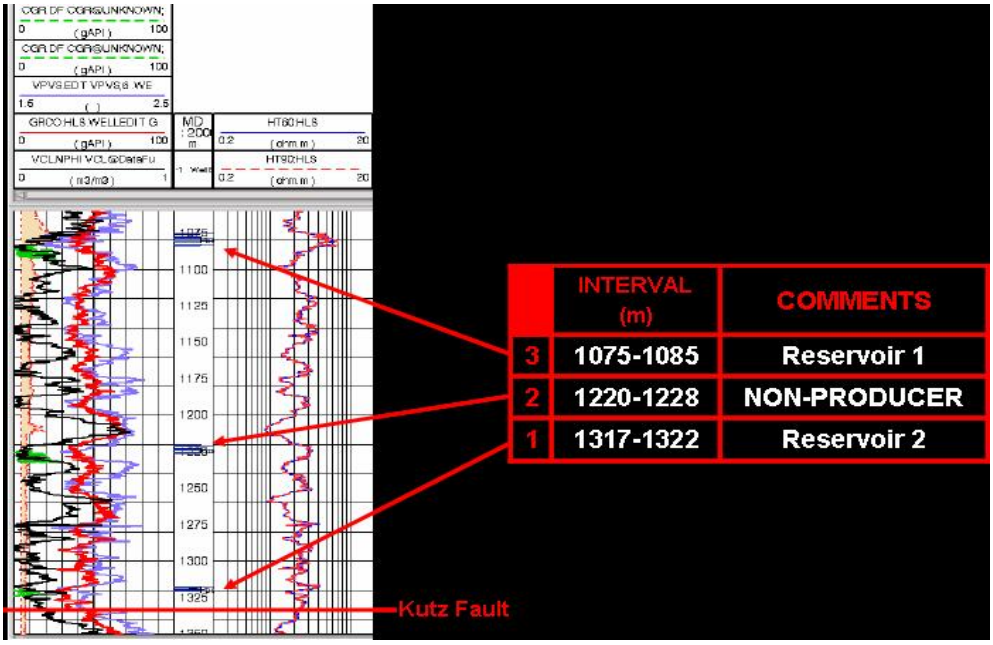


**Figure 2.20: Tested intervals in Utan well.**

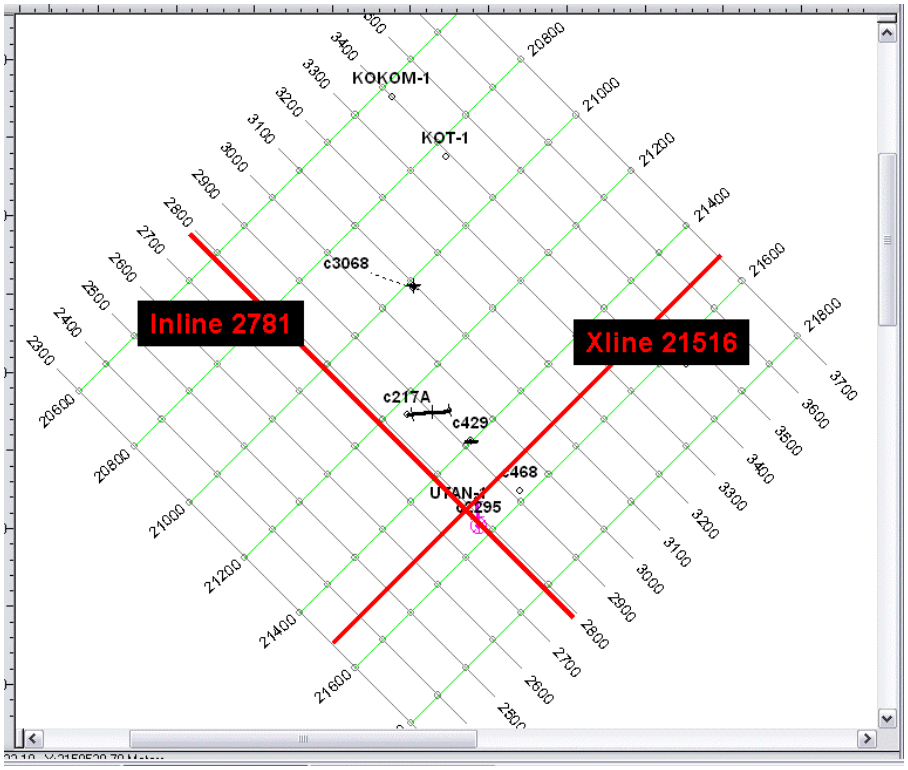


**Figure 2.21: Location of the Utan-1 well related to the seismic cube. Intersection seismic lines over this well (in-line 2781 and cross-line 21516) are also shown.**

# Chapter 3

# BASIC CONCEPTS IN SEQUENCE STRATIGRAPHY

## 2.2 Introduction

Little is known about the late Tertiary depositional systems, their time/spatial distributions and the proper location of gas producing facies in Utan field. This fact provides unique challenges that require new concepts and thinking and provides a favorable environment for systematic and multidisciplinary research in the study area.

This chapter includes basic definitions and concepts useful to understand the importance of a sequence stratigraphic framework in the development of this dissertation. Such concepts were applied to understand the high-frequency depositional setting, facies and rock quality distribution in a methodic and predictable manner.

## 3.2 Basic definitions and concepts in Sequence Stratigraphy

The growth of applied stratigraphy in the 20$^{th}$ Century has been unprecedented. Modern stratigraphy has evolved rapidly because of the growing need for more accurate chronostratigraphic techniques for subsurface correlation. This section contains basic definitions and concepts useful to understand the importance of a sequence stratigraphic framework in the development of this dissertation and how such concepts will be later applied to understand the facies and rock quality distribution in a

methodic and predictable manner. Sequence stratigraphy as a multidisciplinary tool for basin analysis is a very extensive topic and the following overview is far from an exhaustive treatment.

### 3.2.1 Early developments

Stratigraphy, from the Latin *stratum* and the Greek *graphia*, is the study of rock successions and the correlation of geological events and processes in time and space (Koutsoukos, 2005). It is a fundamental science of all geological studies, allowing reconstruction of the sequence of events of Earth history, the evolution of life on Earth and speculations on the nature of Earth´s structure and processes. As a natural science, stratigraphy is a science as old as philosophy itself, which was originated with the early observations of Earth´s natural phenomena allowing wise minds to establish the foundations of the scientific methods of investigation by careful observation of the physical world.

Stratigraphy as a science evolutes from the Ancient Greeks and Romans through the Middle Ages and Renaissance, the Eighteenth and Nineteenth Centuries until the Twentieth Century, the latter known as the Age of Applied Stratigraphy. Particularly, the history of stratigraphy during the Twentieth Century is referred to the history of the individual branches which contributed to the development of modern stratigraphy. Plate Tectonics, Geochronology (Radiometric Stratigraphy), Magnetostratigraphy, Stratigraphic Classifications, Facies Stratigraphy, and Seismic and Sequence Stratigraphy have together contributed to refine the stratigraphic

resolution and basin modeling studies for both scientific and commercial applications. The latest advance is the young field of Seismic Geomorphology developed by Posamentier about 2003 (Roger Slatt, personal communication).

Modern stratigraphy had its major advances by the mid-20$^{th}$ Century, with the increase of petroleum exploration activities and the development of seismic exploration techniques. In 1949, L.L. Sloss and coworkers established the term –sequence- as an unconformity-bounded stratal unit (Van Wagoner et al., 1990). The concept received further support with the works of H.E. Wheeler in the late 1950´s, who introduced the concept of the chrono-lithostratigraphic chart, and Sloss, who in 1963, consolidated the term –stratigraphic sequence- and its employ into regional chronostratigraphic correlations (Koutsoukos, 2005). A passage from Sloss, originally written in 1963, and cited by Van Wagoner (1990), points out "The sequence concept is not new and was already old when it was enunciated by the writer and his colleagues in 1948. The concept and practice is as old as organized stratigraphy". In spite of this fact, Sloss has received the credit for being the scientist who developed the unconformity-bounded sequence as a genetic stratigraphic tool.

On the other hand, the seismic reflection method has been an efficient way to sample the subsurface at the interwell scale through the last 70 years. Seismic applications have been extensively employed in the petroleum industry and successful in reservoir delineation, characterization and even fluid monitoring. It is precisely the improvements in seismic sampling and resolution which contributed to the development of seismic stratigraphy and then to sequence stratigraphy.

In a series of publications starting in the late 1970´s, Peter Vail and his Exxon colleagues presented a revolutionary stratigraphic method of basin analysis which became known as “Sequence Stratigraphy” (AAPG Memoir 26, edited by Payton, 1977), which focused on the analysis of geometric patterns of seismic reflections to infer depositional systems and sequences. As a result of Memoir 26 and new improvements in seismic reflection technology, the sequence as a practical, unconformity-bounded unit for stratigraphic analysis provided a quantum leap in basin analysis. In the beginning, seismic stratigraphy concepts were applied to basin analysis at the scale of seismic data with a lack of enough precision to analyze sedimentary strata at the reservoir scale. Thus, seismic stratigraphy preceded the discipline of sequence stratigraphy (Slatt, 2006).

Sediments can only accumulate where there is space for them to be deposited and preserved. This important concept commonly referred as “accommodation space” was first developed by Jervey (1988) in the volume published by The Society of Economic Paleontologists and Mineralogists (SEPM), titled “Sea-Level Changes: An integrated approach”. That volume introduced many of the modern concepts of sequence stratigraphy.

In 1989, Galloway proposed the term “genetic stratigraphic sequence” for a model of a genetic sequence or depositional episode bounded by maximum flooding surfaces. The concept implied a certain discrepancy with the Exxon approach of the unconformity bounded depositional sequence. The reason is simple, because Exxon uses seismic data, such an approach is a stratigraphy of (reflection) surfaces however,

Galloway´s approach rests more on sedimentological interpretation, facies relationships and geometries. The Exxon scheme however, is by far the most widely used because the widespread erosion surface at the sequence boundary is often more easily recognized than the maximum flooding surface. Galloway´s approach is particularly useful in those areas where there is little or no available seismic data to properly identify sequence boundaries and where flooding surfaces and maximum flooding surfaces are in these cases easier to identify (Koutsoukos, 2005).

Some other lines of research have been developed by several authors including the study of high-frequency sequences with details on how sequence stratigraphic concepts are applicable at the scale of wells, cores, and outcrops (Van Wagoner et al. (1990); Mitchum and Van Wagoner (1991)).

Further developments in cyclostratigraphy, chemostratigraphy and isotope stratigraphy have been also developed during the last decade. Modern stratigraphy is multidisciplinary in nature and future developments of this science will be expected in fields as fractal geometry, complexity theory and computer-aided sequence stratigraphic interpretation. New technology will be useful in modeling successively more complex depositional systems and improving our capabilities to face new scientific problems and understand how to explore and exploit natural resources in a sane and sustainable development of the human community while preserving Earth´s ecosystems diversity.

For those interested in knowing more about the development of the stratigraphy concepts and the corresponding schools of knowledge, an excellent source can be found in Koutsoukos (2005).

### 3.2.2 The basic depositional sequence

Sequence stratigraphy is the study of sedimentary rock relationships within a chronostratigraphic or geologic-time framework (Slatt, 2006). Sequence stratigraphy combines well logs with biostratigraphy and seismic patterns to understand the relationships among rock layers, their seismic expression and depositional environments for a more accurate prediction of reservoir settings, source rocks and seals.

Sequence stratigraphy establishes criteria to define a predictive model, in which a series of systems tracts within a depositional sequence is interpreted to be deposited in a cycle of fall and rise of sea level related to the concept of globally synchronous eustatic changes. Sedimentary patterns along continental margins are controlled by sediment supply, rate of subsidence and sea-level change. The combined effects of regional tectonics and eustasy determine the accommodation potential for the sediments and the distribution of facies within the genetically related packages (Haq et al, 1988).

A sequence is defined as a stratigraphic unit composed of a relatively conformable genetically-related succession of strata that are bounded (at their top and

base) by unconformities or their correlative conformities (Slatt, 2006). It represents a period of deposition between two episodes of significant sea level fall. Using the sequence stratigraphy approach, depositional sequences are the primary means of sub-dividing a basin fill succession. If the relative changes in sea level are basin-wide events, the sequence boundaries may be recognized in different vertical sections and used as a means of correlation provided that the same sequence boundary can be confidently recognized in different places.

The space-temporal distribution of sequences is defined by accommodation space, which is in turn dictated by eustasy and tectonism. The sediment supply will fill the space created. If the rate of sediment supply is greater than at which accommodation space is created at a given point, facies belts will migrate toward the basin centre and water depth will decrease. This process is named progradation. Conversely, if the rate of sediment supply is less than the accommodation space created at a given point, facies belts will migrate toward the basin margin and water depth will increase. This process is named retrogradation. On the other hand, if the rates of sediment supply and creation of accommodation space are in relative equilibrium, i.e. as the rate of sea level rise decreases the rate of creation of accommodation space becomes balanced by the sediment supply, facies belts will stack vertically in a process termed aggradation (figure 3.1).

In sequence stratigraphy, stratal surfaces and rock bodies between the surfaces are defined on the basis of stratigraphic intervals that are time-synchronous, laterally continuous and regionally correlative (e.g., bentonites or condensed sections), rather

than on the basis of the lithologic character of the rocks and their stratigraphic relations. Thus, sequence stratigraphy differs fundamentally from lithostratigraphy, and chronostratigraphic horizons that often crosscut lithostratigraphic horizons (Figure 3.2). Therefore, well-log correlations differ substantially between these disciplines (Slatt, 2006).

### 3.2.3 Systems tracts and key surfaces

A sequence can be internally subdivided into a succession of systems tracts interpreted to be deposited between eustatic-fall inflection points (Posamentier et al., 1988). A systems tract is defined as a linkage of contemporaneous depositional systems (e.g. alluvial-fluvial-deltaic-coastal-shelfal-bathyal). Each is defined objectively by stratal geometries at bounding surfaces, position within the sequence, internal parasequence patterns and interpreted to be associated with a specific segment of the eustatic curve. The chief types are the lowstand systems tract (LST), the transgressive systems tract (TST) and the highstand systems tract (HST).

Mitchum et al. (1993), point out that the general sequence-stratigraphic model consists of a depositional sequence with a lowstand systems tract consisting of basin floor fan, slope fan complex, and prograding complex; a transgressive systems tract; and a highstand systems tract. They emphasize that each systems tract is deposited at a predictable position in an interpreted base level cycle caused by eustasy, and has recognizable signatures in well logs and seismic data. As a consequence, reservoir sand distribution is characteristic for each systems tract.

In outcrop sections, well logs and seismic data the systems tracts can be identified and correlated between three prominent depositional surfaces:

1. The LST and the TST are separated by the transgressive surface (TS) which is defined as the first significant marine flooding surface within a sequence, marking the beginning of the more rapid sea-level advance over the shelf (Haq et al., 1988). This surface is usually marked by a contrast in lithology fining upward. The lowstand deposits below this surface belong to the most regressive phase of the sequence. However, when lowstand deposits are lacking, the transgressive surface may coincide with the underlying unconformable portion of the sequence boundary. The transgressive systems tracts, formed during the period of most rapid rise in sea level, will be characterized by a general landward shift in facies belts, that is, shallow water facies are overlain by deeper water deposits. The rate of creation of accommodation space will be greater than the supply of sediment and outer shelf deeper water mudstones will overlie inner shelf shallower marine sandstones, for instance.

2. The TST and the HST are separated by the maximum flooding surface (MFS), which is defined as the surface corresponding to the time of maximum flooding of the shelf. This surface is seismically interpreted as a “downlap surface”. A physically condensed section occurs at the MFS and forms partially within the transgressive- and partly within the highstand systems tracts of the sequence (Haq et al., 1988). “Condensed section” is defined as a thin marine stratigraphic unit consisting of pelagic to hemipelagic sediments characterized by very low

sedimentation rates. Because of the lack of terrigenous input, the condensed section may contain a high pelagic-fossil concentration, rich glauconitic or phosphatic layers, or a hardground caused by marine lithification. The condensed sections are most areally extensive at the time of maximum regional transgression and this extension increases basinward. The downlap surface separates the TST from the HST. Because of the abundant and diverse planktonic and benthonic microfossil assemblages that the condensed section contains, it is an excellent correlation surface with the open oceans and for calibration against the global standard biostratigraphic zonation schemes. As such, this surface provides the key chronostratigraphic and correlative framework for sequence analysis and in delineating systems tracts (Wynn, 1996).

3. The third surface is the sequence boundary. A relative sea level fall will have a dramatic effect on the shallow marine environment. Rivers may respond to the fall in base level by cutting down into their floodplain and also into the newly exposed shelf area in the process of adjusting to a new equilibrium profile. The exposed beach will be subject to erosion on the coastal plain. This erosion will be preserved as an unconformity surface in the stratigraphic record. Further basinwards, the relative sea level fall may not have exposed the outer parts of the shelf to create an erosion surface, but shallow water deposits of the beach and shoreface will overlie outer shelf deeper water facies. In this case, upward shallowing facies will be preserved in the stratigraphic record. If the sea level fall is as great as the depth of water at the shelf edge, an unconformity may develop over the whole shelf. In

sequence stratigraphic terminology this surface created by the sea level fall is called a -**sequence boundary**-. A sequence boundary normally consists of an unconformity and its -**correlative conformity**-, the equivalent surface in the outer shelf where there was no erosion (Nichols, 1999). As such, the sequence boundary is expressed as the downward (basinward) shift of the coastal-onlap pattern, or by truncation on seismic profiles depending on the position of the section along the shelf to basin profile and the rate of sea level fall. For instance, if the position of a section is proximal (landward) on the shelf, the probability of lowstand deposition in the area is reduced and restricted to transgressive and highstand deposition. In these cases, the sequence boundary may be an unconformity that coincides with the position of the transgressive surface.

### 3.2.4 Cyclicity in changes in sea level

Figure 3.3, shows a relative-sea-level curve, comprising one complete cycle from one highstand to the next highstand (Slatt, 2006). As a first step in an idealized model of sea level fluctuations, the cycle is assumed with a simple sinusoidal curve to describe the rise and fall, and constant sediment supply (Nichols, 1999). The falling limb of the curve reflects a falling stage of relative sea level, and the rising limb reflects a rising stage of relative sea level over an interval of time. In this sense, eustatic change is a curvilinear function punctuated by inflexion points. These are points on the curve where absolute slope or rate of change is greatest (Posamentier et

al., 1988). The different components of the lowstand, transgressive and highstand systems tracts deposited in relation to the position of relative sea level are also shown.

Patterns of changes in sea level through the Phanerozoic had been recognized for many years but the biggest impact on sedimentology and stratigraphy resulted from the publication of the AAPG Memoir 26 in 1977 by Vail and co-workers from Exxon oil company. In the 1977 work and a later paper in 1988 (Haq et.al. 1988), the Exxon group presented a global sea level curve for parts of the Phanerozoic which indicated several orders of cyclicity superimposed upon each other. In this way, the chronology of sea-level fluctuations in the Cenozoic, Cretaceous, Jurassic and Triassic were published in a composite fashion where the cycle charts combine the linear time scale (in My) with magneto-chronostratigraphy, standard-chronostratigraphy, bio-chronostratigraphy, and sequence-chronostratigraphy (Haq et.al. 1988). Particularly, on the Cenozoic-cycle chart the bio-chronostratigraphic data include planktonic foraminiferal zones, calcareous nannofossil zones, radiolarian zones, and diatom zones.

No general agreement exists on the tectono-eustatic mechanisms which may cause sea level fluctuations of either **first-order cycles**, which show a duration of hundreds of millions of years, or **second-order cycles** showing a pattern of rises and falls with duration of ten millions of years (Nichols, 1999).

Rises and falls of sea level with a magnitude of several tens of meters and a periodicity of 1-2 million years are recognized throughout the Phanerozoic stratigraphic record and identified as **third-order cycles**. The fundamental third-order

cycle has an average frequency of 1-2 m.y. duration, with a range of 0.5-5 m.y. (Mitchum and Van Wagoner, 1991). Shallow marine sediments are very sensitive to changes in sea level of this magnitude and display shifts in facies which reflect changing water depth. Close inspection of strata deposited in these environments from many parts of the world and different ages reveal that such sea level changes are common features (Nichols, 1999). Based on these assumptions and using a combination of subsurface and outcrop data the Exxon group constructed the curve which documents fluctuations every few million years which they considered to be synchronous global sea level changes.

Once again, there is no general agreement on the mechanisms which may cause sea level fluctuations at this third order of cyclicity. However, the Haq (Exxon) model assumes that third-order cyclicity is essentially glacio-eustatically controlled and that the tectonism does not override the eustatic signal. Even though it has been questioned by a number of authors (Weimer and Posamentier, 1993; Wynn, 1996), the generated curves showing variations of sea level through time, enhance the predictive utility of the sequence stratigraphic model.

Haq et al. (1988) also produced a conceptual two-dimensional model of the development of second and third order Vailian sequences in relation to essentially glacio-eustatic changes in sea-level. The figures 3.4 and 3.5 present more descriptive diagrams showing the so-called “sea-slug” model and its corresponding systems tracts, first presented by Vail (1987).

### 3.2.5 High-frequency sequences. The parasequence model

In addition to the previously referred orders of cyclicity, shorter-term changes in sea level have also been recognized as being superimposed upon longer-term cycles. These are **fourth-order cycles** which show a duration of 100,000-200,000 years, and **fifth-order cycles** lasting 10,000- 20,000 years (figures 3.6 and 3.7). According to the Exxon models, the magnitude of sea level change in these cycles ranges from a few meters to 10-20m, although short-term sea level changes and high depositional rates in the Quaternary have much higher magnitudes (Nichols, 1999). This cyclicity has been related to climatic changes caused by Milankovitch effects, which are cycles of planetary orbital irregularities, such as eccentricity, obliquity and precession (Mitchum and Van Wagoner, 1991). Evidence for frequent relative changes in sea level of about 10m has been found in successions throughout the stratigraphic record. In sequence stratigraphy terminology these are referred to as **parasequences**.

The parasequence is one of the fundamental stratal units in sequence stratigraphy. A parasequence is defined as a relatively conformable, genetically related succession of beds or bedsets bounded by marine-flooding surfaces or their correlative surfaces (Slatt, 2006). The parasequence boundary is a marine-flooding surface, which represents a relative rise in sea level (unlike the sequence boundary, which represents a relative fall in sea level) (Mulholland J.M., 1998). In special positions within the sequence, parasequences may be bounded either above or below by sequence boundaries (Mitchum and Van Wagoner, 1991).

Most siliciclastic parasequences are progradational in nature, resulting in an upward-shoaling (upward-coarsening and -cleaning) association of shallow marine lithofacies. If the rate of sediment supply to a shoreline area exceeds the rate of water deepening as a result of subsidence and/or sea level rise, then sediments will prograde in the basinward direction (figure 3.8, Stage 1). If water depth increases more rapidly than sediment can be supplied, then marine waters will flood landward over the preceding parasequence, forming a condensed section/marine flooding surface that marks the base of a new parasequence (figure 3.8, Stage 2). If the rate of sedimentation then exceeds that of relative sea level rise, another progradational parasequence will form, giving rise to two progradational parasequences bounded by a shaly condensed section (which can vertically isolate the two sandstone intervals (figure 3.8, Stage 3) (Slatt, 2006).

In the scope of observations regarding the parasequence concept, Mitchum and Van Wagoner (1991) indicate that parasequences have been identified in coastal plain, deltaic, beach, tidal, estuarine, and shelf environments where the shallow marine sediments are very sensitive to changes in sea level, and corresponding shifts in facies (figure 3.9). They point out that it is difficult to identify parasequences in fluvial sections where marine or marginal-marine rocks are absent, and in slope or basinal sections, which are deposited too far below sea level to be influenced by an increase in water depth.

Sequences and their boundaries are interpreted to form as a response of relative fall and rise of sea level. Jervey (1988) and Posamentier et al. (1988) presented an

analysis of the interaction between eustasy and basin subsidence that is interpreted to form sequence boundaries (see figure 7, Posamentier and Vail, 1988). Parasequences and their boundaries also can be interpreted as responses to hierarchies of cycles of relative fall and rise of sea level. The relationship among this hierarchy of eustatic cycles, subsidence, and the deposition of sequences and parasequences is illustrated in Figure 3.10. The curve of sea level fluctuation during the deposition of a sequence therefore consists of a high-frequency oscillation superimposed on the longer-period sinusoidal wave (figures 3.6, 3.7 and 3.10). These curves may be generated by the combination of different orders of sea level fluctuation (third- and fourth- order sea level variations, for instance).

A parasequence set is defined as a sucession of genetically related parasequences that form a distinctive stacking pattern, bounded in many cases by major marine-flooding surfaces (Mitchum and Van Wagoner, 1991). Each systems tract is therefore likely to be composed of a set of parasequences. In most cases each parasequence represents an upward shallowing of the depositional environment. The trends through a set of parasequences are recognized by considering the relative shift in the position of the shoreline when going stratigraphically from one parasequence to another. Figure 3.11 illustrates the variation in stratigraphy that can result by the variation of rate of deposition versus rate of accommodation to produce different parasequence sets. These are the same trends of progradation, retrogradation and aggradation described above for the systems tracts of depositional sequences.

High-order cyclicity depends on seismic resolution to extend the well log interpretation at the interwell space through basic seismic interpretation..

### 3.2.6 Practical sequence stratigraphy

Several considerations have to be taken in order to develop a sequence stratigraphic framework (Vail, 1987; Homewood, 2001; Koutsoukos, 2005; Slatt, 2006). Firstly, it has to be reminded that sequence stratigraphy is multidisciplinary in nature (Slatt, 2006). Therefore, a comprehensive dataset of seismic, well logs, cores, biostratigraphic and geochemical data has to be joined and considered for the interpretation. A reasonable dataset should include:

- A grid of good-quality 2D/3D seismic reflection data
- A reasonable number of wells on or near the seismic sections with a comprehensive dataset of cores, detailed core analyses, high-resolution biostratigraphy, paleobathymetric information, and well log data
- Velocity data in the form of VSP, checkshots and/or sonic logs to make synthetic seismograms, time to depth conversion, and tie wells to seismic data
- Engineering data

Once the dataset has been screened for quality control, several rules and considerations have to be taken into account for the interpretation:

- Review of previous related works in the study area

- Preliminary analysis of well and seismic data: Seismic quality and resolution analysis. Well log edition, corrections and compensation if they are needed.
- Preliminary basin, structural and stratigraphic setting from seismic and well data. Screen the data for seismic terminations and structural interpretation.
- Petrophysical work on key wells
- Annotate biostratigraphic and paleobathymetric information in well logs showing faunal distribution. Identification of paleoenvironments.
- Interpret log patterns and selection of first candidates for regional markers, sequence boundaries, and maximum flooding surfaces. Assign of ages to key surfaces for a preliminary sequence stratigraphic framework
- Regional third-order sequence stratigraphic analysis on key wells: Biostratigraphy and paleobathymetric analysis, confirmation of key surfaces and system tracts definition, correlation with sea level charts. Higher-order sequence identification might be feasible on key wells, however their identification on seismic data will depend on the seismic resolution of the dataset
- Extrapolation of well log signatures of key surfaces to the nearby wells through well log cross section correlations.
- Selection of key seismic sections and construction of synthetic seismograms for well to seismic tie. Once the key surfaces for stratigraphic correlation are identified, they have to be transferred to seismic data for seismic stratigraphic interpretation and correlation. Sequence boundaries are defined from the

geometric relationship of the reflections. Several loops between seismic and well log data have to be performed to assure agreement of interpretations.

- Construction of contour time and depth maps of key surfaces

Once the sequence stratigraphic framework has been defined, it will be able to be applied to the purpose for which the study is being made. Applications of sequence stratigraphy for petroleum exploration include regional correlations of stratal units and prediction of seal, source, trap, and reservoir rocks and their location in both time (geologic and seismic) and space (within a basin) (Slatt, 2006), for a proper basin analysis, petroleum systems and reserve evaluations, prospect predictions and recommendations for future G&G prospectivity work in the study area. For reservoir analysis, the applications vary from analysis of reservoir quality and extrapolation of reservoir properties as well as more detailed reservoir configuration, compartmentalization analysis and prediction of new sites for delimitation, infill and to delineate improved enhanced oil and gas recovery strategies.

### 3.2.7 Misunderstandings in sequence stratigraphy

From the development of early works on sequence stratigraphy there have been several controversies to the acceptance of this tool by the geological community. Some of them are described by Weimer and Posamentier (1993), Weimer (1999), and Mendez and Acuña (1999), and are cited below:

- The “sea-slug” model (Vail, 1987) is a generalized diagram which has been drawn to integrate the common characteristics of many different sedimentary basins in the world under the sequence stratigraphic concepts. However, stratal patterns that look entirely like the “sea-slug” model have never been observed in a sedimentary basin in the world. Even though, certain portions of many basins have similarities with this model this is not a rigid template to apply to all sedimentary basins. For instance, the thick TST seen in the model is fairly rare in siliciclastic settings, although they are more common in carbonate settings.

- The eustatic curves currently published are not really “global charts”. They have been developed from observations from a number of sedimentary basins around the world. Some critics maintain, for instance, that there is not conclusive evidence about the cause of third order sea level cycles. Regardless of the validity of the sea-level curves, the sequence stratigraphic concepts can be applied to any sedimentary basin to enhance understanding of basin fill evolution. Also, this debate does not affect a major aspect of sequence stratigraphy: lithology prediction for reservoir rocks, source and seals. Clearly due to the relative imprecision of most geochronologic tools, one must be careful with the correlation of stratigraphic packages from different basins, the way that sequences should be defined in a aparticular setting, the scales at which the sequence concepts are applicable and the importance of local tectonism in the eustatic curves to be employed.

- The models presented by Jervey (1988) are conceptual and use a set of simplifying assumptions for a specific kind of Atlantic basin. However, these models have been used in the evolution of newer concepts. The treatment of eustacy, subsidence and sediment influx, as independent variables, can be totally unrealistic. Therefore, the effects of local factors such as slope changes, sediment supply and tectonics must be incorporated together into the modeling for a particular basin

- Seismic expression was only represented qualitatively in Jervey´s models. In fact, there has been little incorporation of seismic synthetic models into sequence stratigraphic analysis. Geological modeling should be combined with forward seismic modeling (ray tracing) to obtain a real "seismic expression", showing the effects of frequency bandwidth on them. For instance, Anselmetti et al. (1997) show how 60 Hz onlaps in a seismic section can be converted to 20 Hz toplaps, making it relatively difficult to recognize a third order sequence boundary (figure 3.12).

- It is believed that sequence stratigraphy concepts can be applied only to passive margins. That controversy is false and once the general model is modified to different physiography and tectonic regimes, the sequence concepts can be applied successfully.

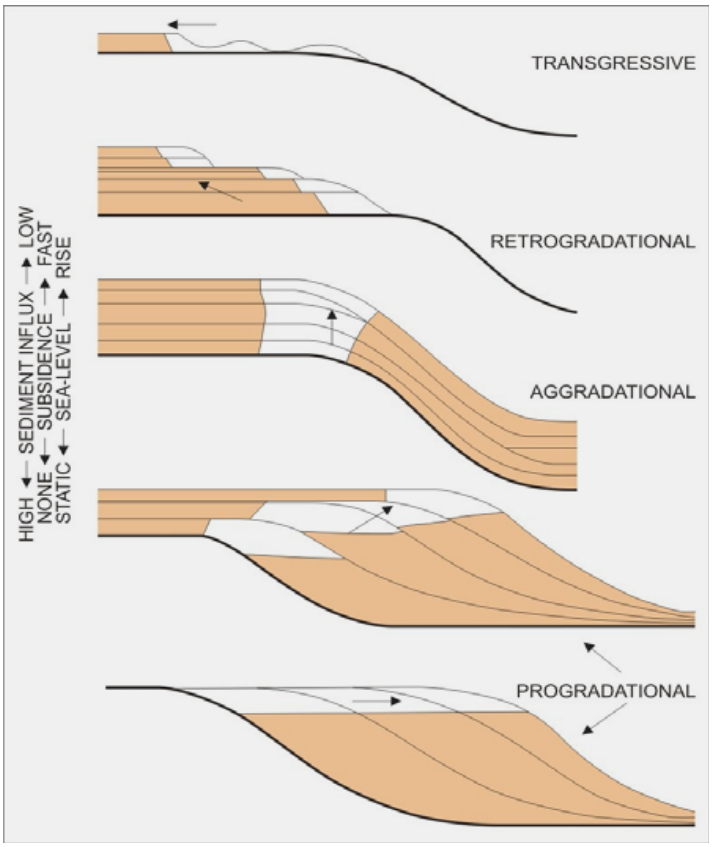


**Figure 3.1: Depositional architecture as defined by sediment influx, subsidence, and sea level (i.e., accommodation). Progradational patterns form when the rate of deposition exceeds the rate at which accommodation increases. Aggradational patterns form when the rate of deposition is approximately equivalent to the rate of increase in accommodation. Retrogradational patterns form when the rate of deposition is less than the rate at which accommodation increases (Slatt, 2006).**

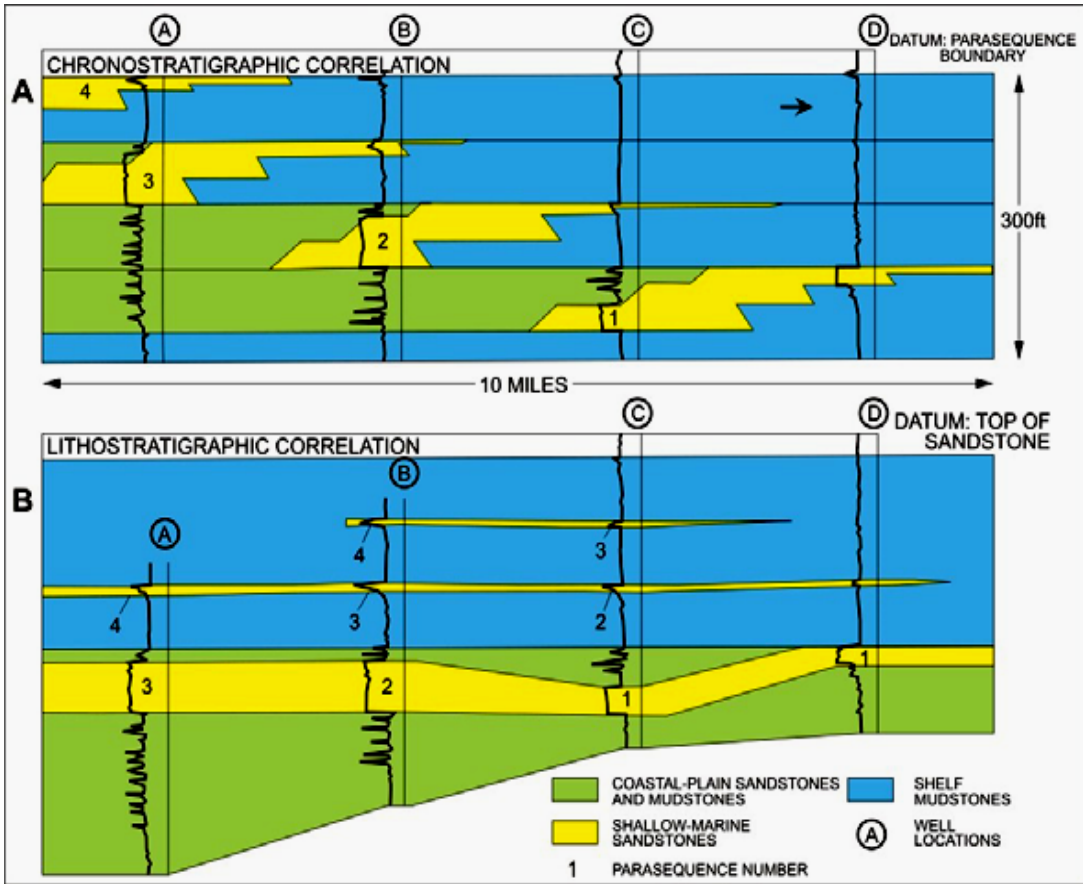


**Figure 3.2: Comparison of well log cross sections correlated on the basis of (A) chronostratigraphy and (B) lithostratigraphy. The datum for the chronostratigraphic correlation is a parasequence boundary. The datum for the lithostratigraphic correlation is a formation top. The chronostratigraphic correlation indicates deposition of four parasequences, with each subsequently younger parasequence stepping progressively toward the left (landward) and the total defining a retrogradational parasequence set. Based on the chronostratigraphic correlation, sands 1–4 are not connected, which they are according to the lithostratigraphic correlation in (B) (Slatt, 2006).**

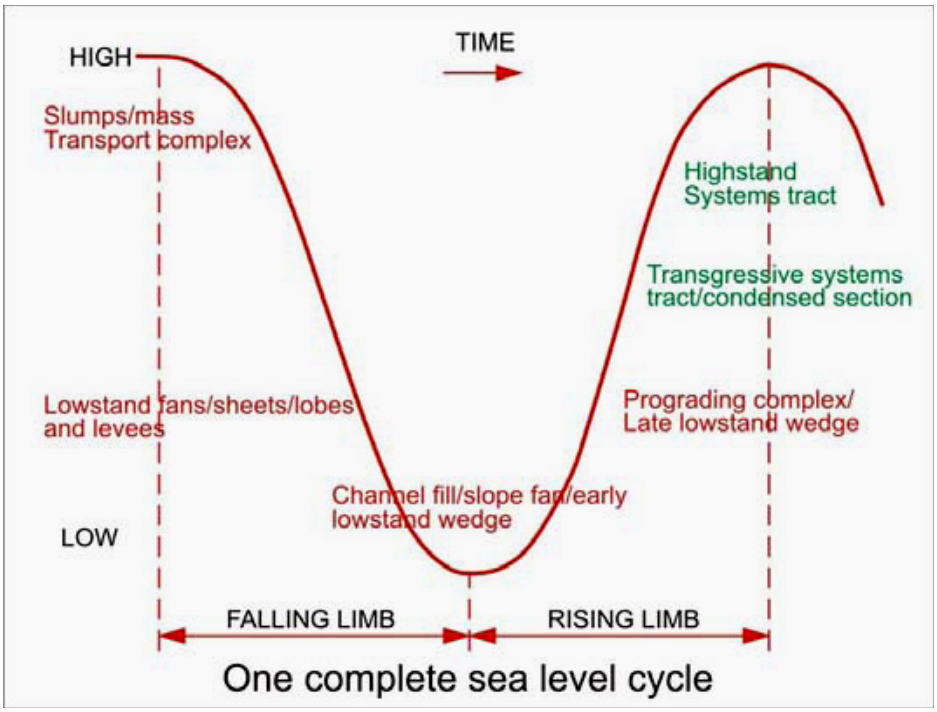


**Figure 3.3: Relative-sea-level curve, comprising one complete cycle from one highstand to the next highstand. The falling limb of the curve reflects a falling stage of relative sea level, and the rising limb reflects a rising stage of relative sea level over an interval of time. Red indicates times during which components of the lowstand systems tract were deposited, in relation to the position of relative sea level. Transgressive and highstand systems tracts are shown in green (Slatt, 2006).**

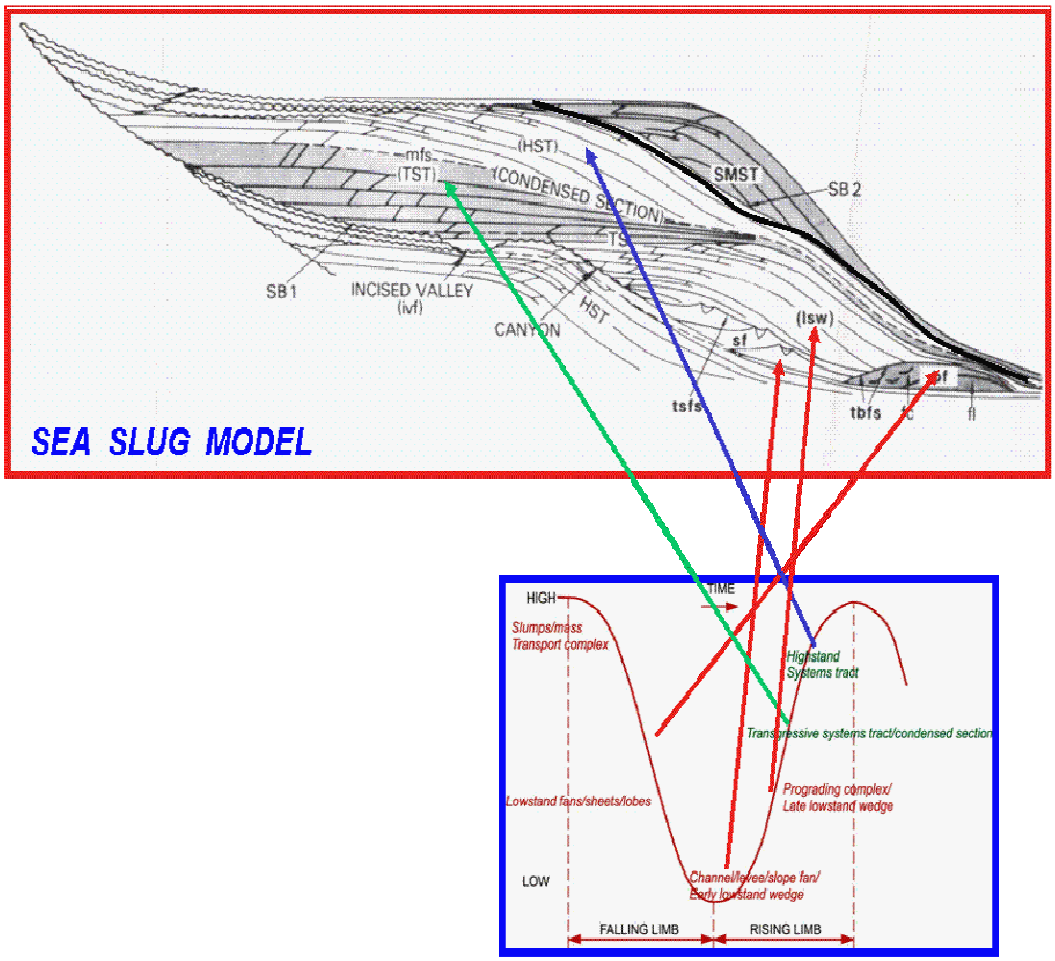


**Figure 3.4: Sea-slug model and corresponding systems tracts for one complete sea-level cycle (Slatt, 2005).**

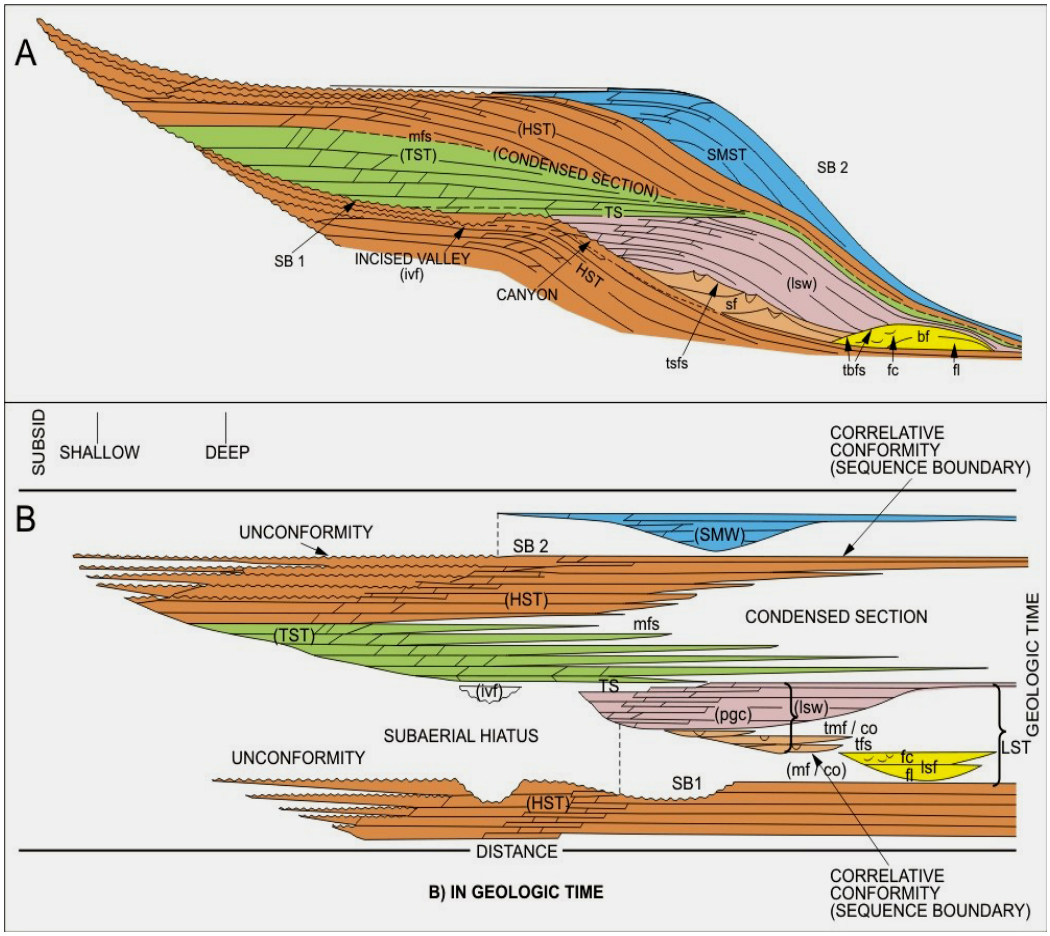


**Figure 3.5: Schematic cross section across one idealized third-order depositional sequence for siliciclastic strata ("sea slug diagram"). (A) illustrates the distribution of sediment and systems tracts in depth and space; (B) shows the distribution in time (vertical axis) and space. Blank areas on diagram (B) record the lack of deposition and/or the erosion that would occur in different areas at a specific time interval. Colored areas record deposition of strata in different areas at a specific time interval. Pgc = prograding complex; Bf = basin floor fan; fl = fan lobe; fc = fan channel, sf = slope fan, tbsf = top basin floor fan surface; tsfs = top slope fan surface; lsw = lowstand wedge; TS = transgressive surface; ivf = incised valley; SB1 = Type 1 sequence boundary; SB2 = Type 2 sequence boundary; TST = transgressive systems tract; mfs = maximum flooding surface; HST = highstand systems tract; smst = shelf margin systems tract; pgc = prograding complex (Slatt, 2006).**

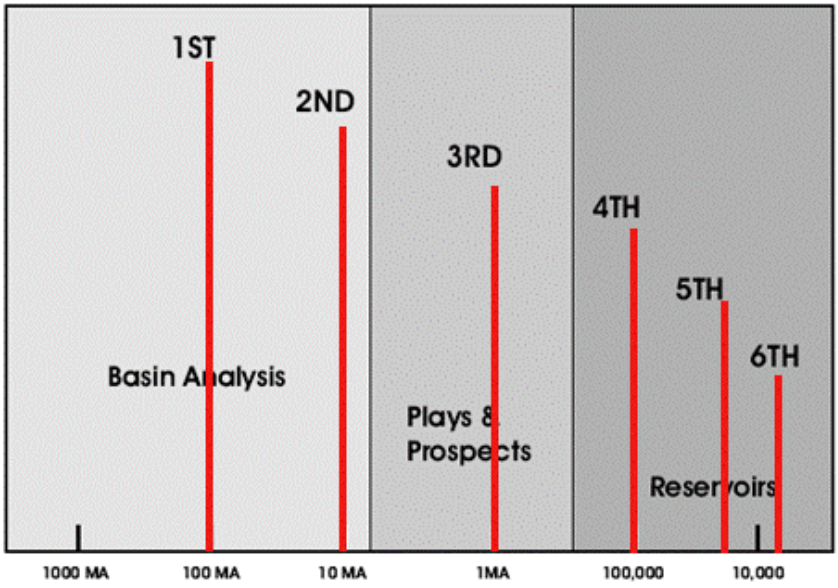


**Figure 3.6: Diagram showing the different frequencies (first through sixth order), and the typical scales for exploration and development (after Slatt, 2005).**

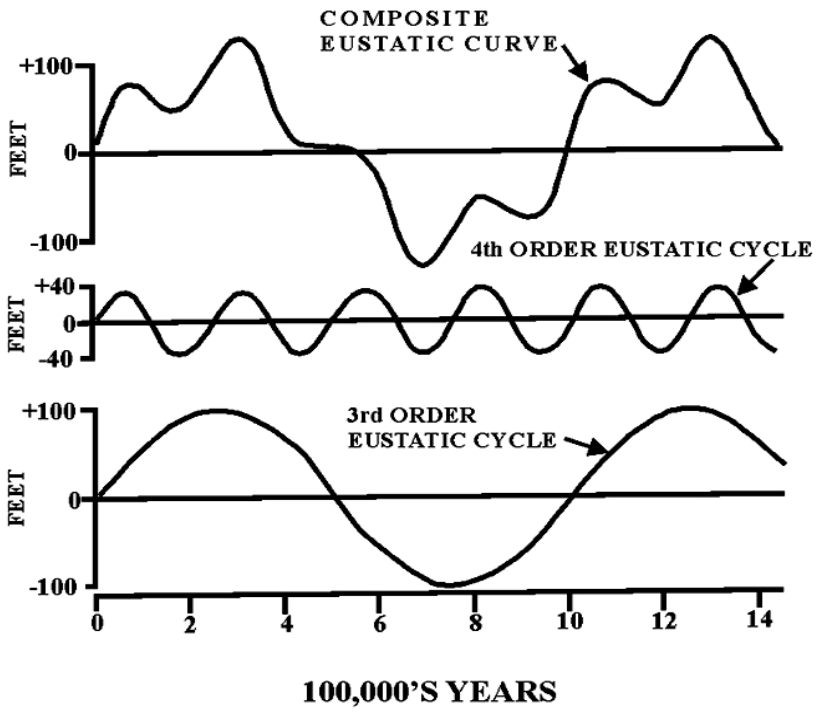


**Figure 3.7: Interaction of 3rd. and 4th. Order eustatic cycles (Slatt, 2005).**

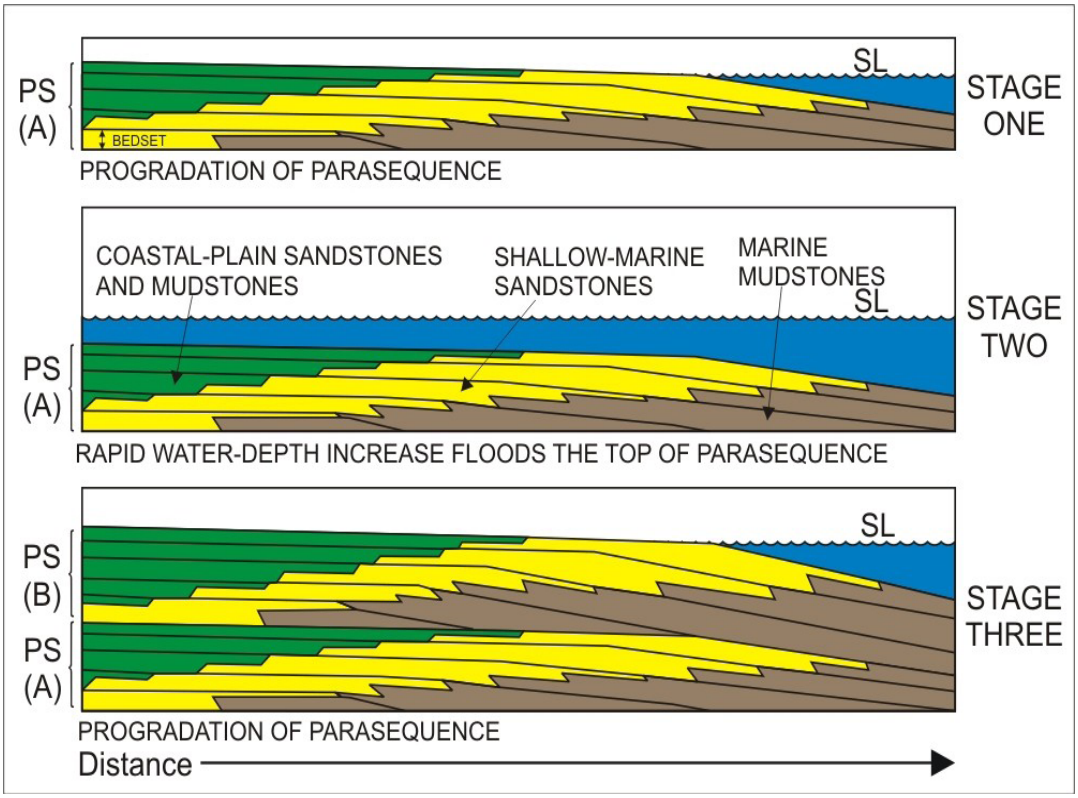


**Figure 3.8: Schematic illustration of the formation of two parasequences. Stage one shows the progradation of Parasequence A at a time when the rate of deposition exceeds the rate of increase in water depth. Stage two shows a rapid water-depth increase, which floods the top of parasequence A, creating a transgressive surface of erosion or non-deposition with respect to siliciclastic sediment with chemically precipitated minerals, volcanic ash beds (glauconite), and/or relatively coarse inorganic or organic grains concentrated on the surface. Stage three shows deposition of marine shale upon the transgressive surface of erosion, followed by progradation of a second parasequence when the rate of deposition again exceeds the rate of water-depth increase. Bedsets in parasequence B downlap onto the transgressive surface of erosion. After Slatt (2006).**

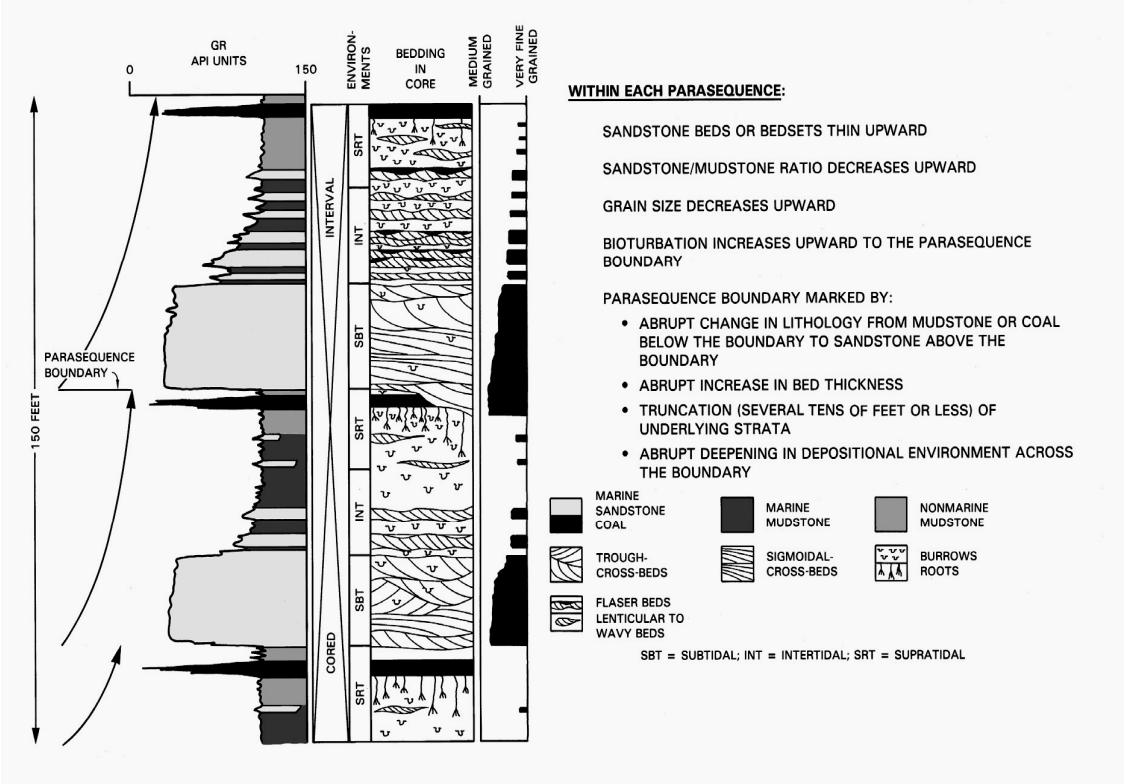


**Figure 3.9: Example of stratal characteristics of two upward-fining parasequences. These types of parasequences are interpreted to form in a tidal flat to subtidal environment on a muddy, tide-dominated shoreline (Van Wagoner et al., 1990).**

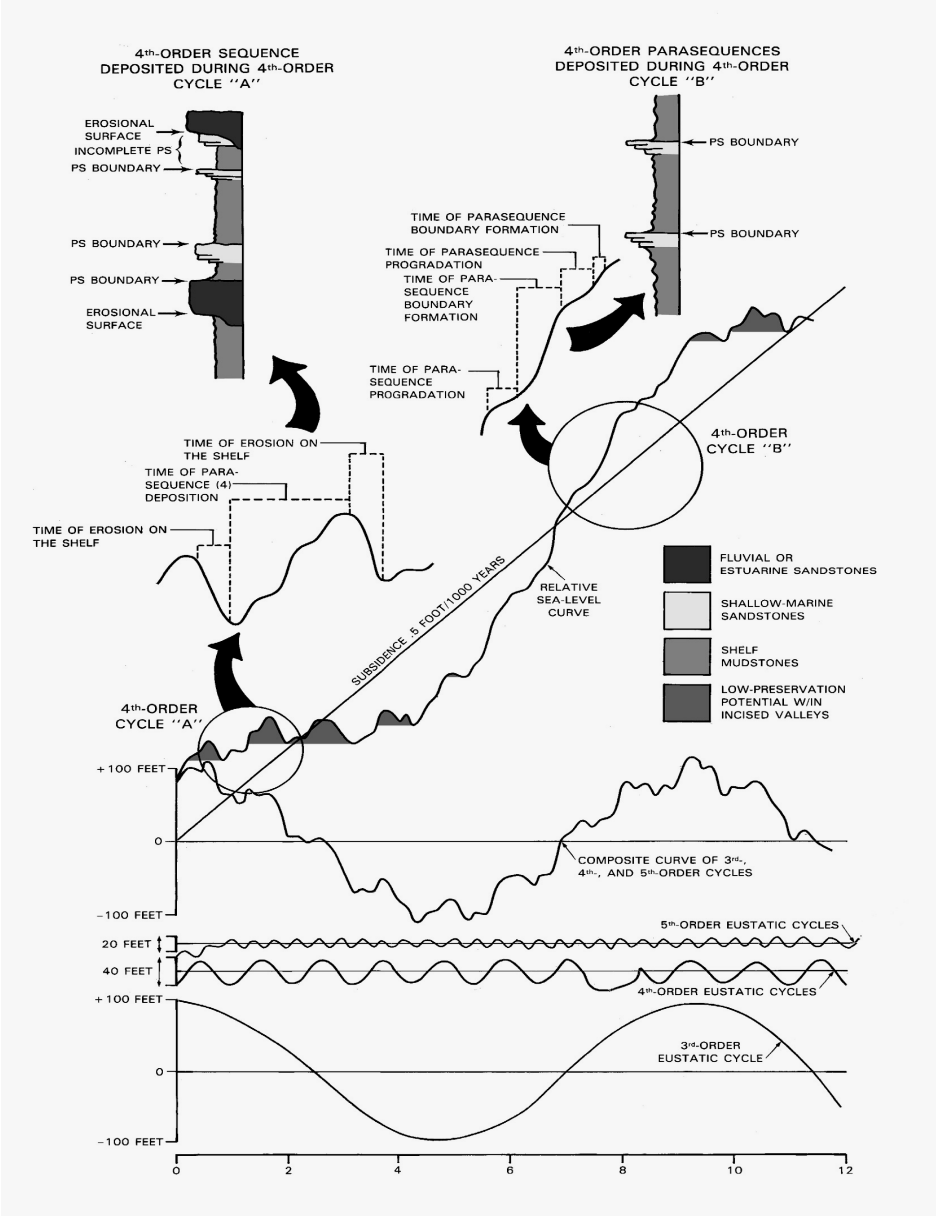


**Figure 3.10: Interaction of eustacy and subsidence to produce parasequences and high-frequency sequences. Lower diagram shows superposition of three eustatic curves with different frequencies into a composite eustatic curve. Addition of a constant basinal subsidence (middle diagram) produces a relative curve of sea-level change. During periods of overall eustatic third-order fall, high frequency falls are exaggerated to produce erosion and fourth-order Type I sequence boundaries (upper diagram). During periods of third-order rise, high-frequency rises are exaggerated to produce high-frequency parasequences or Type II sequences (VanWagoneer et al., 1990).**

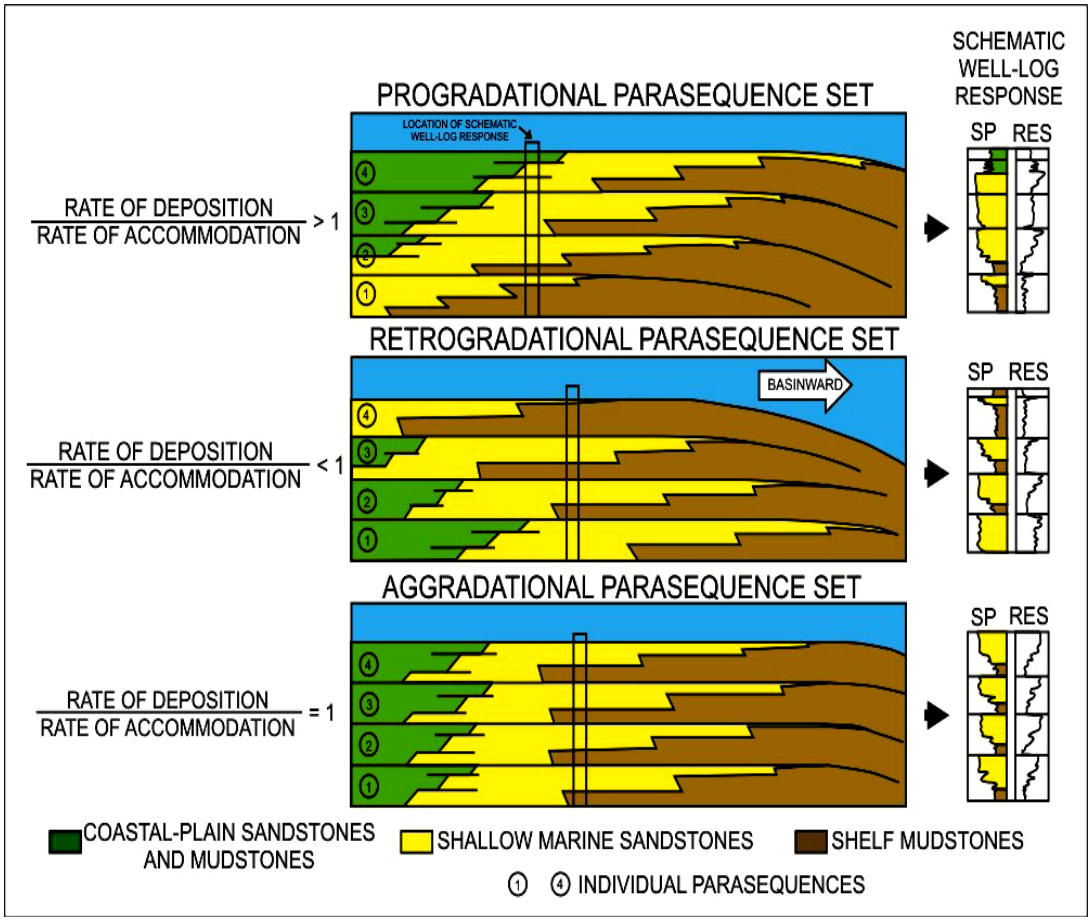


**Figure 3.11: Schematic figure showing four parasequences (prsq´s) stacked to form prsq sets, and their well log patterns. For the progradational case, each prsq progrades seaward to a greater extent than did the preceding, giving rise to a coarsening- and thickening-upward well log pattern. Such a prsq set forms when the rate of deposition exceeds the rate of accommodation. The overall progradation is punctuated periodically by a rise in relative sea level, which results in a flooding surface upon which the next younger prsq is deposited. For the retrogradational case, each prsq progrades seaward to a lesser extent than did the preceding prsq, giving rise to a fining- and thinning-upward well log pattern. For the aggradational case, each prsq progrades seaward the same distance as did the preceding prsq, giving rise to a uniform well log pattern for the four prsqs. (Slatt, 2006).**

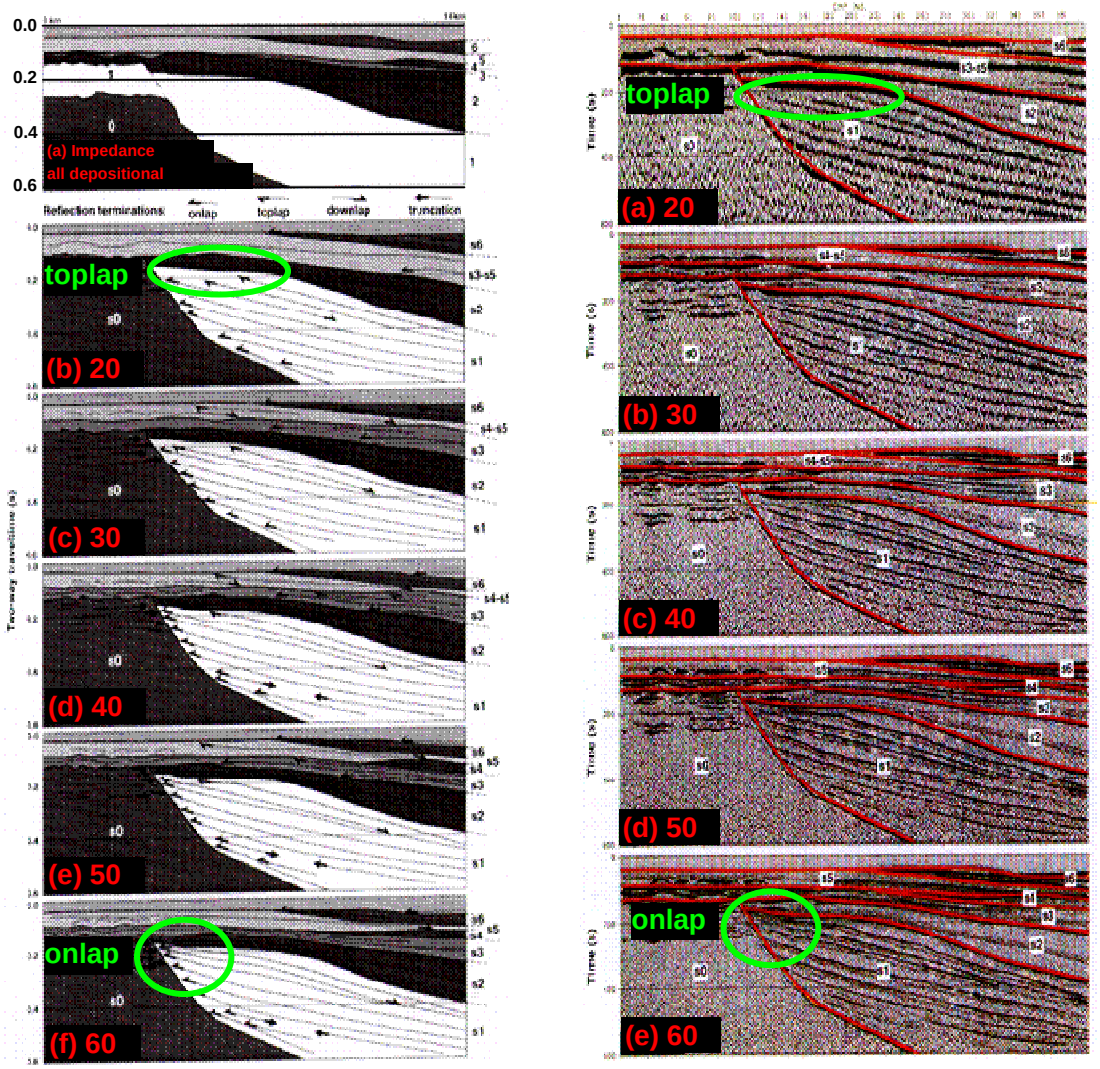


**Figure 3.12:** **Seismic forward modeling of a carbonate platform margin showing the effect of reducing the frequency content on a stratigraphic interpretation of seismic terminations. Left side: impedance model with six depositional sequences and their corresponding seismic terminations; Right side: seismic synthetic traces. Particularly, note how properly modeled 60 Hz onlaps (bottom sections) become toplaps when the medium frequency is reduced to 20 Hz (top sections), which could cause misconception of a sequence boundary (after Anselmetti et al., 1997).**

# Chapter 4

# FORMATION EVALUATION AND PETROPHYSICS

## 4.1 Introduction

Most of the wells available in the study area were drilled for Paleocene-Upper Cretaceous targets. In consequence, many wells had logging tools run just for stratigraphic sections deeper than the Neogene reservoirs. This required detailed inventory of all log runs to identify not just the availability of logs for the shallow section, but also to evaluate log quality.

After screening, a formation evaluation and petrophysical workflow was developed for the Miocene-Pliocene section which consisted of initial quality control, well log editing, petrophysical analysis, pseudo shear velocity prediction, invasion/dispersion corrections and fluid substitution analysis. The workflow is described in detailed below.

This workflow resulted in reliable well logs for well correlation, depositional system and sequence stratigraphic analysis, as well as for time to depth conversion, synthetic seismograms, fluid substitution, well-tie to stacked data, seismic attribute analysis and well-seismic integrated interpretation.

## 4.2 Well data inventory and initial QC

The first step in the well log analysis was to identify the other wells that had the best logs suitable for comprehensive petrophysical analysis. Two immediate disadvantages emerged from most of the wells available for this research:

1- Many wells have some logging tools run only for the deeper stratigraphic section. On the other hand, some runs for the shallow section were not merged. This required detailed inventory of all log runs to identify not just the availability of logs for the shallow Neogene section, but also the log quality.

2- The hole condition, and consequently log quality, is bad for the shallow section due to drilling practices. In particular, interpreting thin beds in siliciclastic sequences requires a good borehole where shales do not wash out and acquisition of high-quality data is likely. Drilling mud, logging speed and borehole size can make a difference in log quality. For instance, typically, logging tools that make direct contact with the borehole wall are designed for optimal contact in 21.6 cm (8.5 in) diameter wellbores. The fixed curvatures of the contact pads may cause some loss of contact in larger or smaller boreholes. Nowadays, most high-resolution log measurements are made with these contact-type tools (Passey et al., 2006).

Out of the dozens of available wells in Cantarell field, over 45 wells were checked for well logs availability and screened under the criteria of having a suitable suite of well logs for correlation and application of sequence stratigraphic concepts as well as for petrophysical work. As a part of the process, LAS files were available for

11 of these wells. These LAS files were loaded and plotted for visual quality control. Some wells had many files for different log runs, which had to be sorted out. Some runs had different sampling rates, and had to be re-sampled for consistency.

Because Pliocene facies in the study area were developed in a mixed platform environment, a multi-mineral analysis was required as an integral part of the petrophysical analysis. The data needed for reliable multi-mineral analysis includes: gamma ray, density, neutron, sonic, and Pe logs. After detailed inventory, it was found that these logs were available, although incomplete in some cases, for the Miocene/Pliocene section in only four wells, which were identified as the key wells for this process: **Utan-1, C-429, C-3068, and C-468**. A complete multi-mineral petrophysical analysis and modeling study was performed for these 4 wells. It was not feasible to include additional wells in this process because they lack several or all of the required logs for the analysis. Figures 4.1 to 4.4 show examples of the plotted logs including wells where there is a suitable suite of well logs for petrophysical work and where data needed for multi-mineral analysis are not complete for the Miocene/Pliocene section.

The following are key conclusions from the data screening and inventory:

- In the study area, only the Utan-1 well was drilled for Pliocene objectives, maintaining an average 8.5 in. diameter hole at target levels. However, environmental problems remained. Majority of the remaining wells, drilled for deeper parts of the stratigraphic section, had bad borehole conditions in the shallow section as indicated by both caliper and deltha-rho (drho) logs.

- The data needed for reliable multi-mineral analysis includes gamma ray, density, neutron, sonic, and Pe logs. These logs were available for only four wells in the Miocene/Pliocene section: **C-429**, **Utan-1**, **C-3068, and C-468**. Yet some logs in some parts of these four wells were either absent or not reliable due to bad hole conditions.

### 4.3 Well log editing

Considering the limited logging suites at shallow levels and the presence of older well data, editing of well logs was a critical step in the petrophysical analysis. This process was especially important because the producing intervals are very thin, and clear resolution of these intervals on well logs is critical. Additionally, continous and consistent well log curves are always needed to make good synthetic seismograms and for multi-mineral analysis.

All logs used in the analysis were edited to correct for spikes, cycle skipping, bad data due to environmental effects as well as by merging different runs, and filling small data gaps or null values.

A set of criteria by which to define a “bad hole flag”, was needed. For instance, the depth of investigation of the neutron and density tools is different. The density log “sees” only about five to ten centimeters (two to four inches) into the formation, within the so-called “flushed zone”, whereas the neutron tool “sees” about thirty centimeters (a foot) into porous rocks and less in less porous rocks. Commonly the caliper, in combination with the delta-rho (drho, from the density) log, are used to flag hole

conditons. An algorithm for the nuclear porosity logs used by Hurley and Peeters (1998) is:

"If caliper > (an amount defined by the analyst) or a delta-rho> of 0.10 or 0.15

….then ignore porosity readings"

In particular, bad hole conditions caused by sloughing or collapse of borehole walls, as indicated by caliper log and the drho curve, would require some editing for the multimineral analysis.

The final edited log curves for the four Utan wells were given an "_ED" extension. If the original sonic was labeled "DT", then the edited sonic was labeled "DT_ED". These curves were formatted in LAS files for each well. Figure 4.5 show some results of wireline log editing.

In addition to the C-429, Utan-1, C-3068, and C-468 logs, the sonic and density logs for some other wells were edited to create synthetic seismograms for later seismic ties.

Editing also included generating pseudo logs to fill missing data gaps or to replace bad data that was not consistent with other logs. Multi-linear regression was utilized to create log relationships to reconstruct relatively large log segments. These log segments have missing and/or bad data values caused by borehole condition or log run changes. The following equation is an example of log relationship using multi-linear regression to reconstruct the PEF log in the C-3068 well (Figure 4.6):

**PEF_ED=-0.1539+2.53325*RHOB_ED- 0.0095*DT_ED- 0.0042*GR_ED**

## 4.4 Formation evaluation and petrophysical analysis

One of the most common problems of traditional log analysis is to establish the composition of the logged rocks in terms of the volumes of fluids and gases contained within the pore space and, secondarily, to determine their mineral content (Doveton, 1994). For rocks with simple binary and even ternary compositions the use of litho/porosity crossplots with two or three porosity tools allows a rough volumetric estimation of mineral and fluid proportions as well as sufficiently accurate estimates of porosity for routine reservoir analysis. For more complex rock types, compositional analysis by traditional crossplots is more challenging and analytic solutions instead of graphical ones are preferred because of the increased number of components that must be incorporated. According to Bassiouni (1994), the true advantage of a graphical solution over an analytical one is that the graphical solution makes detecting the presence of gas, shale or secondary porosity easier by shifting the position of the points with respect to their true lithologies.

Well log analysis was developed for the Miocene-Pliocene section and emphasized on the Utan-1 well, which contained the best suite of well logs, paleontology reports, cored intervals and other useful analysis at the target level. According to drilling fluid characteristics (extracted from Sclumberger records) and the well logging tools available in each interval, the Utan-1 well was divided into three parts (check casing variations on the caliper curve behavior in figure 4.1):

- Upper interval (200-600m): Bentonite/polymer water-based drilling mud, density: 1.06 gr/cc, Tf = 38° C, Bs =12.5”, Rm = 1.9 ohm-m @ 32° C, Rmf = 1.1 ohm-m @ 32° C, Rmc = 3.1 ohm-m @ 32° C, water = 98%, solids = 2%
- Middle interval (600-1035m): Bentonite/polymer water-based drilling mud, density: 1.06 gr/cc, Tf = 43° C, Bs =12.25”, Rm = 1.8 ohm-m @ 32° C, Rmf = 1.6 ohm-m @ 32° C, Rmc = 2.8 ohm-m @ 32° C, water = 97%, solids = 3%
- Lower interval (1035-1452m): Inhibited water-based drilling mud, density: 1.52 gr/cc, Tf = 66° C, B s= 8.5”, Rm = 0.65 ohm-m @ 25° C, Rmf = 0.37 ohm-m @ 24° C, Rmc = 0.8 ohm-m @ 27° C, solids = 19% (barite as a weighting agent)

Water salinity can be determined by direct analysis when water samples are available. In the absence of water samples, salinity is estimated in terms of the electrical conductivity using conventional well logging interpretation techniques. Rw is first calculated from the SP log. The salinity is then obtained using available correlations.

To determine water salinity at the Utan-1 well, four water samples were taken at the interval 1317-1322m. Initially, the salinity resulted in different values for each water sample, which was considered an effect of possible contamination. Therefore, Schlumberger´s Ionic Balance Method was used to select the sample for salinity estimation with both the lower ionic balance and the lower associated error in the procedure.

Salinity refers to the total dissolved ionic solids in water. Atoms in salts are held together by ionic bonds (e.g. NaCl), which are easily broken by polar water molecules. Assuming that most of the dissolved substances in the formation water are just salts, then simple ionic compounds typically disassociate completely into positive and negative ions in water.

Theoretically, the sum of the anions in a water sample, expressed in milliequivalents per litre, should exactly equal the sum of the cations expressed in the same manner (UN GEMS/Water, 2004). The following are some concepts useful in understanding this process (Gore, 2005; Moore, 2008):

- pH= -log10[H+]
- For pure water $[H^+]=[OH^-]=10^{-7}$, so pH=7.
- As [H+] increases, pH decreases: more acidic
- As [H+] decreases, pH increases: more alkaline
- Sea water is slightly alkaline and remains relatively constant: average pH ~7.8
- Ocean salinity is 35 parts per thousand (ppt) and varies between 32 and 37 ppt
- Fresh water salinity is less than 0.5ppt

Table 4.1 shows the results obtained from the experiment as well as the salinity value obtained through this process for an ionic balance of 0.39%. Therefore the salinity value chosen for the initial petrophysical analysis was 32200ppm (32.2ppt). An ionic balance is regarded as correct if the difference between anions and cations relative to the sum of the ions is less than 2%; a greater difference is usually an indication either of the presence in the sample of one or more ion species that have not

been taken into consideration for the calculation, or of analytical errors concerning one or more of the major ion species taken for the calculation (UN GEMS/Water, 2004).

| **Day** | 23 – 01 - 2004 | 25 – 01 – 2004 | **25 – 01 – 2004** | 26 – 01 – 2004 |
|---|---|---|---|---|
| **Hour** | | 9 am | **11 am** | 7 am |
| **Salinity** | 21875 | 17985 | **32211** | 40468 |
| **Rw** | 0.275 | 0.327 | **0.193** | 0.158 |
| **PH** | 8.00 | 6.80 | **7.70** | 7.00 |
| **Density** | 1.01 | 1.01 | **1.02** | 1.03 |
| **Ionic Balance** | 0.61 | 3.54 | **0.39** | 1.60 |
| **Error** | 0.08 | 0.57 | **0.03** | 0.11 |

**Table 4.1: Salinity analysis from water samples at surface**

The effects of formation-water salinity and temperature on rock resistivity has been pointed out by Bassiouni (1994), who refers how for some salts the conductivity increases as concentration increases and presents a nomogram developed from experimental data, which shows the resistivity of NaCl solutions as a function of concentration and temperature. The importance of accurate salinity values comes from the fact that overestimation of n, Rw, and m causes overestimation of Sw and that the sensitivity of Archie´s equation to errors in these interpretation parameters increases as water saturation increases.

X-ray diffraction work was essentially important in the study area for complete analysis of bulk rock composition and clay characterization that cannot be performed using thin section petrography or scanning electron microscopy alone. An automated X-ray diffractometer and specialized software was utilized by Corelab laboratories to provide the results shown in Table 4.2 for the cored intervals in the Utan-1 well.

| CORE | DEPTH | Rock Composition (weigth %) | | | | | | | | Clay Relative Abundance (Normalized to 100%) | | | | | Grain density (g/cc) |
|---|---|---|---|---|---|---|---|---|---|---|---|---|---|---|---|
| | | Quartz | K Feldspar | Plagioclase | Calcite | Dolomite and Fe-dolomite | Aragonite | Pirite | Total clays | Illite/Esmectite* | Ilite & mica | Kaolin | Clorite | % Esmectite in I/E | |
| 1 | 1084.85 | 23 | 7 | 8 | 35 | 18 | 1 | 3 | 5 | 44 | 32 | 0 | 24 | 80-90 | 2.711 |
| 1 | 1086.90 | 8 | 1 | 3 | 54 | 11 | 11 | 3 | 9 | 59 | 26 | 0 | 15 | 80-90 | 2.717 |
| 1 | 1092.44 | 8 | 1 | 4 | 55 | 15 | 8 | 1 | 8 | 63 | 22 | 0 | 15 | 80-90 | 2.714 |
| 2 | 1225.09 | 7 | 1 | 4 | 67 | 12 | 2 | 1 | 6 | 65 | 18 | 0 | 17 | 80-90 | 2.705 |
| 2 | 1227.96 | 9 | 1 | 4 | 65 | 10 | 4 | 1 | 6 | 68 | 20 | 0 | 12 | 80-90 | 2.713 |
| 2 | 1230.39 | 12 | 2 | 6 | 33 | 17 | 13 | 3 | 14 | 71 | 19 | 0 | 10 | 80-90 | 2.724 |
| 3 | 1321.56 | 8 | 1 | 3 | 56 | 26 | 0 | 1 | 5 | 55 | 25 | 0 | 20 | 80-90 | 2.731 |
| 3 | 1322.70 | 4 | 1 | 1 | 74 | 14 | 0 | 1 | 5 | 51 | 31 | 0 | 18 | 80-90 | 2.718 |
| 3 | 1324.21 | 4 | 1 | 2 | 64 | 21 | 1 | 1 | 6 | 47 | 31 | 0 | 22 | 80-90 | 2.727 |
| AVERAGE: | | 9 | 2 | 4 | 56 | 16 | 6 | 2 | 7 | 58 | 25 | 0 | 17 | | |
| MIN: | | 4 | 1 | 1 | 33 | 10 | 1 | 1 | 5 | 44 | 18 | 0 | 10 | | |
| MAX: | | 23 | 7 | 8 | 74 | 26 | 13 | 3 | 14 | 71 | 32 | 0 | 24 | | |

**Table 4.2: X-ray diffraction analysis on samples of cored intervals in Utan well (adapted from non-published Pemex internal reports)**

From these results it can be interpreted that the sampled intervals represent a carbonate rock with an average composition: calcite (56%), dolomite (16%), quartz (9%), aragonite and pyrite (8%), feldspar and plagioclase (6%), and clay (7%). The same Table 4.2 shows the normalized clay characterization and grain density values, the latter of which varies slightly about 2.71, which also corresponds to carbonates. It has to be noticed that at the sampled reservoir intervals (first sample of cores labeled as 1 and 3) the percentage of quartz increases while the carbonate content decreases.

A major application of this analysis was the estimation of shale content, which is on average below 10%, and 5% for the reservoir intervals.

Pliocene facies in the study area were deposited in a mixed platform environment. This fact is supported by the petrographic description of the three cored intervals (Chapter 6 of this dissertation), which show light gray carbonate – siliciclastic mixed mudstones, as well as the X-ray diffraction analysis (Table 4.2) at

the discovery well. Without continuous core present throughout the entire interval that is being analyzed, it is only possible to approximate the matrix composition using petrophysical techniques tied to the core analysis.

Sonic-neutron, density-neutron, and density-sonic crossplots were qualitatively analyzed for the discovery well at reservoir levels (figure 4.7). The dispersion and movement of the center of the crossplotted points indicating the presence of different lithologies also reinforce a multimineral composition (the plots suggest dolomite in one case and a mixed limestone-sandstone in the other case). However, the false indication of lithology could be associated with a combined effect of vugular porosity (which affects sonic log readings), and washed out zones (Hurley and Peters, 1998; Asquith and Krygowski, 2004). In particular, all lithology plots that require a sonic log may be unreliable if there is a large amount of vuggy porosity. In such cases, sonic readings underestimate porosity. In the end-member cases, sandstones normally have only matrix or intergranular porosity whereas carbonates often have all three porosity types: matrix, fracture and vugular (Johnson and Pile, 2006).

In making multimineral analyses, if the response of tools other than the porosity logs can be expressed in terms of volume fraction of the formation constituents, then more than four simultaneous equations can be written and solved for more than three unknowns. This kind of analytical approach can be used when more than three minerals are present (Bassiouni, 1994). They correspond to the statistical approaches which derive from the so-called “global” methods (Worthington, 2003).

The photoelectric index (Pe) is the latest generation of density logging tools, which is usually included with other lithology-porosity tools in multimineral analysis. The Pe index records the absorption of low-energy gamma rays by the formation, which is a direct function of the aggregate atomic number of the elements in the formation, thus is an excellent indicator of mineralogy. The index is scaled on a range between 0 and 10, in units of barns per electron. Basic mineral references are: quartz 1.81; dolomite 3.14; calcite 5.08 barns/electron.

Multimineral analysis was performed on the Miocene/Pliocene section of the Utan-1, C-429, C-3068, and C-468 wells using available log data (gamma ray, Pe, bulk density, neutron, and sonic logs), and Fusion® proprietary software. In order to set up the simultaneous equation system following the global approach, it was necessary to assume the mineral components of the selected interval (Worthington, 2003). For the analyzed mixed platform environment, a rock composition might have the following components: calcite, quartz, dolomite, clay and even anhydrite. Table 4.3 lists the matrix parameters used for each lithology in the multimineral analysis.

The statistical method assumes an effective porosity system. It means a computed Vsh value at every digital sampling level and is based on every input log. Therefore, the petrophysical results included the calculation of the following properties: Volumes of shale, calcite, dolomite, anhydrite, quartz, effective porosity, water and hydrocarbon (gas) saturations. In addition, formation temperature, formation water resistivity corrected for formation temperature, and pore pressure were calculated based on the following information: bottom hole temperature, formation

water resistivity from water sample, and mud densities respectively. The petrophysical results for all the four wells at which the multimineral analysis was applied are presented in Figures 4.8 to 4.11.

| Lithology | Gamma ray (API) | Neutron (fraction) | Density (gm/cc) | Sonic (μsec/ft) | Pe (b/e) |
|---|---|---|---|---|---|
| **Quartz** | 20 | -.05 | 2.65 | 52 | 1.8 |
| **Dolomite** | 15 | 0.065 | 2.87 | 43.5 | 3.12 |
| **Calcite** | 15 | 0.0 | 2.71 | 47.5 | 5.08 |
| **Shale** | 80-85 | 0.4-0.55 | 2.0-2.2 | 85-110 | 3.5 |
| **Anhydrite** | 5 | -.002 | 2.98 | 50 | 5.04 |

**Table 4.3: The log parameters for each lithology in the multimineral analysis**

The lithological components and porosity resulting from the petrophysical analysis were calibrated to the available core data of the Utan-1 well (figure 4.8).

The Miocene/Pliocene stratigraphic section in the wells is mainly composed of muddy carbonates with some quartz. The lithology at the Utan-1 well reservoirs becomes cleaner upward from a Miocene shaly carbonate interval and is mainly composed of calcite with some dolomite and quartz, with porosity as high as 23%. Porosities of 30-45% occur within the upper 1000 meters in the wells due to their non-consolidated nature. Yet, the data quality at these shallow depths is bad and the results are out of the context of this dissertation.

The presence of shale or clay minerals in a reservoir causes erroneous values for water saturation and porosity derived from logs. These effects are not limited to sandstones, but also occur in carbonates (Asquith and Krygowski, 2004).

Asquith and Krygowski (2004) based on Hilchie (1978), mention that the most significant effect of shale in a formation is to reduce the resistivity contrast between oil or gas, and water. Clays commonly contain bound-water, thus they are generally conductive of electricity. In this sense, if the formation is shaly, Archie's saturation equation fails because it implies that the formation is clean or relatively clean (Bassiouni, 1994), and that only the formation fluids can conduct electricity. As a result, conventional approaches provide higher water saturation values for shaly formations, thus complicating interpretation if a zone is productive.

Hurley and Peeters (1998), and Asquith and Krygowski (2004) conclude that for shale to significantly affect log-derived water saturations, shale content must be greater than 10 to 15%. In this case the formation can be considered as shaly and $V_{shale}$ methods have to be utilized to correct porosity for clay content and to calculate the bound-water saturation.

Consequently, the shale content, which resulted in average 7% and 5% for the reservoir intervals in Utan field, is below the cutoff value for shaly formations, which avoids making the shale correction to well log curves. Above and below the Pliocene intervals the formation becomes dramatically shalier and future interpretations have to consider such intervals as shale-prone.

In the studied wells, zones that have considerable gas have relatively good porosity and high resistivity. Different models for estimating fluid saturations were applied. It was found that both Archie and Simandoux equations were the most robust (e.g., did not generate spikes) and consistent with production test data, giving the closest results, so their average was used. It can be interpreted that the low shale content in the Pliocene intervals provided or caused such similar results. The Utan-1 well has the highest hydrocarbon (gas) potential followed by the C-3068 well (Figures 4.8 and 4.9). Both the C-429 and C-468 wells are mainly wet (Figures 4.10 and 4.11).

The best reservoir in the studied wells is at a depth of 1075-1085m in the Utan-1 well. In-situ gas saturation in this reservoir does not exceed 60%. This indicates very small grain size or shaly content (Dr. James Forgotson, The University of Oklahoma, personal communication). There will always be an irreducible water fraction which avoids having fully gas saturated rock. Gas does not displace the wetting phase of the rock (water) due to capillary pressure. Gas is always considered the non-wetting phase.

Potential reservoirs in the study area have lower volumes of shale and are mainly composed of calcite with some dolomite and quartz, with porosity as high as 23%. Increase in the amount of quartz indicates higher-energy depositional environment, which may enhance development of porous zones (Bahamon, 2006).

Changes in carbonate content result in large changes in permeability. According to the EMI log, at reservoir levels in the Utan-1 well there is high-frequency scale interbedding, which is beyond the resolution of visual core analysis and standard logging tools. It represents high cyclicity in depositional energy to

produce alternate sand-shale interbeds which may indicate a intratidal- to subtidal-dominated mixed carbonate-siliciclastic depositional environment (Bahamon, 2006).

## 4.5 Pseudo shear velocity prediction, invasion/dispersion corrections, and fluid substitution

Drilling activities can profoundly affect the characteristics of a formation. The drillbit changes the rock somewhat, but the main alterations are caused by the drilling mud. After drilling, well log measurements are made in a borehole filled with drilling fluids (mud) and frequently the radius of investigation does not penetrate beyond that part of formation that is invaded to some extent with these fluids (figure 4.12). The sonic and density measurements are among the most adversely affected and can be particularly pronounced in gas bearing rocks.

Measurement of true resistivity of formation is one of the key goals of resistivity logging. Unfortunately no single device has been able to completely eliminate the effects of invaded zone and a common practiced solution is to measure the resistivity with several arrays having different depths of invasion. Because water saturations are typically computed from a deep resistivity device (which looks several feet into the formation), calculated Sw values most likely do not reflect the saturation seen by the sonic and density logs, which have much shallower depths of investigation (Smith et al., 2003). Consequently, invasion correction sometimes may be needed prior to utilizing sonic and density logs for seismic applications (Smith, 2003; Chi et al., 2004; Mahob and Castagna, 2000).

Mahob and Castagna (2000) consider that when utilizing sonic logs, the frequency dependence of P-wave velocity should be evaluated, pointing out that velocities are dispersive, particularly in partially fluid saturated rocks. Velocity dispersion from seismic to ultrasonic frequencies mainly occurs when gas exists in the reservoir, which leads to velocity variation at different gas saturations (figure 4.13). In this sense, it is commonly assumed that sonic logs are acquired at frequencies that may be considered in the low frequency range, thereby justifying the use of Gassmann's equations. However, Peeters (1998), Hofmann (2000), and Mahob and Castagna (2000), report that dispersion in the low frequency band can occur –between seismic and sonic log frequencies– particularly in hydrocarbon bearing rocks, which has strong implications on seismic attribute analysis.

On the other hand, a prior knowledge of the shear-wave velocity is required for AVO analysis and for pore fluid identification from seismic data. However, when shear-wave logs are not available, S-wave velocities (VS) are estimated from P-wave velocities (VP) using statistical empirical relationships (Castagna et al., 1993; Mahob and Castagna, 2000). In the Utan-1 well, the results of the petrophysical analysis were used for prediction of pseudo-shear velocity using Fusion proprietary software. Since the Utan-1 well has a shear sonic log, the shear velocity prediction was performed for the Miocene/Pliocene stratigraphic section in the three remaining wells (Figure 4.14).

Along the same line, one of the most important problems in the rock physics analysis of logs, cores and seismic data is the prediction and comparison of seismic

velocities in: (a) rocks saturated with one fluid from rocks saturated with a second fluid; (b) equivalently, saturated rock velocities from dry rock velocities.

Fluid substitution is the rock physics problem of understanding and predicting how seismic velocity and impedance depend on pore fluids (Avseth et al., 2005). Mahob and Castagna (2000) refer to this process as the mechanism by which new acoustic parameters (i.e., moduli, densities, and velocities) are theoretically calculated when the pore fluids are changed from a known saturation to a new saturation. Such a need arises during seismic modeling and amplitude variation with offset (AVO) analysis where such fluid substitution provides a valuable tool for modeling various fluid scenarios which might explain an AVO anomaly (Smith et al., 2003).

The equations generally used for fluid substitution are those from Gassmann (developed in 1951), which predict how the rock modulus changes with a change of pore fluids, and Biot (developed in 1956). The combined formulation is the Biot-Gassmann theory.

The most widely accepted theoretical approach for fluid substitutions employs the low-frequency Gassmann theory. Gassmann's equation relates the saturated bulk modulus of the rock to its porosity, the bulk modulus of the porous rock frame, the bulk modulus of the mineral matrix, and the bulk modulus of the pore-filling fluids (Smith et al., 2003). The bulk modulus or incompressibility (the inverse value of compressibility), is defined as the ratio of hydrostatic stress to volumetric strain:

$$K_{sat} = K^* + \frac{\left(1 - \frac{K^*}{K_o}\right)^2}{\frac{\phi}{K_{fl}} + \frac{(1-\phi)}{K_o} - \frac{K^*}{K_o^2}},$$

$K_{sat}$ = the saturated bulk modulus (undrained of pore fluids)
$K_o$ = the bulk modulus of the mineral matrix
$K_{fl}$ = the bulk modulus of the pore fluid
$K^*$ = the bulk modulus of the porous rock frame, (drained of any pore-filling fluid)
$\Phi$ = porosity.

Along the process it is important to recognize that the shear modulus (a measure of the ratio of shear stress to shear strain), is insensitive to pore fluid, that is:

$$G_{sat} = G_{dry}$$

$G_{dry}$ = effective shear modulus of dry rock
$G_{sat}$ = effective shear modulus of rock with pore fluid

Additional relationships necessary to perform the process of fluid substitution are (Smith, 2003):

$$K = \rho_B \left(V_p^2 - \frac{4}{3} V_s^2\right),$$

which relates the bulk modulus of a rock, ***Ksat,*** to its compressional velocity, shear velocity, and bulk density.

$$G = \rho_B V_s^2.$$

A fourth equation expresses the relationship between the fluid density ($\boldsymbol{\rho_{fl}}$), porosity ($\boldsymbol{\Phi}$), grain density of the rock matrix ($\boldsymbol{\rho_g}$), and the rock bulk density ($\boldsymbol{\rho_b}$), as follows:

$$\rho_B = \rho_g(1-\phi) + \rho_f\phi.$$

Several assumptions are considered in applying Gassman´s equations. The model assumes an isotropic and homogeneous medium with interconnected porosity (note that Gassmann makes no implications statements about pore structure); the pores are filled with a frictionless fluid (liquid, gas or mixture) (Wang, 2001). It is assumed that all fluid phases are immiscible and homogeneously distributed (violation = "patchy" saturation). The model is valid only at low frequencies such that pore pressures are equalized over a length scale much greater than a pore dimension and much less than the wavelength of the passing seismic wave (Smith, 2003).

A lot has been written about Gassman´s equations, its benefits and limitations. For those interested in a deeper knowledge and practical aspects of this theory, see: Castagna et al. (1993); Mavko et al. (1998); Wang (2001); Smith et al. (2003); Avseth et al. (2005).

In addition to the petrophysical analysis results mentioned in the previous section, the following parameters were included in the computing program (Fusion´s SVlog software) for the application of invasion and dispersion correction and fluid substitution based on Gassman's equation: temperature gradient estimated from

bottom hole temperatures, and pressure gradient based on mud densities and pressures. Also, the input fluid parameters in Utan were: gas gravity=0.60, GOR=1000, and brine salinity=32,200 ppm (Table 4.1).

Invasion and dispersion corrections as well as fluid substitution were performed in the same intervals for selected potential reservoirs in all four wells. The following criteria were employed for zones selection: clean rock (low volume of shale), high resistivity, good porosity, good hole condition, and/or has in-situ gas saturation.

Invasion correction was performed to obtain the in-situ condition for the sonic and bulk density log measurements by substituting the flushed (invaded) zone fluid saturations with virgin (non-invaded) formation fluid saturations. Next, the invasion-corrected (in-situ) P- and S-velocities are used to correct for dispersion between sonic and seismic frequencies using formation saturations by substituting the sonic frequency effective fluid modulus with the low frequency fluid modulus, according to Mahob and Castagna (2000). Maximum dispersion correction for measured velocity logs resulted for porous zones that have the lowest gas saturations but are not fully water-saturated. It agrees with what was observed by Mahob and Castagna (2000), for a negligible dispersion correction for clean gas sands, whereas the correction was maximum (6%) for partially saturated shaly gas sands.

After invasion and dispersion corrections, fluid substitution was performed either to generate the brine case from the in-situ gas, or the full gas case from the in-situ brine, i.e. 100% brine saturation, in-situ saturation, and full gas. Bulk density, P-

and S-velocities, and Poisson's ratio curves were derived from the process. Examples are shown in Figures (4.15 and 4.16). Full gas saturation (1-Swmod) means the potential reservoir interval was assumed to be filled with gas at irreducible water saturation (Swmod). The effects of fluid substitution on Vp, bulk density, and Poisson's ratio increase at higher rock porosity (Figure 4.15). This is due to the decrease in rock stiffness as the porosity increases. A noticeable effect occurs when gas is introduced in the Miocene/Pliocene rocks in the project area, which is indicated by the difference between the full-gas-saturated case and the brine case (Figure 4.16). Results of AVO and spectral modeling for fluid substitution in the Utan area will be later analyzed in Chapter 7 of this dissertation.

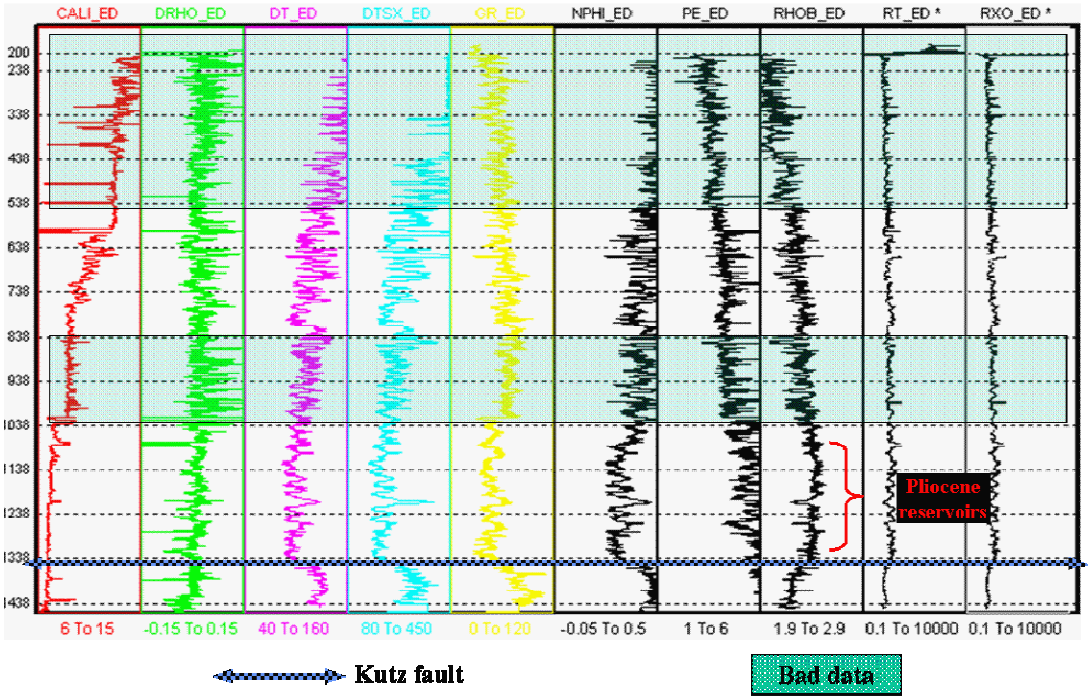


**Figure 4.1: Display showing available logs and depth of the runs for the Utan-1 well. The studied Pliocene section and the Kutz fault are outlined. Major bad data zones within this section are squared. Data needed for multi-mineral analysis exists for the Miocene/Pliocene section in this well.**

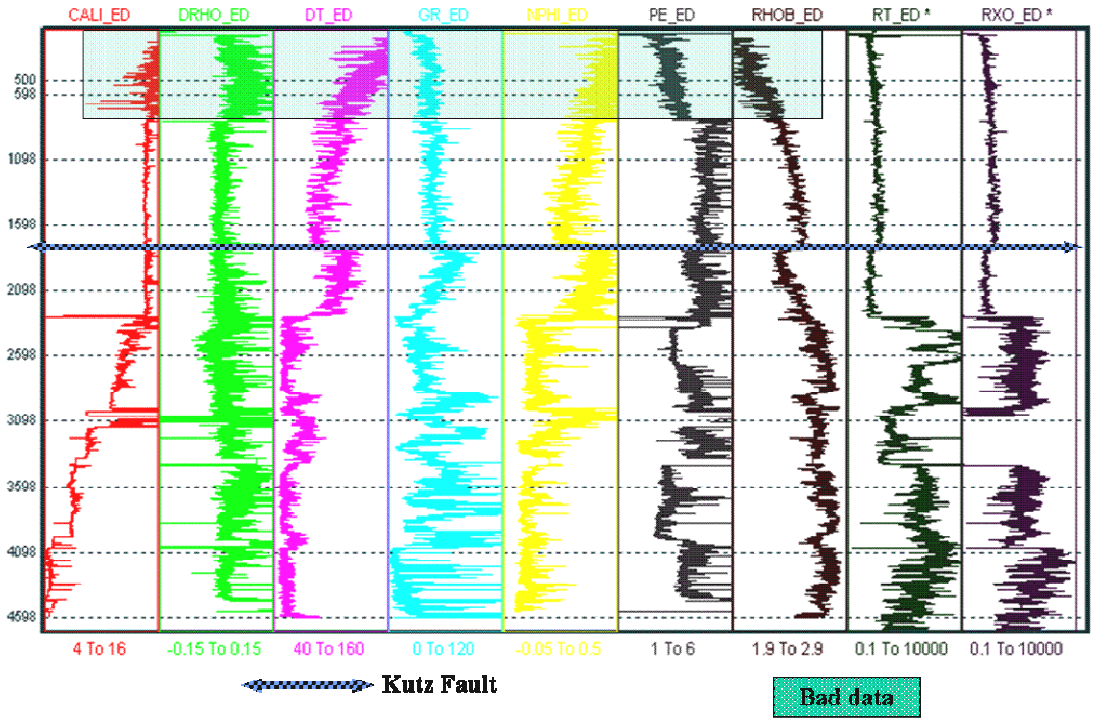


**Figure 4.2: Display showing available logs and depth of the runs for the C-3068 well. The Kutz fault position is outlined. A bad data zone within this section is squared. Data needed for multi-mineral analysis exist for the Pliocene section in this well, above the Kutz fault.**

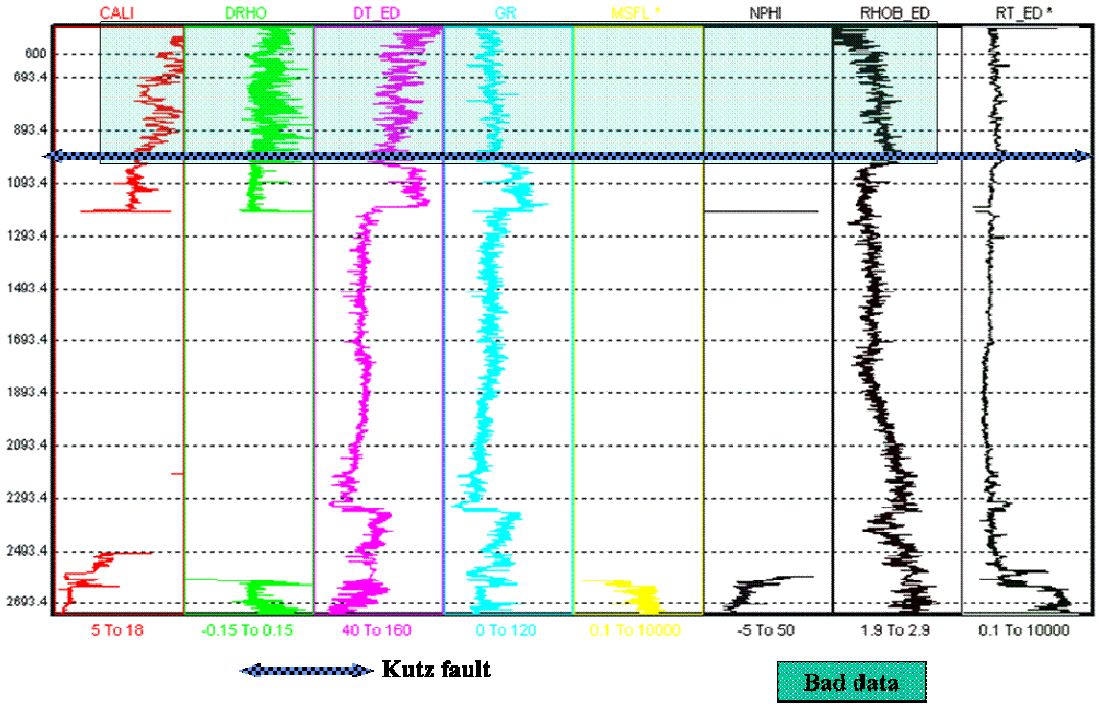


**Figure 4.3: Display showing available logs and depth of the runs for the C-2295 well. The Kutz fault position is outlined. A bad data zone within this section is squared. Data needed for multi-mineral analysis are not enough for the Miocene/Pliocene section in this well.**

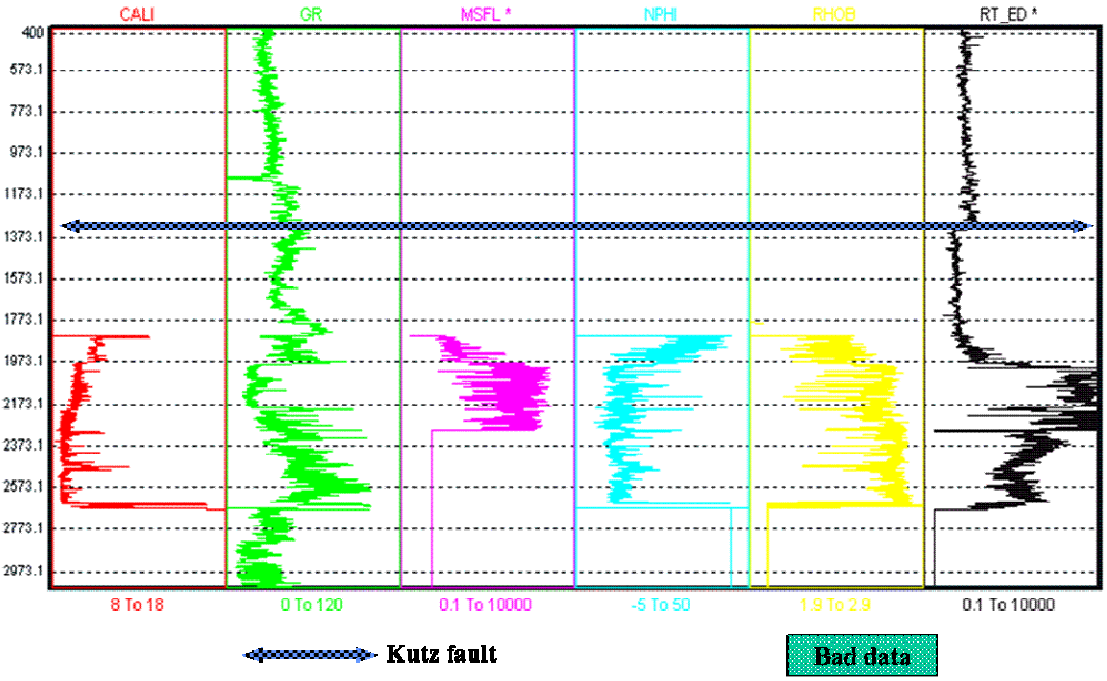


**Figure 4.4: Display showing available logs and depth of the runs for the C-219 well. The base of the Pliocene section is outlined (Miocene top). There are no data available for multi-mineral analysis at the Miocene/Pliocene section in this well.**

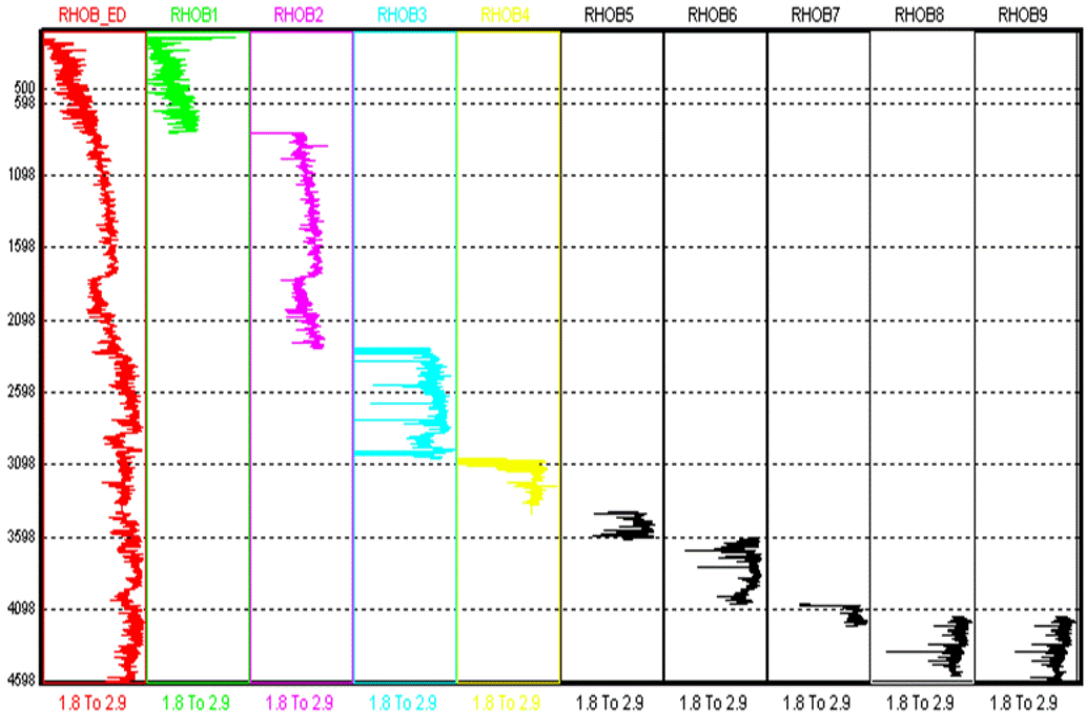


**Figure 4.5: Editing example (merging, gap filling and despiking) for the bulk density log in the C-3068 well. Composite density log in this well (first panel on left) was the result of merging the 9 runs of the remaining panels. Then the composite log was edited for spikes and data gaps. Final edited log ends with _ED suffix.**

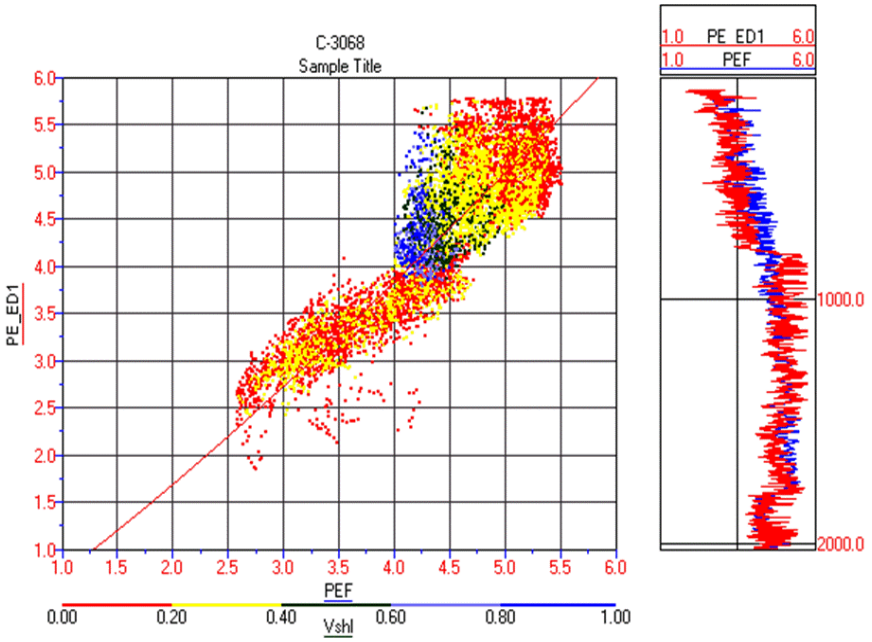


**Figure 4.6: Correlation between measured and reconstructed PE log in C-3068 well. Multi-linear regression was used to reconstruct bad segments of data. Multi-linear regression equation used: PEF_ED=-0.1539+2.53325*RHOB_ED- 0.0095*DT_ED- 0.0042*GR_ED**

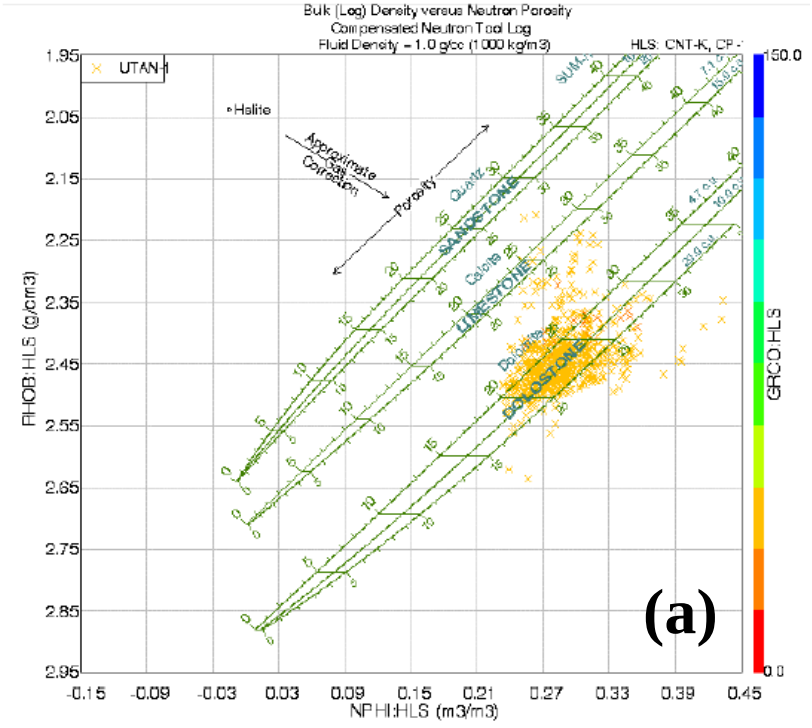


**Figure 4.7a: Dual mineral crossplots for the interval 1076-1450m in the Utan well: (a) density - neutron (non-published Pemex internal reports).**

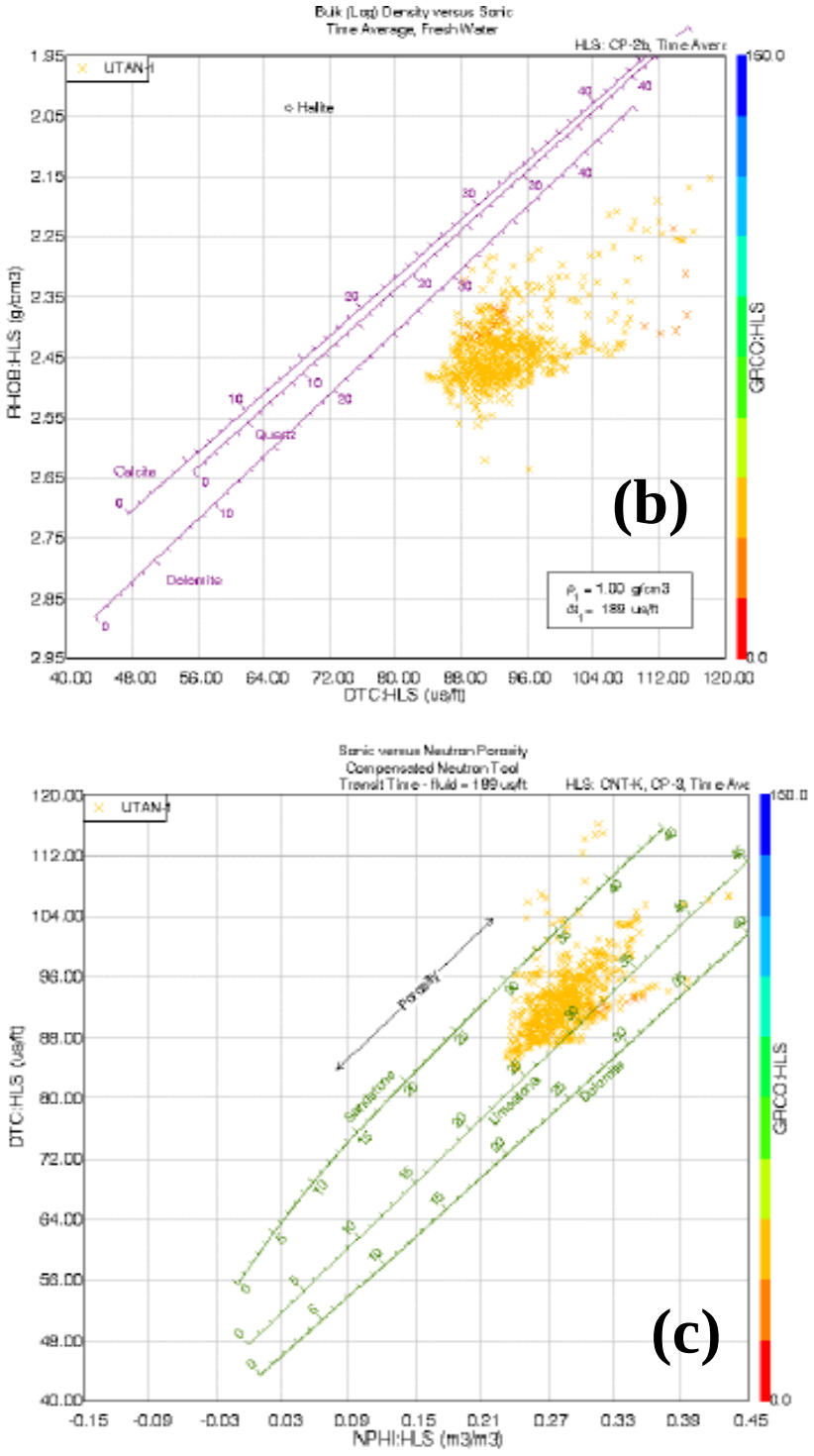


**Figure 4.7b: Dual-mineral crossplots for the interval 1076-1450m in the Utan well: (b) density-sonic; (c) sonic-neutron (non-published Pemex internal reports).**

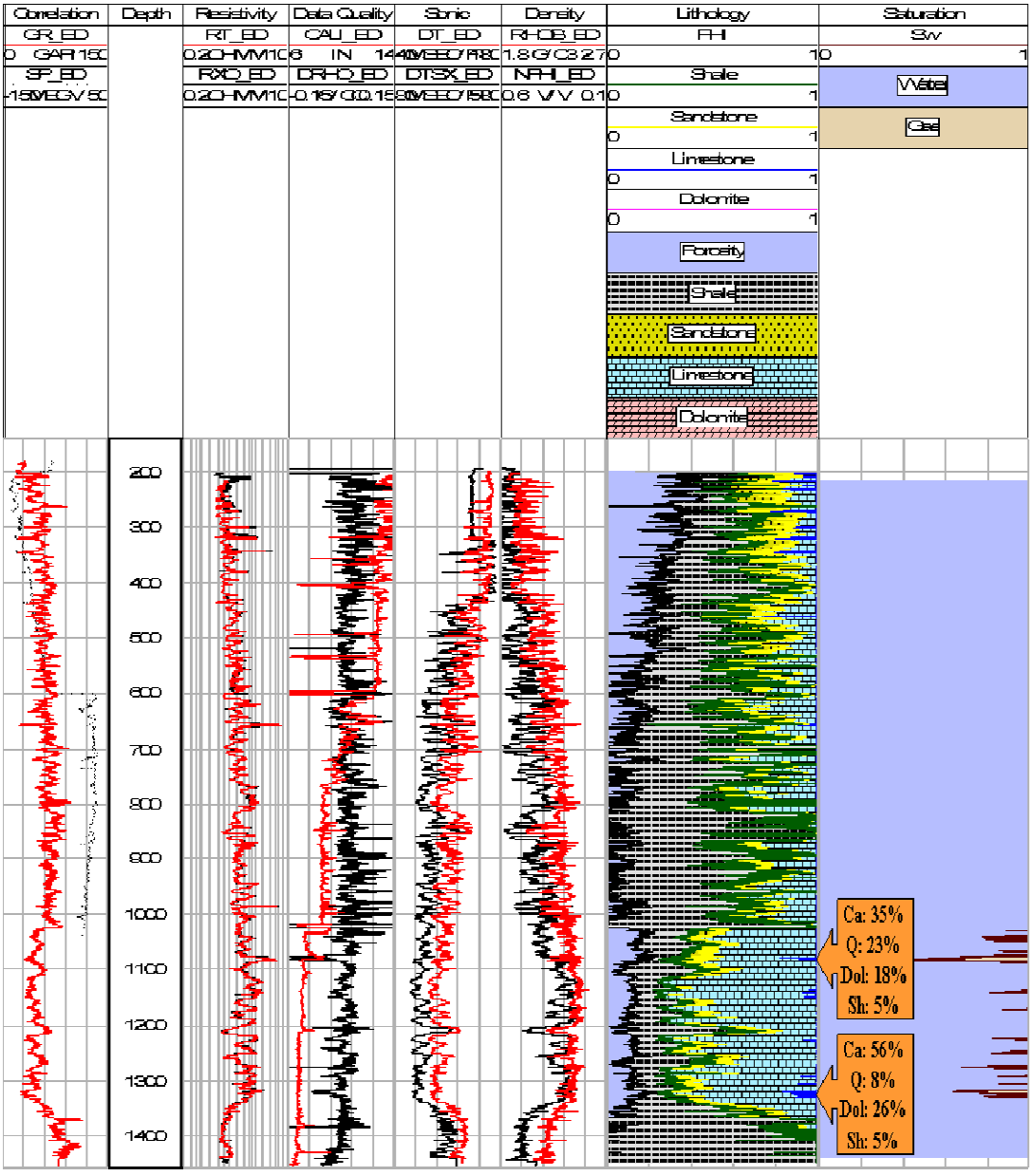


**Figure 4.8: Lithologies, porosity, and fluid saturation distribution from the multimineral analysis in the Utan-1 well. Orange symbols show calibration points with X-ray diffraction of core samples at the base of producing intervals. The calibration results acceptable for the carbonate-quartz-shale content. The Pliocene section becomes cleaner than the shalier Miocene section (below 1340m), and the reservoir intervals are mainly composed of calcite with increased quartz presence and higher effective porosity. The reservoir intervals correlate with high resistivities and good gamma ray response. The upper tested interval was the best tested interval reaching porosities as high as 23% from the multimineral analysis. The higher porosities shown at the first 700m could be indicative of non-compacted rocks and due to the bad quality of the log data they have to be carefully considered for future analyses (figure 4.1).**

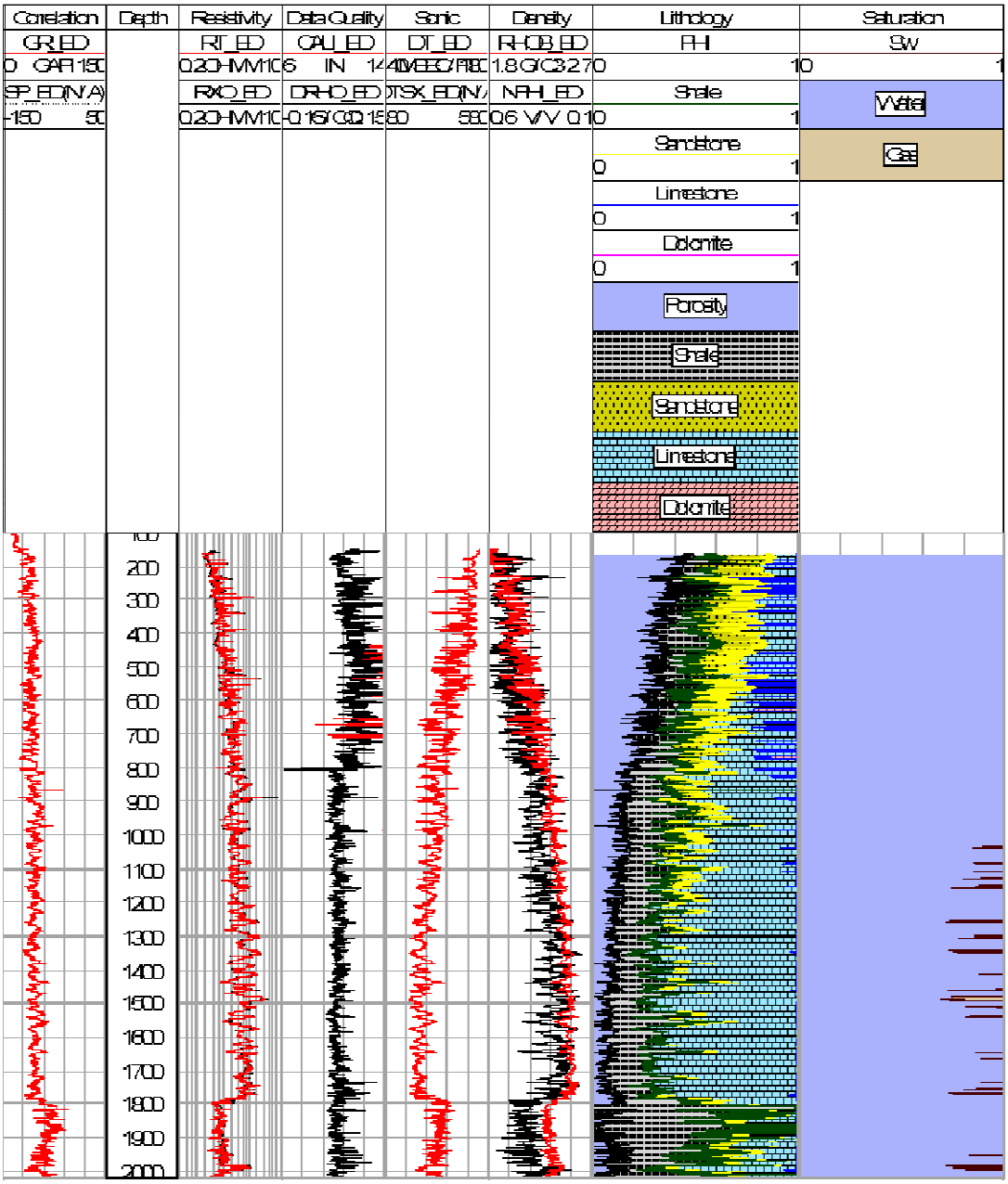


**Figure 4.9: Lithologies, porosity, and fluid saturation distribution in the C-3068 well. This well is located northward of the Utan-1 well (figure 2.21). After the high potential hydrocarbon content of the Utan intervals, this well exhibited the better hydrocarbon potential in some intervals between depths of 1200m and 1500m. These intervals show high resistivity response, increased quartz content and high effective porosity. There were no calibration points due to the lack of cored intervals, however as it happened with the Utan-1 well, the Pliocene section becomes cleaner than the shalier Miocene section (in this case below the Kutz fault at 1790m, approximately). Bad hole conditions (figure 4.2), avoided reliable petrophysical results above 820m, approximately.**

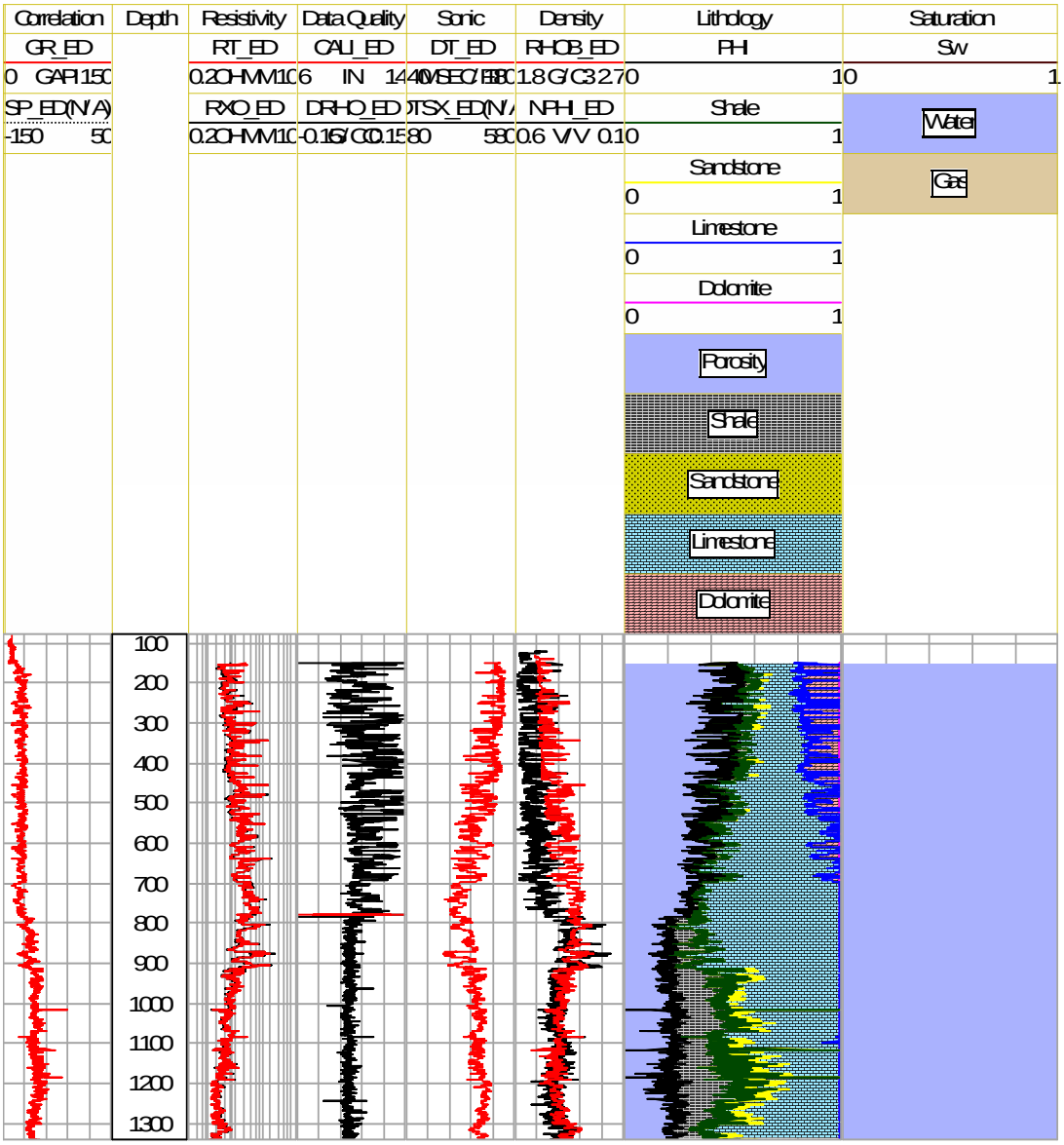


**Figure 4.10: Lithologies, porosity, and fluid saturation distribution in the C-429 well. Pliocene levels are located at upper structural levels on the eastern side of the Kutz fault and not easily correlated to Utan tested intervals. The well was wet.**

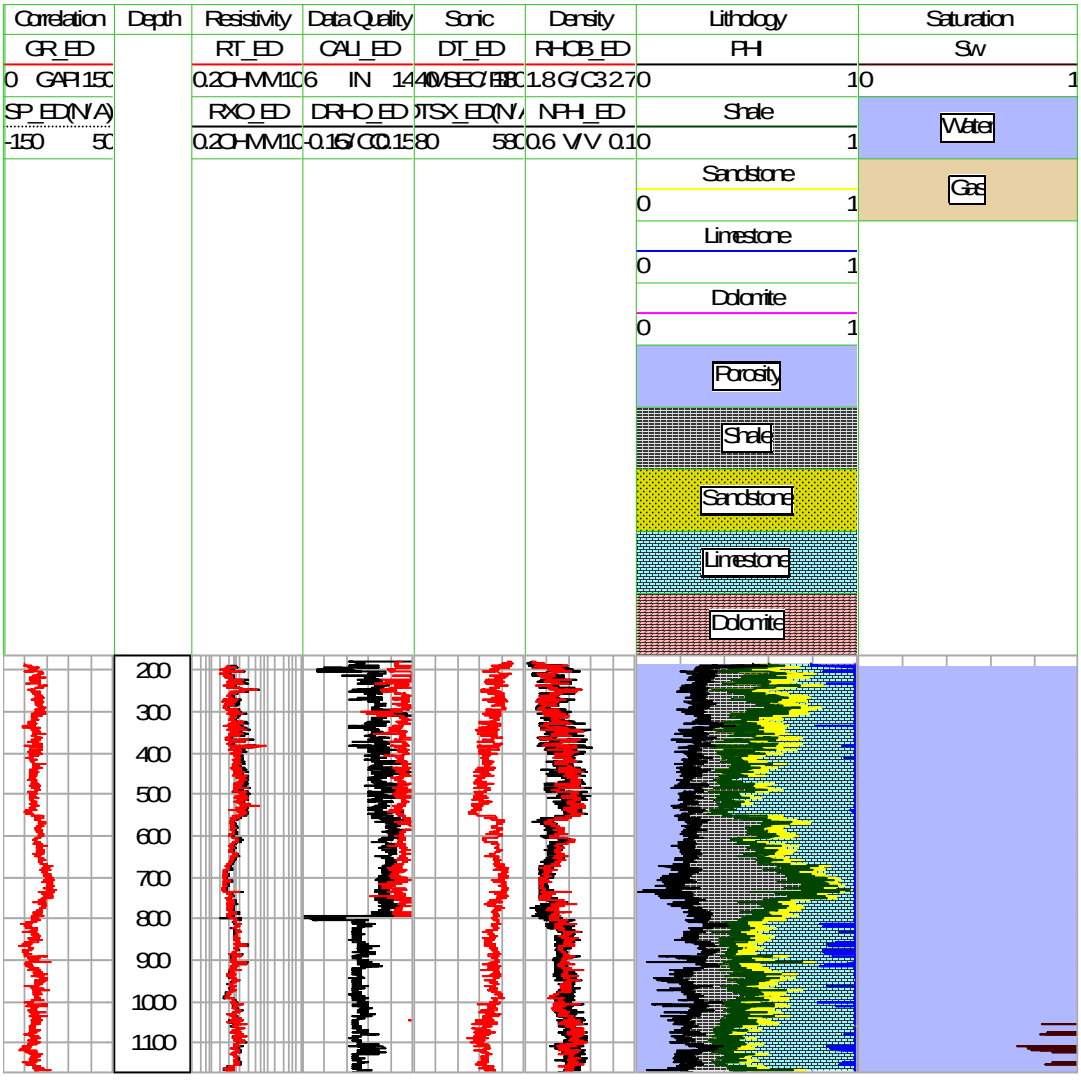


**Figure 4.11: Lithologies, porosity, and fluid saturation distribution in the C-468 well. Pliocene levels are located at upper structural levels on the eastern side of the Kutz fault and poorly correlated. The well was mainly wet.**

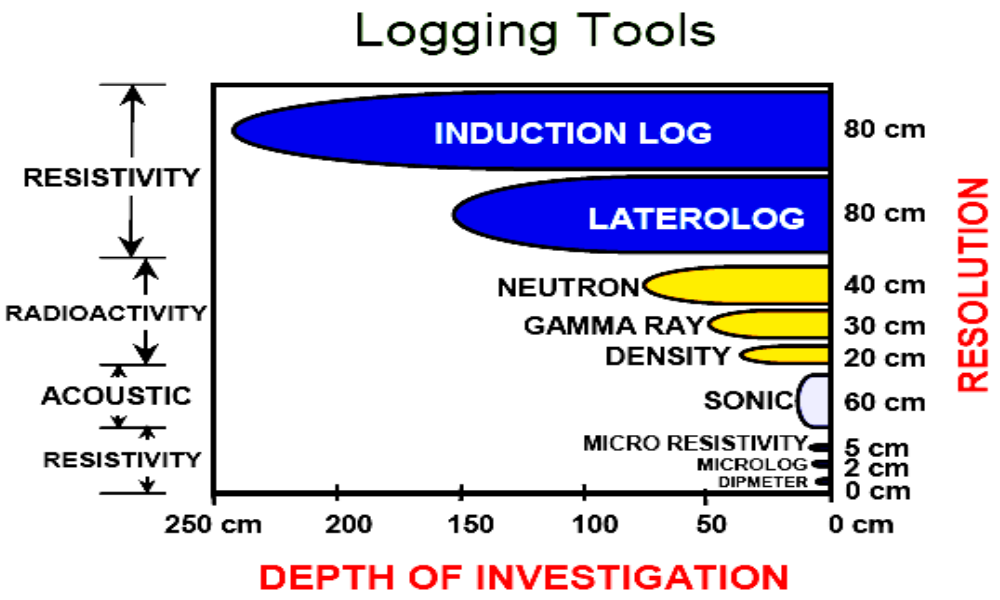


**Figure 4.12: Depth of investigation of logging tools (Youniz, 2006).**

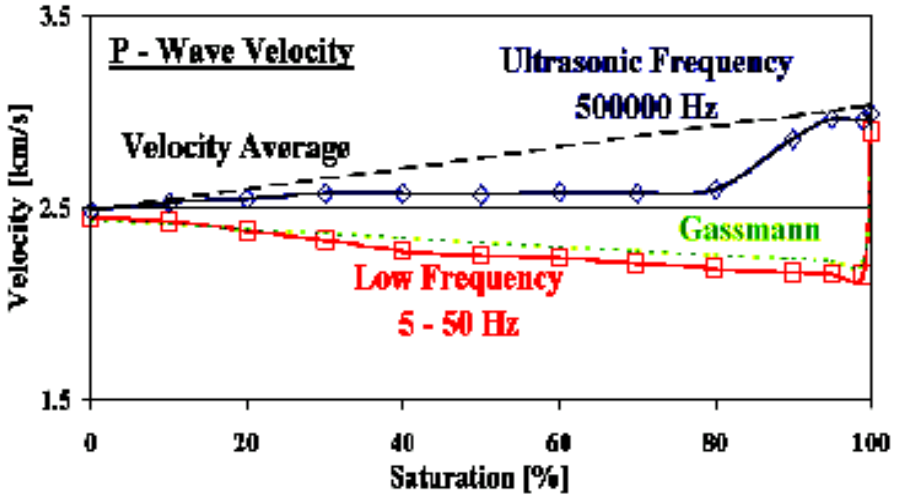


**Figure 4.13: Velocity dispersion from seismic to ultrasonic frequencies occurs when gas exists in the reservoir which leads to velocity variation at different gas saturations (Hofmann et al., 2000).**

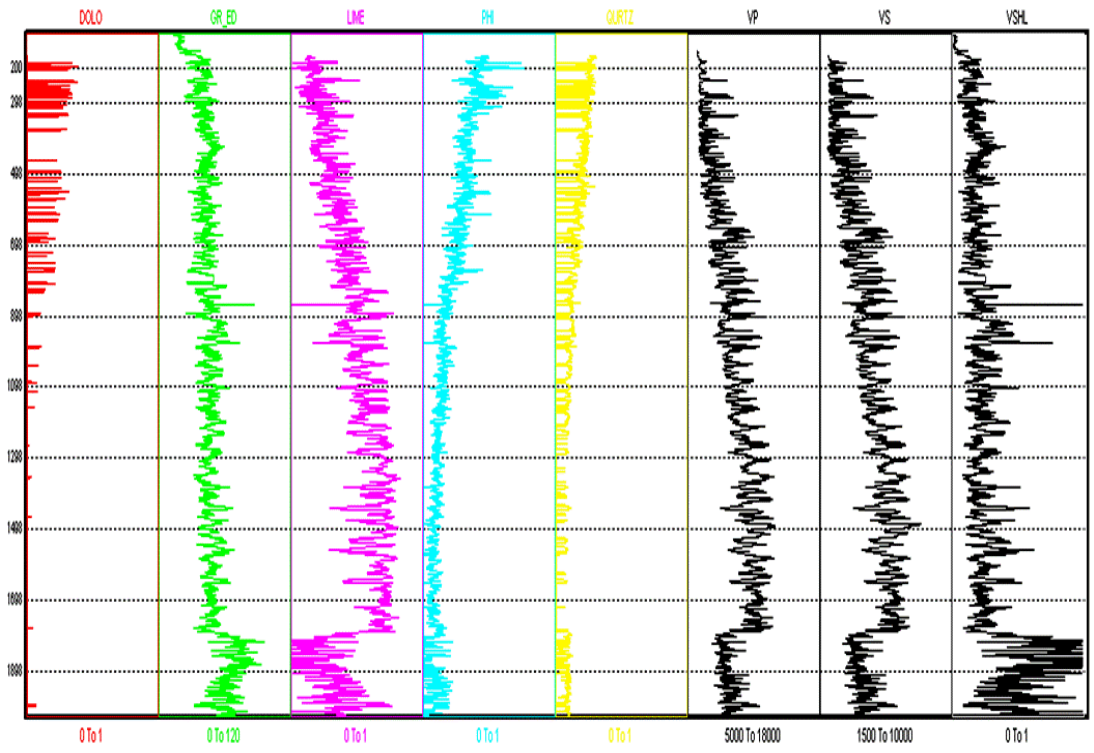


**Figure 4.14: Example of shear velocity prediction performed for the studied stratigraphic section in the C-3068 well. Input data included lithological composition and measured compressional velocity. The seventh panel (second from the end), shows the predicted shear velocity function.**

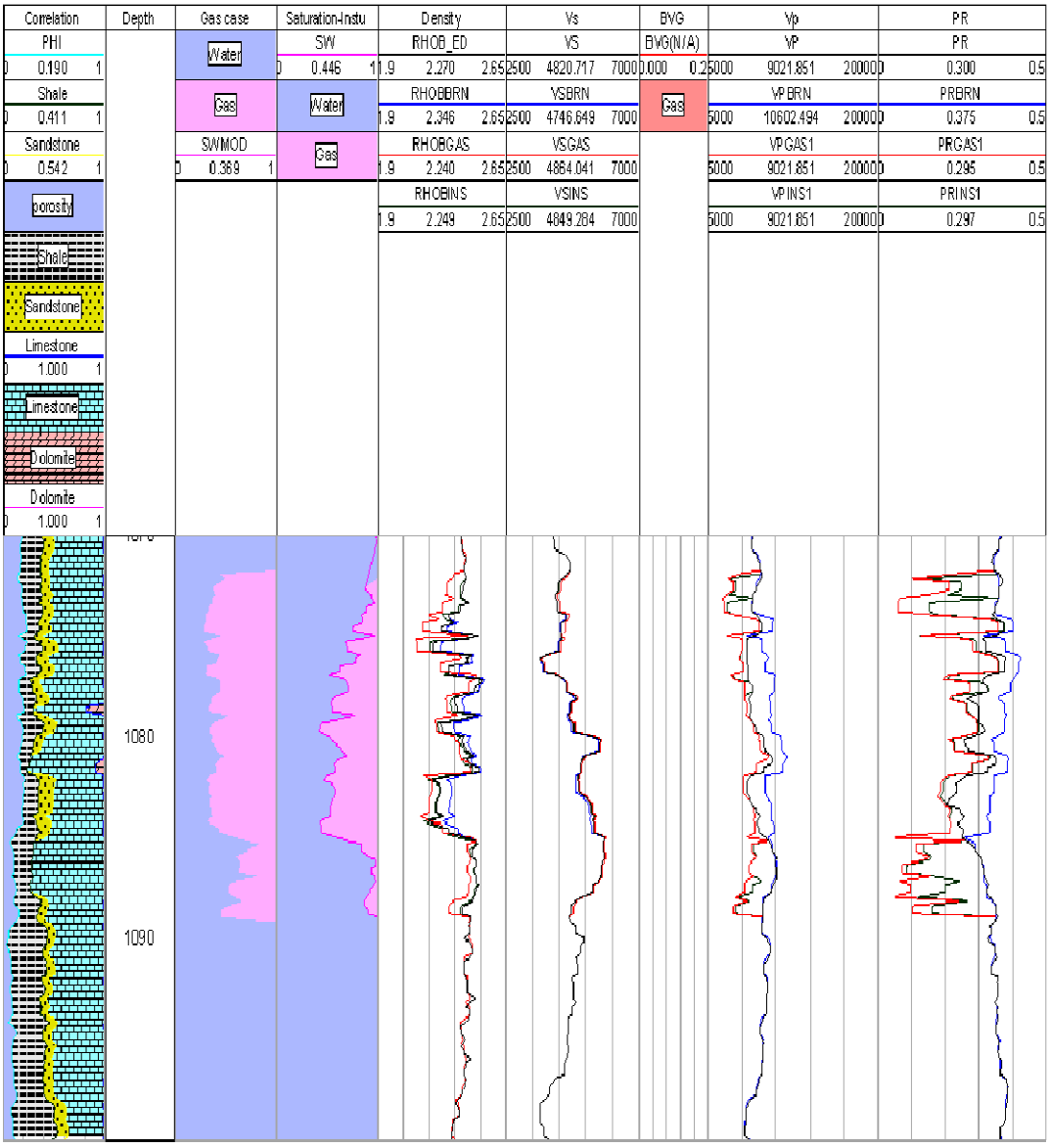


**Figure 4.15: Fluid substitution was performed to obtain the bulk density, s-velocity, and p-velocity, Poisson's ratio curves (displayed from left to right) for the following cases: 100% brine saturation (blue line), in-situ saturation (green line), and full gas (red line). Measured/reconstructed curves are in black. Figure is for zone at depth range 1070-1100m, which includes the upper reservoir in the Utan-1 well.**

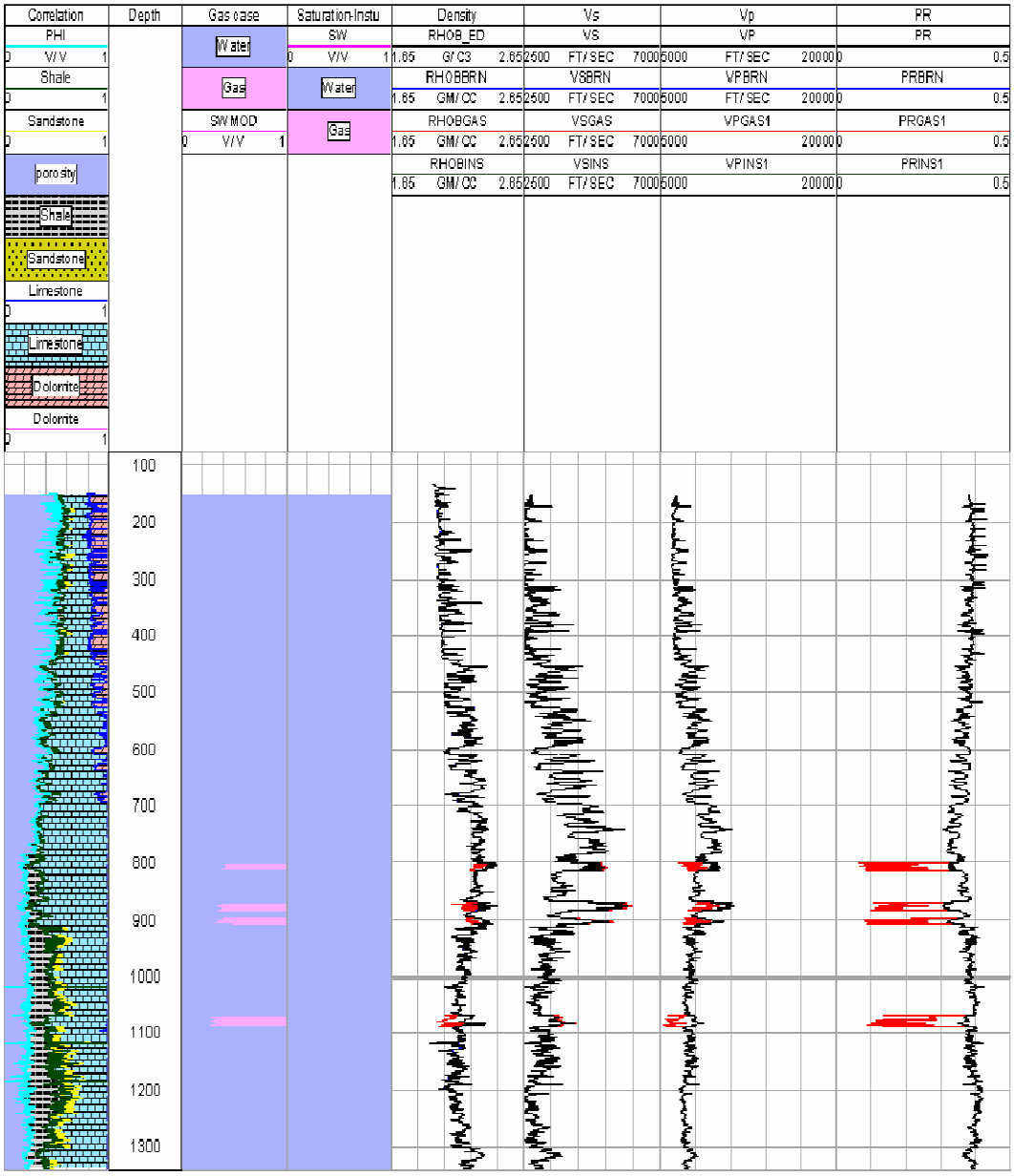


**Figure 4.16: Fluid substitution was performed on selected zones to show the effect of introducing gas in wet zones. The effect is noticeable as shown in this example from the C-429 well, which resulted wet (gas effect is shown in red).**

# Chapter 5

# SEISMIC DATA ANALYSIS

## 5.1 Introduction

Cantarell Field is located in a complex system of compressive structures that has always constituted a great challenge for seismic velocity analysis and structural interpretation. Three different seismic surveys were acquired over this field using different field designs and acquisition approaches to enable better definition of this structural complexity at the Upper Cretaceous-Paleocene level. As a consequence, seismic data have limited use for interpreting the shallower and mostly stratigraphic targets, which are the focus of this research.

Therefore, a first step in the seismic analysis was to evaluate the seismic dataset and attempt to enhance data quality at shallow levels for basic interpretation and the later application of sequence stratigraphic concepts and seismic attributes. The seismic database provided for this research is a 3D seismic Ocean Bottom Cable (OBC) survey acquired in 1996, which was reprocessed in 2003 to improve the signal to noise ratio at Cantarell-Sihil reservoir depths.

## 5.2 OBC Data Acquisition and Processing Parameters

The study area was defined by the limits of seismic and well data provided by Pemex, and encompassed an area of approximately 300 $km^2$. The geophysical database included seismic PSTM-CDP gathers and stacked data from the 3D seismic survey over Cantarell Field. Figure 2.21 showed the location of the discovery well on the seismic base map, which was used for the analysis. In the same figure, locations of inline 2781 and cross-line 21516 were shown. These two lines intersect at the Utan #1 location and, therefore, they are repeatedly used in the following analysis.

The Cantarell 3D OBC original seismic dataset consisted of approximately 620 $km^2$ of 60 fold data acquired in water depths ranging from 20 to 70m. It was recorded by Western Geophysical, from July to November 1996, using Compact Sleeve Source and an OBC receiver spread. Recording time was of 6.144 seconds at a 2-millisecond sample interval.

The Cantarell OBC survey was the second of three 3D seismic surveys acquired in the Cantarell area. The first of them was the so-called Campeche Sound Block "A", which was acquired by GSI in 1978 utilizing a conventional single-streamer. This survey represented the first 3D seismic survey acquired in Mexico, providing valuable information to interpret the structural configuration of Cantarell field although the resolution was not adequate for stratigraphic purposes.

A third 3D seismic survey was the Sihil node 3D/4C survey, overlapping the previous two 3D surveys in approximately 220 $km^2$ of 106 fold data. The objectives of this survey were to delineate the Cantarell-Sihil boundary and to evaluate converted

wave technology for planning better development strategies. It was recorded by SeaBed Geophysical from November 2003 to March 2004 using an air gun as source and a set of 4C autonomous nodes. Such a multicomponent seismic dataset was being processed during the course of this research, thus is not available for the interpretation.

In particular, the OBC survey provided for this dissertation was carried out to increase seismic resolution for structural purposes at Cantarell and Sihil depths. Therefore, the survey design was focused on Paleocene and Mesozoic intervals using the following parameters (figure 5.2):

### Field Parameters

| | |
|---|---|
| Survey | : 3D Cantarell OBC |
| Location | : Campeche Sound, Mexican Gulf of Mexico |
| Survey carried out by | : Western Atlas International |
| Date | : July-November, 1996 |
| Type of survey | OBC (Ocean Bottom Cable) "Dual Sensor" |
| Total number of swaths | : 18 |
| Total number of source points | : 320,008 |
| Bin size | : 25 x 12.5 meters |
| Total number of bins | : 1984000 |
| Nominal fold | : 50 |
| Maximum offset | : 6000 meters |
| Type of operation | : single vessel operation |

### Energy source

| | |
|---|---|
| Type of energy source | : Airguns-Compact Sleeve Source (CSS) |
| Shot point interval | : 25 meters |
| Source line spacing | : 200 meters |
| Number of sources | : 32 |
| Source array | : 4 sub-arrays (750 cubic inches/array) |
| Volume source | : 3000 cubic inches (750 x 4) |
| Air pressure | : 1800 psi |
| Source depth | : 6 meters |

## Cables and Receivers

| | | |
|---|---|---|
| Type of receivers | | Dual sensor “Hydro-geophone”: HGS 2 |
| Type of cables | : | OBC (Ocean Bottom Cable) |
| Cable depth | | Sea floor depth |
| Number of cables | : | 2 |
| Nominal cable interval | : | 650 meters |
| Active cable length | : | 12,000 meters (2 cables of 6000m each) |
| Seismic channels per cable | : | 240 (2 cables of 120 each) |
| Group interval | : | 50 meters |
| Number of phones (channels) per group | : | 2 (1 hydrophone and 1 geophone) |

## Instruments

| | | |
|---|---|---|
| System | : | WG-24A S/N 016 SYNTRON, Syntrak 480 |
| Tape format | : | SEG-D 8015 |
| Filters | | |
| • Low cut | : | 3 Hz, 6 dB/oct |
| • High cut | : | 218 Hz, 484 dB/oct |
| Record length | : | 6.144 seconds |
| Sample interval | : | 2 milliseconds |
| Channels | : | 240 per active cable |
| Recording delay | : | 32 milliseconds |
| Recording format | : | SEG “D” 8015 |

♦ *Polarity: for minimum phase data, « normal polarity » is defined as :*
***Compression = Negative number = Onset of white trough.***

## Positioning

| | | |
|---|---|---|
| Reference datum | : | WGS - 84 |
| Ellipsoid name | : | WGS - 84 |
| Projection | : | Universal Transverse Mercator (UTM) |
| Zone | : | 15 UTM |
| Central Meridian | : | $93^{o}$ West |
| Scale factor of Central Meridian | : | 0.9996 |
| False Northing (m) | : | 0.0 |
| False Easting (m) | : | 500000.00 |
| Latitude of origin | : | $0^{o}$00 North |

The raw Cantarell 3D OBC dataset was originally processed by Western Geophysical using the Omega System® in 1996-1997 as a part of the same acquisition-processing service agreement. This dataset has been reprocessed and conditioned more than once for different applications. In particular, the dataset used in this dissertation was reprocessed by Veritas DGC in 2003. The main goals of this reprocessing work were to improve the signal to noise ratio, to increase the frequency bandwidth at Cantarell-Sihil depths (which was demonstrated to have a dominant frequency of 8 Hz), and therefore to improve the structural image and faulting in the Sihil structure below Cantarell field. A Kirchoff Prestack Time Migration (PSTM) algorithm was added to address these purposes on an amplitude preservation basis. The following processing sequence and parameters were used by Veritas on the proprietary Tango System®:

### Data Processing Parameters

| | |
|---|---|
| Processing length | : 6 seconds |
| Processing sample rate | : 4 milliseconds |
| Resampling | : 2 milliseconds to 4 milliseconds |
| Nominal stacking fold | : 56 |
| Datum plane | : Mean sea level |

### OBC Reprocessing Sequence (Amplitude and Phase Preservation)

1. RAW DATA LOADING (Reformatting from SEG " D " TO TANGO® INTERNAL FORMAT)
2. NAVIGATION DATA LOADING (FORMAT P1-90)
3. SOURCE DESIGNATURE (MINIMUM PHASE CONVERSION)
4. RESAMPLING (2 msec to 4 msec)
5. SPHERICAL DIVERGENCE CORRECTION: $G(t) = t^2$
6. RECEIVERS AND SOURCES REPOSITIONING
7. RMS AMPLITUDE EDITION (ON STACKS OF COMMON SOURCES AND RECEIVERS)

8. PRELIMINAR VELOCITY ANALYSIS (ON A GRID OF 650 m X 650 m)
9. FAST-TRACK POST-STACK MIGRATION (hydrophone and the hydrophone-geophone summation independently). Both cubes were used just for preliminary interpretation purposes and for making decisions on the benefits of using the summation for ghost removal
10. ADAPTIVE FILTERING FOR PLATFORM NOISE REMOVAL
11. ADAPTIVE FILTERING FOR PIPES NOISE REMOVAL
12. HYDROPHONE AND GEOPHONE SUMMATION
13. PREDICTIVE SURFACE CONSISTENT DECONVOLUTION (Sources and receivers terms designed separately for velocity and pressure for a common minimum phase output and design of a predictive filter)
14. RANDOM NOISE ATTENUATION
15. 3D CDP BINNING
16. TIME VARIANT FILTERING (high-cut for high-frequency remotion)
17. PSTM Velocity model construction
18. KIRCHHOFF 3D PRE-STACK TIME MIGRATION WITH AMPLITUDE PRESERVATION
19. DATA PROCESSING AFTER PSTM AND STACKING
    - Residual Velocity Analysis (650m x 650m)
    - REVERSE NMO (using PSTM velocity field to remove this velocity field)
    - NMO (using residual velocity field)
    - MUTE (30 degrees, calculated with the PSTM velocity field)
    - STACK
    - FXY DECONVOLUTION
    - FK FILTERING (0 – 800 ms)
    - TRACE INTERPOLATION FOR FINAL CUBE PREPARATION (from a 25x12.5m grid to a 12.5x12.5m grid)
    - TIME VARIANT BANDPASS FILTERING
    - AGC (window: 1000ms)
    - TIME SHIFT TO SAME REFERENCE LEVEL AS THE ORIGINAL CUBE (–60 ms)

Figure 5.3 shows the fold coverage obtained after reprocessing of the seismic OBC survey over Cantarell field, whereas figure 5.4 shows a comparison between a

seismic line extracted from the reprocessed cube and the same line derived from the original dataset processed in 2003.

Additional comments regarding the seismic data quality and data conditioning are provided in the following sections.

### 5.3 Preliminary Seismic Data Evaluation

Cantarell Field is an operating field and ambient noise levels are high. Therefore, the first step in the seismic workflow of this dissertation was to evaluate the seismic data provided and attempt to enhance data quality at shallow levels where ambient noise and the seismic acquisition footprint disrupts the seismic signal, making the basic interpretation difficult. An extra objective was to determine the feasibility of conducting modeling and AVO analysis to help in the delineation and extension of the Utan #1 reservoirs and for further exploration of surrounding areas.

As a part of a larger collaborative project among Pemex-The University of Oklahoma-Fusion Geophysical, this research included seismic data conditioning, seismic-well tie and seismic attribute extraction activities led by the author of this dissertation and carried out at Fusion Geophysical offices in Norman, Oklahoma, and Houston, Texas, with the use of MicroSeismic Technology Kingdom Suite. Many of the seismic analyses conducted as part of this dissertation were done using this platform. Some other complementary seismic analyses and attribute extractions were

carried out with Hampson&Russell and Fusion proprietary software with participation of Fusion´s geoscientists.

The seismic OBC dataset reprocessed by Veritas gave some satisfactory results according to the objectives; nevertheless the complex Cantarell-Sihil system of compressive structures has always constituted a great challenge for seismic velocity analysis and structural interpretation even after the three seismic surveys were acquired. A basic seismic frequency analysis on the extracted subcube (figure 5.1) shows that the reprocessed PSTM volume has a fairly good frequency content for the first two seconds (Figure 5.5) with a bandwidth of 5-48 Hz and a dominant frequency of about 22 Hz.

Seismic resolution is a measure of how large an object needs to be in order to be seen on seismic data. The key parameter for extracting stratigraphic details from seismic data is the vertical and horizontal resolution. The vertical resolution refers to the ability to distinguish two close seismic events corresponding to different depth levels, and the horizontal or spatial resolution is concerned with the ability to distinguish and recognize two laterally displaced features as two distinct, adjacent events (Chopra et. al., 2006).

Broad frequency bandwidths, higher frequencies and short wavelengths provide better vertical and lateral resolution. These parameters are the main focus of seismic contractors specializing in acquisition designs, processing algorithms, seismic attributes and other applications of seismic interpretation. In particular, after seismic data have been acquired, data processing can greatly affect resolution: a proper

deconvolution can improve vertical resolution by producing a broad bandwidth with high frequencies and a relatively compressed wavelet, whereas migration techniques can improve lateral resolution by reducing the size of the Fresnel zone.

While both aspects are important for interpreting small features on seismic data, migration procedures have their own niche in collapsing the Fresnel zones to enhance spatial resolution whereas the way to improve the vertical resolution has still many variants in the market.

The vertical resolution is derived from the predominant wavelength of the seismic signal. A commonly used measure of vertical resolution inherent to the seismic data is referred to as the one fourth of a wavelength (¼λ), which is referred to as the tuning wavelength (Brown, 1996). With increasing depth the frequency of the signal will decrease while the velocity and wavelength normally increase assuming the sediments are gradually more compacted with depth. This means that with increasing depth the seismic resolution will be diminishing. The high frequencies are reflected from relatively shallow reflectors and the lower frequencies penetrate to greater depths.

The dominat frequency is normally used when calculating seismic resolution. This may lead to an underestimate, as high frequencies in the data may improve the resolution (Rafaelsen, 2003). Yilmaz (1987) indicates that not only the high frequencies resolve thin beds, but he shows examples of the importance of considering both low and high frequencies in a broad bandwidth for better time resolution.

The seismic wavelength is calculated by:

$$\lambda = v/f$$

where:

$\lambda$ = wavelength
f = seismic frequency
v = seismic velocity

Therefore, for the study area the average spectrum of the seismic wavelet at reservoir levels is centered around: $f_{dom}$=22Hz, whereas the velocity transmission is v= 2200m/s, so $\lambda$ = 100, and the vertical seismic resolution is calculated by: $\lambda/4$ = 25m. It means that reservoirs having a thickness less than 25m may not have their top and base resolved. Reservoirs at the study area are below this vertical resolution, thus are considered as thin beds from the seismic point of view.

Seismic velocity control was supplied in the form of a checkshot survey for the Utan-1 well (Figure 5.6); these time/depth pairs were used to initially tie the wells to the seismic data, thus the top of the upper pay zone was located at a TWT of approximately 0.979 seconds, the middle non-producer interval at 1.079 seconds, and the lower pay zone located at 1.146 seconds. Synthetic seismograms later provided the final ties. Very little lateral velocity variation was seen between wells in the shallow section. Therefore, the single Utan time-depth relation was used for the remaining selected wells in the study area.

## 5.4 Seismic Data Conditioning and Preparation for Attribute Extraction

After a quick-look review of the provided final stacks and unstacked gathers and having recognized the presence of noise and acquisition footprints in the seismic signal, pre- and post-stack analyses were performed to verify seismic quality at Tertiary levels and to evaluate the type of conditioning required to enhance the signal to noise ratio prior to basic seismic interpretation and attribute extraction. The process included determining if AVO studies would be feasible in the study area. After evaluation of processing tests, it was determined that data conditioning should include proper amplitude balancing, noise suppression on seismic gathers and the application of an adaptive filter. As a result of this procedure, ambient noise levels and the acquisition footprint effects were reduced, and more continuous reflections were finally obtained, even though the fold coverage was low at reservoir levels.

### 5.4.1 Seismic Prestack conditioning and AVO feasibility analysis

Tests were performed on CDP gathers to determine the best applications for noise reduction without affecting amplitude preservation. Bandpass filtering, Radon transform in the mode for noise suppression, and FX deconvolution (pre- and post-stack) to reduce random noise levels were applied to the data.

Additional tests were also taken into account to evaluate whether stack quality could be improved by eliminating the traces present at angles above 35 degrees, since these did not appear to contribute to the signal.

Based on evaluation of these and other results, it was decided to restrict the data in the final stack to 35 degrees. On the other hand, it was decided that FX Deconvolution should not be applied before stacking. Additional parameters selected for pre-stack seismic conditioning were:

- Bandpass Filtering (ormsby filter) with frequency bandwidth of 4-12-60-72 Hz
- Various noise reduction techniques on the gathers were evaluated. Radon filtering was selected using the next parameters: time windows: ±100 ms in the interval of interest; maximum number of values in the interval: 61; frequency bandwidth allowed: 6-60 Hz under parabolic modeling

Figure 5.7 shows a group of original gathers taken from the survey processed by Veritas without any other process applied, and the corresponding corrected gathers after conditioning. Ambient noise levels were effectively reduced and more continuous reflections were obtained even though the low fold coverage was low at Pliocene reservoir levels, indicating that reliable AVO analysis would not be feasible. As a matter of fact, figure 5.8 presents a closed caption of the same gathers showing the low number of traces available for shallow intervals, which corresponds to the fold coverage analysis presented in table 5.1. This low coverage can be considered a result of the original seismic design and acquisition geometry, which were designed for deeper targets.

| FOLD COVERAGE | | | | | |
|---|---|---|---|---|---|
| **TWT (ms)** | 400 | 600 | 800 | 1000 | 1400 |
| **Number of traces** | 2 | 4 | 5 | 6 | 9 |

**Table 5.1: Fold coverage analysis for shallow intervals**

### 5.4.2 Seismic Poststack conditioning

Once it was decided to restrict the data in the final stack to 35 degrees, new stacks for the survey were prepared. After post-stack analysis, severe acquisition footprint effects were noticed (figure 5.9). To enhance data quality, a Fusion proprietary data-adaptive noise-reduction filter (GradMAN®) was applied to the seismic data. The program performs a 3D adaptive gradient filtering based on a principal component analysis to remove components with undesirable spatial characteristics. The filter improves the lateral continuity without affecting the gradient to preserve the structural component of the data. For the application of this process a parameter setting the number of points to filter along the gradients (nxn) has to be defined by the user. The larger the number of points the smoother the filtered signal and the better the noise suppression. However, much care has to be taken to avoid losing the small details of the signal that may be related to stratigraphic features.

Several filter sizes were tested for a better preservation of stratigraphic features (3x3, 5x5, and 7x7). The 3D adaptive filter with a 3x3 size gave a satisfactory improvement to the output signal. As a result of this procedure, more lateral continuity and amplitude balance were obtained without affecting the small details of the signal. As a consequence, the acquisition footprint effects were much reduced at the target

level, although shallow footprints remain strong. Figure 5.10 shows a comparison between final pre- and post-stack conditioning on a seismic line extracted from the filtered seismic cube. The improvement in both continuity and signal to noise ratio is clearly seen after conditioning.

### 5.4.3 Synthetics and Phase tie

Zero-phase seismic data is an issue when thin layers are involved at reservoir level. Also, since spectral decomposition and seismic inversion for reflectivity require zero-phase data, an important part of this study was to perform a phase tie, between synthetic seismograms generated at control wells, including the discovery well, and the 3D seismic data. Figure 5.11 shows the base map with the wells considered for the seismic-well tie.

As a part of this process, the wavelet was extracted from the seismic using the adjacent traces in a subvolume surrounding the discovery well in a time window defined around the reservoir. The resulting wavelet gives a good estimate of the assumed zero-phase wavelet embedded in the seismic data. Afterward, a synthetic trace was generated using the extracted wavelet and the density and sonic log information. The resulting trace was compared to the seismic traces in the data volume at the well location. Using a zero phase wavelet a very poor correlation was obtained, which indicates that either the original seismic data is not zero-phase or the logs are unreliable. It was assumed that after the petrophysical analysis (Chapter 4) the well log data was reasonably acceptable so it was assumed that the seismic data should be

rotated to achieve the zero-phase requirements. A phase rotation was applied until the best tie between the synthetic and data traces was achieved. Finally, a +70 degrees phase rotation was applied to the seismic data in order to achieve the best regional correlation through the zero-phase requirement.

Synthetic seismograms were calculated by using a 25Hz Ricker wavelet, which proved to be a good representation of the "regional" wavelet, and correlated for 5 of the control wells in the study area (figure 5.11). Good ties were obtained for the Utan-1, C-3068 and C-429 wells (figures 5.12 to 5.14), whereas poor correlations were obtained for the C-2295 and C-468 wells, which reached the Pliocene targets at upper structural levels on the other side of the Kutz fault where a different seismic character, both lower signal to noise ratio and frequency content, are observed; consequently a different wavelet behavior could be expected. Both lower well log quality and low seismic signal to noise ratio might explain the poor tie for the C-2295 well. Figure 5.15 shows a random seismic line crossing all the control wells used for the well-seismic tie.

The tie between the synthetic seismogram for the discovery well and the +70 degrees rotated seismic data is shown in Figure 5.12. A reasonable tie can be observed. The same figure illustrates the final time tie of the log data to the seismic data for the three tested intervals in the Utan-1 well: the upper pay zone (Interval III) ties to a low-amplitude peak at approximately 0.940s, the lower pay zone (Interval I) ties to a low-amplitude peak at approximately 1.100s, whereas the middle tested interval ties at 1.035s.

The rotated data were then used for the following processes and analysis. A critical step to compare effectiveness of various attributes in the study area, particularly the spectral decomposition and the seismic inversion for reflectivity, was the good tie achieved between the wells and seismic data after this process.

## 5.5 Some basic concepts on the seismic attributes used in this research

Chopra and Marfurt (2005), define a seismic attribute as "a quantitative measure of a seismic characteristic of interest". Nowadays, the seismic industry accounts for dozens of attributes applied to the interpretation of geologic structure, stratigraphic features, and rock/pore fluid properties.

Basic and advanced attributes were applied to the seismic data in the study area in order to enhance subtle or hidden features for stratigraphic correlation as well as for fluid detection and discrimination, with the intent to better interpret the seismic data.

### 5.5.1 Basic seismic attributes

Some basic attributes were extracted from the seismic signal by the use of the Petrel™ software and attribute library. The library includes basic attributes divided into the system according to specific tasks: complex trace attributes, structural attributes and stratigraphic attributes. Among them, the following attributes were selected to be applied to key sections of the seismic database used for this dissertation. Due to the nature of these basic attributes, no input parameters were required in all of the cases.

**Instantaneous Phase (complex-trace attribute)**

When a seismic trace is considered as an "analytical signal g(t)", it can be expressed as a complex function $g(t)=f(t) - i\,H[f(t)]$. Complex-trace analysis treats the seismic trace amplitude as the real part of the (complex) analytical signal while the imaginary part of the signal is computed by taking its Hilbert transform. Hilbert transform can be seen as a type of filter which changes the phase in ±90° without affecting the amplitude of the spectral components (Larner, 1998).

The above argument is the base for the well known single-traced "instantaneous attributes": instantaneous envelope, instantaneous phase and instantaneous frequency, as well as other seismic attributes derived from them including the cosine of phase. Complex-trace analysis numerically quantifies subtle changes in envelope, amplitude and phase (Chopra and Marfurt, 2005).

Instantaneous phase is the phase of the analytic signal derived from the Hilbert transform. The attribute is calculated on a sample by sample basis without regard to the waveform. The attribute provides an amplitude independent display which is especially useful for tracking reflector continuity which vary greatly in their amplitude. The attribute appears as discontinuous at trough locations (±180 degrees). The instantaneous phase emphasizes spatial continuity/discontinuity of reflections by providing a way for weak and strong events to appear with equal strength. The attribute tends in this way to enhance weak events, detect unconformities, and to distinguish small faults and dipping events but also enhances noise. Seismic sequence

boundaries, sedimentary layer patterns and regions of onlap/offlap patterns often exhibit extra clarity when used together with Cosine of Instantaneous Phase.

**Cosine of Instantaneous Phase (complex trace attribute)**

Also derived from the Hilbert´s transform, this attribute, also known as "Normalized Amplitude", is the cosine of the instantaneous phase. It has the same uses as Instantaneous Phase with one additional benefit: it is continually smooth. It is -1.0 for both 180 degrees and -180 degrees, avoiding the ± 180 degrees discontinuity that occurs with instantaneous phase, thus many times more preferred by the interpreters. Amplitude peaks and throughs retain their position, but with strong and weak events now exhibiting equal strength.

It may help to enhance the definition of structural delineations and stratigraphic features, providing better continuity to the seismic signal when used together with Instantaneous Phase for comparison. No inputs parameters are required.

**Gradient Magnitude (structural attribute)**

This attribute is the magnitude of the instantaneous gradient (first derivative) computed in three-dimensions of the sample neighborhood. No input parameters are required.

**Relative Acoustic Impedance (stratigraphic attribute)**

This attribute is a running sum of regularly sampled amplitude values. It is calculated by integrating the seismic trace, and passing the result through a high-pass Butterworth filter, with a hard-coded cut-off at (10*sample rate) Hz. This is not a

seismic inversion for impedance process but a type of fast-track attribute which does not require input parameters.

Figures 5.16 and 5.17 show the application of the above attributes to the seismic lines crossing the Utan-1 well in both in-line and cross-line directions. These basic attributes do not require any parameter input so they are not model-based and have to be used only as a first approach in initial seismic interpretations. In the study area, the most useful basic attributes for enhancing and picking key horizons in low signal to noise regions were Instantaneous Phase and Cosine of the Instantaneous Phase.

### 5.5.2 Advanced seismic attributes

Advanced seismic attributes such as spectral decomposition, seismic inversion for reflectivity, seismic inversion for impedance, and amplitude versus offset were considered at the planning phase of this dissertation to validate how much they could enhance some stratigraphic features, or how sensitive they might be to quantify rock/pore fluid properties in this type of mixed siliciclastic-carbonate setting. The accuracy of predicting a reservoir property from seismic data improves when those attributes that statistically are different, but present a significant correlation to certain physical properties, are properly combined for the interpretation.

## Spectral Decomposition

Broadly speaking, we apply the principles of spectral decomposition any time we extract a wavelet or look at a spectrum (Hall, 2006). While seismic processors have long used spectral decomposition, over the last seven years or so, spectral decomposition has become a more powerful seismic interpretation process. Recent qualitative applications include seismic geomorphologic analysis (e.g., Chopra and Marfurt, 2006), and quantitative schemes to compute variability of temporal bed thickness (as described by Partyka et al., 1999). It has also been applied to direct hydrocarbon detection (e.g. Burnett et al., 2003). Particularly, over the last years spectral decomposition applications have been more widely used for the detection of gas in conventional and unconventional reservoirs (e.g. Mendez et al. 2003, Decker, 2004).

Spectral decomposition analysis is conceptually analogous to AVO analysis: because a conventional stacked trace is made up of data from different offsets each of which can be analyzed independently, a conventional stacked trace is also made up of data from different frequencies each of which can be analyzed independently (figure 5.18). The range of frequencies and dominant frequency present in a seismic data set and the corresponding amplitude spectrum at any given subsurface point depend on several factors, including seismic field acquisition parameters, processing flow and the earth filtering effects. Therefore, a conventional stacked trace or volume contains

information from a range of frequencies and when conventional amplitude analysis is performed, it is effectively based on the dominant frequency of the seismic data.

Traditionally, spectral decomposition techniques have used methods that require the use of a time window (windowing methods) including Fourier transforms and maximum entropy to decompose the seismic trace into its constituent frequencies. These windows produce serious distortion of true spectra and/or severely limit the vertical resolution, introducing unwanted artifacts into the data according to the selected time window size. Discrete spectral energy from individual reflection events that fall inside the window are mixed together, and when the window length is shortened to minimize this problem, frequency discrimination is compromised. The windowed techniques do not preserve the individual reflection events and introduce distortions and artifacts. (Burnett et al, 2003; Hall, 2006).

In order to avoid windowing effects, different methods have been tested. Continuous wavelet methods (CWT) and Matching Pursuit Decomposition (MPD) have been two of the most commonly applied methods.

The CWT has a great disadvantage in that the wavelets utilized must be orthogonal (Castagna and Sun, 2006). On the other hand, MPD is a more computationally intensive process which involves cross-correlation of a wavelet dictionary against the seismic trace. Castagna and Sun (2006), describe the MPD process as:

> *The projection of the best correlating wavelet on the seismic trace is then subtracted from that trace. The wavelet dictionary is then cross-correlated against the residual, and again the best correlating wavelet*

> *projection is subtracted. The process is repeated iteratively until the energy left in the residual falls below some acceptable threshold. As long as the wavelet dictionary meets simple admissibility conditions, the process will converge. Most importantly, the wavelets need not be orthogonal. The output of the process is a list of wavelets with their respective arrival times and amplitudes for each seismic trace.*

Mathematically speaking, MPD provides a good estimation of regularity. Physically speaking, MPD is based on certain assumptions as genetic algorithms do. The decomposition of a signal emulates an atomic decomposition where the signal is made over elements (atoms) from some selected set (dictionary) of uniquely defined elements. The matching pursuit algorithm consists of subtraction from the decomposed signal that atom, which one has, at the given iteration, the greatest coherence with the signal, which is left out after the previous subtractions (Kouzoub and Ronquillo-Jarillo, 2002). In any case, the selection of base atom (prototype) for layout of the dictionary results is of primer importance in the process. The prototype, retrieved from the seismic section itself–adapted dictionary and an analytical basic wavelet based on the second (or higher) derivative of the function of probability of Gauss–not adapted dictionary are two options explored by Kouzoub and Ronquillo-Jarillo (2002).

The wavelet transform time-frequency spectral analysis based on MPD eliminates windowing and consequently has higher temporal resolution avoiding distortions (Shengjie and Castagna, 2002). Nowadays, according to Chopra and Marfurt (2005): *most workers prefer the wavelet transform-based approach introduced by Castagna et al. (2003) over the original discrete Fourier transform*. Castagna´s technique is a high-resolution spectral analysis that utilizes wavelet transforms and a

derivation of MPD, the Exponential Matching Pursuit Decomposition (EPD), to eliminate windowing problems.

By using the technique of instantaneous spectral decomposition, it is possible to generate multiple seismic volumes for each frequency, providing a frequency spectrum for each time sample of each seismic trace that will require subsequent analysis of particular sub-attributes like peak amplitude and peak frequency (figure 5.19). Spectral decomposition provides this by generating a series of sections, maps or cubes.

Spectral decomposition analysis is conceptually analogous to AVO analysis. Individual “events” on a frequency gather can be picked and their amplitudes plotted, thereby showing the variation of amplitude of that subsurface point with changing frequency. The data resulting from spectral decomposition can be used to prepare a range of displays or volumes that observe the response of the reservoir to different frequencies. These are then animated allowing the interpreter's eye to catch subtle changes in the reservoir, tuning frequencies and peak frequencies. The different products include (figure 5.20):

- A frequency gather corresponding to a single seismic trace
- A single frequency vertical section, time slice or 3D cube
- Single frequency maps for a given horizon (showing lateral variation in amplitude for that frequency)
- Peak frequency vertical displays, 3D volumes or maps
- Peak amplitude vertical displays, 3D volumes of maps

Typical applications of the spectral decomposition data have included:

- direct detection of hydrocarbons through a distinctive spectral response or attenuation/low frequency shadows beneath reservoirs
- bed thickness estimation
- reservoir quality prediction

The spectral decomposition attributes have been particularly successful in delineating stratigraphic traps and identifying subtle frequency variations caused by hydrocarbons (Portniaguine and Castagna, 2004). For instance, spectral decomposition, using wavelet transforms, has been successfully applied with these purposes by the author of this dissertation in all the gasiferous basins of Mexico, i.e. Burgos and Macuspana basins (Mendez, 2003; Mendez et al, 2003; Burnett et al., 2003) (figure 5.21), as well as in Veracruz and Lankahuasa basins during the past few years. Therefore, the attribute was selected to be tested in the Pliocene gas plays of the Utan area.

**Thin bed seismic spectral inversion for reflectivity**

As reviewed in Chapter five, seismic resolution involves two aspects, vertical resolution and horizontal resolution. They are the key for extracting stratigraphic detail from seismic data. From them, seismic industry has paid more attention on how to enhance vertical resolution assuming that, independently of acquisition data effort, migration techniques in data processing are the best way to collapse Fresnel zones and improve horizontal resolution. It is also well known that vertical resolution is driven

by the wavelength of the seismic data, which in turn is closely related to the frequency content of the seismic signal.

Seismic inversion has been a largely used process to extract more comprehensive information from seismic data and a way to improve vertical resolution. Conventional seismic inversion for impedance, i.e. acoustic inversion, involves post-stack inversion techniques, which provide an acoustic impedance model with increased bandwidth through the inclusion of a low frequency component. On the other hand, spectral inversion is a post-stack inversion technique, which operates in the frequency domain removing the seismic wavelet and extracting reflectivity without blowing up noise at high frequencies, with corresponding improvement in seismic resolution (Chopra et al., 2006). The result ia a novel way of extracting reflection detail and stratigraphic features from seismic data.

Spectral inversion is a last generation technique whose principles came out to the seismic industry in 2004 (Portniaguine and Castagna, 2004), being refined in 2005 (Portniaguine and Castagna, 2005), and recognized by the industry in the following years (Chopra et al., 2006; Mendez et al., 2006; Dwan et al., 2007; Chopra et al., 2008). Commercial application is the algorithm known as Thinman$^{TM}$. According to Chopra et al. (2006), the benefits of this technology in deconvolving the complex seismic interference patterns from seismic data are changing the conventional mind set of interpreters and yield interpretable stratigraphic patterns with remarkable detail.

Inverse spectral decomposition is a method which spectrally decomposes a seismic trace by solving an inverse problem. Portniaguine and Castagna (2004)

postulate the principle that the reverse wavelet transform with a library of complex wavelets could serve as a forward operator in the inverse spectral problem. The inversion reconstructs the wavelet coefficients that represent the seismic trace satisfying an additional constraint needed to reduce the non-uniqueness of the inverse solution. After testing, the authors conclude that the sparse-spike constraint produces solutions with better time and frequency resolution than the minimum L1 norm, and the minimum L2 norm. The choice of the wavelet library (and hence the choice of forward operator) is a critical factor in determining the utility of the spectral decomposition. These were the basis of the named "spiky spectral decomposition".

After the above reasoning developed in 2004, spectral inversion was later refined as a form of sparse-spike inversion in that it outputs a sparse reflectivity series (Portniaguine and Castagna, 2005). However, the spectral inversion rather than being driven to achieve maximum sparseness, computationally relies on aspects of the local frequency spectrum obtained using spectral decomposition. Therefore, thin bed inversion resulted in a trace-by-trace operation which takes in a single stacked seismic trace, applies spectral decomposition and produces high-resolution reflectivity model trace as an output. Details of the process are still proprietary but the method essentially consists of following steps (Chopra 2008):

1. *Making accurate estimation of a time and space varying set of wavelets from the data. For this purpose having some well control is desirable. In the absence of any well control, a statistical method of wavelet estimation is adopted.*
2. *Wavelets estimated in step 1 are removed from the data using seismic inversion with spectral constraints that have their roots in spectral decomposition procedures. It is important to note that*

> *no starting earth model or interpretation is used in the inversion procedure. The trace-by-trace procedure requires no starting model and has no lateral continuity constraints.*

Under the spectral inversion assumptions, the spectrum of a local seismic response is taken to be a superposition of sinusoidal transfer functions associated with reflection coefficient pairs. Thus, the output time domain reflectivity series is a superposition of odd and even impulse functions; spectral inversion, by appropriately weighting odd and even components of reflection coefficient pairs, can thus achieve the best possible combination of resolution and robustness to noise (Dwan et al., 2007). As it happens with all sparse-spike type inversion techniques the frequency bandwidth of the output reflectivity series is broader than the input seismic data.

The inverted reflectivity as a series of impulses can then be integrated to produce a band limited impedance estimate that is unbiased by existing well information. While the impedance estimate will show lower apparent vertical resolution than the reflectivity, it is especially useful for stratigraphic differentiation of the strata themselves rather than the stratal boundaries (Portniaguine and Castagna, 2005).

Chopra (2006), making reference to Tirado (2004; "*Sand thickness estimation using spectral decomposition"*, MS Thesis, University of Oklahoma), points out a strong dependence of peak frequency extracted from spectral decomposition on bed thickness (Figure 5.22). A particular simulated case is represented by Chopra et al. (2006) as a 2-point reflectivity sequence shown at the top of figure 5.23. Mathematically, the model can be represented as the sum of an odd part consisting of a

pair of equal and opposite reflection coefficients (Widess model-type), and an even part composed of two reflection coefficients of the same polarity. The odd part resulted in this particular case with stronger reflection response than the even part. After modeling on these two components, for the odd component the amplitude first increases (tuning) and then decreases as the thickness gradually reduces. For the even part this variation is just the opposite (base of figure 5.23).

The above was a particular case of thin bed reflectivity, however most real situations would require both of these contributions, depending on the relative magnitude of the reflection coefficients in the two additive components to provide more possible contribution from one component with respect to the other. The even part may be relatively weak as in the case of bright spots, so noise rather than the dominant frequency, would control the fundamental limit of resolution (Portniaguine and Castagna, 2005).

Figure 5.24 shows the peak amplitude and peak frequency variation respectively with thickness for the same case of figure 5.23, where the odd part is significantly stronger than the even part. Notice that the total peak frequency (sum of the contributions from the odd and even components) shows a variation. When the reflection coefficients at the top and the base of a thin bed are not exactly equal and opposite, a more general behavior is observed, where the peak frequency decreases as thickness decreases below about half of the tuning frequency. Exactly at what thickness this rollover occurs depends on the relative magnitudes of even and odd

reflection coefficients. Contrary to the Widess model, below this rollover there is a strong dependence of peak frequency on thickness.

The importance of the even component in the final resolution of the output time domain reflectivity series, considered as a superposition of odd and even impulse functions, is illustrated by Dwan et al. (2207), when punctuate that:

a) Odd impulse functions (as Widess model) shows have a resolution limit of about 1/8λ, below which the response is approximately the derivative of the seismic wavelet, irrespective of layer thickness. As an odd impulse pair thins below this limit, the peak frequency of the response remains relatively constant while the amplitude decreases almost linearly with thickness. According to this model, for layer thickness below 1/8λ one cannot separate differences in reflection coefficient magnitude from changes in layer thickness (even in the absence of noise), so this value is generally considered the theoretical limit of seismic resolution (it was shown before that due to noise presence and wavelet imperfections this value could be taken as 1/4λ).

b) For even impulse pairs, response frequency varies continuously with layer thickness and, in the absence of noise, layer thickness and reflection coefficient magnitude can both be precisely determined. Thus, for an isolated layer with an even component of reflectivity, resolution is nearly perfect in the absence of noise.

Spectral inversion, by appropriately weighting odd and even components of reflection coefficient pairs, can thus achieve the best possible combination of

resolution and robustness to noise. As is the case with all sparse-spike inversion methods, the output reflectivity series contains frequency components outside the band of the original seismic data. This suggests that the seismic response is more sensitive to thin beds than generally thought previously. From this analysis Chopra et al. (2006) conclude that the Widess model for a thin bed is a very special case of a more accurate combination of reflection coefficients and that the behavior predicted by Widess becomes more atypical as thickness approaches zero.

As the seismic amplitude and frequency vary continuously far below the conventional view of the limit of seismic resolution, it is possible to infer thickness below the seismic sample rate. This implies that frequency beyond the seismic data bandwidth can be recovered and thicknesses far below tuning can be resolved. As the spectra of impulse pairs are sinusoids with infinite frequency content, in the absence of noise, all frequencies out to Nyquist can theoretically be recovered. Dwan et al. (2007) mention that filtering back to the original bandwidth of the data reproduces original data – the process is thus amplitude preserving and does not introduce “false” events.

Chopra et al. (2008) emphasize that this method is driven by geological rather than mathematical assumptions and keys on aspects of local frequency spectrum obtained by using spectral decomposition. In this row, Dwan et al. (2007) refer that if one uses the a priori knowledge that sedimentary rocks are generally layered, and if one assumes that only layers of significant thickness are of importance, then the broad-band spectrum is simply a superposition of sinusoids.

Recapitulating, the increased resolution to resolve thin layers below the tuning thickness of the spectral inversion process, can be achieved by the contribution of the even part of the seismic waveform by appropriately weighting odd and even components of reflection coefficient pairs, thus achieving the best possible combination of resolution and robustness to noise as well as by the proper knowledge of the wavelet. Also, the broader the bandwidth of the original data, the more robust the process is against noise.

Resolution deteriorates as the even part is weaker (especially in bright spots, where noise rather than dominant frequency will control the level of resolution), the noise level increases and imperfections in the wavelet estimation are present. If wrong parameters are selected, non-geological artifacts may result, thus Dwan et al. (2007) remark that some quality control displays including inversion result panels as a function of stabilization and wavelet parameters are imperative during the process.

Dwan et al. (2007) conclude that if the original bandwidth is broad enough, the signal-to noise ratio is high enough, there is sufficient even component to the signal, and the assumptions about layering are valid, experience indicates that useful results that tie well control can be obtained out to 2 or 3 times the original bandwidth. This broadband sparse reflectivity spectral inversion, i.e. thin-bed inversion, outputs a reflectivity series and its apparent resolution is far superior to the input seismic.

Common applications of this technology include precise mapping of tops and bases of thin layers, layer thickness determination, stratigraphic visualization and DHI analysis of thin reservoirs. The algorithm has been applied successfully in Mexican

basins as Veracruz, Lankahuasa, and Tampico-Misantla (figure 5.25). Current applications include a project led by the author of this dissertation in the onshore Chicontepec basin of Mexico (figure 5.26).

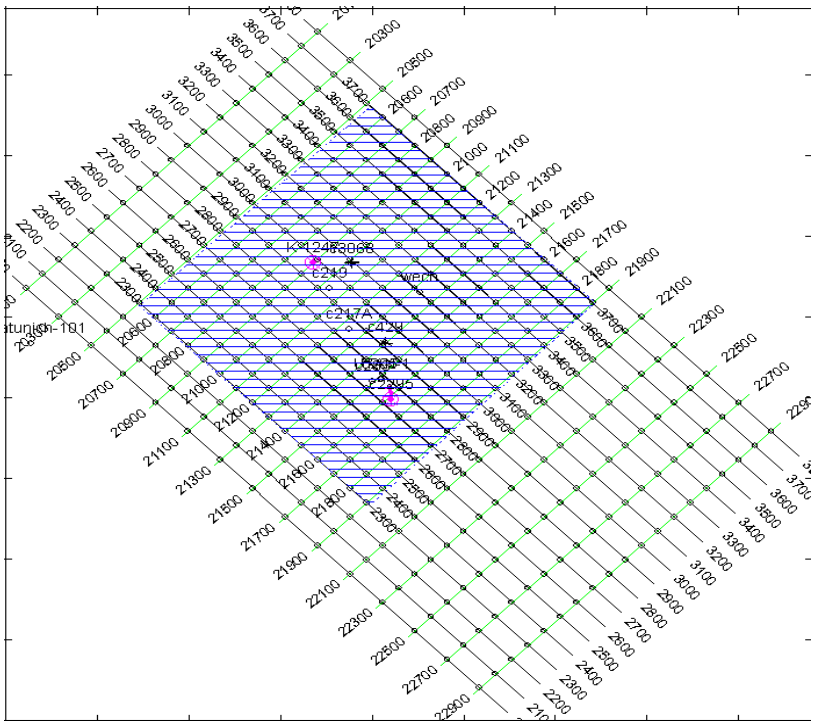

**Figure 5.1: Seismic base map of the entire Cantarell OBC 3D volume area showing survey orientation and the extracted study area.**

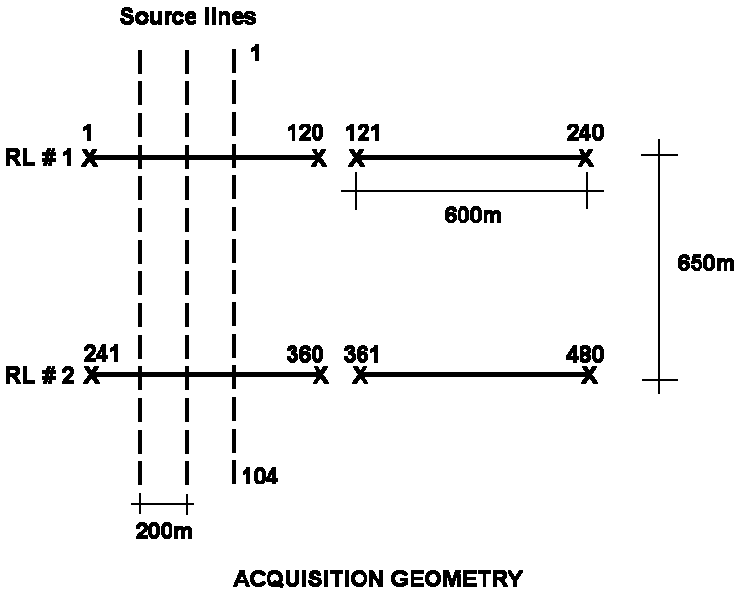


**Figure 5.2: Acquisition geometry layout for the 3D seismic Ocean Bottom Cable (OBC) survey, acquired in 1996 over Cantarell Field.**

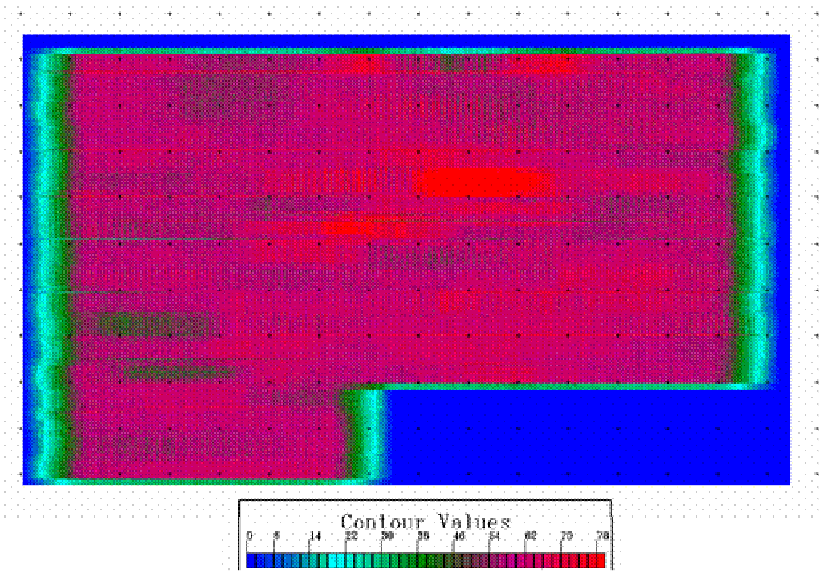


**Figure 5.3: Fold coverage for the entire 3D seismic OBC-PSTM survey reprocessed by Veritas in 2003 (non-published Pemex internal reports).**

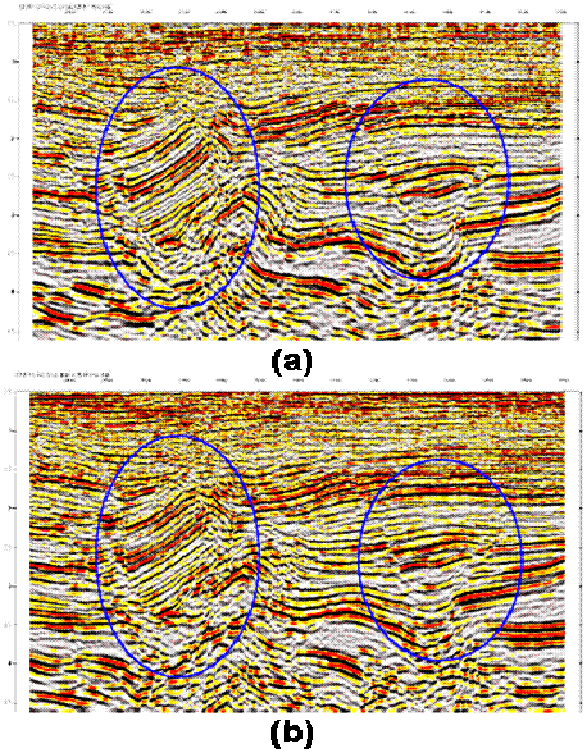


**Figure 5.4: Comparison between a line extracted from: (a) the seismic OBC dataset reprocessed in 2003 (wider frequency bandwidth for structural objectives), and (b) the original seismic data set processed in 1997 (non-published Pemex internal reports).**

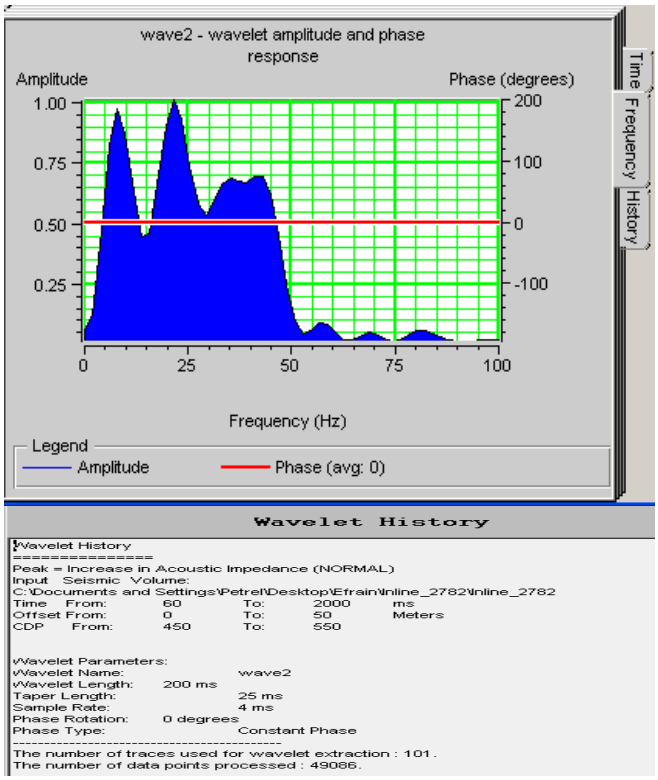


**Figure 5.5: Frequency spectrum of Cantarell OBC PSTM volume. Note dominant frequency of about 22 Hz. The history of the statistical wavelet extraction is also shown.**

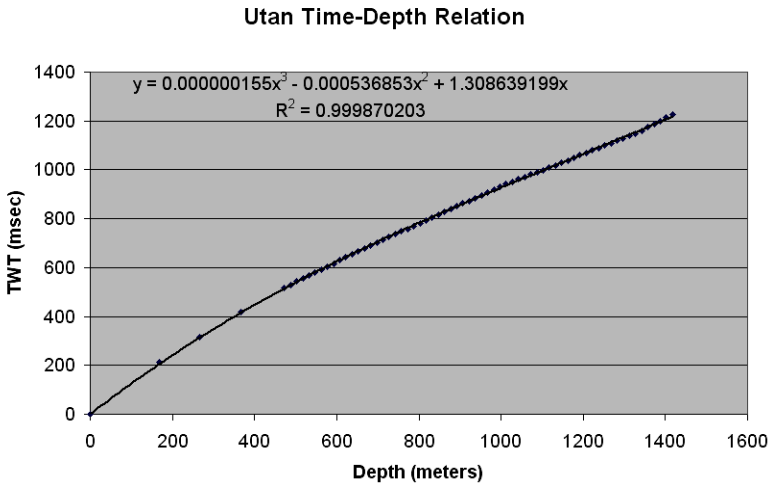


**Figure 5.6: Check shot data for the Utan-1 well. A third-order polynomial fits the points very well.**

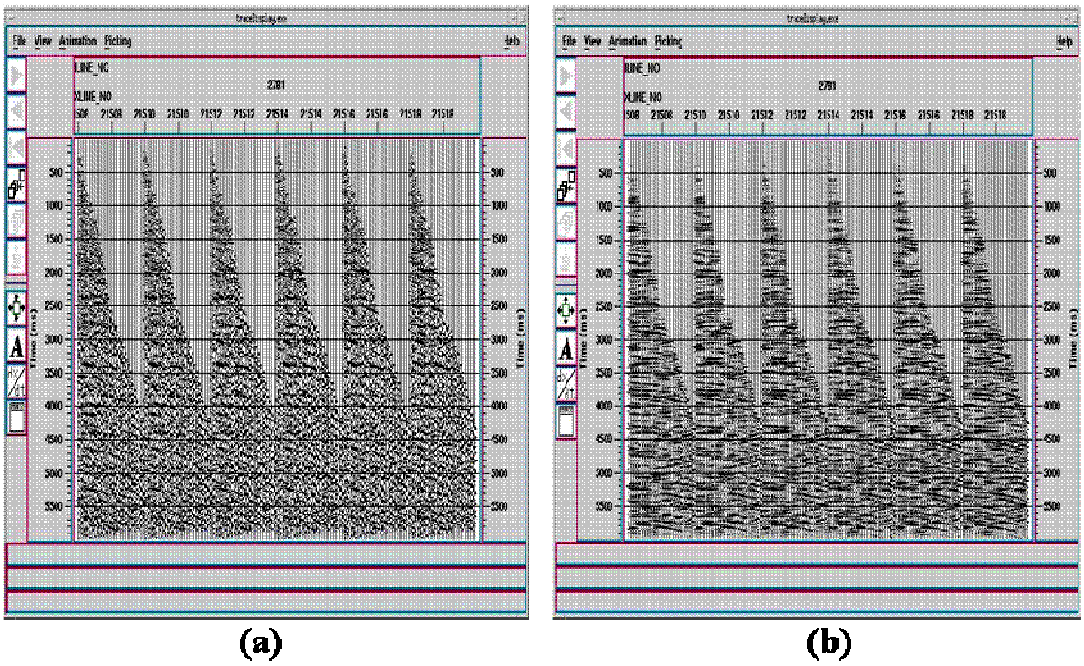


**Figure 5.7: Seismic pre-stacked time migrated CDP gathers a) pre-, and b) post-conditioning. After conditioning, ambient noise levels were reduced and more continuous reflections were obtained.**

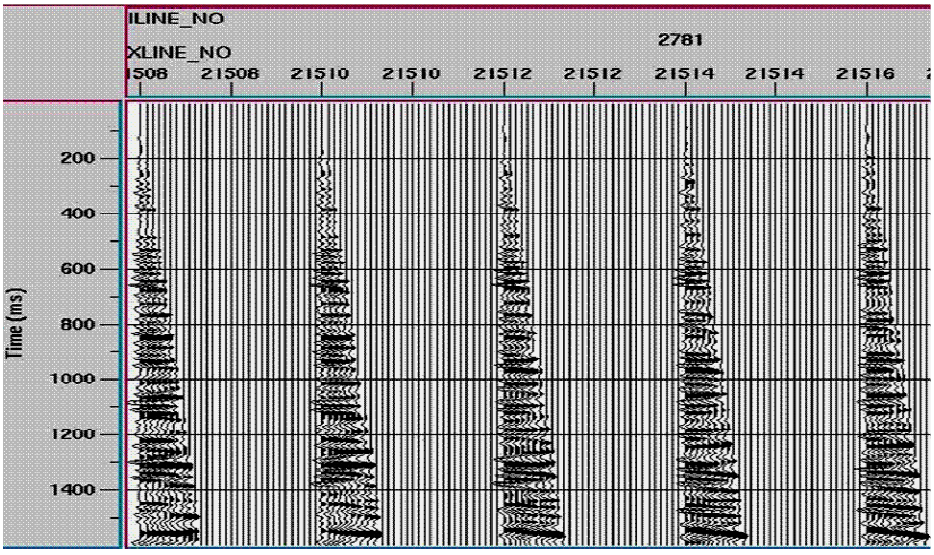


| FOLD COVERAGE | | | | | |
|---|---|---|---|---|---|
| TWT (ms) | 400 | 600 | 800 | 1000 | 1400 |
| Number of traces | 2 | 4 | 5 | 8 | 9 |

**Figure 5.8: Fold coverage analysis for shallow intervals in the Cantarell seismic OBC - PSTM volume.**

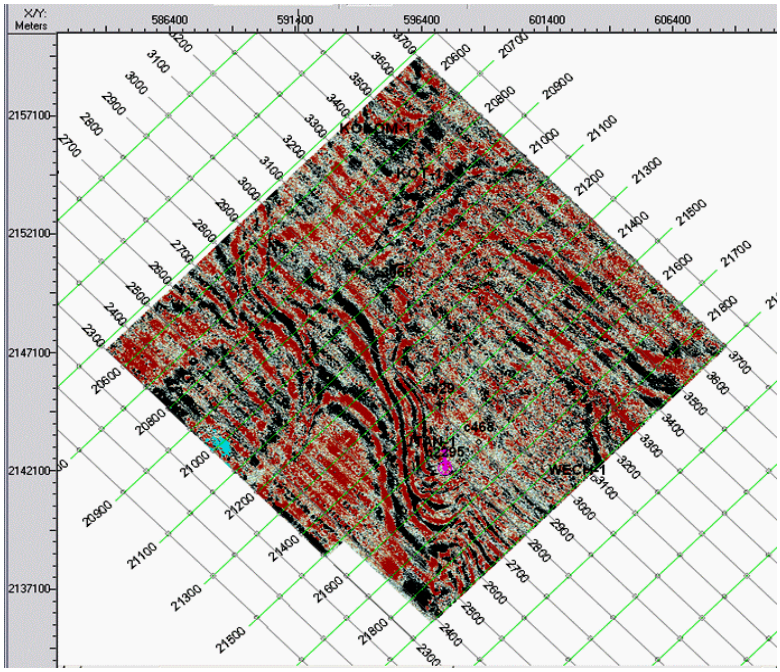


**Figure 5.9: Time-slice extracted from the Cantarell seismic OBC volume showing effects of acquisition footprint on shallow level amplitudes (strips northwest-southeast oriented).**

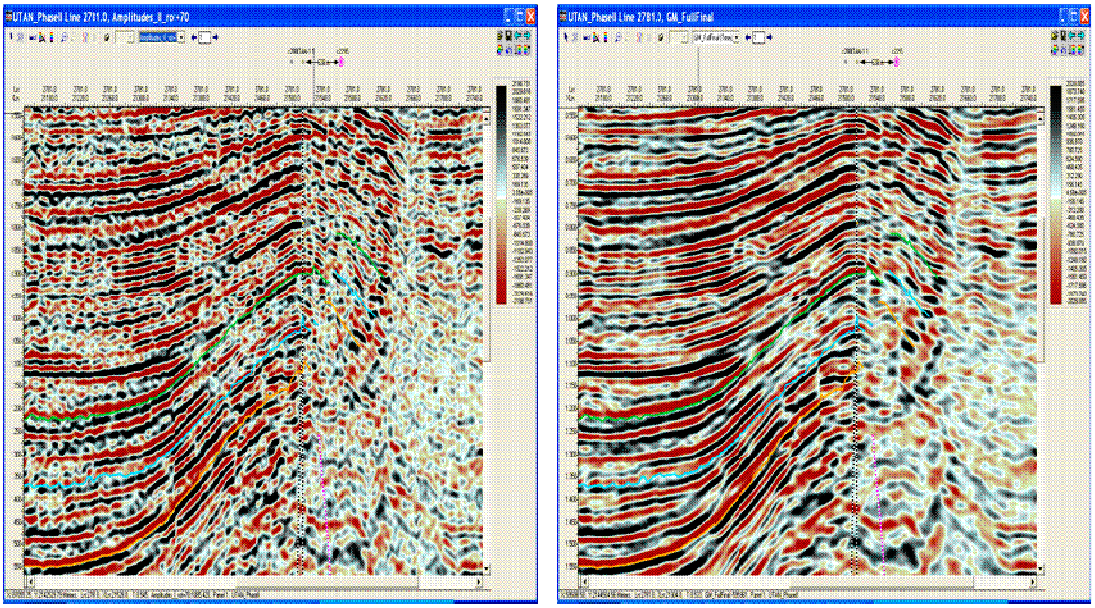


**Figure 5.10: Post-stack seismic data a) pre-, and b) post-conditioning. Ambient noise and the acquisition footprint effects were favorably reduced after conditioning to obtain more continuous reflections.**

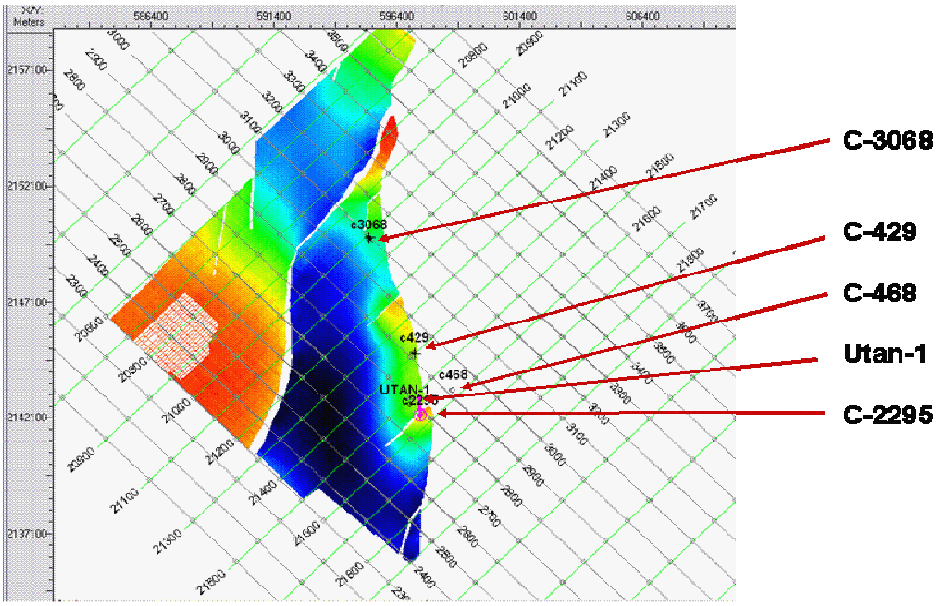


**Figure 5.11: Base map of the Cantarell OBC 3D volume area. Also displayed are the well locations used as control and the time structure of the upper reservoir.**

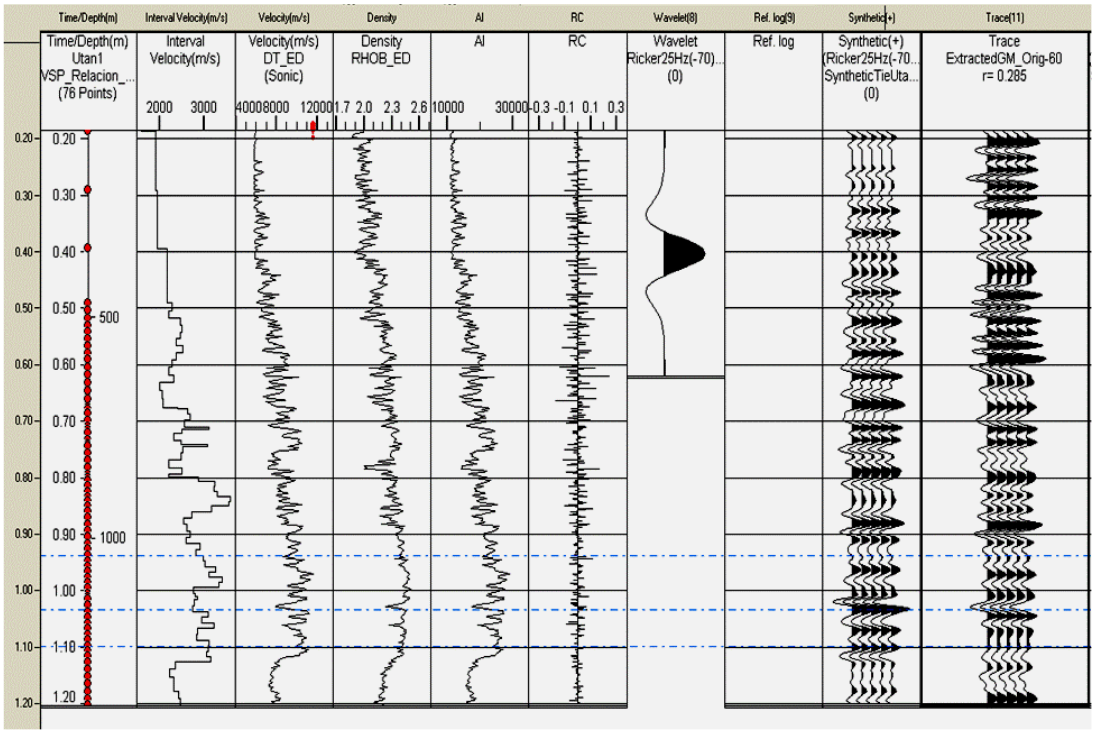


**Figure 5.12: Seismic-well tie for the Utan-1 well. A 25Hz Ricker wavelet demonstrated to work as a good "regional" wavelet for the west side of the fault. The wavelet size in the figure is schematic. The three tested intervals are shown.**

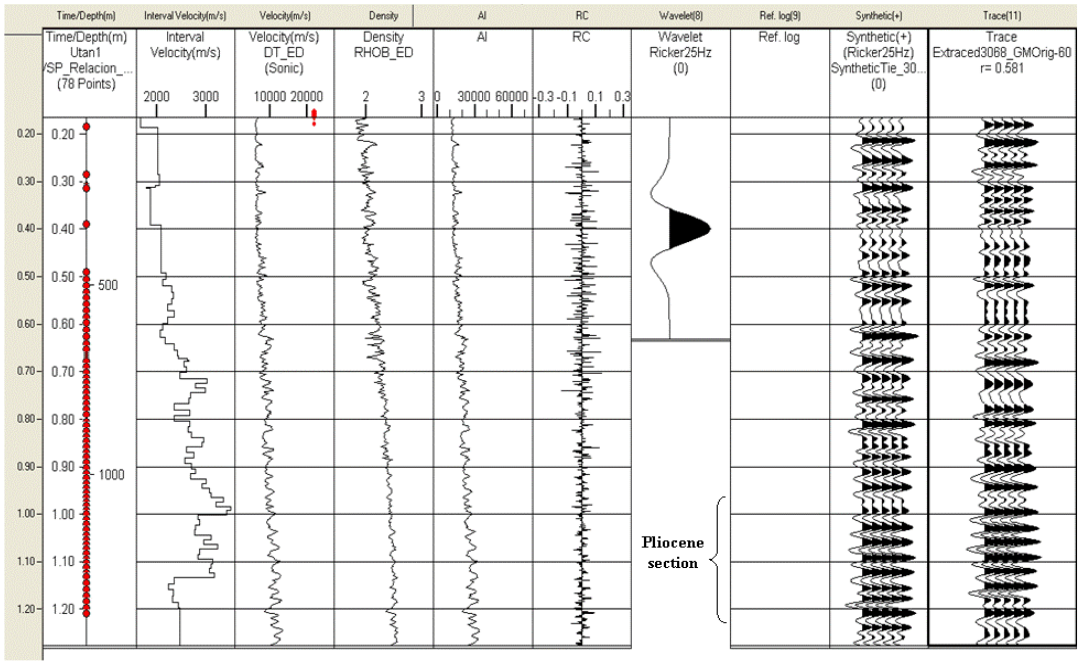


**Figure 5. 13: Seismic-well tie for the C-3068 well. Good seismic to well tie is reached. The wavelet size in the figure is schematic.**

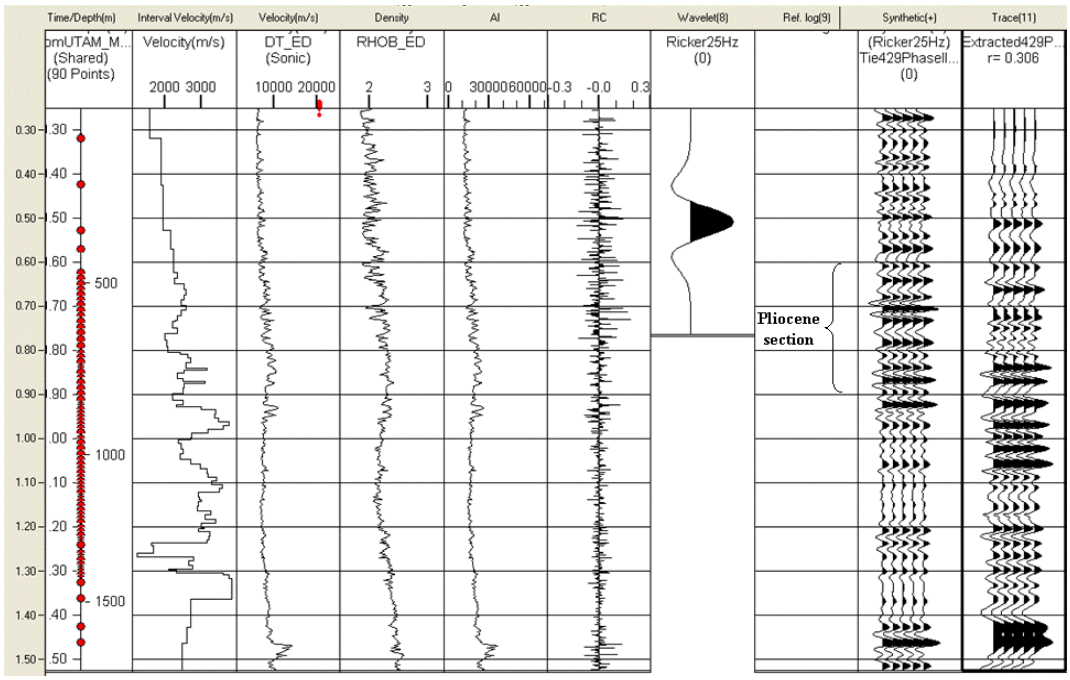


**Figure 5. 14: Seismic-well tie for the C-429 well. Pliocene section is shallower at the east side of the Kutz fault where both signal to noise ratio and well to seismic tie diminish. The wavelet size in the figure is schematic.**

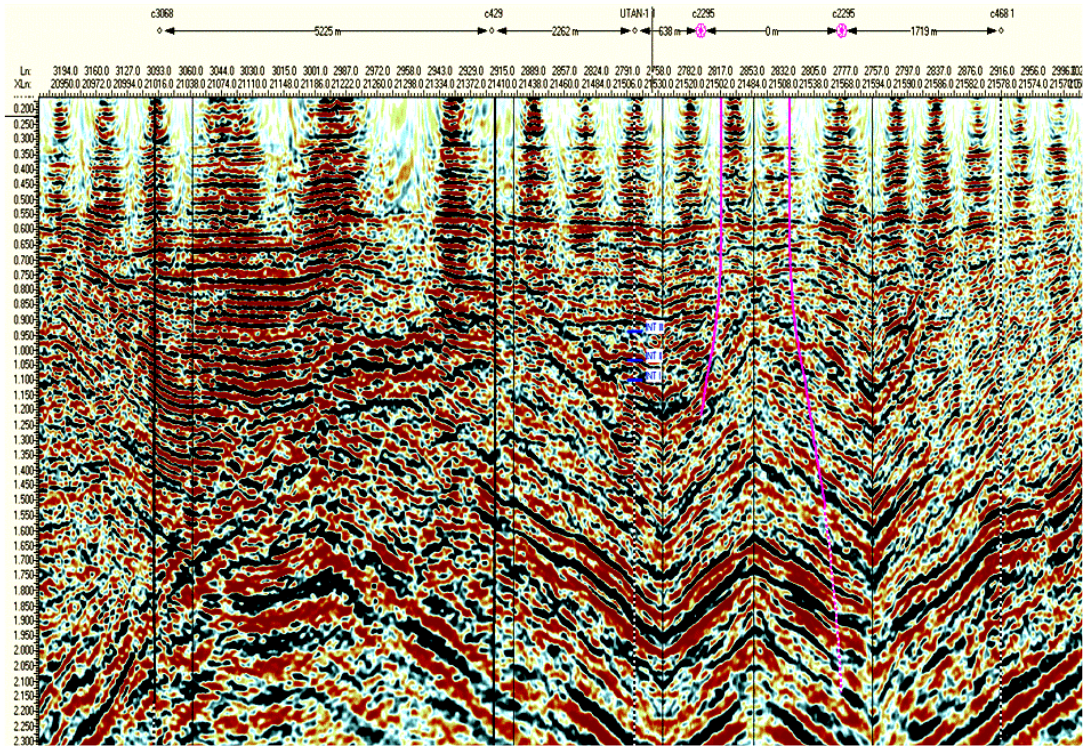


**Figure 5.15: Random line crossing the control wells utilized for the seismic-well tie and phase rotation. The Kutz fault cut the continuity of the lower intervals affecting the well to well correlation.**

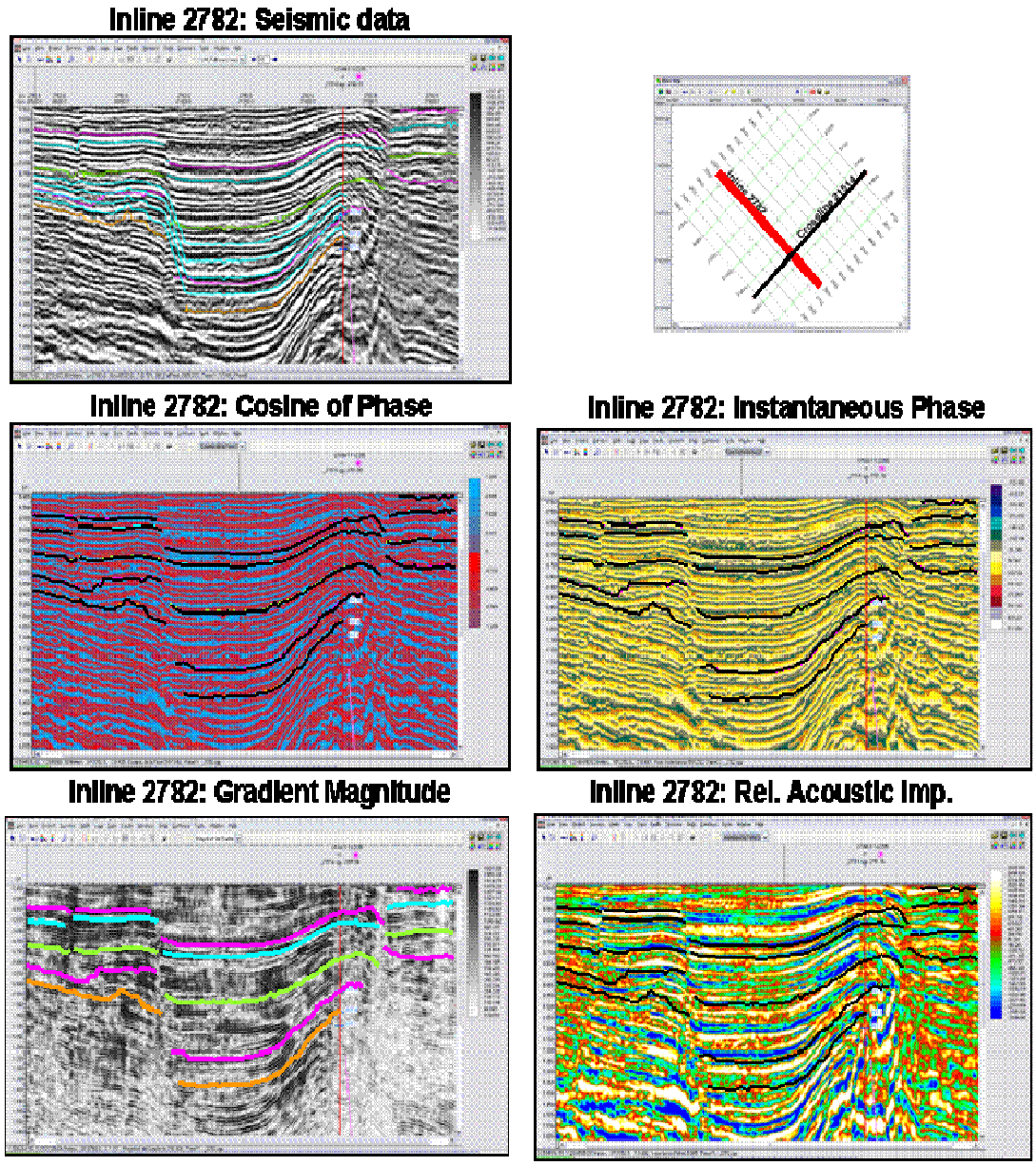


**Figure 5.16:** **Basic attributes applied to In-line 2782. Original seismic data and corresponding picked marker horizons are shown as reference. These attributes do not require any parameter input. Therefore, they were only used to provide better continuity to the seismic signal in order to enhance the definition of structural delineations and some stratigraphic features. Cosine of Phase and Instantaneous Phase were the most helpful in this sense.**

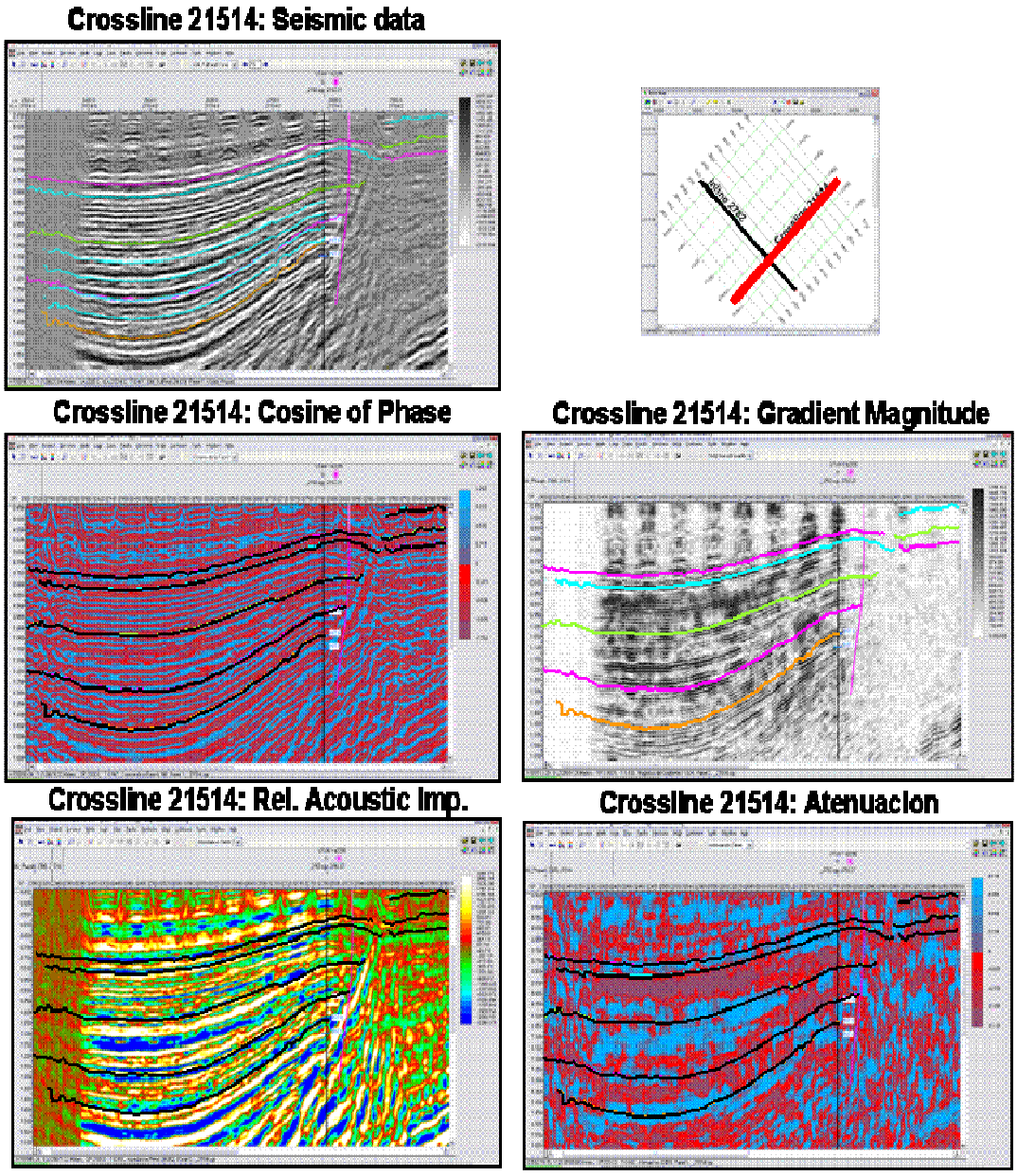


**Figure 5.17: Basic attributes applied to Cross-line 21514. Original seismic data and corresponding picked marker horizons are shown as reference. As it was explained in figure 5.16 these basic attributes do not require any parameter input. Therefore, they were only used to provide better continuity to the seismic signal in order to enhance the definition of structural delineations and some stratigraphic features.**

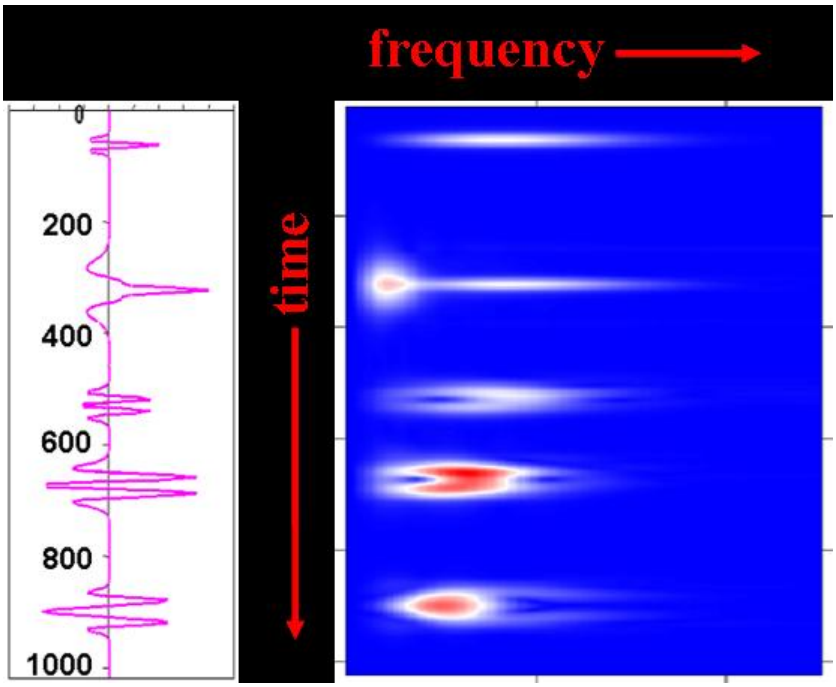


**Figure 5.18: Spectral-decomposition is a continuous time-frequency analysis of a seismic trace providing a frequency spectrum at each time sample.**

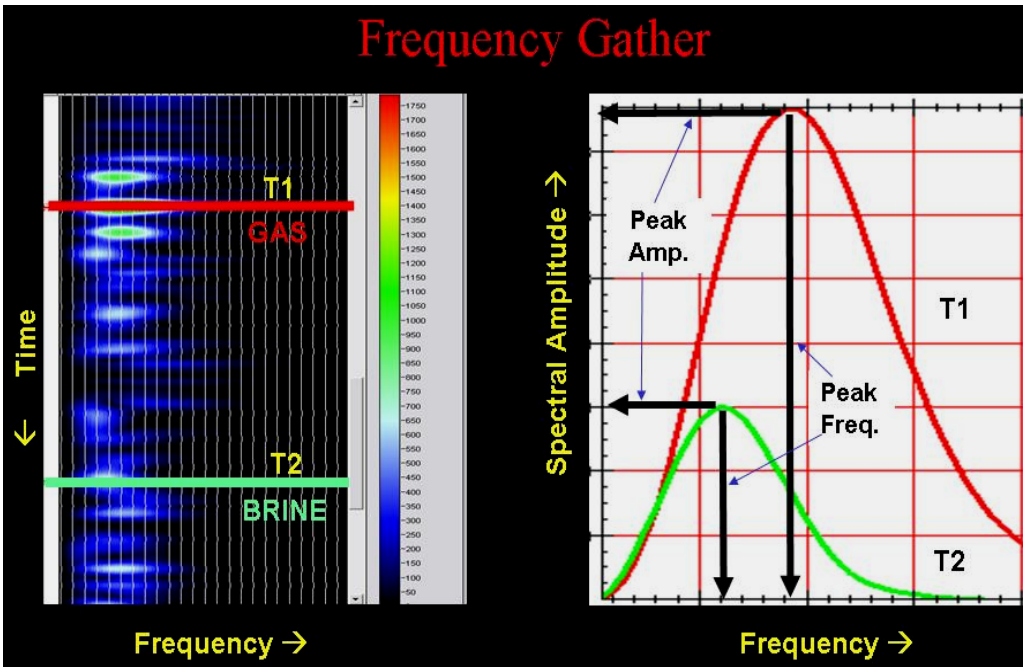


**Figure 5.19: Useful Spectral-Decomposition parameters on a frequency gather.**

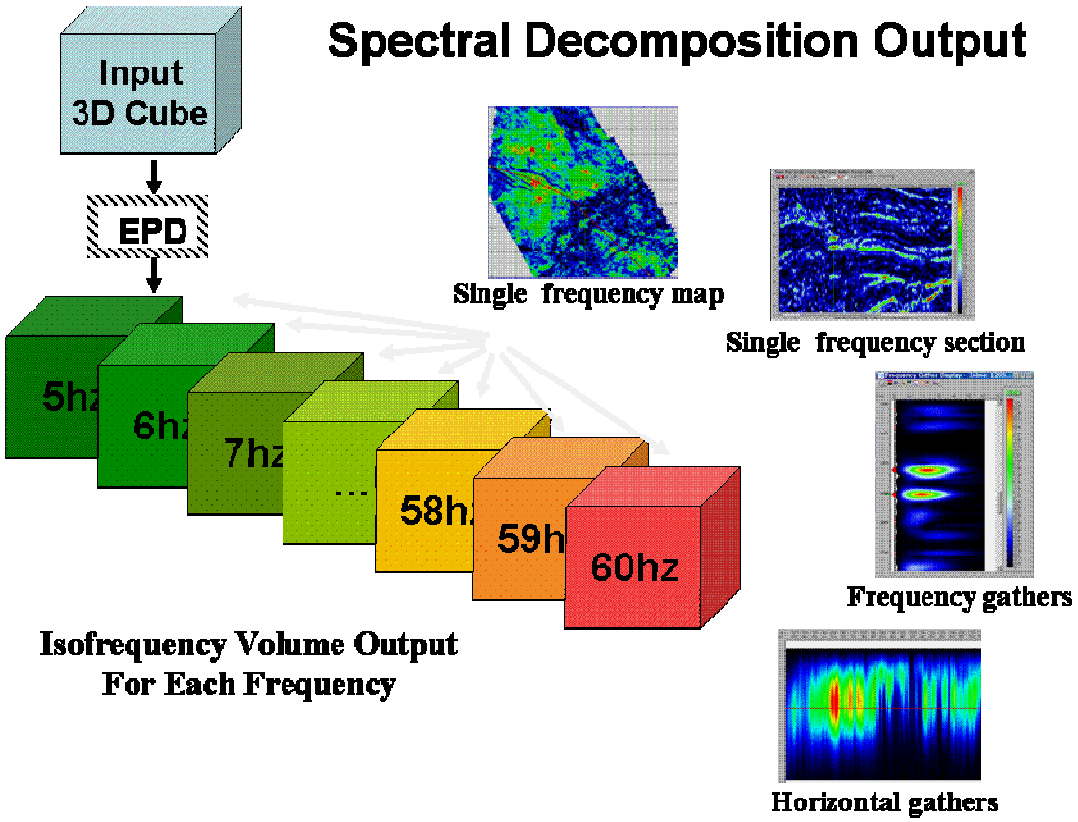


**Figure 5.20: Spectral-Decomposition products include: single frequency volumes for each frequency, frequency gathers corresponding to single seismic traces, and single frequency vertical section and maps.**

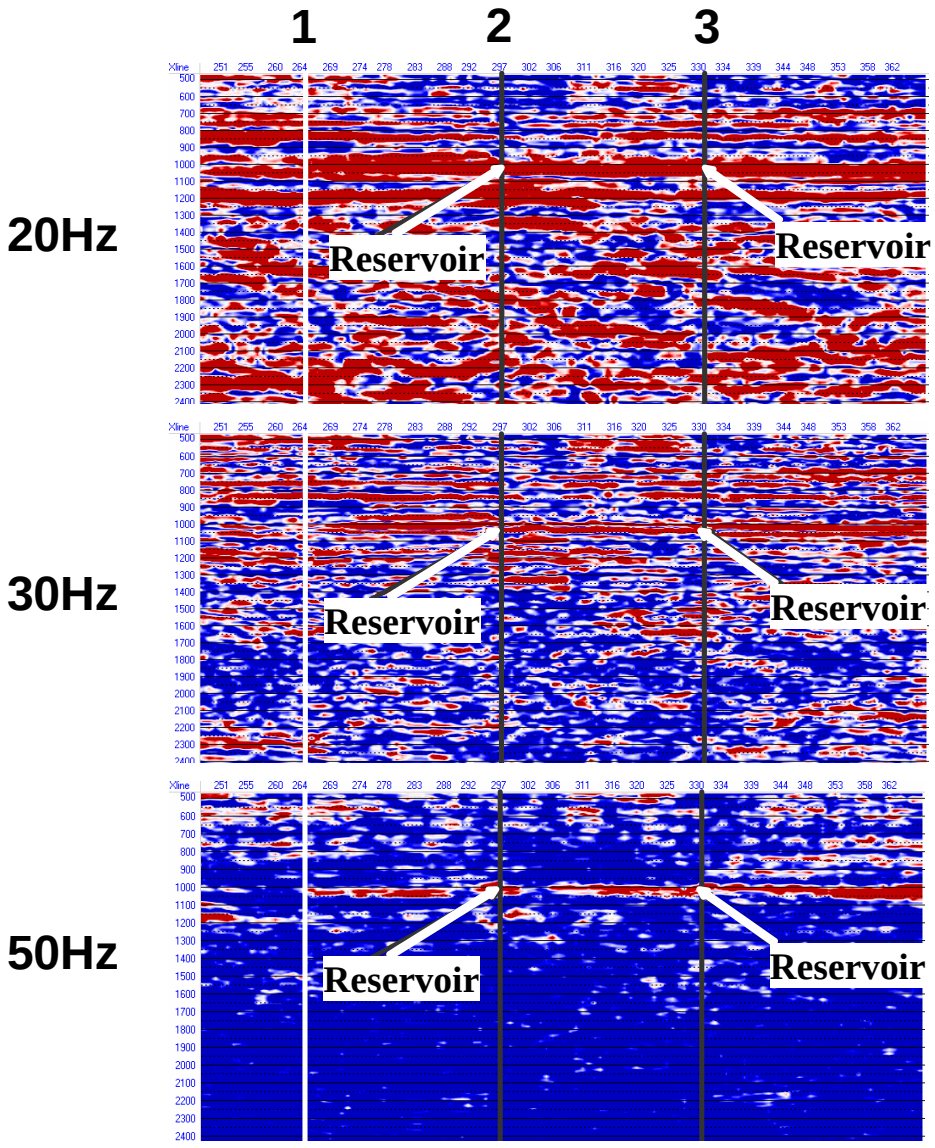


**Figure 5.21: Arbitrary line showing differential illumination through wells 1-3 for 20, 30, and 50 Hz in Cobo Field, Macuspana Basin, Mexico. Higher amplitudes at 50 Hz (red) correspond to a compartmentalized producing interval. Note that well #1 has no anomaly and no production (Mendez et al., 2003).**

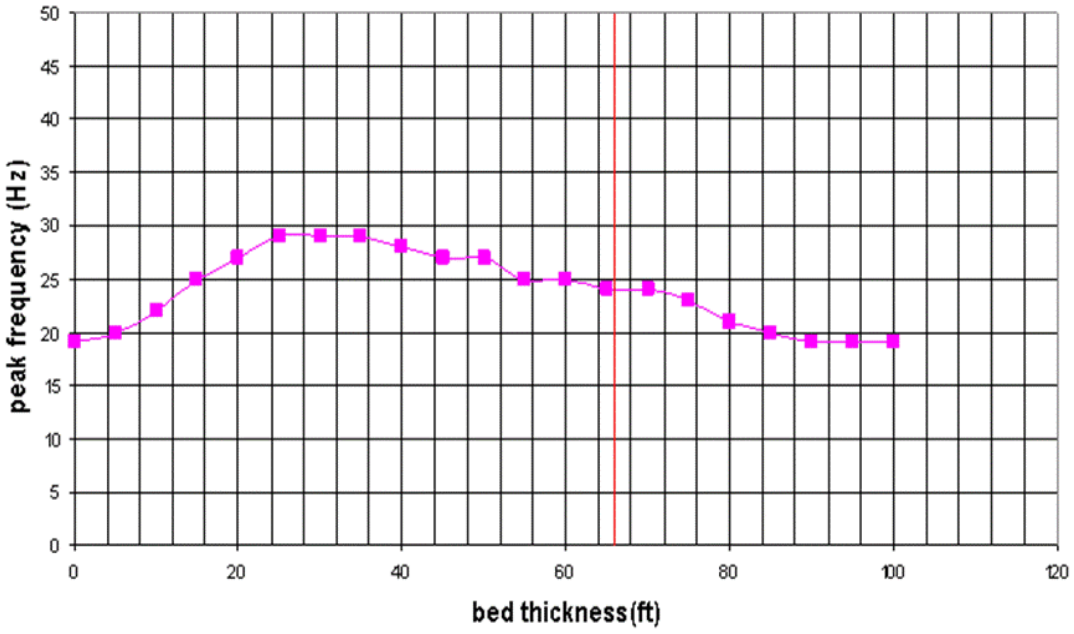


**Figure 5.22: Variation of peak frequency with bed thickness. There is a gradual increase in frequency as the thickness of the bed decreases and beyond some fraction of the tuning frequency it rolls off (Chopra et al., 2006).**

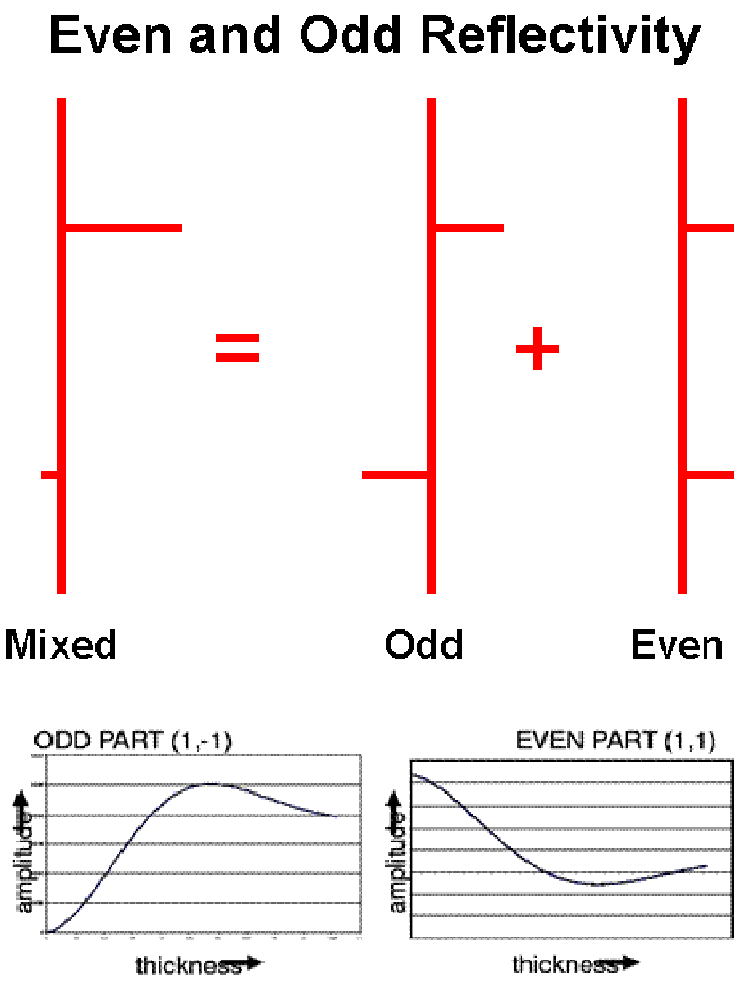


**Figure: 5.23: A practical thin bed subsurface situation represented with a two point reflectivity sequence corresponding to the top and bottom of a layer. This series may be shown as the sum of a pair of sequences, an odd part with a pair of equal and opposite reflection coefficients (like in the Widess model), and an even part made up of two reflection coefficients of the same polarity. After modeling, for the odd component the amplitude first increases (tuning) and then decreases as the thickness gradually reduces. For the even part this variation is just the opposite (after Chopra et al., 2006 and non-published Fusion™ technical literature).**

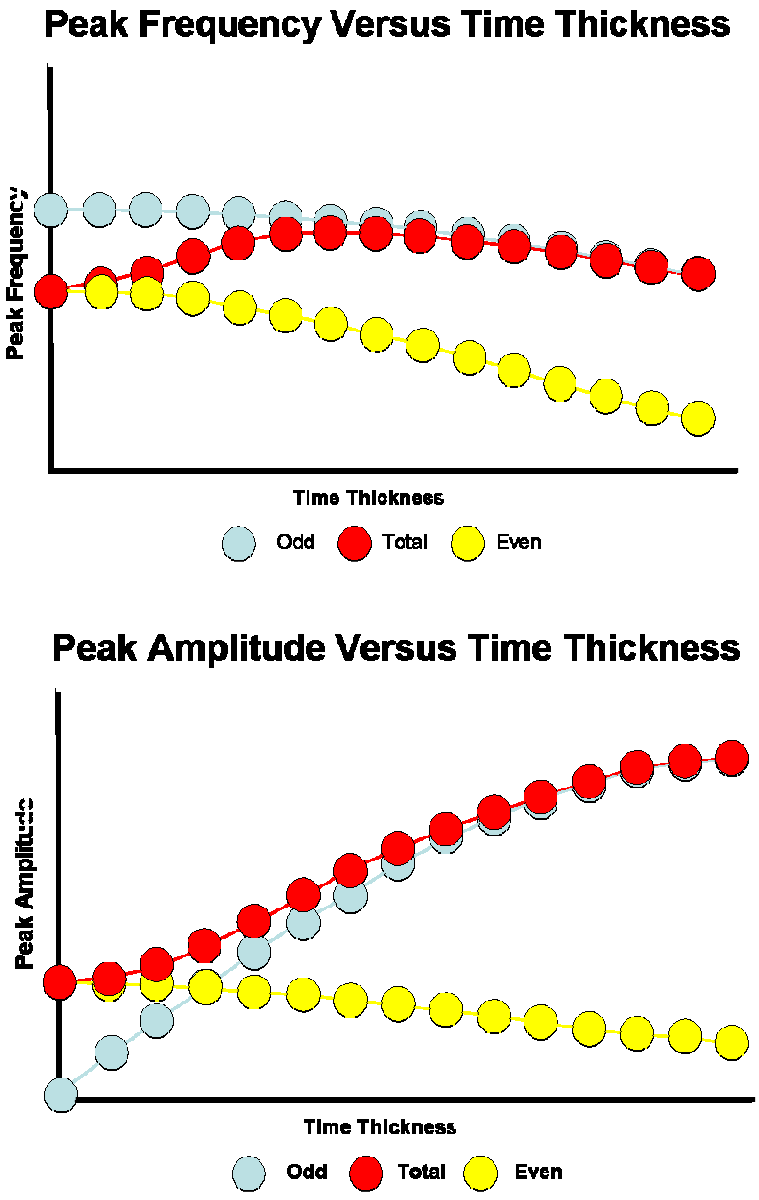


**Figure 5.24: Top: Peak frequency variation as a function of time thickness of the beds; Base: Peak amplitude variation as a function of time thickness of the beds. Both figures show the contributions from the odd and the even components shown in figure 7.15 as well as their sum (after Chopra et al., 2006 and non-published Fusion™ technical literature).**

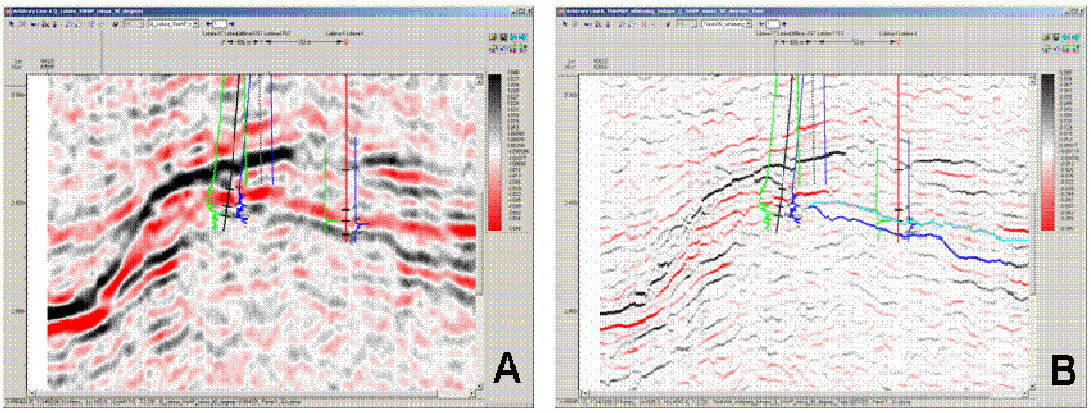


**Figure 5.25: Spectral inversion in Tampico Basin, Mexico. A) original seismic section; B) spectral inverted section (non-published Pemex internal reports).**

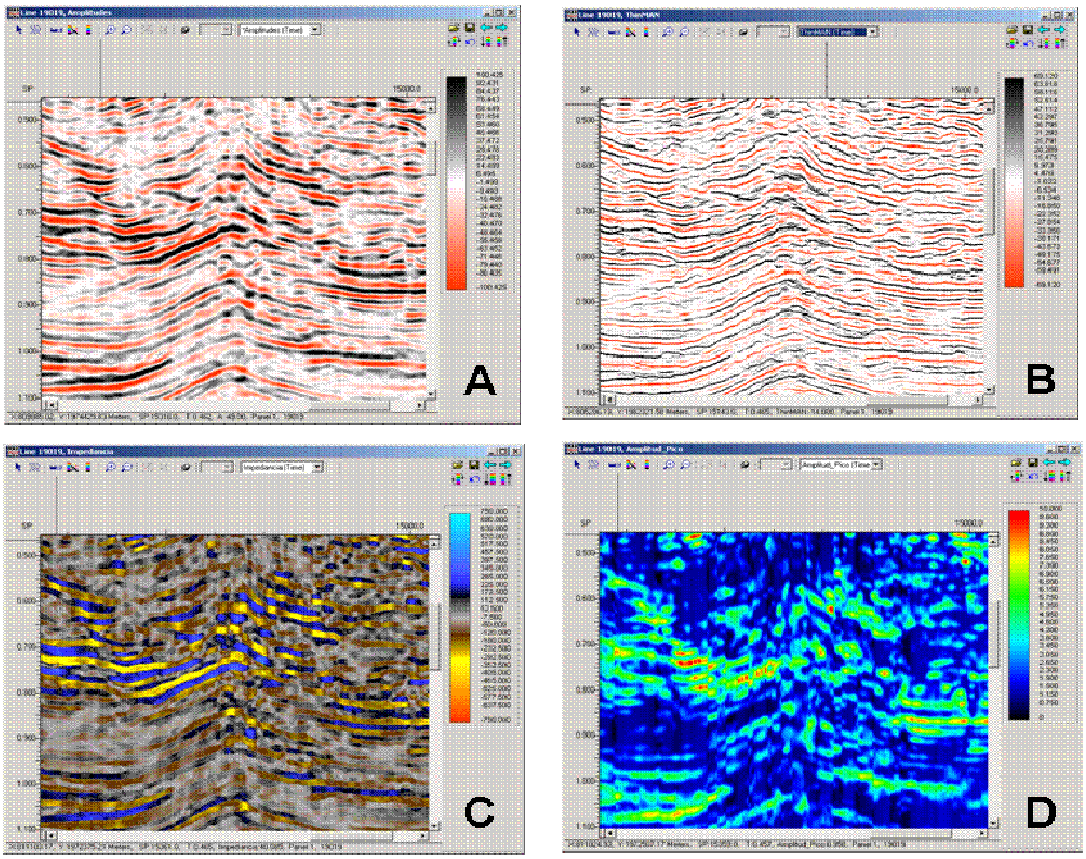


**Figure 5.26: Composite figure showing spectral decomposition products in Chicontepec Basin, Mexico. A) Original seismic section; B) spectral inverted section; C) relative impedance derived from spectral inverted section; D) spectral decomposition section at 35Hz (non-published Pemex internal reports).**

# Chapter 6

# SEQUENCE STRATIGRAPHIC FRAMEWORK AND INTEGRATED ANALYSIS (I)

## 6.1 Introduction

Sequence stratigraphic tools were utilized as a framework for the integrated interpretation in the study area. The benefits of establishing a sequence stratigraphy framework were fundamental for the correlation of strata and for more accurate facies interpretation, allowing predictive models for more reliable reservoir rock mapping.

An important aspect of defining a sequence stratigraphic framework is the depositional model and its corresponding lithofacies used during the interpretation. Therefore, a depositional model which supported the evidence provided by the integrated interpretation of cuttings, cores, well log and biostratigraphical data was corroborated at the discovery well, which contains the most comprehensive database for the late Tertiary stratigraphic intervals. The current chapter describes the establishment of the depositional model in the study area and sets some of the basis for the construction of the sequence stratigraphic framework which is discussed in the following chapter.

## 6.2 Depositional Model

Interpretation of lithology and depositional environments is a first step in defining a sequence stratigraphic framework. Before starting this research in 2005, a depositional model for the Pliocene Utan facies, including an understanding of their spatial and temporal variations, had not been well established. Previous unpublished basic interpretations identified these facies as corresponding to either outer neritic environments of a mixed carbonate-siliciclastic platform or deepwater basin floor fan deposits. On the other hand, the lack of a widely accepted and systematic way of classifying mixed litologies and environments has contributed to the controversy over the Pliocene sediments present in the Utan area.

Sediments are normally either siliciclastics or carbonates and classifications are based on simple fabric and mineralogical criteria of these end members, ignoring the spectrum of 'mixed' sediments and depositional environments. According to Mount (1985), this stems, in part, from the limited abundance of mixed siliciclastic and carbonate sediments, and the belief that, due to the inhibiting effects that siliciclastics have on carbonate-secreting organisms, the two sediments should not occur together.

The integrated analysis developed in this work diminishes such misunderstandings by proposing a depositional model following the workflow described in figure 3.1 of this dissertation and based on cuttings descriptions, core analyses, well log analysis including borehole image logs, and biostratigraphic data. The following analysis complements those developed by Bahamon (2006) and Mendez et al. (2006).

### 6.2.1 Lithology in the discovery well

Pliocene facies in the study area were deposited in a mixed platform environment. This fact was supported initially by the basic macroscopic description as well as by both the petrographic and the X-ray diffraction analyses (Table 4.2) completed on the three cores in the discovery well. Based on these control points and without any other core throughout the entire drilled interval nor in nearby wells, the matrix composition was estimated by consulting the cutting descriptions from the well site mud logger report, as well as by the use of detailed thin section petrographic and petrophysical analysis (Chapter 4 of this dissertation).

#### 6.2.1.1 Well cuttings

Lithology analysis begins at the well site where the mud logger collects representative samples of drill cuttings from the shale shakers, which have to be prepared for lithological interpretation and hydrocarbon show evaluation. In this stage, it is important to remove the coarser *cavings* (formation fragments which originate from the sides not from the bottom of the borehole), which could produce erroneous interpretations of the depth of stratigraphic horizons.

Based upon the mud logging report of the Utan well, the interpreted lithology of the recovered cuttings in the drilled interval (200-1450m) (figure 6.1), was divided as follows, from base to top:

**1450-1364m:** Shale-prone. Dominantly light gray to light green, calcareous mudstone. Shales are light green with a plastic texture; they are tight. A few intercalated thin limestone layers are also present.

**1364-455m:** Dominantly light gray, shelly calcareous mudstone interbedded with light green to white, fine-grained calcareous sandstone containing angular to subangular quartz grains. A 68m interval of mudstone at 724-792m is present. Three cores and the three tested intervals are located in this interval.

**455-210m:** Sand-prone. Dominantly light green, unconsolidated, shelly, calcareous sands at the base of the interval and shelly sands upward.

**210-200m:** Shale-prone. The logger´s description is inferred to be shelly unconsolidated shale. This interval is not shown in Figure 6.1.

The cuttings description from the mud logger established an almost pure siliciclastic description in which the carbonate component of this mixed sequence was not referred to, even though the ditch samples as well as the cores react to hydrochloride acid. This fact resulted in a false conceptual framework of the drilled interval, even though the sandier composition of the three tested intervals was reported. The non-reported high carbonate content was later revealed from both the macroscopic and the microscopic core analyses.

#### 6.2.1.2 Core data analysis

Examination and analysis of cores are probably the most important basic technique available to the petroleum industry for obtaining optimum recovery in the exploitation of reserves (Monicard, 1980).

As a wildcat exploration well, once the potential productive intervals were determined, programs for coring and testing were completed for the Utan well. Three intervals associated with three tested intervals were cored (figure 6.2 and Table 6.1). Two of the three, the upper and the lowermost, were reported as producers. Unfortunately, the cores were taken mainly from below the tested intervals; only about one meter of the tested intervals were recovered.

During the development of this research, the Core Storage Department of Pemex Marine Region was visited by Dr. Roger Slatt, Carlos Bahamon, and the author (figure 6.3) to perform comprehensive visual analyses of the cores, including detailed non-destructive description of sedimentology and sedimentary structures, mineralogy, and biological components as well as whole-core and close-up photography. These data provided information about depositional environments, and vertical stratigraphic changes, which were later correlated with the microscopical analyses, the borehole image logs, and the biostratigraphic data.

After these analyses, it was concluded that all three cores exhibited a general dominant lithology composed of very fine to fine-grained, light gray, bioturbated, mixed calcareous-siliciclastic mudstones (Figure 6.4). Some wavy laminations and lenticular cross-bedding were present, as well as shell fragments of molluscs. Some

ichnofossils, vertical open fractures and bioturbated zones are also present. Fine-scale stratification visible on the image log was not readily visible in the core until the core was washed with water, which revealed wavy laminations and lenticular bedding. The white shell fragments, ichnofossils and organic matter present as black specks of coal (figure 6.5) all indicate a shallow (inner neritic) environment of deposition rather than a deep marine environment. It has to be emphasized that none of the three cores were fully representative of the tested intervals.

| CORE | DEPTH (meters) | RECOVERY | COMMENTS |
|---|---|---|---|
| 1 | 1084-1092.5 | 9m (100%) | Only the lowermost meter of Reservoir II was cored |
| 2 | 1225-1232 | 7.2m (80%) | |
| 3 | 1321-1324.4 | 3.75m (42%) | Only the lowermost meter of Reservoir I was cored |

**Table 6.1: Core intervals recovered in the Utan well**

Reports of conventional analyses conducted on these cores by Corelab and Schlumberger, and provided for this research included: core photographs, core descriptions, thin section sedimentologic and petrographic analysis, scanning electron microscopy (SEM), X-ray diffraction (XRD), and other analyses. Three samples per each core, for a total of nine samples (Table 6.2), were selected by Pemex geoscientists for thin-section preparation and used for detailed thin section analysis and for the XRD and SEM studies. Only samples 1M and 7M are representative of the upper and lower reservoirs, respectively.

From the detailed core characterization the main composition of the three cores was found to be similar, consisting of well-cemented, light gray and medium brown shaly and calcareous siltstone. Some laminations exhibit thin shell fragments and bioturbation. Ichnofossils include clay-filled tunnels produced by the excavation of echinoderms and molluscs.

Cores 1 and 3, which did not sample more than one meter of the producing intervals exhibit a few 5-10cm thick beds of very fine-grained shaly and calcareous sandstones with vertical and wavy stratification and open fractures; the middle core does not exhibit such features. Irregularly distributed patchy dolomitization is also present in cores 1 and 3. Accurate placement of each cored section within the well bore was possible with the spectral core gamma scan measured in the laboratory.

| Core | Sample number | Depth (meters) | Thin section | SEM | DRX |
|---|---|---|---|---|---|
| **1** | **1M** | **1084.85** | **X** | **X** | **X** |
| 1 | 2M | 1086.90 | X | X | X |
| 1 | 3M | 1092.44 | X | X | X |
| 2 | 4M | 1225.09 | X | X | X |
| 2 | 5M | 1227.96 | X | X | X |
| 2 | 6M | 1230.39 | X | X | X |
| **3** | **7M** | **1321.56** | **X** | **X** | **X** |
| 3 | 8M | 1322.70 | X | X | X |
| 3 | 9M | 1324.21 | X | X | X |

**Table 6.2: Core samples selected for detailed thin section analysis, XRD and SEM in the Utan well. Only the samples 1M and 7M (shaded) were representative of the upper and lower reservoirs, respectively**

Corelab´s procedures for preparing samples for detailed petrographic thin section analysis include cleaning and impregnating with an epoxy solution to ensure the cohesion of the sample and to prevent loss of material during the grinding procedure. A blue dye is added to the epoxy solution to highlight in light blue the pore spaces. Each of the samples is mounted on a frosted glass slide and then cut and ground in water to a thickness of approximately 30 microns. To make carbonate cement identification easier, the cut samples are impregnated in a solution composed of red alizarin and potassium ferricyanide which highlights calcite in pink, ferric dolomite in dark blue and ferric calcite in purple. An extra solution of sodium cobaltnitrite highlights potassium feldspars in yellow.

Corelab reports included sedimentologic, petrographic, XRD and SEM analyses. The following conclusions were reached:

The analyzed samples could not be easily classified as a siliciclastic or carbonate rock.

Corelab classified the rocks as calcareous sands and silts, and indicated that “the depositional environment does not seem to be an active carbonate platform system”.

Quantitative petrographic analysis by point counting revealed a high content of calcite minerals (Table 6.3), resulting from the recrystallization of detrital carbonates and from dissolution of other calcium, iron, and magnesium minerals (Nichols, 1999). Aragonite, is present in minor amounts in the Utan samples.

| SAMPLE | 1M | 2M | 3M | 4M | 5M | 6M | 7M | 8M | 9M |
|---|---|---|---|---|---|---|---|---|---|
| Depth (m): | 1084.85 | 1086.90 | 1092.44 | 1225.09 | 1227.96 | 1230.39 | 1321.56 | 1322.70 | 1324.21 |
| Texture | | | | | | | | | |
| Average size (mm): | 0.11 | 0.05 | 0.04 | 0.04 | 0.05 | 0.06 | 0.06 | 0.06 | 0.05 |
| Grains | | | | | | | | | |
| Monocrystalline quartz | 14.8 | 7.6 | 4 | 6 | 6 | 8.4 | 9.2 | 7.2 | 7.6 |
| Policrystalline quartz | 0.8 | 0.4 | 0 | 0 | 0 | 0 | 0 | 0 | 0 |
| Potassium feldspar | 2 | 1.2 | 0.4 | 0.4 | 0 | 1.2 | 0.8 | 0.4 | 0.8 |
| Plagioclase | 2.8 | 2.8 | 0.8 | 3.6 | 1.2 | 2.4 | 2 | 1.6 | 2.4 |
| Total - igneous fragments | 0.8 | 0.4 | 0 | 0 | 0 | 0 | 0 | 0.4 | 0 |
| Total - metamorphic fragments | 0 | 0 | 0 | 0 | 0 | 0 | 0 | 0 | 0 |
| Total - carbonated fragments | 3.6 | 3.2 | 6.8 | 3.6 | 3.6 | 2 | 2 | 0.4 | 0 |
| Total - siliciclastic fragments | 0.4 | 0 | 0 | 0 | 0 | 0.4 | 1.2 | 0.4 | 0 |
| Total - lithic fragments | 4.8 | 3.6 | 6.8 | 3.6 | 3.6 | 2.4 | 3.2 | 1.2 | 0 |
| Total - micas | 1.2 | 0 | 0.4 | 0 | 0 | 0 | 0.4 | 0.8 | 0 |
| Total - heavy minerals | 0 | 0 | 0 | 0 | 0 | 0 | 0 | 0 | 0 |
| Total - foraminiferal-planktonic | 1.6 | 4 | 2 | 0.8 | 3.2 | 1.6 | 2.8 | 4.4 | 4 |
| Total - foraminiferal-benthic | 0 | 0 | 0 | 0 | 0 | 0 | 0 | 0 | 0 |
| Total - skeletal grains | 10.4 | 23.2 | 19.6 | 18.8 | 12.8 | 12.4 | 14.4 | 25.6 | 16.8 |
| Total - non-skeletal grains | 0 | 0 | 0 | 0 | 0 | 0 | 0 | 5.2 | 4 |
| Total - other grains | 0 | 0 | 1.2 | 0 | 0 | 0.8 | 0 | 0 | 0 |
| Total Grains | 36.8 | 38.8 | 33.2 | 32.4 | 23.6 | 27.6 | 30 | 42 | 31.6 |
| Replacement grains | | | | | | | | | |
| Total- replacement grains | 0 | 0 | 0 | 0 | 0 | 0 | 0 | 0 | 0 |
| Detrital matrix | | | | | | | | | |
| Total-detrital matrix | 3.2 | 9.2 | 12 | 8.8 | 10.8 | 16.8 | 14.4 | 23.2 | 42 |
| Authigenic minerals | | | | | | | | | |
| Total-authigenic clays | 0 | 0 | 0 | 0 | 0 | 0 | 0 | 0 | 0 |
| Total-authigenic quartz | 1.2 | 0.4 | 0 | 0.4 | 0.4 | 0 | 0 | 0 | 0 |
| Total-authigenic feldspars | 0 | 0 | 0 | 0 | 0 | 0 | 0 | 0 | 0 |
| Total-authigenic carbonates | 43.6 | 46 | 52 | 54.8 | 62.8 | 52.4 | 48.4 | 30.8 | 25.6 |
| Total-sulfates | 0 | 0 | 0 | 0 | 0 | 0 | 0 | 0 | 0 |
| Total-sulfurs | 0 | 3.2 | 1.6 | 0.4 | 1.2 | 2.8 | 2 | 3.2 | 0.8 |
| Total-zeolites | 0 | 0 | 0 | 0 | 0 | 0 | 0 | 0 | 0 |
| Total other authigenic minerals | 0.8 | 0.4 | 0.8 | 0 | 0 | 0 | 0 | 0 | 0 |
| Total-no shaly cements | 45.6 | 50 | 54.4 | 55.6 | 64.4 | 55.2 | 50.4 | 34 | 26.4 |
| Total-cements | 45.6 | 50 | 54.4 | 55.6 | 64.4 | 55.2 | 50.4 | 34 | 26.4 |
| Porosity | | | | | | | | | |
| Total-primary porosity | 12.4 | 2 | 0.4 | 3.2 | 1.2 | 0.4 | 5.2 | 0.4 | 0 |
| Total-secundary porosity | 2 | 0 | 0 | 0 | 0 | 0 | 0 | 0.4 | 0 |
| Porosity- Others | 0 | 0 | 0 | 0 | 0 | 0 | 0 | 0 | 0 |
| Total-porosity | 14.4 | 2 | 0.4 | 3.2 | 1.2 | 0.4 | 5.2 | 0.8 | 0 |
| TOTAL (%) | 100 | 100 | 100 | 100 | 100 | 100 | 100 | 100 | 100 |

**Table 6.3: Quantitative petrographic results from point-counting analysis practiced to the 9 core samples of Utan well. Only the samples 1M and 7M (highlighted in yellow) were representative of the upper and lower reservoirs, respectively (adapted from non-published PEMEX´s internal technical reports)**

The samples labeled in Table 6.3 as 1M and 7M, are from the base of the upper and lower reservoirs respectively. An increase in both grain size, and the amount of quartz grains and porosity as well as a reduction in calcite differentiate these samples

from the remaining ones. The abundance of detrital quartz and the quartz grain size diminish beneath the cored reservoir intervals and skeleton grains and carbonate cement increase in abundance.

Figure 6.6 shows the results of the point counting analysis for the uppermost core and its samples 1M, 2M and 3M. The top sample 1M was the only one located within the reservoir. Pie diagrams illustrate how the quartz content increases and the carbonate content decreases beneath the reservoir interval. Photomicrographs accompany this petrographic analysis of reservoir quality controls. The same trend occurs for the lower reservoir.

A high percentage of carbonate cement is common in all the core samples, reaching 45-55% of the average total volume of the rock.

A digital color spectrophotometer was used by Corelab for high-resolution color profiles of each core sample. Two color photomicrographs at different scales were included in the reports. The very high magnification scanning electron microscopy images (SEM) provided additional information on the pore network, and the effects of cements, matrix, and authigenic clays on reservoir quality. For instance, the SEM image in figure 6.5 shows that the carbonate cement also fills open fractures in deeper intervals. Analysis of the individual clay crystal morphology by Corelab suggested that no authigenic clays are present; all are detrital in origin.

X-ray diffraction analysis performed by Corelab provided the weight percentages of quartz, feldspars, carbonates and specific clay minerals (e.g., kaolinite,

chlorite, illite, smectite, and mixed-layer illite/smectite). Results for the sampled intervals were previously listed in Table 4.2 of this dissertation.

The X-ray bulk rock composition indicated the sampled intervals are composed on average of calcite (including Fe-calcite) (56%), dolomite (16%), quartz (9%), aragonite and pyrite (8%), feldspar and plagioclase (6%), and shale (clay minerals) (7%).

The quartz content is highest within the reservoir intervals. Clay minerals are: illite/smectite (80-90% of smectite), illite and chlorite. The matrix in all of the samples varies heterogeneously as a mixture of carbonate mud or micrite, particles of detritical clay, organic material, particles of quartz and clay-sized feldspars. This fine carbonate mud is commonly found in many carbonate-forming environments. According to Nichols (1999), the small size of the particles usually makes it impossible to determine their origin, which may be the result of chemical precipitation from water saturated in calcium carbonate, or of the breakdown of skeletal fragments, or to have an algal or bacterial origin.

Visual examination of cores from five additional wells, revealed a similar mixed composition.

#### 6.2.1.3 Borehole Image log

An **EMI$^{TM}$** log acquired over the interval 1070m-1450m in Utan well was available for the interpretation. The **EMI$^{TM}$** (Electrical Micro-Imaging tool, a mark of

Halliburton) belongs to the electrical micro-imaging tools developed over the past two decades, for water-based muds, capable of producing wellbore images.

The imaging tools contain microresistivity electrodes which become arranged around the wellbore by pads that are pressed against the borehole wall. Electrical current is forced to flow into the rock through the electrodes, and remote sensors measure the current after it interacts with the formation, thus displaying an image of the borehole wall (Hurley, 2004). Passey et al. (2006) provides details of borehole image logs.

Initially, the EMI™ images were interpreted for dipmeter information in the Utan-1 well. The resulting structural interpretation established that the bed dips are not significant and that the structural dip is not greater than 15 degrees in most of the recorded interval. A preferential dip orientation is toward SSW and SW. There were only two intervals where bed dips are higher than 15 degrees, reaching 30 to 60 degrees at 1270 and 1350m, indicating normal faults. The deeper fault is the master Kutz fault against which the Utan rollover structure was formed (Figure 6.7).

Electrical borehole images represent variations in electrical conductivity related to lithology, fluid type, hole rugosity, speed correction errors and other factors (Passey et al., 2006). The image log in the Utan-1 well revealed finely-stratified, conductive, and resistive intervals of shales and sandstones, respectively which were not easily visible in the core.

Bahamon (2006), interpreted the borehole images to identify sedimentary structures in the Utan-1 well, including wavy and planar laminations, ripples, cross

stratification, and hummocky cross stratification (figure 6.8). Bahamon indicated these features were intercalated with several thick high resistivity intervals (from 1 to 9m thick, with a mean value of 3m), associated with an increase in carbonate content making them more resistive.

### 6.2.2 Biostratigraphic data

Fossils are essential for establishing a detailed stratigraphy and correlation scheme in sedimentary rocks. The level of detail achieved in each case is determined by the nature of the depositional environments and the way in which different taxa lived and evolved.

According to Nichols (1999), the ideal fossil for stratigraphic purposes would be “an organism which lived in depositional environments all over the world and was abundant; it would have easily preserved hard parts and would be part of an evolutionary lineage which frequently developed new, distinct species”. Unfortunately, no such ideal fossil taxon has ever existed, however many plants and animals occupy ecological niches which are defined by such factors as water depth, temperature, nutrient supply, nature of substrate and so on.

Shelves are areas of oxygenated waters rich in life and nutrients. They provide enough organisms to interpret their remains in terms of chronostratigraphy. In open ocean areas all organisms either float (planktonic), are free-swimming (nektonic) or

live on the surface or within the upper column of sea floor sediment (benthonic or benthic).

Algae, which are at the base of the food chain, belong to the group Chrysophyta and include coccoliths which have spherical bodies of calcium carbonate a few tens of micrometers across; planktonic algae organisms of this size are commonly referred to as **nannoplankton**. Slightly larger are **foraminifera**, a group of single-celled animals which includes planktonic forms with a calcareous shell about a millimeter or a fraction of a millimeter across. These organisms have lived in warm seas since the Mesozoic and their remains contribute to soft calcareous muds on the sea floor, nannoplankton ooze or foraminiferal ooze. Both regional and world-wide zonation schemes using forams for correlation in the Mesozoic and Cenozoic are widely used in the hydrocarbon industry because microfossils are readily recovered from boreholes (Nichols, 1999).

To preserve the chronostratigraphic record, a variety of schemes are commonly used in **biostratigraphy**, including assemblages of taxa for zonation schemes. If the ecological niche of a fossil organism can be determined, this can provide an excellent indication of the depositional environment. McGowran (2005) points out that a good index fossil marks a well-tested and narrow interval of time. Usually, the main types of zones are defined on the first appearance (evolution) and last appearance (extinction) ranges or concurrent ranges or acmes of selected marker species. Particularly, in the oil industry, the main type of zone is defined as the last appearances datum (LAD),

colloquially known as “tops”, due to the fact that the first appearances (“bases”), are impossible to locate accurately using drilled cutting samples (Wynn, 1996).

Considerable information has been published for integrated bio- and sequence-stratigraphic schemes for the Plio-Pleistocene of the Gulf of Mexico, including Armentrout (1987); Bowen and Shaffer (1987); Haq et al. (1988); Allen et al. (1991); Armentrout and Clement (1991); Coterill et al. (1991); Galloway et al. (1991); Clement and Thompson (2005). Currently, the groups of planktonic organisms used for biostratigraphic analysis of shelf and slope Cenozoic strata in the Gulf of Mexico are planktonic foraminifera and calcareous nannoplankton (Wynn, 1996).

Hydrocarbon exploration activities in Tertiary sediments from the southeastern Gulf of Mexico have highlighted the importance of biostratigraphic studies in defining the geological setting of this relatively poorly known section of the Mexican geology. During the last few years the number of contributions to the Tertiary paleontology in Mexico has increased considerably through high-resolution biostratigraphic studies for petroleum exploration applications. In particular, marginal, shallow and deep-marine environments can be differentiated on the basis of benthonic foraminiferal biofacies or the ratio of planktonic to benthonic foraminifera. Biozones and LAD have been established by Pemex for the Cenozoic chronostratigraphy for the southeastern Gulf of Mexico.

Particularly, planktonic foraminifera and calcareous nannoplankton data define the chronostratigraphy of the Pliocene intervals examined in the Utan area. Figure 6.9 shows the recently adjusted (August 2005) chronostratigraphic distribution of

planktonic foraminifera in the Neogene of the Southeastern Basins. The new adjustments included a new chronostratigraphic position for *Globerigerina nepenthes* from the Upper Miocene to Lower Pliocene. This fact favorably supported the sequence stratigraphic interpretation developed by Bahamon and the author of this dissertation for the study area (Bahamon, 2006, Mendez et. al., 2006).

The LAD ages of the index planktonic foraminifera used in this study closely agrees with published tables for the –Late Miocene–Pleistocene Sequence Chronostratigraphy for the Gulf of Mexico- (figure 6.10), developed by Micro-Strat Inc. (Wornardt et.al., 2002). This chart is also employed as a reference chart in the sequence stratigraphic work to be developed later in this dissertation.

Internal paleontologic reports from Pemex for the Utan-1 well were provided and reviewed for this dissertation (one of these reports is shown in figure 6.11). It was first noticed that planktonic foraminifera comprise ages between Lower (Early) Pliocene (*Globerigerina nepenthes,* 4.18my) (at ~1452m) to Recent sandy sea floor sediments. Beneath this depth, LAD´s of index Pliocene planktonic foraminifera were correlated to the table for the Southeastern Basins (figure 6.9).

Based on this biostratigraphy, the interval 1390-1452, was considered as Lower Pliocene (N-19) due to the presence of *Globorotalia margaritae* and *Globoquadrina altispira altispira*, as well as the LAD of *Globigerina nepenthes*. LAD of *Globorotalia margaritae* marks the Middle Pliocene-Lower Pliocene boundary (N19-N20). Middle Pliocene is marked as a biozone by *Globorotalia miocenica,* and the LAD of this index fossil marks the Middle Pliocene-Upper Pliocene boundary.

Figure 6.12 schematically shows the stratigraphic distribution and zonation of the selected planktonic foraminifera which were analyzed for the Utan well. Additionally, calcareous nannoplankton biozone tops were considered as a second level of importance for the correlation work.

Summarizing, from the planktonic foraminifera analysis in the Utan-1 well, three major biozones were identified at the following depths:

- **210m – 800m:** ***Globorotalia truncatulinoides truncatulinoides***
- **830m – 1390m:** ***Globorotalia miocenica,***
- **1390m – 1452m:** ***Globorotalia margaritae.***

Last appearance datums (**LAD**) were also determined from the planktonic foraminifera. Additionally, ages were taken from the table for the Southeastern Basins developed by Pemex (figure 6.9) and from Wornardt et al. (2002):

- **660m:** ***Globigerinoides trilobus cf. Fistulosus*** **(1.7my)**
- **830m:** ***Globorotalia miocenica*** **(2.3my)**
- **900m:** ***Globorotalia obliquus extremus*** **(2.4my)**
- **1100m:** ***Globoquadrina altispira s.l.*** **(3.09my)**

  ***Globoquadrina altispira conica***
- **1380m:** ***Globorotalia margaritae margaritae*** **(3.58my)**

  ***Globoquadrina altispira altispira***
- **1400m:** ***Globoritalia nepenthes*** **(4.18my)**

Establishing the water depths at the time of deposition is problematic beyond certain upper and lower limits. The effects of waves, tides and storm currents can usually be recognized in sediments deposited on the shelf and are absent below 200m water depth (Nichols, 1999). Some authigenic minerals, such as glauconite, are indicative of shelf environments.

| INTERVAL (m) | BATHYMETRY |
|---|---|
| 200 - 210 | TRANSITIONAL |
| 260 - 270 | TRANSITIONAL |
| 270 - 280 | TRANSITIONAL- INNER NERITIC |
| 380 - 390 | TRANSITIONAL- INNER NERITIC |
| 390 - 400 | INNER NERITIC |
| 400 - 410 | INNER NERITIC |
| 410 - 420 | INNER NERITIC - MIDDLE NERITIC |
| 450 - 460 | INNER NERITIC - MIDDLE NERITIC |
| 460 - 470 | INNER NERITIC |
| 840 - 850 | INNER NERITIC |
| 850 - 860 | INNER NERITIC - MIDDLE NERITIC |
| 890 - 900 | INNER NERITIC - MIDDLE NERITIC |
| 900 - 910 | INNER NERITIC |
| 940 - 950 | INNER NERITIC |
| 950 - 960 | INNER NERITIC - MIDDLE NERITIC |
| 970 - 980 | INNER NERITIC - MIDDLE NERITIC |
| 980 - 990 | INNER NERITIC |
| 1000 - 1010 | INNER NERITIC |
| 1010 - 1020 | INNER NERITIC - MIDDLE NERITIC |
| 1030 - 1040 | INNER NERITIC - MIDDLE NERITIC |
| 1040 - 1050 | INNER NERITIC |
| 1200 - 1210 | INNER NERITIC |
| 1210 - 1220 | INNER NERITIC - MIDDLE NERITIC |
| 1290 - 1305 | INNER NERITIC - MIDDLE NERITIC |
| 1305 - 1310 | INNER NERITIC |
| 1340 - 1350 | INNER NERITIC |
| 1350 - 1360 | MIDDLE NERITIC |
| 1400 - 1410 | MIDDLE NERITIC |
| 1410 - 1420 | OUTER NERITIC - MIDDLE NERITIC |
| 1450 - 1450 | OUTER NERITIC - MIDDLE NERITIC |

**Table 6.4: Interpreted bathymetric configuration derived from benthonic foraminifera and the ratio planktonic vs benthonic foraminifera**

In particular, the abundance of benthic organisms decreases as the water depth increases in the same way that planktonic forms are likely to be more abundant in deeper water. Therefore, the ratio of planktonic to benthonic foraminifera is commonly used as a relative depth indicator and provides a crude measure of the distance from the paleo-shoreline.

A benthonic foraminiferal bathymetric range chart of the Southeastern Basins of Mexico (adapted from non-published Pemex internal reports) is provided in figure 6.13. Benthonic foraminifera abundance and the ratio of planktonic vs benthonic foraminifera indicated (Table 6.4) that inner neritic environments, at depths from 0-30m, prevailed during deposition of the producing facies in Utan-1 well with an oscillating sea during deposition of most of the stratigraphic interval.

### 6.2.3 Interpretation of the Depositional Environment

A number of different sets of terms can be used to describe the parts of the marine realm (figure 6.14). The marine environment can be roughly subdivided according to its morphology into the shelf, slope, and deep ocean basin. Water depths define neritic, bathyal and abyssal zones. Shallow marine environments can be also subdivided into inner-middle-outer shelf or inner-middle-outer neritic.

The neritic (shelf) environments are the most complex of all marine environments because of the diversity of processes and bathymetry (Lewis and

McConchie, 1994). The shelf encompasses the shallow-water areas of the ocean lying shoreward of the shelf break where usually the depth of water varies from 0 to ~200m.

The evidences provided by well cuttings, core analyses, biostratigraphy, and well log data, including the EMI log from the Utan-1 well, indicate that the depositional environment where the drilled facies were deposited was a composite inner neritic (shelf) environment, consisting of shoreface, barrier, lagoon, marsh, and tidal flat subenvironments (Fig. 6.14). The inner neritic environment, from 0 to 30m depth, was determined by the benthonic/planktonic foraminifera analysis.

The inner neritic environment is often dominated by tidal, wind-driven, and storm-wave processes (Boggs, 1995). The supply of sediments to shelves is a fundamental control on shallow marine environments and depositional facies (Nichols, 1999). The shallow depths also provide the proper conditions where carbonate and siliciclastics can provide the mixed lithology found in Utan facies.

In particular, for the Middle Pliocene strata which contain the reservoir intervals in the Utan-1 well, the model that best fits the evidence is the shoreface-tidal flat environment, considered to be potential reservoir facies with long distance lateral continuity. This interpretation has previously been proposed by Bahamon (2006), and Mendez et al. (2006).

Tidal flat deposition is dictated by the pattern followed by tidal currents, which regularly change direction from: a) the *flood tide* current, which moves water onshore between the low and high tide, and b) the *ebb tide* current which flows in the opposite direction as the water level returns to low tide (Nichols, 1999) (figure 6.15).

Tidal flats are subdivided into the supratidal subenvironment above mean high water, the intertidal subenvironment, the region lying between the high and low tide range which is alternatively covered and uncovered by the sea, and the subtidal subenvironment, which is the region normally covered by water (figure 6.15). The tidal range is the vertical amplitude between low and high tide levels. Because of the normal variation in tidal range and the effect of storms, the boundaries between these tidal zones are transitional rather than sharp (Hardie, 1986a).

The importance of tides in sedimentary processes is that they involve the movement of water at patterns and velocities that are capable of moving sediments. Particle transport is vigorous and rapid, making the tide an effective sedimentation agent (Biju-Duval, 2002).

Tidal flats are low-relief environments which contain unconsolidated and unvegetated sediments that accumulate within the intertidal range, including the supratidal zone (Davis, 1983). Tidal flats can occupy a broad or narrow band, depending on the gradient of the coast and on the tidal range (Lewis&McConchie, (1994); Middleton (1991).

The most characteristic feature of tides is their cyclicity, indicating flood-ebb bipolar currents showing opposite directions. One of the currents may be much stronger and dominant that the other. In consequence, the tide creates a a wide spectrum of erosion and cross-stratification patterns superimposed upon another (Davis, 1983).

As a response to such cyclicity, the main sedimentary structures generated by the tidal currents, useful as criteria for recognition of ancient tidal sediments are (Middleton, 1991; Nio and Yang, 1991; Nichols, 1999): ripples; tidal bundles and evidence for other neap-spring rhytms; the interbedding of thin strata of rippled sand and mud forming structures called flaser, wavy and lenticular bedding particularly when present in fining-upward cycles with evidence for deposition on prograding tidal flats; crossbedding with evidence for current reversals, such as opposed cross-strata, regularly spaced reactivation surfaces, and mud drapes.

Tide-dominated shoreline-shelf systems pass laterally into estuaries and deltas, and landward into tidal flats. Subtidal flats and the lower portions of intertidal flats tend to be sandy, and to pass landward into muddy and then vegetated, intertidal and supratidal flats (Emery and Myers, 1996). In consequence, tidal flats usually generate fining upward successions (figure 6.16). The wide varieties of bedforms commonly contain many organisms and bioturbation may be present throughout the tidal flat sediments, but is more likely in the upper portion where the energy is relatively low (Davis, 1983).

The tidal flat environment includes both the true tidal flats and the higher-energy tidal channels that cut across them. The role of tidal channels is of great importance if it is considered that they form dendritic patterns, from numerous but small channels near mean upper tide level to fewer but deeper and wider ones below mean lower tide level; the smaller channels slowly shift their position, reworking the

tidal flat sediments and introducing coarser sediments into the facies (Lewis and McConchie, 1994) (figure 6.17).

The evidences discussed in this chapter strongly suggest that the model that best fits the prevalent depositional environment for the Middle Pliocene reservoir intervals located in the Utan-1 well is a tidal flat system in the inner neritic shoreface environment, considered to be potential reservoir facies with long distance lateral continuity. This fact agrees with the interpretation of Bahamon (2006), and Mendez et al. (2006). Summarizing this series of facts:

a) The bathymetric configuration from the benthonic/planktonic foraminifera analysis reports an inner neritic environment (0 to 30m depth) for the producing facies. Some oscillations between inner-middle neritic depths are also reported;

b) Broken fossils indicate current action in shallow water;

c) Bioturbated zones indicate oxygenated, shallow water;

d) Laminated strata and sedimentary structures such as wavy, lenticular, and hummocky cross-stratification, indicative of cyclicity, were observed in core and the EMI log images;

e) Stratigraphic cyclicity observed in core and EMI images are interpreted as finely laminated successions of sandy-shaly carbonate bodies that define a systematic stacking pattern indicative of shoreface oscillations;

f) Shallow waters promoted the carbonate-siliciclastic mixture assuming that the reservoir rocks are highly detrital with some quartz grains redistributed by the tidal and current actions;

g) Preliminary seismic interpretation demonstrated that the Utan reservoirs have broad continuity in the mini basin where the rollover structure was formed;

Section 6.3 of this dissertation demonstrates how climatic effects, during the Middle Pliocene promoted the increase in water depths and transgressive seas, thus providing broader intertidal environments.

Previous interpretations developed in the study area (non-published Pemex reports) indicated that the Utan producing facies were deposited as fans in outer shelf and deep water environmets. Other models were related only with water depths without establishing the related subenvironment. The proposed model which agrees with interpretations from Bahamon (2006) and Mendez et al. (2006), defines a more logical sequence of features indicative of shallower inner neritic environments. This new model provides reliability for the sequence stratigraphic framework established in the following chapter of this dissertation.

### 6.2.4 Provenance of sediments

Regarding the Utan sediment provenance, the mixed mineralogy suggests at least two end-member sediment supply sources.

For Pliocene times, the Utan area was bordered in its eastern-northeastern part by the Campeche escarpment, which is the western border of the Yucatan shelf or platform (the Yucatan peninsula is the surface exposed portion of the larger Yucatan platform). The escarpments separated the western side of the Yucatan platform, as an area of submarine high ground, from the Pilar de Akal, formed during the Miocene tectonic compression, of lower ground where the Utan area was located during Pliocene to Recent times (figure 6.18). Therefore, the Yucatan platform, considered an example of unrimmed shelve or carbonate ramp (Boggs, 1995), which has been a stable tectonic element since Triassic times, was the main source of carbonate detritus to the Utan area.

On the other hand, the main source of siliciclastics during the Middle Pliocene was the Chiapas foldbelt (Sierra de Chiapas), located onshore south-southeast of the Utan area. This element provided terrigeneous and volcanic sources, via fluvial systems, to the marine basin. Even though delta systems were far away from the study area, current action and intertidal processes were capable of redistributing terrigeneous sediment to the study area during marine transgressions (figure 6.19).

Some controversy concerning the interaction of carbonates and siliciclastics in the inner neritic environment is clarified by noting that the carbonates accumulate more rapidly in shallow water and more slowly as the water depth increases.

Section 6.3 will illustrate how changes in climatic effects during the Middle Pliocene favor the proposed model.

### 6.2.5 Sediment accumulation rates

Paleonvironmental reconstructions require knowledge of the rate of deposition through time (Bruns and Hans, 1999). Nichols (1999) indicates that the thickness of a biostratigraphic unit at any place is determined by the rate of sediment accumulation during the time period represented by the biozone.

To calculate sediment accumulation rates several considerations have to be taken into consideration: 1) A core section or a stratigraphic succession with biostratigraphic analysis is selected which is assumed to represent a site of continuous, steady sedimentation; b) the positions of biozone markers (FAD and LAD of taxa) and corresponding depths are marked on the core or section; c) the thickness between each FAD and LAD is obtained, then is divided by the age difference of the index fossil to obtain the sedimentation rate.

The sedimentation rates have to be compared with another core or vertical succession of strata containing the same biozone in order to identify lateral changes in rates of sedimentation and hiatuses (Nichols, 1999).

Sedimentation rates have always a relative degree of confidence because they do not necessarily represent the true sedimentation effect. Increasing post-depositional burial depth means increased compaction, thus the measured sedimentation rates naturally decrease with depth although the true sedimentation rate may have remained constant through time. On the other side, deposition may not be constant and gradual,

and the reference index fossils may not be sufficiently close in age to reflect small changes in sedimentation ranges during the calculation.

Bruns and Hans (1999), indicate that this approach defines the sedimentation rates correctly only if the dating method is reliable and compaction between the two reference levels remained constant. The same authors point out that “often the assumption of constant sedimentation rates between datum levels forms one of the most important but sometimes least certain basic assumptions for further interpretations”.

Nichols (1999) claimed that biostratigraphy can provide a fine scale of resolution only in circumstances where the rate of sedimentation was relatively slow and the frequency of speciation events in the zone´s taxa was relatively high. If a biozone is estimated to have lasted a million years the complete zone is more likely to be represented in a single exposure of sediments of a deep marine setting where sedimentation rates are slow (a few millimeters per thousand years) than in shallow marine environments where rates are likely to have been higher (decimeters to meters per thousand years).

Utan structure was formed by a rollover anticline which rotated against a growth fault. Usually, fault movement generates enormous thickness changes in equivalent sediments, however from the structural interpretation of the EMI log (figure 6.7) it was noticed that the well was located on a limb of the structure where the layers are still horizontal, thus at least most of the drilled interval is not affected by the

possible false thickness produced by the growth fault. In this case, only the deeper part of the well shows variability of dips.

Sediment accumulation rates were calculated for the Utan-1 well (figure 6.20) showing values from 28-70 cm per thousand years (28-70 cm/Kyr) and average values for the Middle Pliocene, where the two Utan reservoirs are located, of 52 cm/Kyr, which is similar to values found for shallow Plio-Pleistocene sediments in the northern Gulf of Mexico, of 69-113 cm/Kyr (Armentrout and Clement, 1991). Because the variability in accumulation rates depend more on the time span in which the rate is calculated than on the depositional environment, calculated results for an area could be misleading. Therefore, it is recommended for the Utan area that more detailed biostratigraphy and additional controls are obtained from future wells if the same approach is going to be employed, otherwise further approaches as described by Bruns and Hass (1999), are recommended.

Bahamon (2006) determined sediment accumulation rates for three wells, including the Utan-1 discovery well. Values for the wells in the western downthrown side of the Kutz fault where the Utan structure is located, and lower rates on the opposite side of the fault indicate the structure remained high in the eastern side during Pliocene deposition.

### 6.2.6 An analog model

Ciudad del Carmen Island, Campeche state, Mexico, is located 67km southeast of the Utan-1 well. It represents a good present day analog of tidal flat sequences with

intertidal and supratidal subenvironments in a mixed siliciclastic-carbonate platform, which maintains two end member sediment supply sources, the siliciclastic source from the continent and the carbonate influence from the Yucatan platform northeastward of the island (figure 6.21).

The island represents a barrier island separated from the continent by a lagoon. Several shoreface subenvironments are clearly noticed including tidal channels, tidal deltas, intertidal deposits and ripple structures as well as supratidal environments. The sediment provenance and type of sedimentation maintain the bipolar influence varying in percentage along foreshore subenvironments with an almost purely siliciclastic influence in the west side, where a tidal channel promotes erosion, intrachannels and sediment redeposition, to a mixed or transitional environment at the middle of the island to an almost net carbonate influence eastward, more proximal to the Yucatan platform (figures 6.22 to 6.24).

### 6.3 The Pliocene: Time of change

At time scales of tens and hundreds of thousand of years, global climatic changes astronomically forced climate changes, and their influence upon accumulation rates have to be considered in the analysis. Climate warming is expected to result in rising sea level and the Middle Pliocene was the warmest interval of the Neogene, punctuated by cool intervals (figure 6.25).

In this context, the global climatic effects that occurred during the Mid Pliocene must be understood to complement the understanding of the types of depositional environments in which the Utan reservoirs were developed.

In 1993, the American Association of Stratigraphic Palynologists (AASP) held the symposium “Palynology, Climate and Sequence Stratigraphy of the Pliocene”, whose main contributions were printed by the AASP in the volume “The Pliocene: Time of Change”, in 1999. The key purposes were to understand the chronology of Pliocene geological, biostratigraphical, sea level and climatic events, and their potential use as analogs for future climate change (Leroy, 1999). As a result, regional event charts were published comparing geologic, biostratigraphic, climatic, and sea level events that occurred during the Pliocene in widely separated areas sharing analog climatic background (Wrenn, 1999). The charts show a consistent story that is significant on a global scale, discarding an exclusively regional influence. Additional contributions included the refining of the absolute Pliocene chronology by orbital tuning on oxygen isotopic records, cyclostratigraphy and astronomical calibrations as well as discussions on the controversial mid-Pliocene warming (for instance: Wrenn, 1999; Leroy, 1999; Cita, 1999).

The high quality of the climatic reconstructions showed that numerous climatic fluctuations characterized the Pliocene, giving veracity to the corresponding saying “…a time of change”.

The most widely used organisms for oxygen isotopic analyses are the foraminifera, both benthic and planktonic. As forams live and die and sink to the ocean

floor, they preserve a vertical record of the isotopic composition of seawater over time, and thus oceanic temperature. The variations in isotopic compositions of sediments or fossils have allowed geochemists to construct long oxygen isotopic composition curves that have been also used as stratigraphic markers for correlation purposes. Under isotope records and cyclostratigraphy reconstructions, it has been feasible to distinguish between successive isotopic cycles for the recognition of global signatures, which shows (Leroy, 1999; Cita, 1999) (Figure 6.25):

- The base of the Zanclean (boundary Miocene/Pliocene) has been placed at the base of the Italian Trubi Formation at 5.32My
- The first Pliocene cooling event has been dated at 4.5My. Warmer conditions remain for the rest of the lower Pliocene. Oxygen isotope values also suggest a possible deglaciation event between 4.9 to 4.3My
- The base of the Piacenzian coincides with the Gilbert-Gauss boundary and to an assigned astronomical age of 3.6My (3.58 in this dissertation which coincides with LAD of *Globorotalia margaritae*)
- Just below the Zanclean/Piacenzian boundary (at 3.6Ma) the temperatures began to decrease culminating in cold stages at 3.35-3.3My
- This was followed by a well documented warming about 3.3-3.15My: the Mid-Pliocene warm period, which spans the transition from relatively warm global climates of the Early Pliocene, when glaciers were greatly reduced in the Northern Hemisphere, to the global cooling trend toward the generally cooler

climates of the Pleistocene, with expanded Northern Hemisphere ice-sheets and prominent glacial and interglacial cycles.

- The cooling trend toward the late Pliocene glaciations starts at 3.15My and lasts approximately 0.5My to culminate by the earliest northern hemisphere glacial-interglacial cycles, which began at 2.6My. This was followed by the Gelasian just above the Gauss/Matuyama boundary (2.589My) (this boundary does not coincides with the Mid-Upper Pliocene boundary of the Pemex Southeastern Basins chronologic chart of figure 6.9). This was the most important climatic change of the Pliocene and seems to be diachronous at a global scale with strongly developed glacial events between 2.6 and 1.8My
- The end of the Gelasian, thus the Pliocene has been placed at 1.795My

The long, stable and well-documented warmest interval during the Mid-Pliocene, which resulted in warmer climate than the present, has been selected as an analog of current climate changes providing a potential guide to predict future global trends and the predicted strong green-house warming during the next decades. For these reasons, the mid-Pliocene has been an attractive target for extensive study including climate modeling and simulation studies by international organizations (NASA GISS, 2008; Leroy, 1999).

The ancient distribution of warm-climate ocean plankton, and of animal and plant fossils on land, also indicate that mean annual temperatures in the mid-latitudes

were often several degrees higher than present (Adams, 1998). The period of maximum Neogene warmth and high sea level from 4.0-3.0 My was punctuated by cool intervals.

The causes of these generally warmer climates of the Pliocene are still a matter of discussion. Higher levels of heat transfer through ocean circulation patterns is the most accepted mechanism although higher concentrations of greenhouse gases in the atmosphere is another unproven possibility (Leroy, 1999; Adams, 1998).

Because there was less ice volume near the poles, sea levels may have been as much as 30m higher than at present during the warmest intervals. Leroy (1999) reports high eustatic sea level estimates from the passive continental margin of the eastern United States, derived from oxygen isotopes and Mg/Ca ratios for the period 3.2 to 2.8My, close to the 25 to 40m.

Leroy (1999) refers how the astronomical forcing theory, which has been confirmed in recent years by biostratigraphic and radiometric analyses of long ocean cores, explains the cause of individual glacial-interglacial oscillations (after 2.6My) and warm-cold stages (before 2.6My), being tied to “Milankovitch Cycles”, i.e. variations of the Earth´s position in its orbit around the sun. Leroy (1999), also points out an attempt to correlate the time series of successive obliquity minima and the third order eustatic sea level cycles of Haq (Haq et al., 1988), the latter of which average 1.3My, corroborate that the third-order eustatic cycles are likely to be related to glacial episodes, thus are glacio-eustatically controlled.

The “Milankovitch Cycles”, would be also responsible for producing high-frequency cyclicity in stratigraphic patterns, as explained in Chapter 3. Long sediment cores show that even relatively short subdivisions of the Pliocene were characterized by almost continuous flux and oscillation in aridity and temperature, occurring on the timescale of several thousand years (often with a detectable periodicity of 19,000-21,000 years) (Adams, 1998). Leroy (1999), refers that Mid-Pliocene warming may have been of shorter duration according to new data which detail fluctuations around 3.2My.

It is probable that many other abrupt and shorter timescale Pliocene events remain “hidden” because of the lack of resolution of the long palaeoenvironmental records. In this sense, Adams (1998) recommends summarizing Pliocene climates and their extension to the Quaternary Period in a statistical sense in terms of averages, mean variance, period of oscillation etc. as they appear in the record. These statistical characteristics themselves shift throughout the period of the last few million years going into the Quaternary, with a decline in mean temperature and a trend towards increased aridity, and broader oscillations in both temperature and aridity.

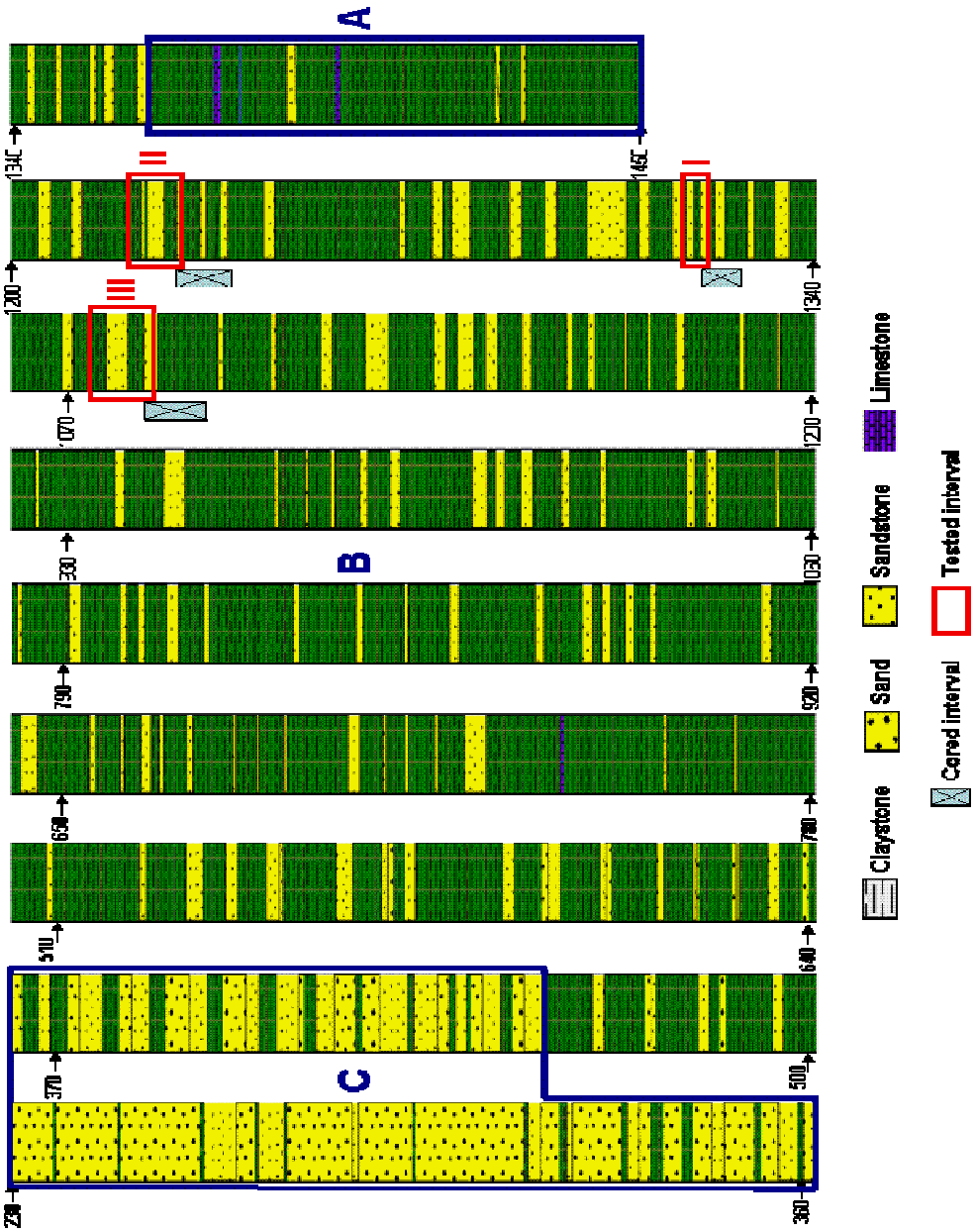


**Figure 6.1: Interpreted lithology from cuttings of the Utan well as extracted from the mud log report. The drilled interval can be divided into three broad lithologic groups (A, B; and C). The three tested intervals are shown in red (I, II and III).**

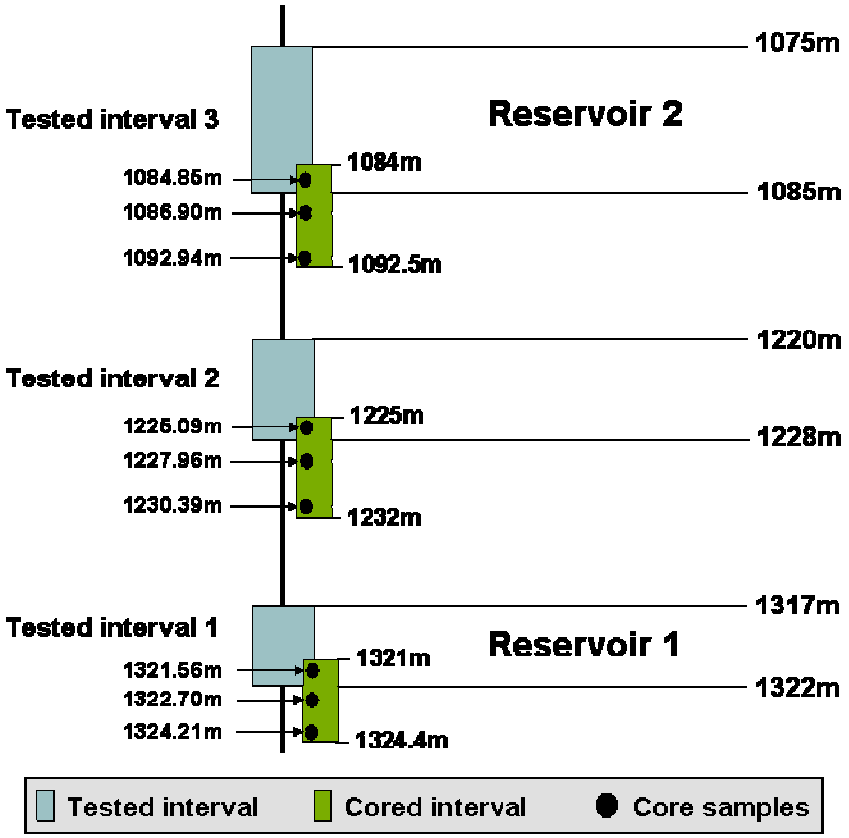


**Figure 6.2: Schematic sketch showing tested intervals, reservoirs, cored intervals and core samples in Utan well, which will be later referred in this dissertation.**

**Figure 6.3: The Core Storage Department of Pemex Marine Region was visited in repeated times for comprehensive visual analyses of the recovered cores available for this work.**

**Figure 6.4: After the comprehensive detailed visual analysis, it was concluded that all three cores of the Utan well exhibited similarities and a general mixed calcareous-siliciclastic lithology. (Upper) Core 3 (1084-1092.5m); (Middle) Core 2 (1225-1232m); (Lower) (1321-1324.4).**

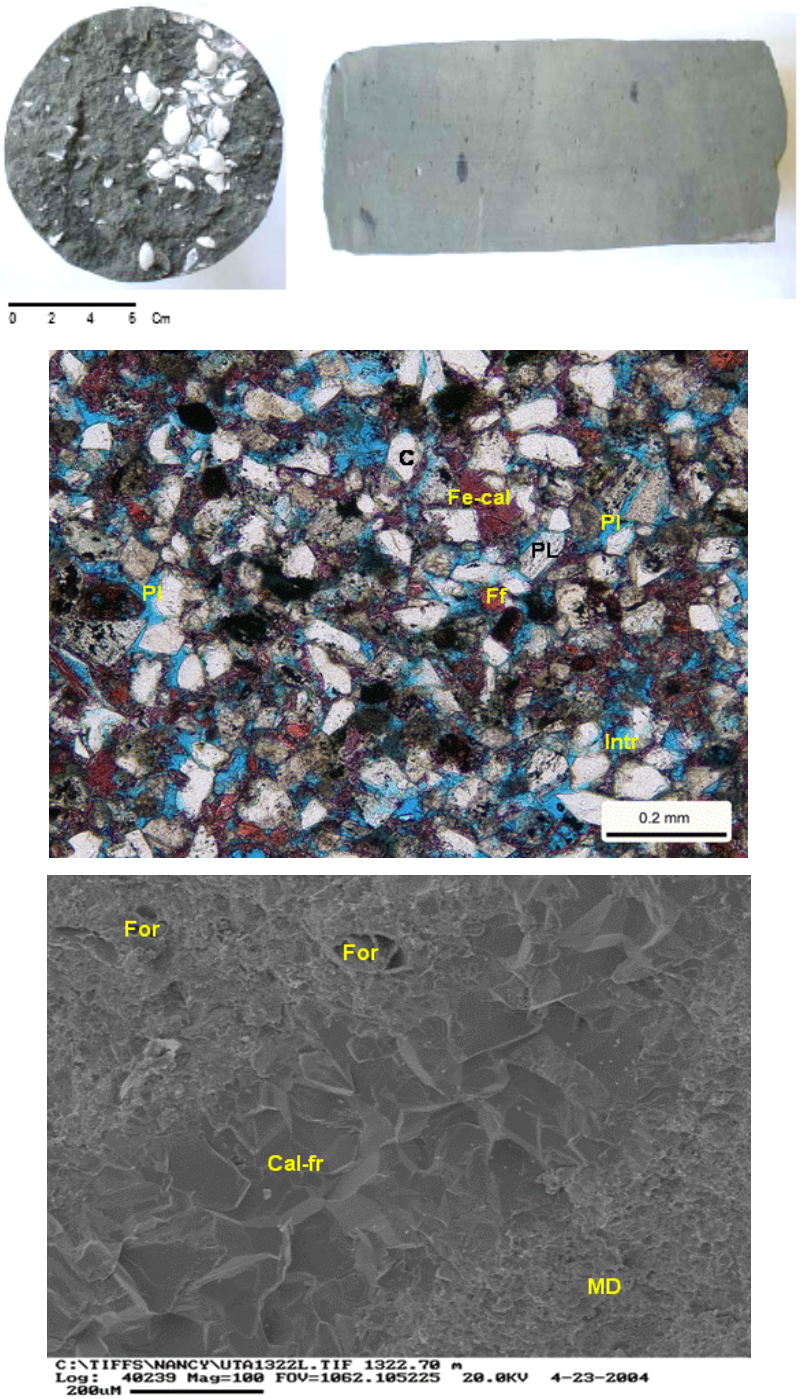


**Figure 6.5: Different scales of core analysis. Upper figure: Core sample at 1088m. Left: white shell fragments. Right: organic matter as black dots of coal; Middle figure: Photomicrograph of sample 1 (core 3) showing quartz grains as the dominant element and plagioclase (PL) in minor amounts. Carbonate detrital grains mainly include undetermined fossils (Ff). Carbonate cement is present as ferric calcite (Fe cal). The porosity system is mainly composed by primary intergrain pores which are locally interconnected (Pl), and intragrain pores (Intra); Lower figure: SEM image of sample 8 (core 3) showing how carbonate cement is also present filling open fractures (Cal-fr).**

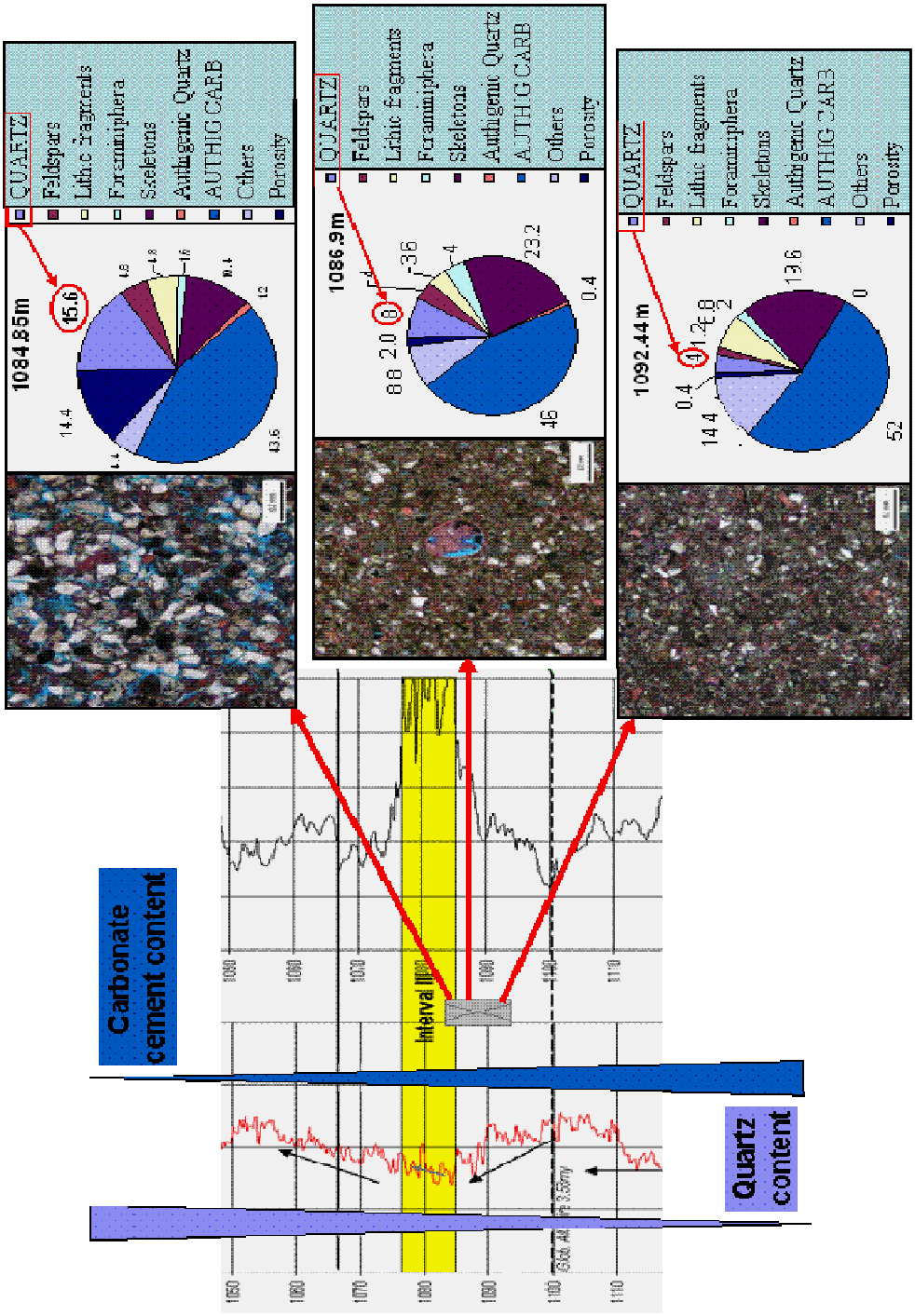


**Figure 6.6: Quantitative petrographic analysis incorporating the use of point counting for the three samples of the core 3 of Utan well (pie diagrams). The upper sample was located into the reservoir 3. An increase of porosity is closely related to an upward progressive increase in quartz content and a decrease of calcareous cement (modified from Bahamon, 2006).**

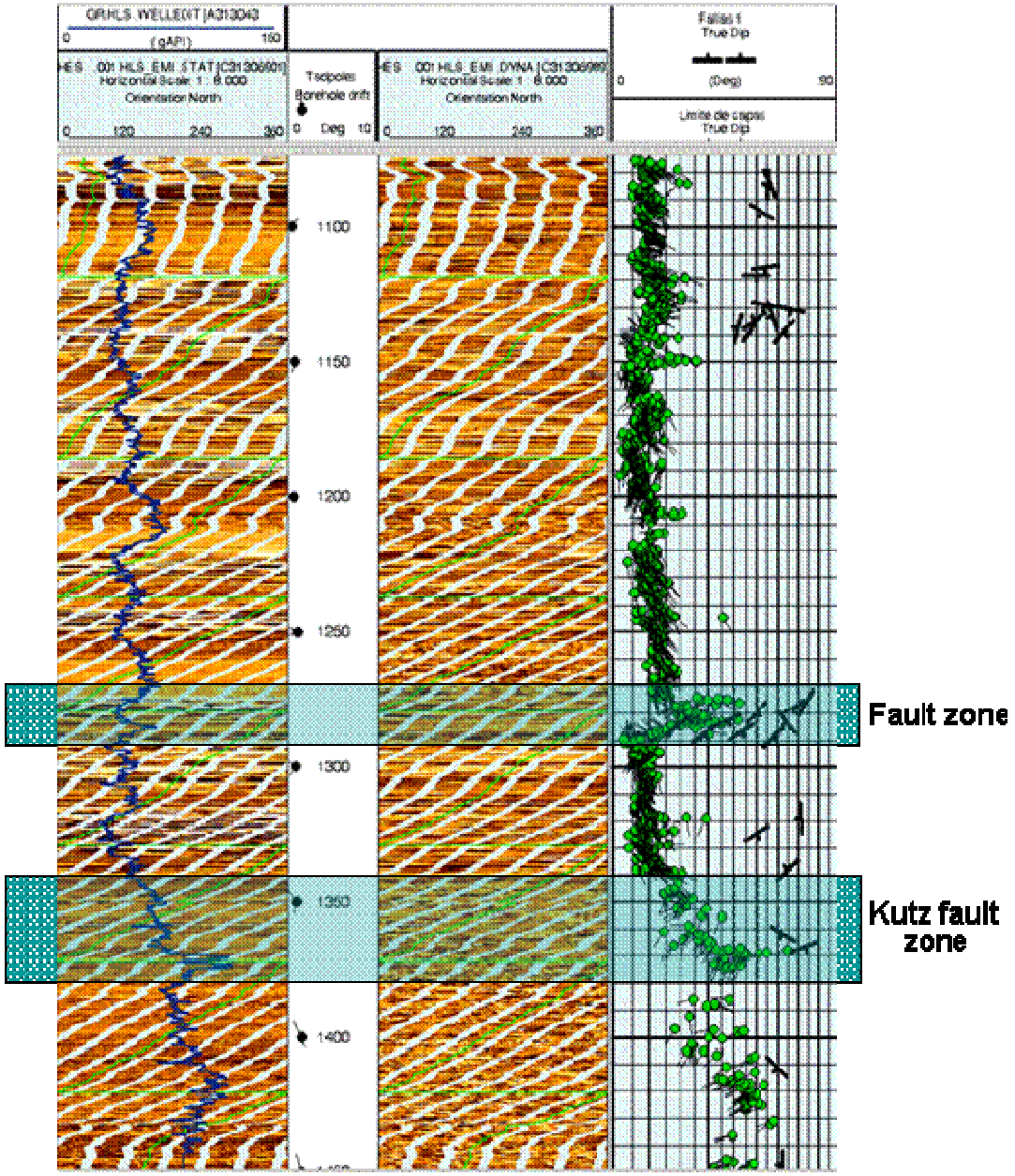


**Figure 6.7: Image well log showing the fault presence interpretation through the dipmeter analysis. The lower fault is the master Kutz fault against which the Utan rollover structure was formed.**

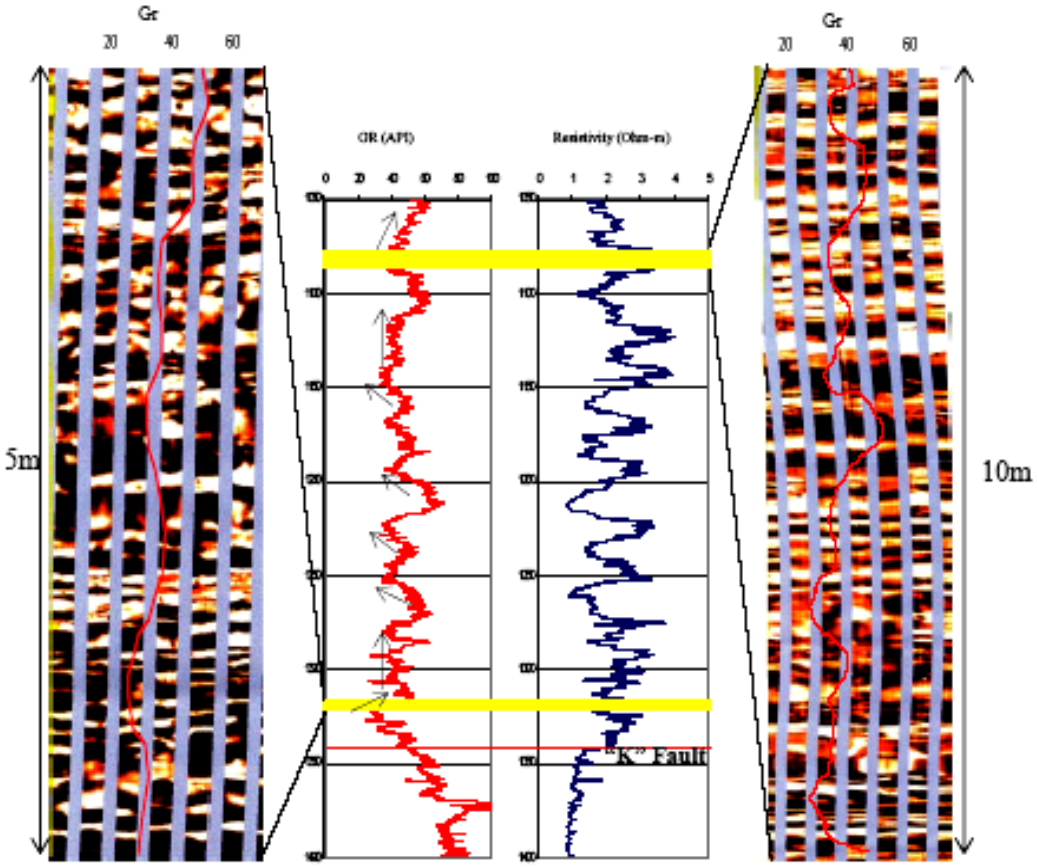


**Figure 6.8: Borehole image log of the two reservoir intervals. Left hand picture is the deepest reservoir at 1317-1322m. Right hand picture is the shallowest reservoir at 1075-1085m Overlying the image log is a gamma ray log in red. Note cyclicity as repetitive sequences of conductive and resistive images associated with intercalations of shale and sandstone respectively and that the productive layers could be the most resistive intervals (Bahamon, 2006).**

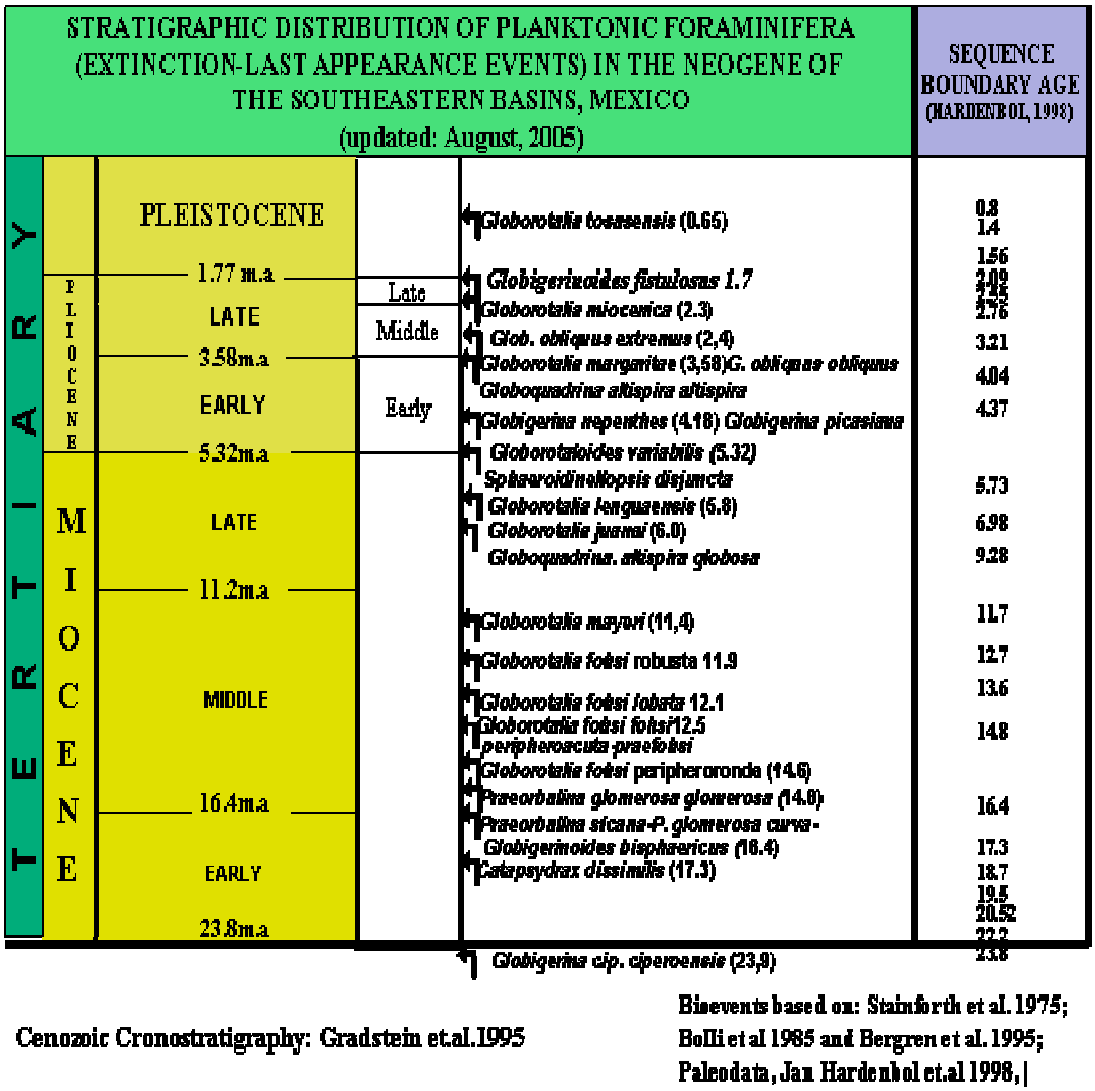


**Figure 6.9: Chronostratigraphic distribution of planktonic foraminifera in the Neogene of the Southeastern Basins of Mexico (adapted from non-published Pemex internal reports).**

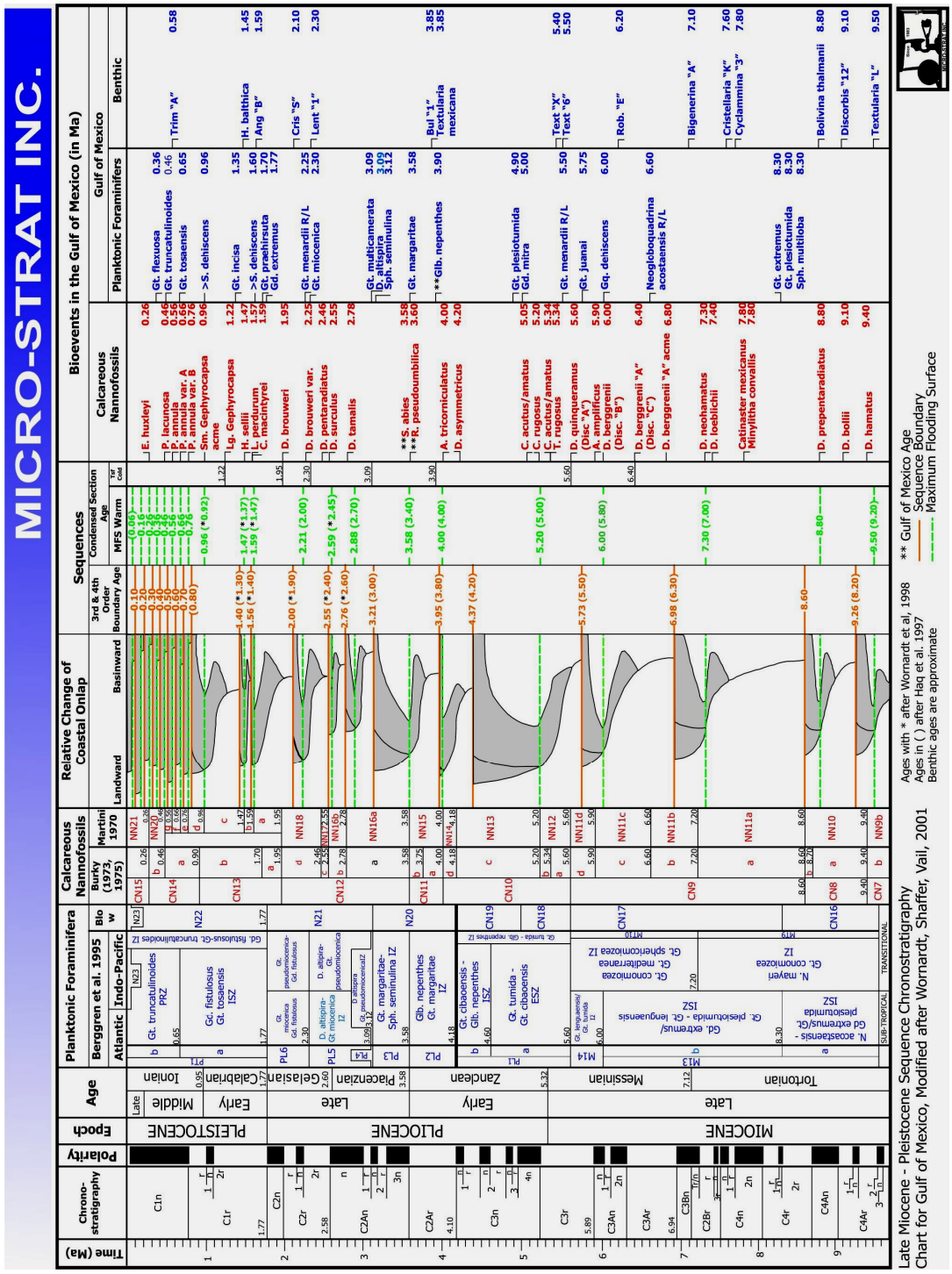


**Figure 6.10: Late Miocene – Pleistocene Sequence Chronostratigraphy Chart for Gulf of Mexico (Wornardt et al., 2002).**

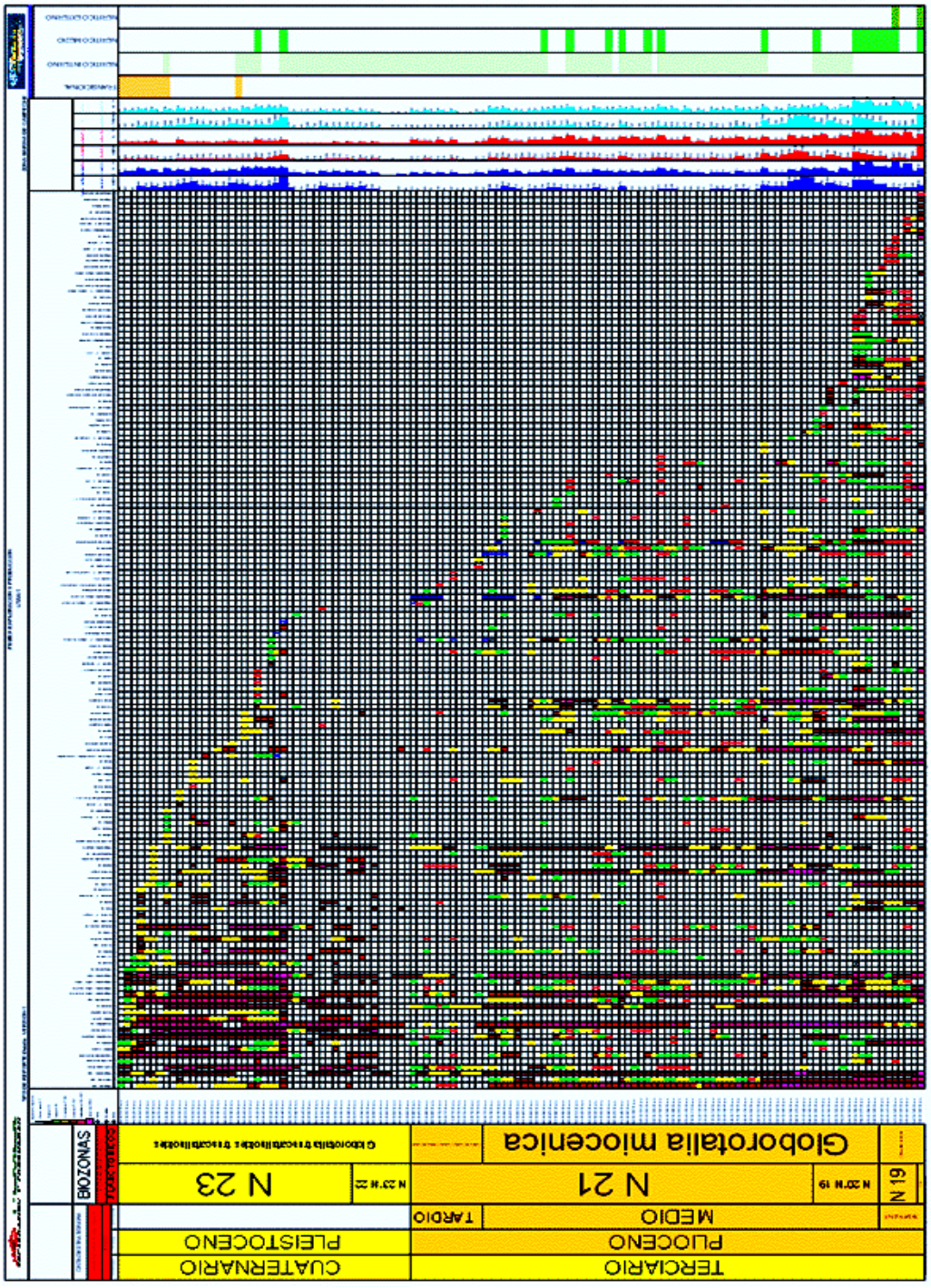


**Figure 6.11: Chart of Stratigraphic distribution and zonation of the selected planktonic and benthonic foraminifera for the Utan-1 well (for schematic purposes, non-published Pemex internal reports).**

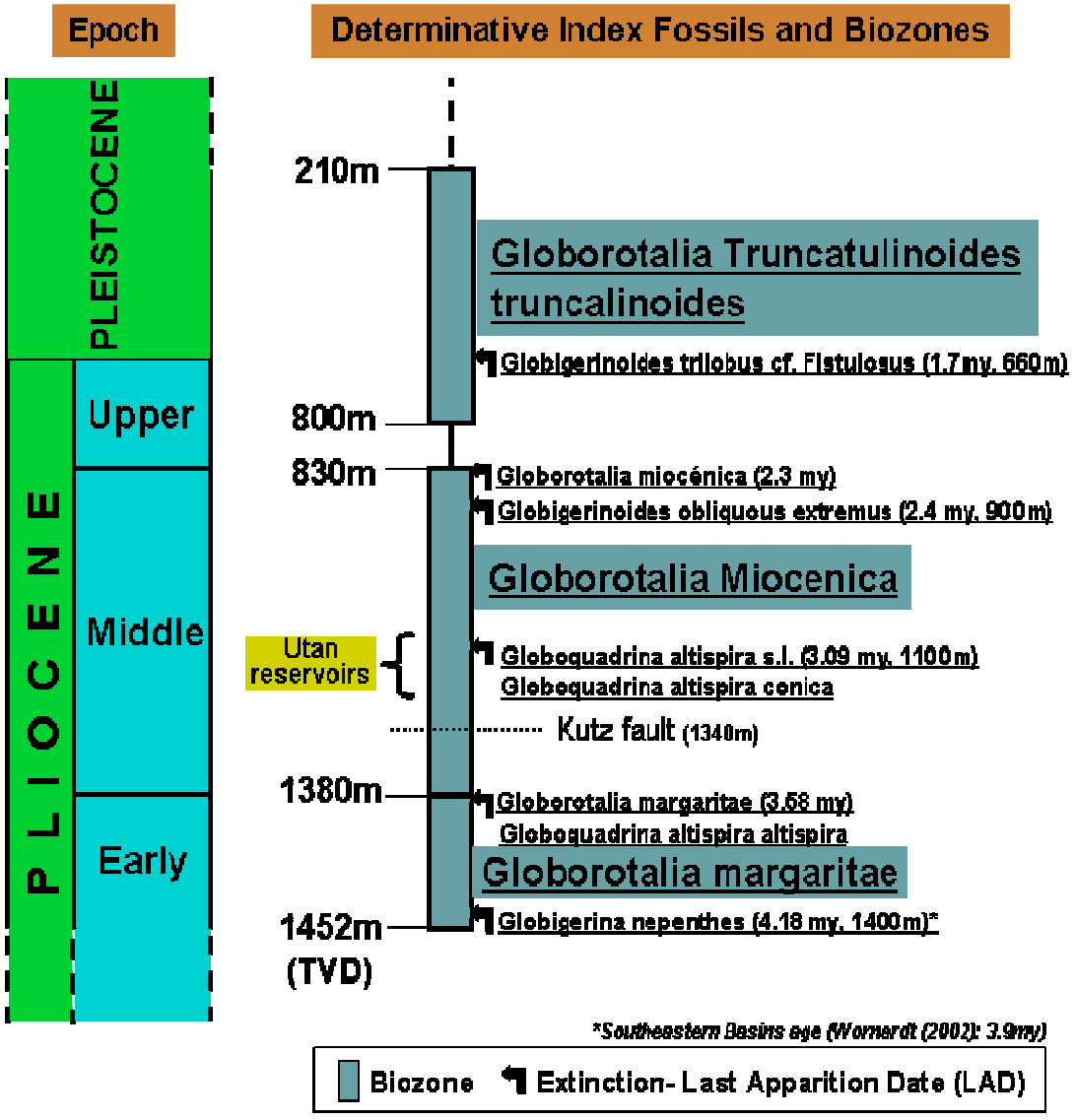


**Figure 6.12: Stratigraphic distribution and zonation of the selected planktonic foraminifera which were analyzed for the Utan well. Major biozones and main index fossils (LAD) are marked.**

| BATHYMETRY | ENERGY | Spp. BENTHONICS |
|---|---|---|
| **Inner Neritic** | High | Charophytes<br>Ostracods<br>Micromolluscs<br>Lignite<br>*Elphidium*<br>*Ammonia*<br>*Lenticulina spp*<br>*Hanzawaia spp* |
| **Middle Neritic** | High<br>Moderate | *Amphistegina spp*<br>*Lenticulina spp*<br>*Hanzawaia spp*<br>*Uvigerina spp*<br>*Brizalina spp*<br>*Siphonina sp*<br>*Sphaeroidina* |
| **Outer Neritic** | Moderate<br>Low | *Globocassidulina*<br>*Cibicidoides spp*<br>*Pullenia*<br>*Nodosaridos*<br>*Rectouvigerina*<br>*Animalinoides*<br>*Nonion affine* |
| **Upper Bathyal** | Low | *Melonis pompiliodes*<br>*Cyclammina spp*<br>*Pyrgo spp*<br>*Usbekistania charoides*<br>*Chillostonella sp*<br>*Hoegundina sp*<br>*Gyroidinoides* |
| **Middle Bathyal** | Low | *Cibicides wuellerstorfi*<br>*Pleurostonella sp*<br>*Nuttalides sp*<br>*Vulvulina sp* |

**Figure 6.13: Paleobathymetric distribution of some benthonic foraminifera index fossils for the Southeastern Basins of Mexico (adapted from non-published Pemex internal reports).**

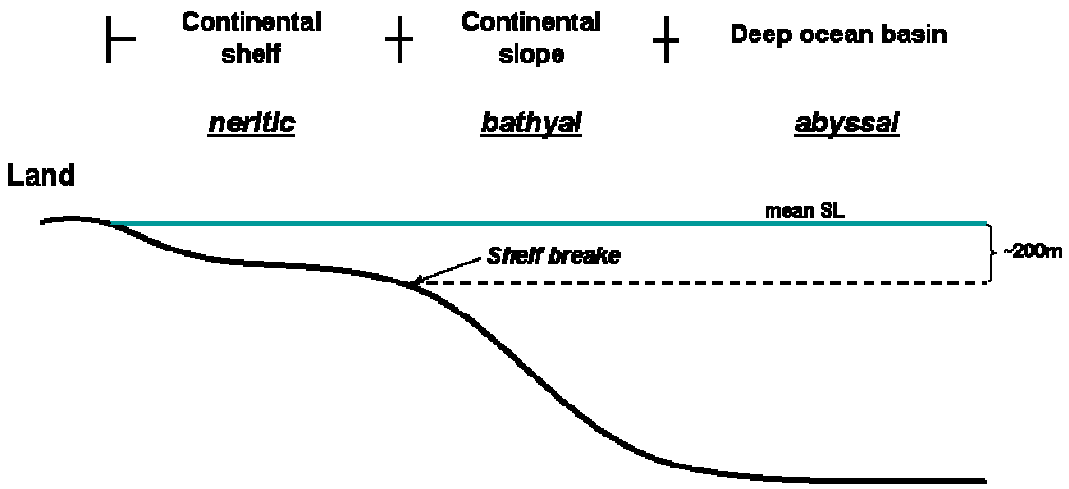


**Figure 6.14: Common terminology for marine environments.**

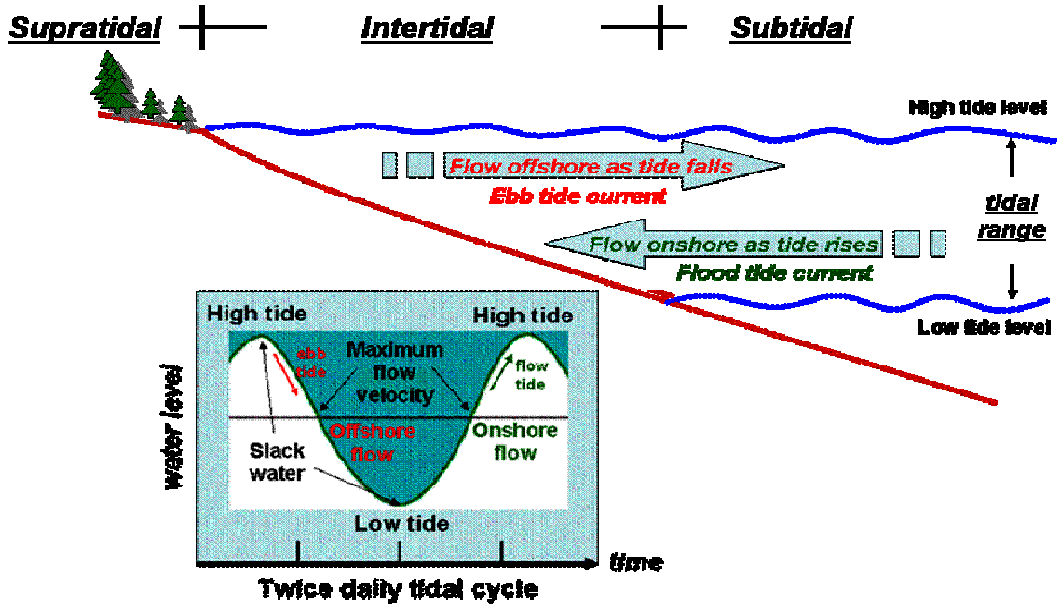


**Figure 6.15: Tidal domain and changes in direction and velocity of flow during a tidal cycle (after Nichols, 1999).**

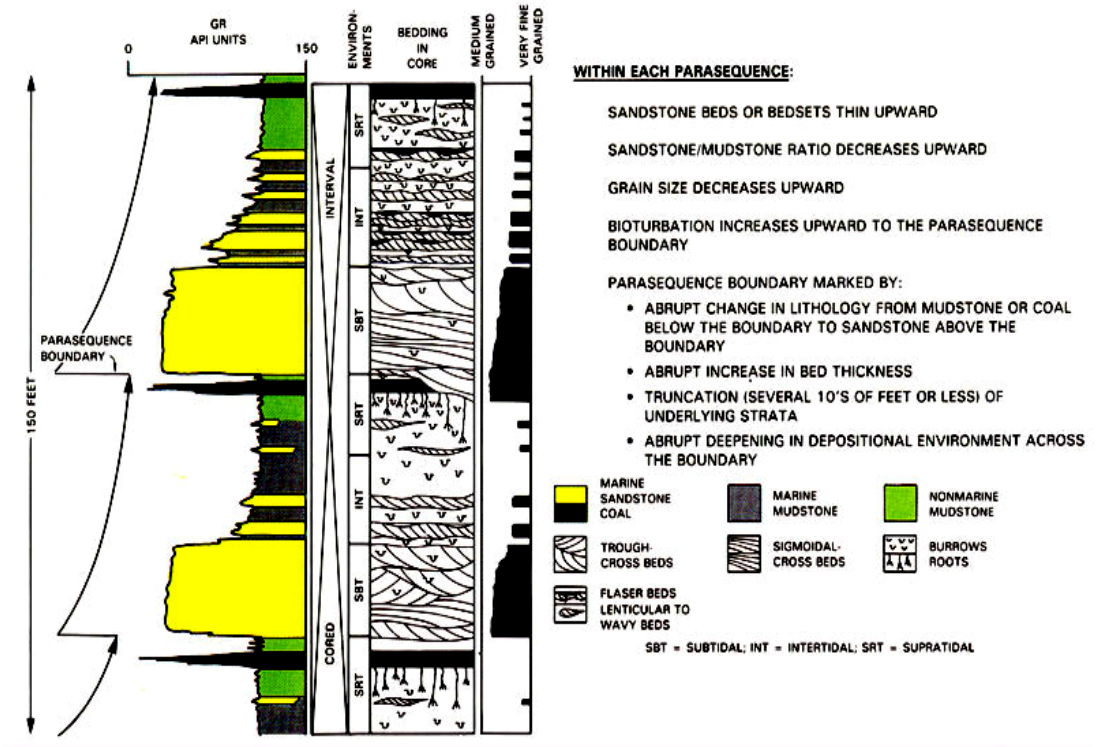


**Figure 6.16: Stratal characteristics of two upward-fining parasequences. These types of parasequences are interpreted to form in a tidal flat to subtidal environment on a muddy, tide-dominated shoreline (VanWagoner et al., 1990).**

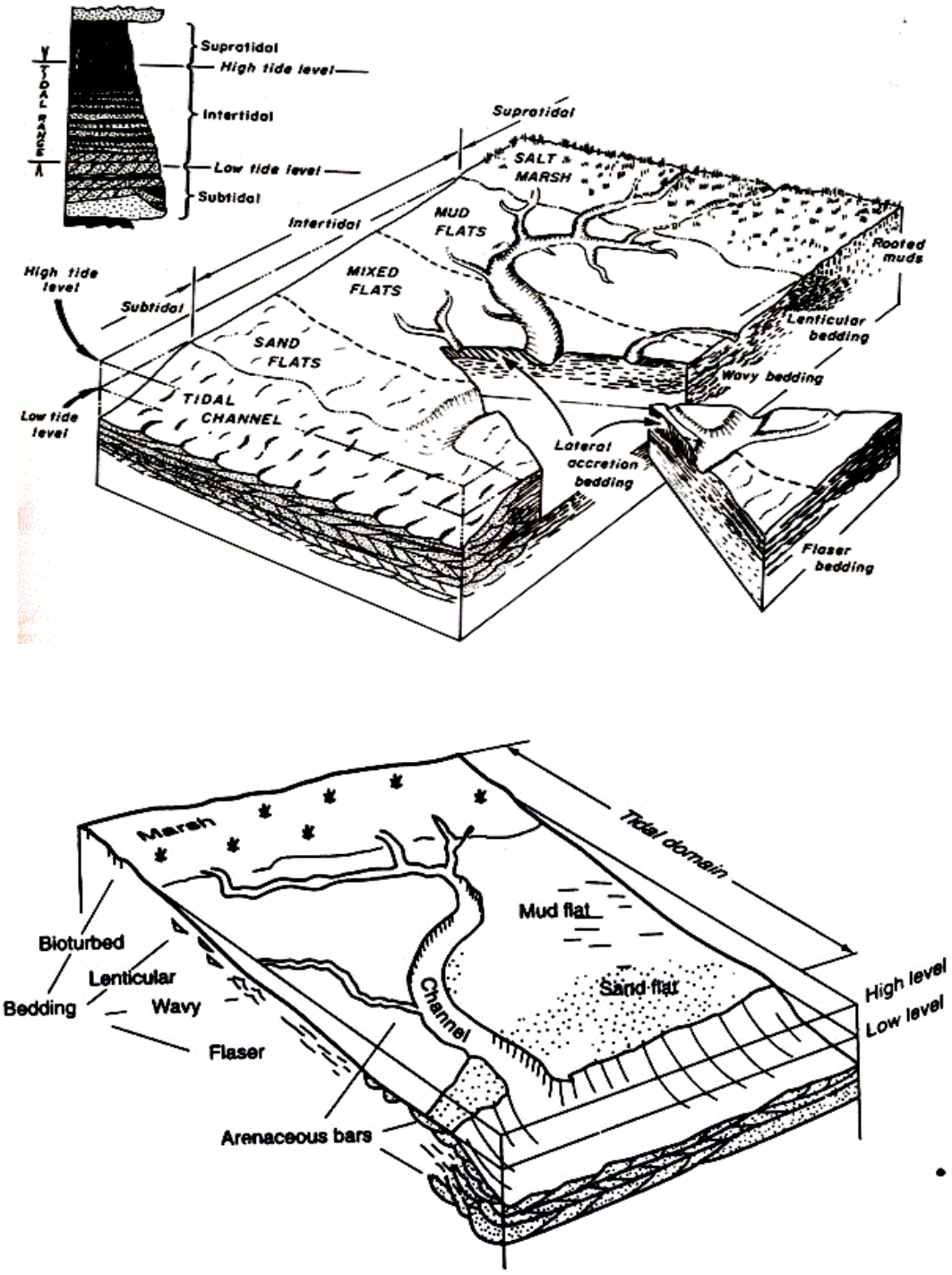


**Figure 6.17: Domain and types of sediments in the tidal zone. Top figure (Dairymple, 1992); base figure (Biju-Duval, 2002).**

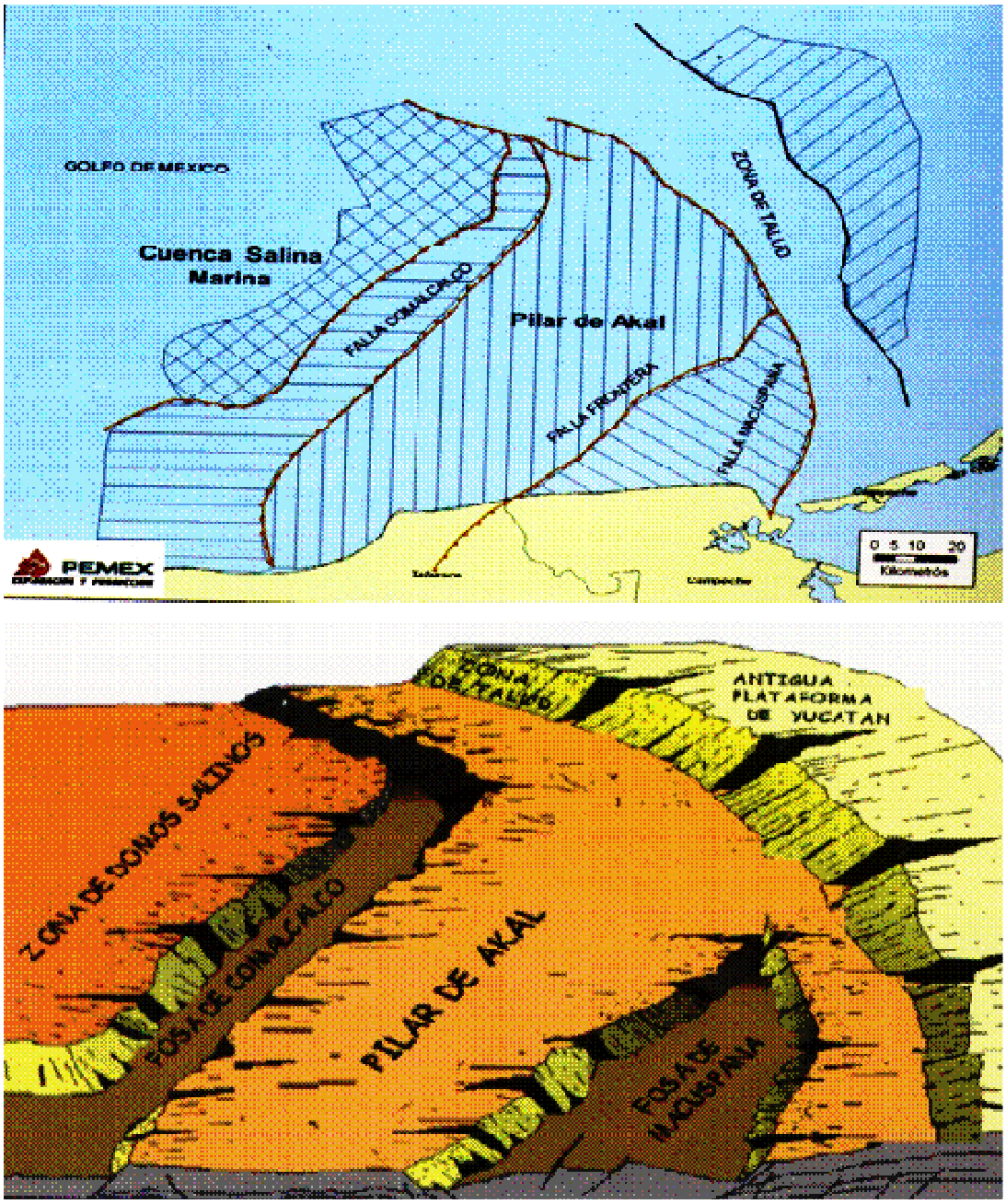


**Figure 6.18: Composite image of major structural features and tectonic provinces of the Campeche Sound. Top figure: areal view; base figure: isometric view ("Zona de talud" menas Campeche escarpment), (Angeles-Aquino, 2006).**

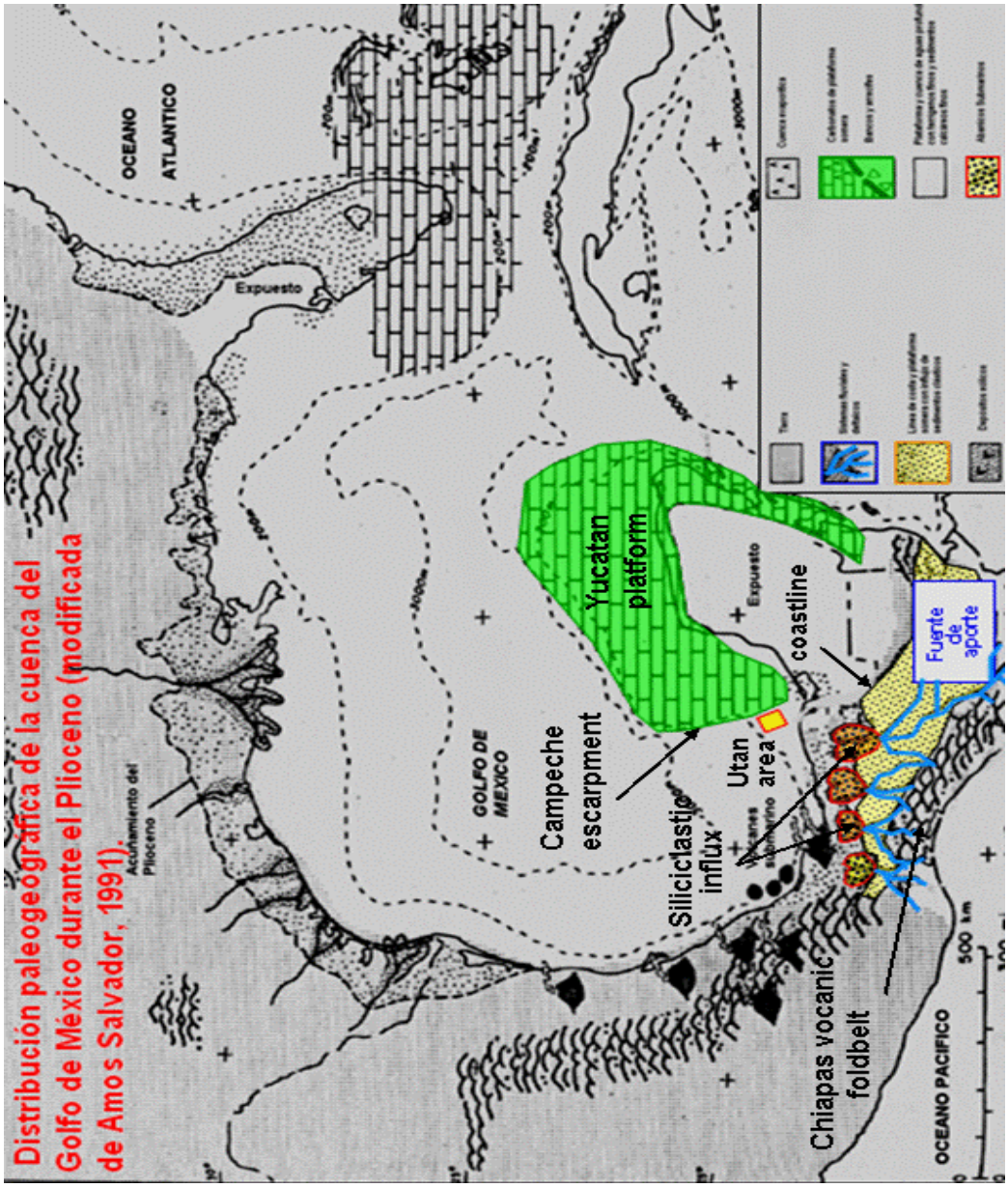


**Figure 6.19: Paleogeographic map for Southeatern Gulf of Mexico in Pliocene times. Sediment influs for Utan area was provided by two end-members, the carbonated Yucatan Platform and the Chiapas foldbelt (non-published Pemex internal reports).**

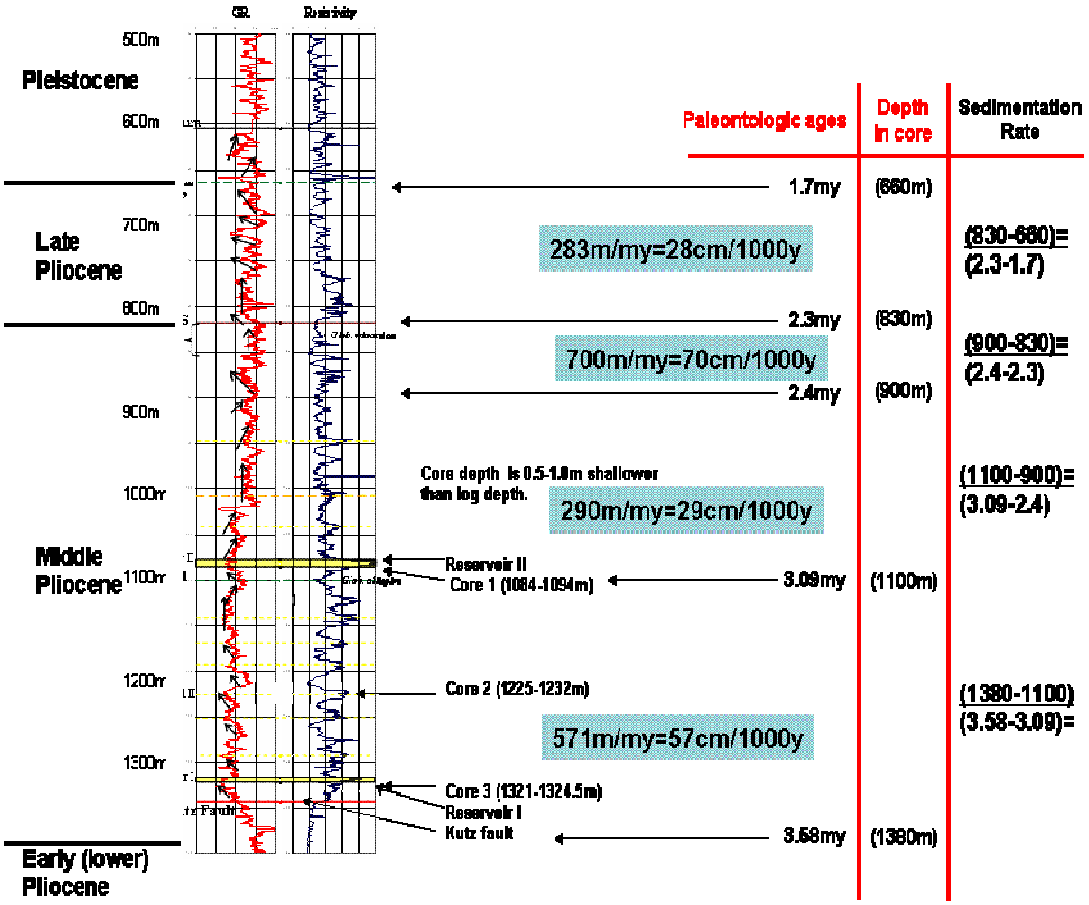


**Figure 6.20: Sedimentation rates in the strata drilled in the Utan well.**


**Figure 6.21: Location of Ciudad del Carmen Island, Campeche State, Mexico, 67km southeastward of the Utan-1 well. Base figure shows the location of subareas A, B, and C of terrigeneous, mixed and carbonate-prone sedimentation, respectively (Angeles-Aquino, 2004b).**

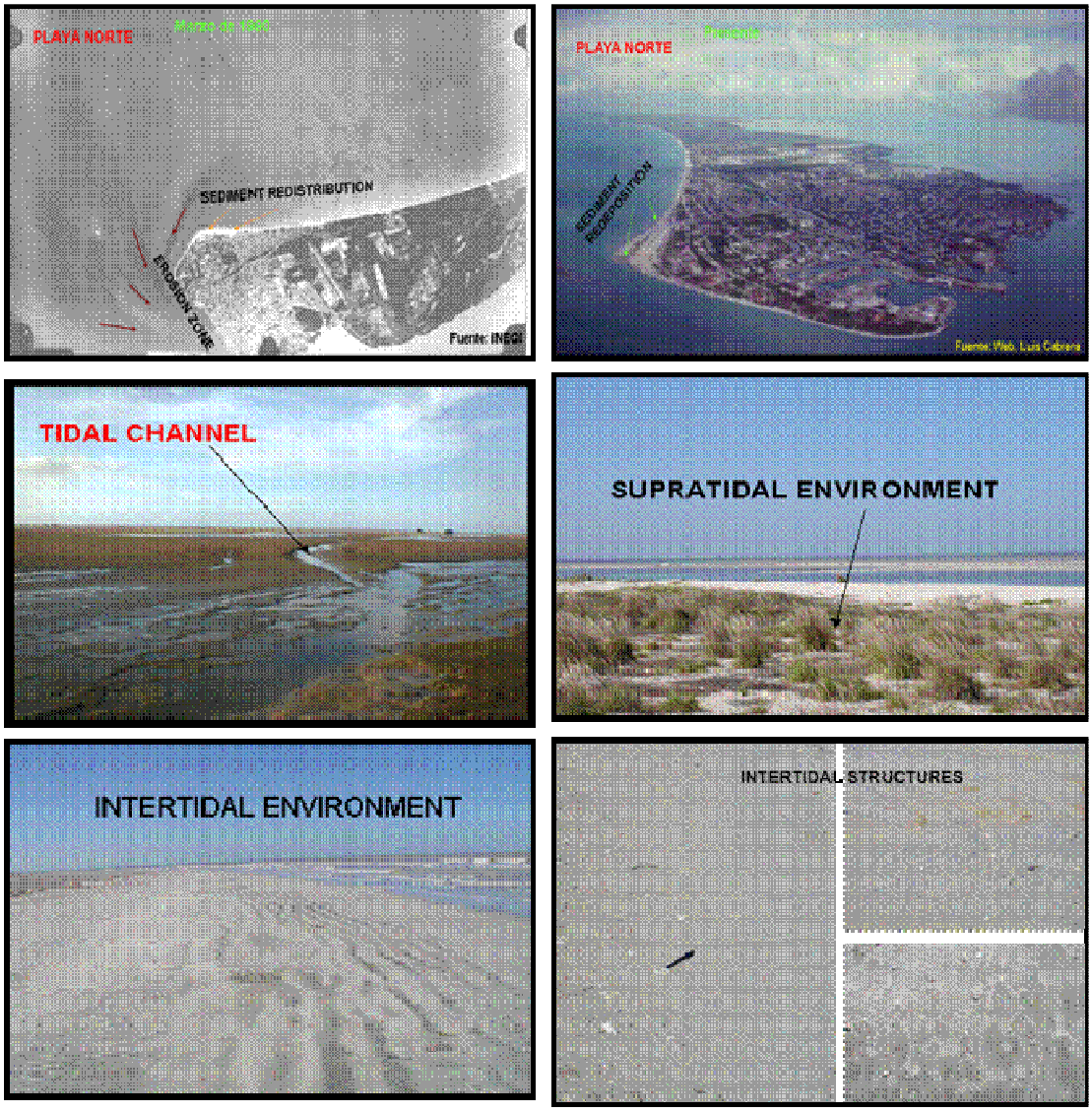


**Figure 6.22: Zone A of figure 6.22 showing Ciudad del Carmen as a barrier island with erosion, tidal channels, tidal deltas and supratidal and intertidal subenvironments with mostly terrigeneous sedimentation (Angeles-Aquino, 2004).**

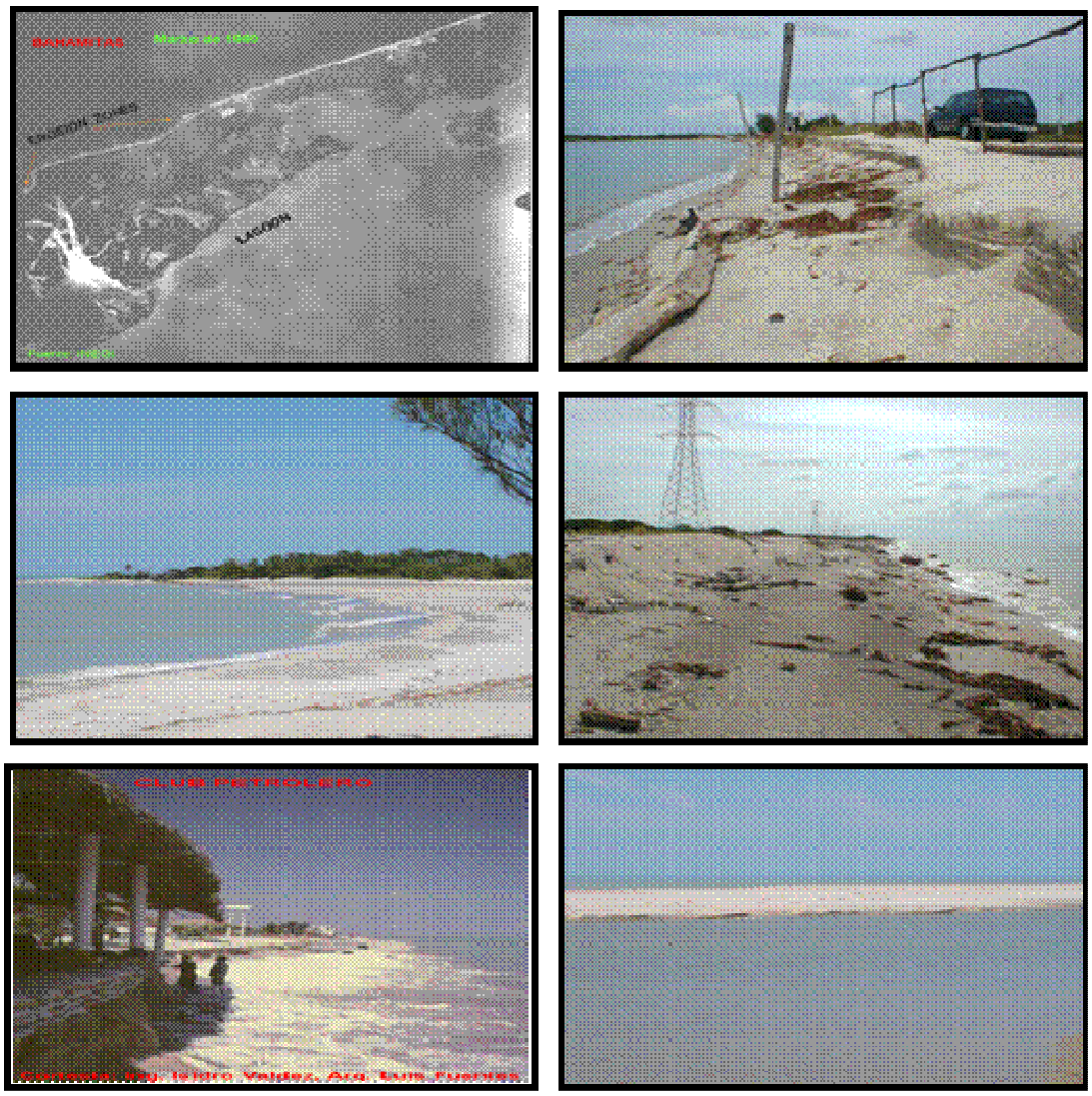


**Figure 6.23: Zone B of figure 6.22 showing depositional environments with a mixed siliciclastic-carbonate influence. Banks, shoreface and intertidal subenvironments look different from the purely siliciclastic influence shown in zone A (figure 6.23) (Angeles-Aquino. 2004b).**

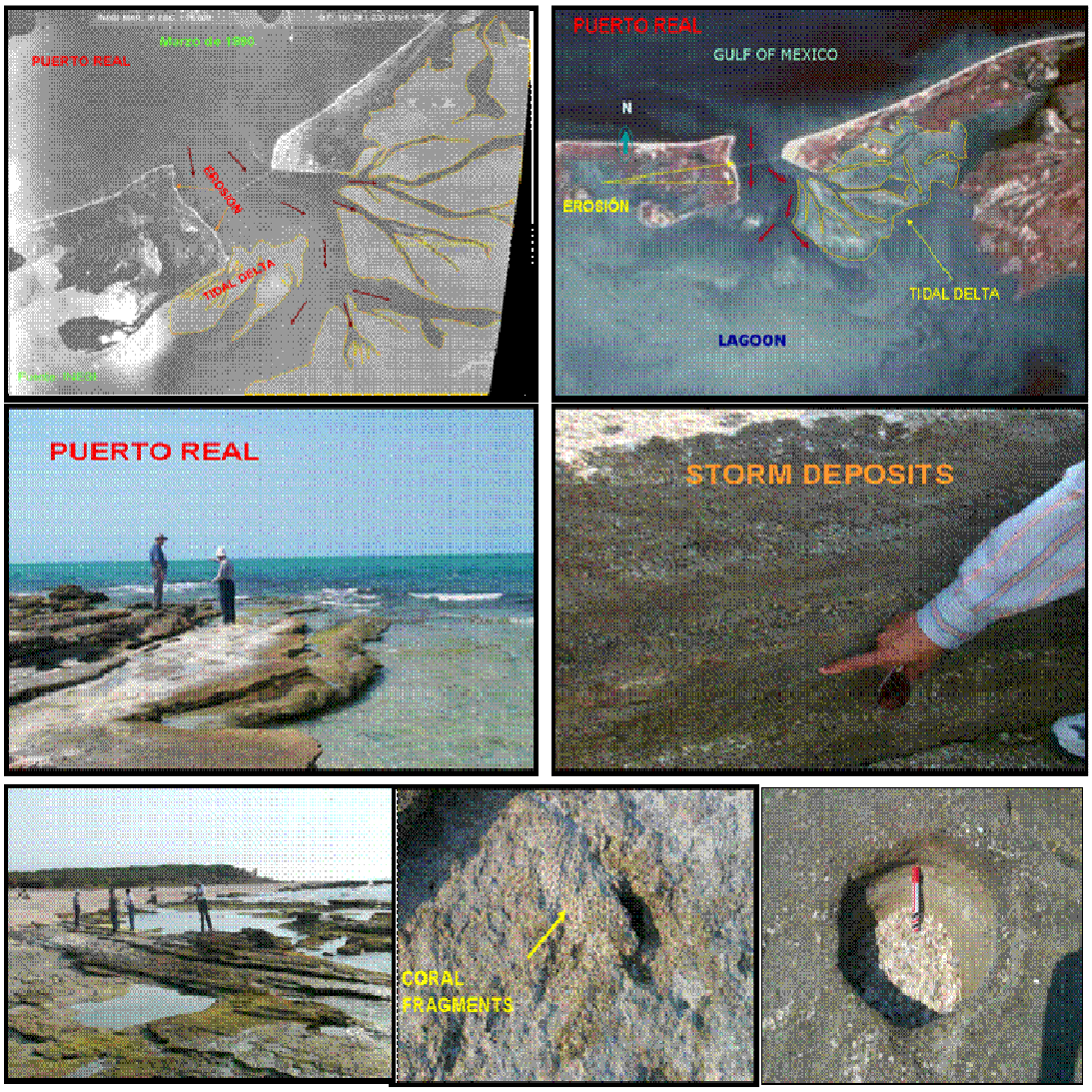


**Figure 6.24: Zone C of figure 6.22 showing depositional environments with a mostly carbonate influence due to the proximity to the Yucatan platform. Banks, shoreface and intertidal subenvironments look more compacted than the purely siliciclastic influence shown in zone A (figure 6.23) (Angeles-Aquino. 2004b).**

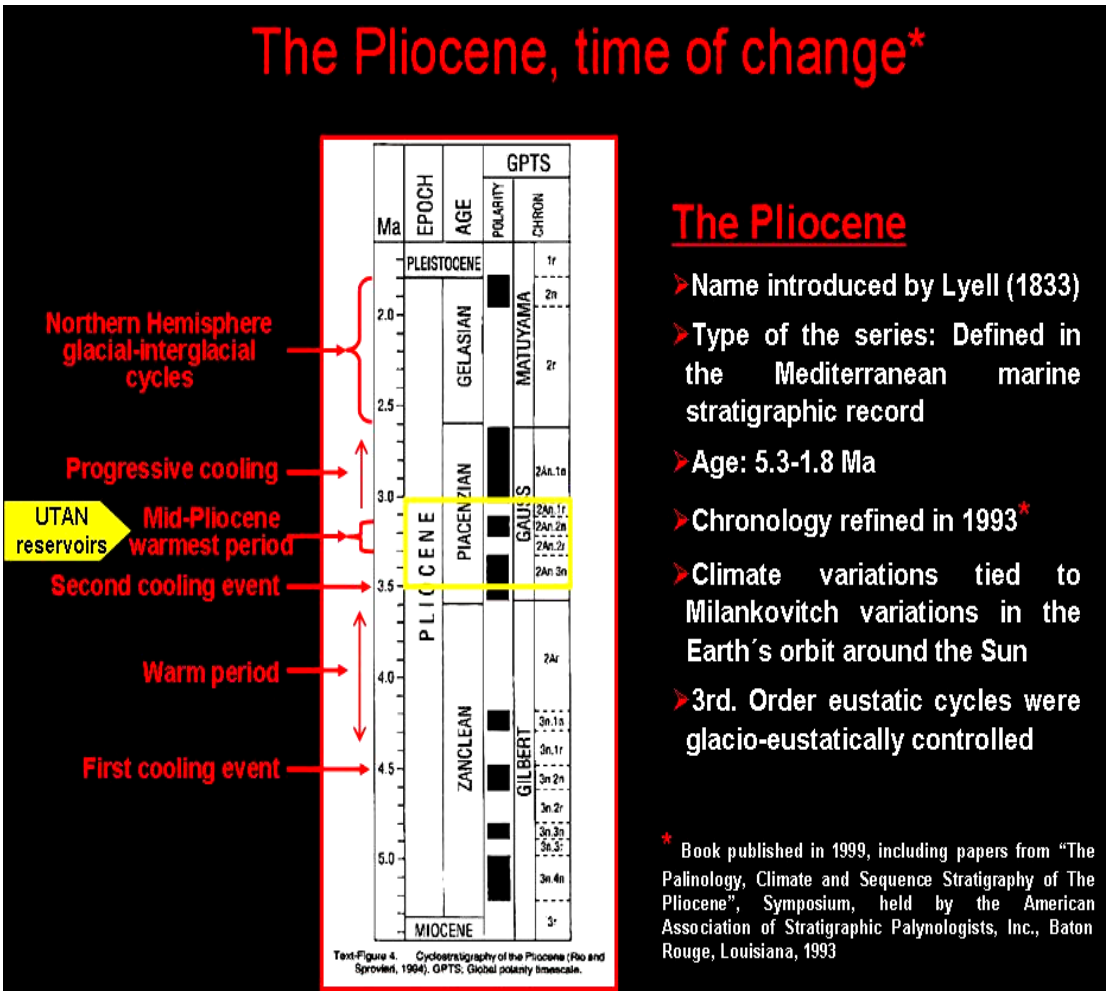


**Figure 6.25: Cyclostratigraphy, climatic events derived from Oxygen isotope records, and some other references of the Pliocene epoch. GPTS: Global polarity timescale (after Leroy et al., 1999).**

# Chapter 7

# SEQUENCE STRATIGRAPHIC FRAMEWORK AND INTEGRATED ANALYSIS (II)

## 7.1 Introduction

Sequence stratigraphy provides a deterministic framework for understanding the relationships in time and space between rock layers, depositional environments and facies in terms of relative sea level changes, and a structured scheme to define reservoir architecture and reservoir quality.

As a follow-up to the depositional model established in Chapter 6 for the facies deposited in the Utan area, and based on the same database, a sequence stratigraphic framework was first established for the Utan-1 discovery well. This well contains the most comprehensive well database for the analyzed late Tertiary stratigraphic targets, thus it was the reference well to build a well log sequence stratigraphic framework and then to extend it to the remaining area for the integrated interpretation.

Once the key surfaces for stratigraphic correlation were identified, the well log signatures were extrapolated to the nearby wells through well log cross section correlations. Finally, the well log data and key surfaces were tied to the seismic data for seismic stratigraphic correlation and interpretation. Several loops between seismic and well log data were performed to assure agreement of interpretations.

After the preliminary framework was established, seismic sequence interpretation and seismic attributes were employed to more accurately delineate the reservoir intervals. This analysis formed the basis for identifying new opportunities in the study area and to plan a development strategy for Pemex.

Establishment of the sequence stratigraphic framework and the integrated interpretation for the Utan area were based on the workflow defined in Chapter 1 and according to the concepts established in Chapters 3 and 6.

## 7.2 Review of the structural framework

Once a reliable depositional model was established for the facies deposited in the Utan area (Chapter 6), a review of the local structural model was made in order to decide whether to segment the study area prior to developing the sequence stratigraphic framework.

As stated in Chapter 2, the Cantarell complex consists of a broad northwest-southeast trending, faulted anticline in the Campeche Sound (figure 2.16), which has been divided into three separate main fault-bounded allochthonous blocks: Akal, Nohoch, and Kutz.

The study area is a linear north-south–trending structure that is separated from the Akal structure by a major north-south–trending Tertiary listric normal fault, i.e. the Kutz fault (figures 2.16 and 2.17). The fault separation decreases from north to south.

Utan field is located in a minibasin formed by growth and antithetic faulting in the southern part of the Kutz block (figures 2.18 and 2.19).

Locally, the Kutz fault divides the study area into two parts (figures 2.16 to 2.19):

1. The hanging-wall to the west of the fault contains the Utan rollover anticline. The hanging-wall rotates into the growth fault as a result of the listric fault geometry and differential loading of the Plio-Pleistocene sediments, above a ductile shaly Miocene surface. The beds within this half-graben are tilted and thicken into the fault. The main trap mechanism is not the fault itself but the rollover closure against the master major listric fault.

2. The foot-wall east of the fault remained as a relative structural high during the rollover process.

Five secondary faults compartmentalize the structure and corresponding reservoirs. Bahamon (2006) reconstructed the structural model in a cross-section displaying the structural style in the study area (figure 7.1). Basic preliminary seismic interpretation developed in Chapter 5 of this dissertation showed how the seismic character changes across the listric fault (figure 7.2). Signal to noise ratio and frequency content of the seismic data are lower on the east side of the fault, consequently a different wavelet behavior could be expected, which has produced poor well to seismic ties on that side of the fault.

### 7.3 Well log sequence stratigraphy in the Utan-1 well

Well logs allow the identification of key surfaces for sequence stratigraphic interpretation and for correlation of these surfaces between adjacent wells. Well log sequence stratigraphic analysis provides a first understanding of the relationships between the depositional environment and how it was affected by sea level changes. In this step, preliminary estimates of sequences and systems tracts are proposed from the interpreted lithofacies, biostratigraphy, and correlation with global cycle charts. In this stage, changes in accommodation space are determined from parasequence stacking patterns.

According to the Utan-1 well position in the structural framework of the study area, and based on the seismic data quality, it was decided as a strategy to set up the sequence stratigraphic framework for the Utan-1 discovery well, extend the Utan well log-seismic interpretation to the nearby wells on the western flank of the Kutz fault, then to attempt to transfer the interpretation across and to the east of the fault.

Gamma ray and resistivity curves were used to identify log patterns and a quick look was carried out on seismic data to delineate candidates for key surfaces, i.e. sequence boundaries, maximum flooding surfaces and other regional marker horizons.

Biostratigraphy and well log data were required for assignment of ages and to identify key chronostratigraphic surfaces. Extinction datums and biozones, determined from the biostratigraphic analysis (see-Chapter 6 and figure 6.11) were annotated in the well log curves. Parallel to this process the interpreted key fossils and ages were

tied to the eustasy curve published for the Gulf of Mexico (modified from Wornardt and Vail in 2002) (figures 6.10 and 7.3).

As a result, two sequence boundaries marking major discontinuities and one maximum flooding surface were identified:

- **Sequence Boundary #1:** It occurs at 1100m, just below the upper reservoir, through the LAD of the index fossil *–altispira-* (3.09ma) corresponding to a sharp drop of sea level according to the eustasy curve.
- **Maximum flooding surface (MFS):** It is at 830m and is associated with a rise of relative sea level indicated by the eustasy curve, the approximate extinction age of *Globorotalia miocenica,* some faunal peaks in the paleontological reports, and the top of a 30m high-gamma ray/low resistivity shale interval (the corresponding condensed section). The Gulf of Mexico coastal onlap chart (Wornardt et al, 2002) also reports this MFS.
- **Sequence Boundary #2:** It is at 660m and corresponds to the LAD of *Globigerinoides trilobus cf. Fistulosus* (1.7my) (figure 6.11), a sharp drop of sea level reported in the eustasy curve, a low gamma-ray/high resistivity response, and a higher rate of drilling penetration and loss of mud fluid reported by the mud logger.

Two additional key surfaces were identified:

- A third SB was inferred by a sharp gamma ray change below the deeper reservoir whose base is at a depth of 1322m, and above the Kutz fault located at

1340m. It is interpreted to occur between the top of a coarsening upward pattern (HST?) and a sand interval above. In practice, the boundaries are not always precise and the proximity of the Kutz fault could favor the presence of a sequence boundary slightly above the fault, but it could also occur at or beneath the fault (Mendez et al., 2006). Unfortunately, the Kutz fault has prevented a more definitive interpretation of this possible sequence boundary.

- A shale interval located at 605m, which will be later used as datum for well log stratigraphic correlation.

According to the interpretation of key surfaces on the Utan-1 well, the time interval spanned between the SB3 and SB1, as well as between the SB1 and SB2 boundaries correspond to Vail´s third-order depositional sequences. Thus, the interval is interpreted as a transgressive systems tract (TST) and a highstand systems tract (HST), separated by a maximum flooding surface (MFS) between SB-1 and SB-2. Another highstand systems tract (HST) is interpreted to occur between SB-3 and SB-1 (fig. 7.4). According to the depositional environment proposed for this study area, shallow waters would imply platform exposure, erosion and the lack of preserved lowstand deposits, which agrees with the proposed interpretation.

Stacking patterns and internal configuration into systems tracts suggest the additional presence of higher-order sequences, i.e. parasequences (Van Wagoneer et al., 1990). According to Mulholland (1998b), parasequences have been identified in coastal plain, deltaic, beach, estuarine and shelf environments whereas they have not

been identified in fluvial sections without marine influence or in deep-water environments where water depth is not an influence.

Eight low gamma-ray, sandy intervals occur between SB-3 and SB-1 (fig. 7.5), which are interpreted as parasequences (Mendez et al., 2006). The lowermost, labeled PS1, which sits upon SB-3, and which comprises Reservoir Interval I, is aggradational to retrogradational based upon the fining-upward log shape. PS2 and PS3 are aggradational; PS4, PS5, PS6, and PS7 are progradational; and PS8 is aggradational. Reservoir Interval II sits atop SB-1; termed PS9, it is also clearly retrogradational (fig. 7.5). Above this parasequence, to SB-2, there are a number of mainly progradational parasequences (figure 7.4).

Variations in the type of parasequence within the well are a result of high frequency variations in rate of sediment supply, eustacy, and subsidence during different geologic time intervals (Mendez et al., 2006). High-order sequence identification might be feasible on key wells, however their identification on seismic data will depend on the seismic resolution of the dataset used in this research. Mulholland (1998b), points out that parasequences and their boundaries (marine flooding surfaces), are easily identified in cores, outcrops, and well logs, however they are too thin to be identified seismically. On the other hand, the same Mulholland (1998c) clarifies that although individual parasequences are generally below seismic resolution, sets of stacked parasequences (termed parasequence sets) are distinguishable by their characteristic stratal patterns.

Only the two retrogradational parasequences between SB1 and SB3 are reservoirs. Lowstand erosion, followed by early transgression, produces high energy at the migrating shoreline, thus concentrating quartz-rich sediments on this surface. The observed increase in porosity caused by the increase in quartz content has resulted in reservoir quality sand occurring as retrogradational parasequences sitting on the sequence boundaries. This analysis has provided a new play concept under this stratigraphic framework. In other words, the delineation of regional sequence boundaries using seismic or well log data should reveal retrogradational parasequences which might be reservoir-prone. Mulholland (1998c) refers to the fact that parasequences stack in orderly and predictable patterns controlled by relative sea level, so that enhanced prediction of depositional environments and subsurface chronostratigraphic correlations can be more reliable.

On this basis, the interval which lies upon SB2 is a retrogradational parasequence (figure 7.4) that was never tested. In this case, the overlying 20-30m condensed section might be a regional seal in the study area.

Mulholland (1998c), has pointed to the widely accepted concept that transgressive shoreline sands are deposited along the shoreline as it migrates landward with the transgressive sea. Such sand bodies are really the retrogradational parasequence sets that comprise the transgressive systems tract.

### 7.4 Well log cross section correlations

The sequence stratigraphic framework developed for Utan-1 well was extended to six additional nearby wells taking into account the gamma ray patterns of the key surfaces and the previously mentioned shale marker as datum. It was not feasible to tie biostratigraphic ages due to either the lack or the reliability of biostratigraphic analyses in the remaining wells. Therefore, the Utan-1 stratigraphic interpretation was tied to seismic lines that crosses other wells in the area, and the seismic then provided correlations from well to well (figure 7.6):

- Section A: North-south oriented, includes wells C-3068, C-219 and Utan-1. Good lateral continuity of the two Utan reservoirs is observed in this correlation. Picked horizons indicate key surfaces from the well log sequence analysis in the Utan-1 well. The structural complexity is clearly noticed and controlled by normal faults that separate these three wells. The faults dip south-north north of the Utan-1 well, and north-south south of this well (figure 7.7). If these faults are sealing, then the reservoir intervals may be compartmentalized.

- Section B: North-south oriented, includes wells C-418D/C-429, Utan-1, C-283/267 and C-2275. This section shows that the two Utan reservoirs are not continuous due to compartmentalization by the Kutz fault system. Among these wells, the main Kutz fault occurs at different seismic time intervals, and is difficult to map (figure 7.8). Both SB-1 and SB-3 are truncated by the fault itself, but the MFS and SB-2 can be traced above the fault plane and provide some measure of correlation.

- Section C: northeast-southwest oriented, includes wells Utan-1, C-283/267 and C-468. This section, plus pressure tests indicate that the Utan-1 reservoirs are not hydraulically connected. The C-468 well was not correlated due to the low signal to noise ratio on the eastern side of the Kutz fault.

These correlations offer an understanding of the lateral extent of Reservoir Intervals I and II. Reservoir Interval I (deeper) sits atop SB-3 and closer to the Kutz fault, so is more areally restricted than reservoir II. It only could be identified in wells C-219 and C-3068. Reservoir Interval II (shallower) sits atop **SB-1**, which can be traced from the Utan-1 well across to wells C-267, and C-2275, then across to wells C-219 and C-3068 (figure 7.8). In all cases, this correlative, potential reservoir exhibits a retrogradational stacking pattern, as in the Utan-1 well (Mendez et al., 2006).

### 7.5 Seismic-stratigraphic analysis

Because reliable age dates are not available for other wells in the area, and because there are so many individual parasequences that appear similar in log character, correlation of seismic reflections from well to well was deemed necessary to extend the geologic interpretation away from Utan-1 to other, nearby wells.

Chapter 5 of this dissertation dealt with initial evaluation of the seismic database provided for this research. As a result of the seismic diagnostics, several pre- and post-stack applications were applied to the data to enhance data quality at shallow levels. To maximize the potential for correlations using seismic reflections, it was

necessary to perform a phase tie between synthetic seismograms generated at the control wells (wells chosen on the basis of good quality and a complete log suite), including Utan-1, and the 3D seismic volume. Additionally, because zero-phase seismic data is a concern when thin layers are involved at the reservoir level, well-seismic tie analysis indicated that the seismic data should be rotated 70 degrees to achieve the zero-phase requirements. The zero-phase assumption was also a requirement for the later application of sequence stratigraphic concepts and advanced seismic attributes.

Vertical resolution was calculated considering an average spectrum of the seismic wavelet at reservoir levels centered around: $f_{dom}$=22Hz, velocity transmission of v= 2200m/s, for a wavelength of $\lambda$ = 100m, and vertical resolution of $\lambda/4$ = 25m. Thus, reservoir intervals having a thickness less than 25m may not have their top and base resolved.

Once the key surfaces for stratigraphic correlation were identified (Chapter 6), they had to be transferred to seismic data for seismic stratigraphic interpretation and correlation. The following are the seismic markers which were firstly identified and correlated from well log information and tied to seismic data, then picked in the west side of the Kutz fault, then picks were attempted on the east side of the fault:

- Shale marker (4_02): Seismic reflector with strong impedance contrast and regional distribution. This marker was used as a datum for the well log stratigraphic correlation and as a guide for seismic interpretation.

- Sequence boundary 1 (SB1) (SB1_02_15): Key surface correlated in wells. Seismic evidences are geometric relations of reflectors against this surface, i.e. seismic terminations (Mitchum, et al., 1977), recognized both in conventional seismic and Thinman-processed lines. This surface has a restricted regional distribution due to its proximity to the Kutz fault.

- Maximum Flooding Surface (MFS) (MFS_4_02): Key surface correlated in wells. Seismically detected as a strong impedance contrast reflector.

- Sequence boundary 2 (SB2) (SB2_4_02): Second sequence boundary recognized and correlated in wells with broad regional distribution. Seismically recognized by seismic onlap and downlap terminations against this surface.

- Deep shale (DeepShale_utan_26.01): Additional seismic marker with strong impedance contrast whose stratigraphic position facilitated positioning and mapping the upper and lower reservoirs in the Utan-1 well.

Third order sequence boundaries were identified on seismic sections as truncations or as a result of lowstand erosional surfaces, and from the geometric relationship of the reflections including onlap and downlap terminations. Higher order sequences were restricted by the resolution of the seismic data. Several loops between seismic and well log data had to be performed to assure agreement of interpretations.

Some other seismic marker horizons not related to any interpreted stratigraphic surface were picked during the development of this work as an aid to basic seismic and

stratigraphic interpretation, as phantom horizons or to delimitate some windows for seismic attribute extraction.

Thinman sections were useful to guide the interpretations in zones of low signal to noise ratio, in smoothing zones of spiky picked horizons, and to refine the stratigraphic interpretation. Figure 7.9 shows the help provided by Thinman sections in the picking process. The picked horizon is a MFS, which is interpreted to separate a TST below from a HST above. The higher resolution provided by the Thinman section allows interpreting this surface as a downlap surface overlain by downlap terminations (prograding complex), which help to verify the MFS interpreted from the well log sequence analysis. Figure 7.10 shows how spectral inversion also helped to identify and guide the interpretation of the sequence boundaries identified during the well log sequence interpretation. Figure 7.11 graphically shows the interpreted key surfaces on seismic data. Basic attributes such as instantaneous phase and cosine of the instantaneous phase were also employed during the process to make some events stronger in areas with low signal to noise ratio (figures 5.16 and 5.17).

Once the key horizons and markers were identified and placed on the well log sequence stratigraphic framework, tied to seismic data at well sites, and seismically extended to the entire study area, seismic time contour maps were constructed for all the interpreted key seismic surfaces (figure 7.12). The minibasin formed by listric and antithetic faulting in which the Utan structure formed is well defined by the contour maps. Even though the foot-wall east of the fault remained as a relative structural high during the rollover process, there is an additional structural high in the eastern side of

the fault, which presumably should have affected the depositional process in the eastern block. This is a possible explanation for the differences in seismic appearance from block to block which additionally limited transferring the sequence stratigraphic interpretation from the Utan block to the other side of the fault. More biostratigraphic data at Neogene ages and a new sequence stratigraphic framework have to be postulated at the other side of the fault in order to constrain the interpretation for future correlation attempts at tying key stratigraphic surfaces from block to block across the Kutz fault.

### 7.6 Advanced attribute analysis

Both AVO and spectral frequency models were created from the petrophysical multi-mineral analysis and fluid substitution referred to in Chapter 4 of this research. For the AVO modeling, the P-wave velocity, shear-wave velocity and density logs resulting from the petrophysical analysis were used as inputs. The modeling was conducted using Hampson Russell's AVO software, and Fusion´s proprietary software, to predict the seismic response at a user-selected range of offsets. The Zoeppritz modeling option was selected. Synthetic gathers resulting from the AVO forward modeling were spectrally decomposed to create spectral gathers.

Modeling was performed for the Utan-1 well as an aid to identify the attribute response in-situ, and to differentiate its response in other fluid conditions (figures 7.13 to 7.16). Modeled AVO and frequency gathers showed effects of fluid substitution from wet to dry gas indicating that fluid presence is seismically noticeable and may

indicate detection in AVO and frequency analysis. The same exercise was repeated for wells C-3068, C-429 and C-468 and compared to the results on the brine synthetic, in-situ and commercial gas synthetic.

Modeling indicated that fluid identification is feasible and that AVO Type II to I, and an amplitude decrease of the spectral response could be indicative of gas presence in the reservoir intervals. Therefore, fluid content and potential gas reservoirs could be identified through lateral variations of these parameters

Lateral variations of these parameters could be used to map lateral reservoir extension and could also be helpful in identifying potential gas reservoirs in analog sites of the study area within the retrogradational parasequences which sit upon sequence boundaries, according to the sequence stratigraphic framework developed in this research.

Even though pre-stack seismic data after conditioning shows both better continuity and signal/noise ratio, low fold coverage at the reservoir levels prevented conducting a regional AVO study.

Instantaneous spectral analysis, i.e. spectral decomposition, was carried out on the conditioned 3D seismic volume provided for this research. The data resulting from this process was used to prepare a range of displays or volumes that document the response of the reservoir to different frequencies. These were then animated as progressive increase of frequency values to catch subtle changes in the reservoir tuning frequencies and peak frequencies. Other products included single frequency sections that intersected the Utan-1 discovery well and other key well locations. Single

frequency maps were also extracted to identify and correlate key surfaces for the stratigraphic interpretation and reservoir analysis.

Frequency gathers showed that the majority of the signal's strength for the reservoir reflections was confined to a narrow band of frequencies centered around 22 Hz. Consequently, single sections and maps were carried out in the vicinity of this peak frequency for the analysis. The apparent dim amplitude of the reservoir intervals following structural contours allowed defining the extension of the upper reservoir and inferring additional attractive analog areas for new drilling, based on the following criteria (figure 7.17): For the main reservoir interval the hydrocarbon signature is a dim spot and mainly Class I AVO. Areas with presumed thin or non-existent reservoir are also dim. Bright amplitudes are indicative of relatively thick or sandy reservoir intervals.

Future exploration strategies following this seismic attribute incorporation into the sequence stratigraphic framework should take into consideration the following points:

(1) Identify retrogradational inner neritic sand sheets which sit upon third order sequence boundaries.

(2) Within those sand fairways, find possible structural trapping locations.

(3) Confirm the probability of hydrocarbons in potential trapping locations within sand fairways by the presence of dim spots imaged by spectral decomposition.

(4) The greatest risk for such prospects is dimming due to reduced reservoir quality. Thus, if fold and S/N ratio permit, perform AVO analysis to confirm both the presence of hydrocarbons and good reservoir quality. If AVO cannot be relied upon, reservoir risk is still significant even in structurally high locations which exhibit dim spots. Relative Acoustic Impedance derived from rotated Thinman$^{TM}$ data is another alternative to be tested if AVO analysis is not feasible.

(5) An overall conclusion is that spectral decomposition provides valuable information not available through other methods of seismic analysis. It can be reliably used as an indicator of gas presence and extension of known reservoirs in the absence of other geological information. However, it does not show promise as a good indicator of reservoir quality in this area and other attribute tools have to be used to support any such interpretation.

## 7.7 Geologic controls on hydrocarbon entrapment and reservoir quality

The accurate prediction of geologic controls on entrapment before drilling a discovery well and on reservoir quality after drilling is a challenge in petroleum exploration and development and has to be analyzed from different scales and perspectives. This is particularly true if, after drilling a wildcat well and due to the lack of infrastructure, it becomes necessary to determine whether a discovery well is commercial before proceeding with its development (Dickey, 1986).

At the macroscopic scale, Utan reservoirs contain both structural and stratigraphic trapping components. Structurally, the reservoirs are contained within a rollover anticline where the deeper reservoir is restricted in size by the Kutz fault. From the sequence stratigraphic point of view, the two reservoir intervals are retrogradational shoreface parasequences sitting atop third-order sequence boundaries (lowstand/transgressive surfaces of erosion).

Limited X-ray diffraction analysis (Table 4.2) and quantitative petrographic analysis (Table 6.3) of Utan-1 core samples provided a basic understanding of the mineralogy and reservoir quality of the field; this was particularly important considering that poor borehole conditions affected the well log quality. Core analyses indicated that the bulk rock composition of the Pliocene stratigraphic section averages (with very few samples): calcite (56%), dolomite (16%), quartz (9%), aragonite and pyrite (8%), feldspar and plagioclase (6%), and clay minerals (6%). Reservoir intervals have cleaner lithology (lower volume of shale) than other intervals which are mainly composed of calcite, with some dolomite and quartz and with thin-section porosity values as high as 14%. Increase in the amount of quartz indicates a higher-energy depositional environment, which enhances development of relatively coarser grain size and more porous zones. Therefore, reservoir quality is mineralogically driven by quartz content in a carbonate rock. As the quartz content increases and the carbonate content decreases the porosity also increases (figure 6.6).

The porosity system at reservoir intervals is composed of primary intergranular pores which are irregularly interconnected locally (middle figure 6.5), microporosity and isolated intraskeleton secondary pores.

Porosity and permeability measurements were completed by Corelab on cored intervals in the Utan-1 well. Twelve, eight and seven measurements at 800 and 1200psi of confining pressure were applied to the upper, middle and lower cores respectively. Porosities and permeabilities to air at 800psi vary in the same proportion: from 5.7% and 0.0021md in the lower core to 17.9% and 1.46md at the top of the upper cored interval. In a general sense, permeabilities were best at the base of the top reservoir at 1084.05m (1.46md and porosity of 17.9%). Out of this value, permeabilities are less than 0.1md (figure 7.18). The top of the lower cored interval, which corresponds to the base of the lower reservoir, registered porosity and permeability values of 10% and 0.034md, respectively.

By considering that the core samples were not totally representative of the tested intervals and after reviewing the porosity-permeability values described above, minipermeameter measurements were required on the top one meter of the upper core, which corresponds to the base of the upper tested interval. Red circles showing the locations of the minipermeameter measurements are shown in figure 7.19. Two measurements were made at each sample point in order to evaluate reproducibility at each stratigraphic level measured. Average grain size was also estimated at each measurement location using a grain size comparator chart. Further explanations on minipermemeter measurements can be found in Selley (1998) and Slatt (2006).

Minipermeameter measurements exhibited higher permeability values than the core plug measurements, with a high of 40md at 1084.1m. Since the core was only taken through the lowermost part of the reservoir interval (figure 7.19), it can only be inferred that porosity and permeability values for the upper tested interval are higher, particularly since the reservoir intervals are fining-upward retrogradational parasequences.

In a general sense, reservoir quality can be classified as moderate to poor. The low permeabilities correspond to gas reservoirs rather than to oil reservoirs. The best Pliocene reservoir in the studied wells is at depths between 1065-1085m in the Utan-1 well. In-situ gas saturation in this reservoir does not exceed 60%.

The best reservoir quality in the cored intervals is associated with intratidal and retrogradational facies. The sequence stratigraphic framework developed in this research predicted the non-reservoir middle tested interval to be a highstand progradational parasequence.

There is reservoir heterogeneity beneath the standard logging tools resolution, as indicated from the EMI log for the Utan-1 well. Such higher levels of heterogeneity may provide additional reservoir-seal relationships. Low depositional energy thin beds alternate with higher depositional energy beds that have much better reservoir quality.

Advanced seismic attributes indicate that there are potentially similar reservoirs northward from the Utan-1 well (figure 7.28). Gas-water contact is presumably defined by the boundary between the dim and the bright amplitude response at 20-25Hz of the spectral decomposition single frequency map.

According to non-published Pemex reports, gas composition is mostly methane (95 to 98%). Selley (1998) infers that biogenic methane is commonly formed in the shallow subsurface by the bacterial decay of organic-rich sediments; as the burial depth and temperature increase, this process diminishes and the bacterial action is extinguished. Thus thermal maturation of organic matter is the main factor in methane encountered in deep reservoirs.

The mostly methane gas composition and the shallow depth of the Utan reservoirs point out a possible biogenic origin, even though a small amount could be thermogenic in nature, assuming the generation associated with the deeper oil reservoirs of Cantarell field connecting through the Kutz fault, and allowing gas migration to shallower Tertiary depths. Bahamon (2006) also agrees with the mostly biogenic origin of the gas contained in Utan reservoirs.

The biogenic nature of the methane, the thin sheet reservoir geometries, and the lack of infrastructure for gas transportation make together, nowadays, unattractive the commercial exploitation and transportation of this resource. However, the current declining phase in which Cantarell field is positioned, makes feasible a future Pliocene gas reinjection to Mesozoic levels to improve the recovery efficiency of the giant field.

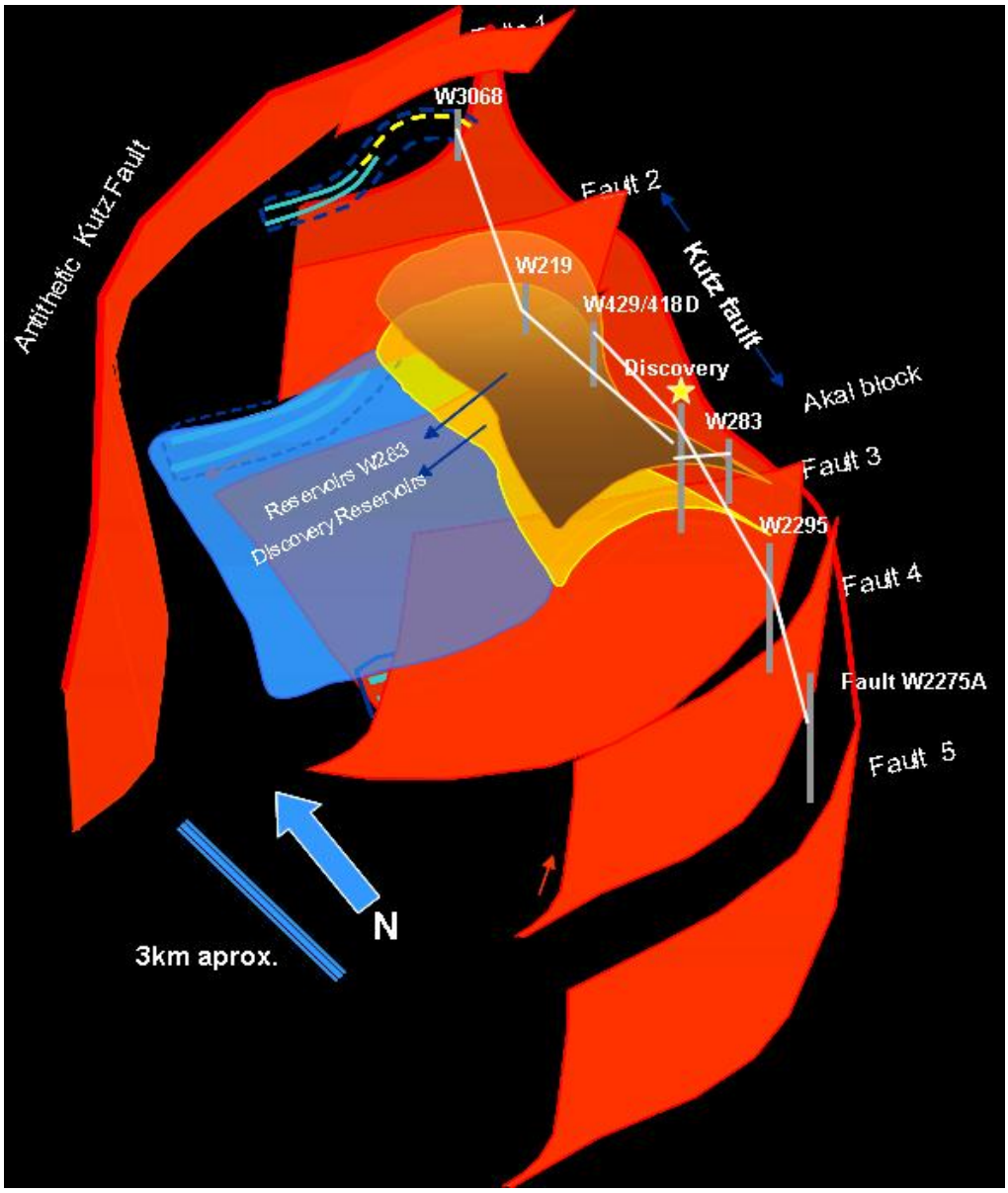


**Figure 7.1: Structural reconstruction of the Utan rollover structure (Bahamon, 2006).**

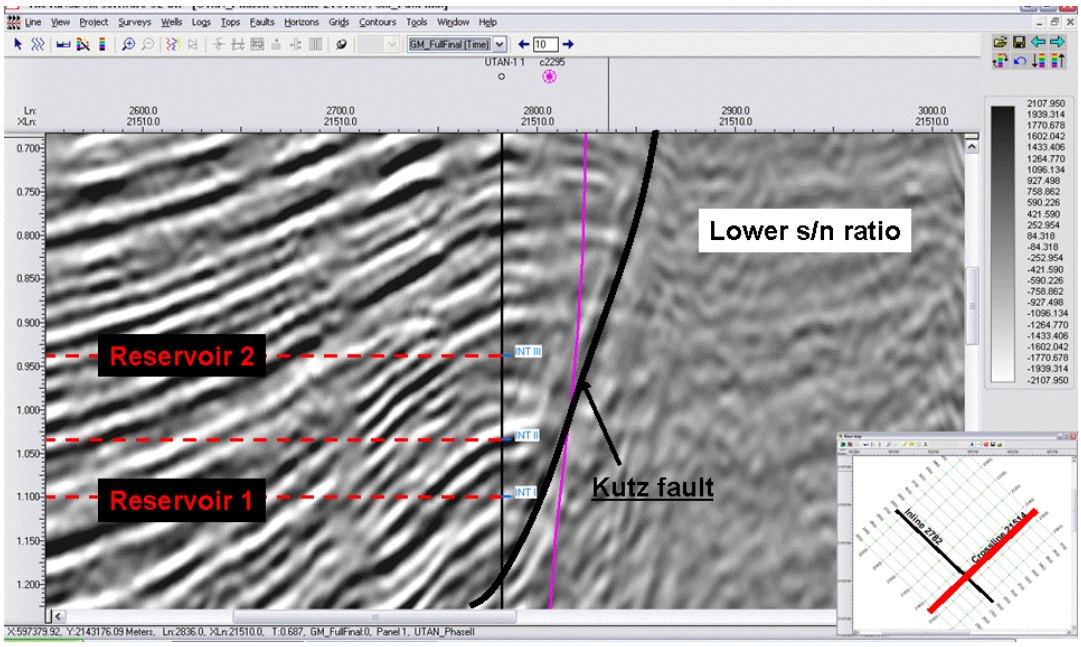


**Figure 7.2: Seismic section crossing the Utan-1 well and the Kutz fault in the southwest-northeast direction. The three tested intervals are shown. Better signal to noise ratio is clearly noticed in the west side of the fault where the Utan structure is located.**

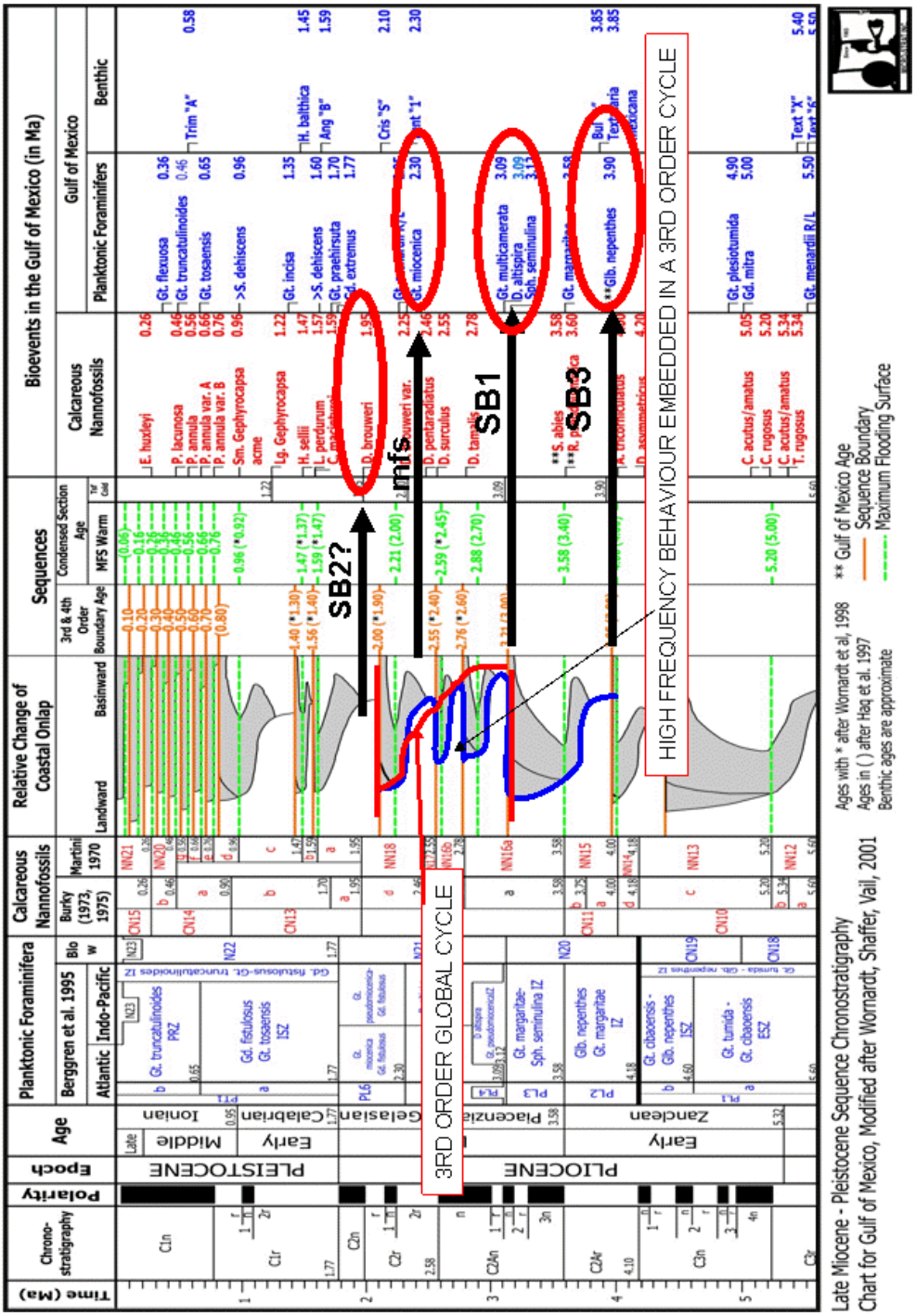


**Figure 7.3: Late Miocene – Pleistocene Sequence Chronostratigraphy Chart for Gulf of Mexico with extinction dates for key fossils, and recognition of key surfaces and depositional sequences for the Utan area (Wornardt et al., 2002).**

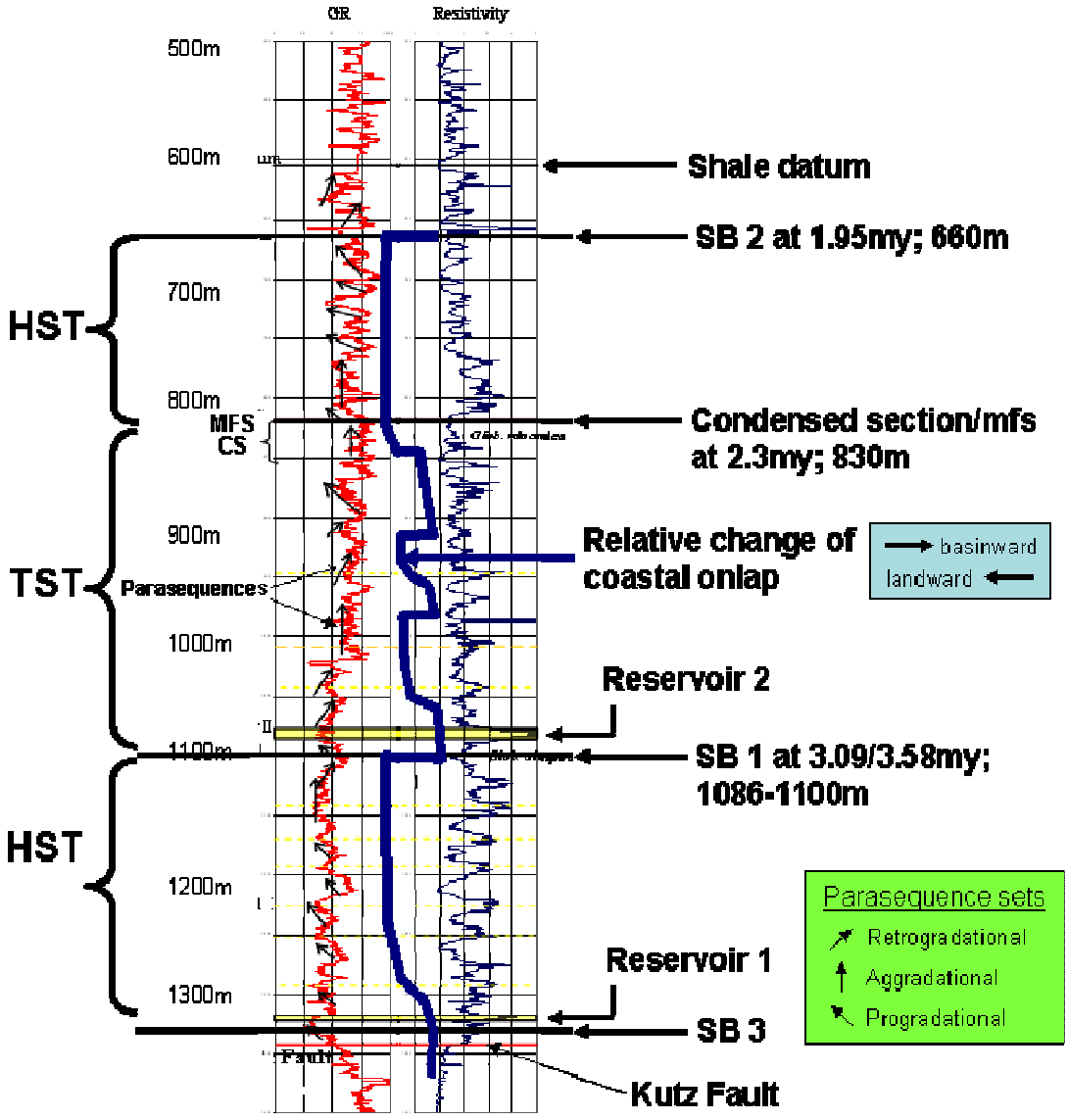


**Figure 7.4: Composite figure of Utan-1 well showing gamma ray and resistivity curves, relative changes of coastal onlap (Wornardt, 2002), key horizons, ages, reservoir intervals, and transgressive and highstand systems tracts. Sequence boundaries represent lowstand surfaces of erosion. Note that the two reservoir intervals sit atop sequence boundaries.**

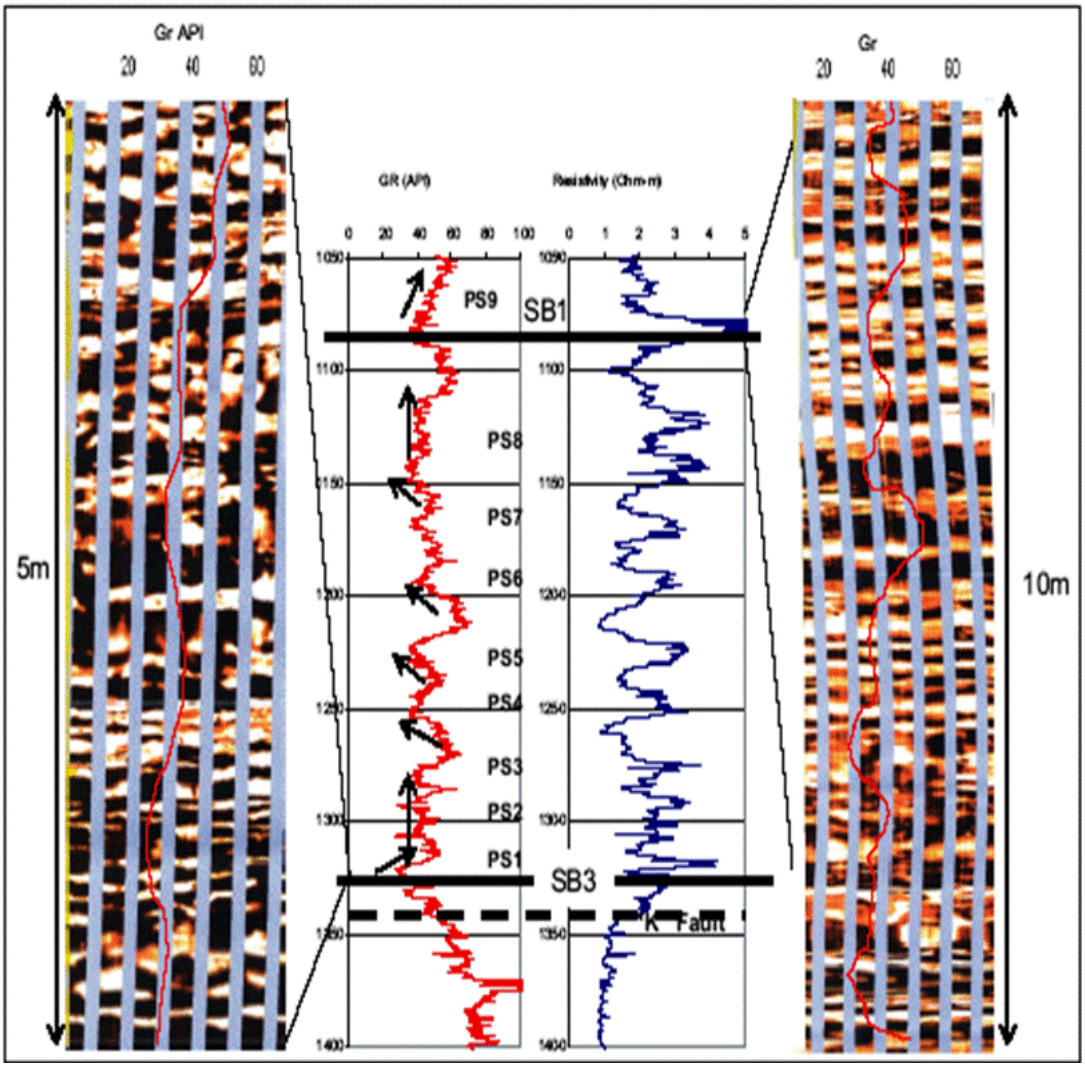


**Figure 7.5: Borehole image log of the two reservoir intervals. The left hand image is the deepest reservoir, at 1317 – 1322m The right hand image is the shallowest reservoir at 1075 – 1085m. Overlying the image log is a gamma ray log in red. Note cyclicity and abundance of parasequences. Also note that the productive layers could be the most resistive intervals (Mendez et al., 2006).**

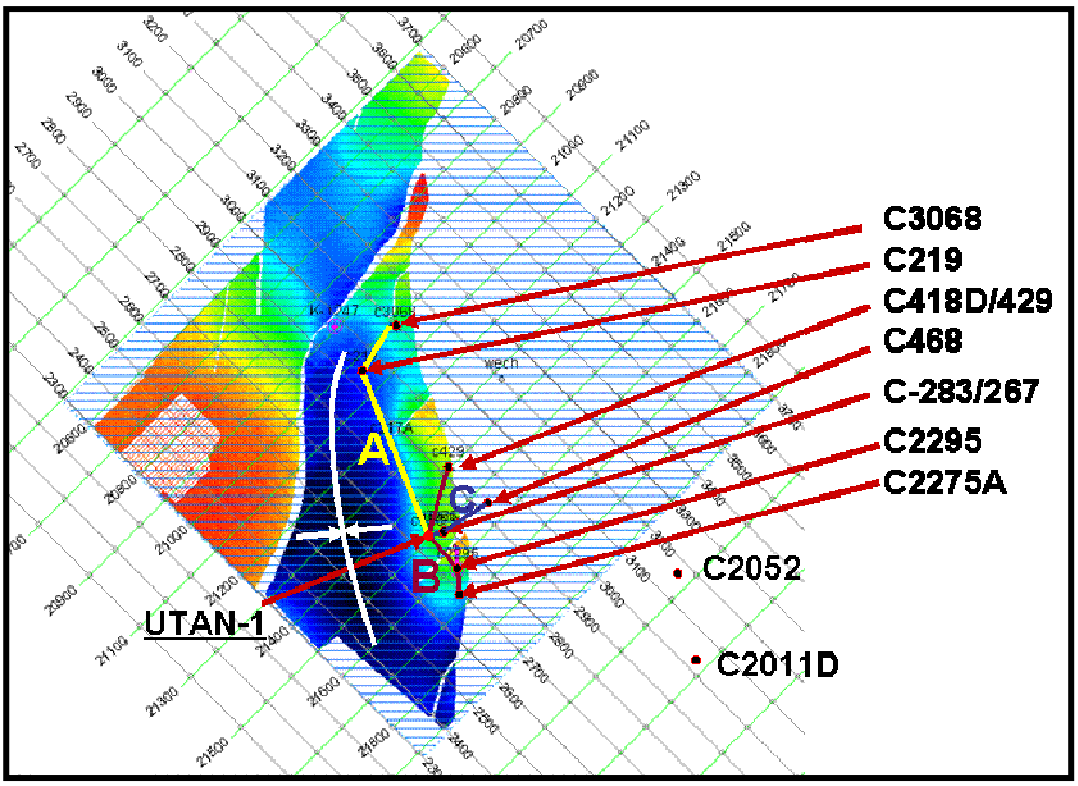


**Figure 7.6: Base map with the location of wells involved in the stratigraphic well log correlation. Cross sections A, B and C are also shown.**

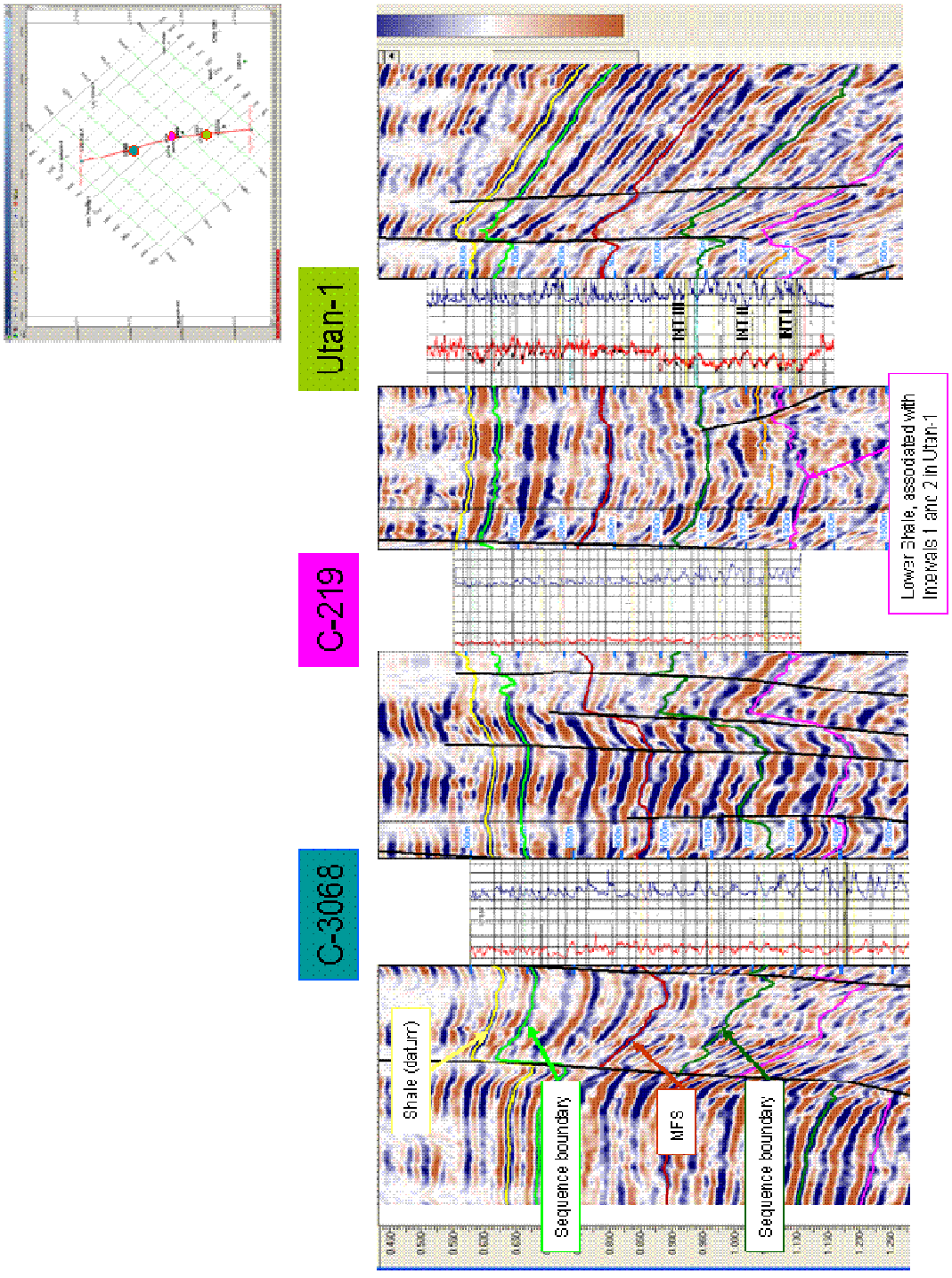


**Figure 7.7: Stratigraphic section A, crossing the wells C-3068, C-219, and Utan-1.**

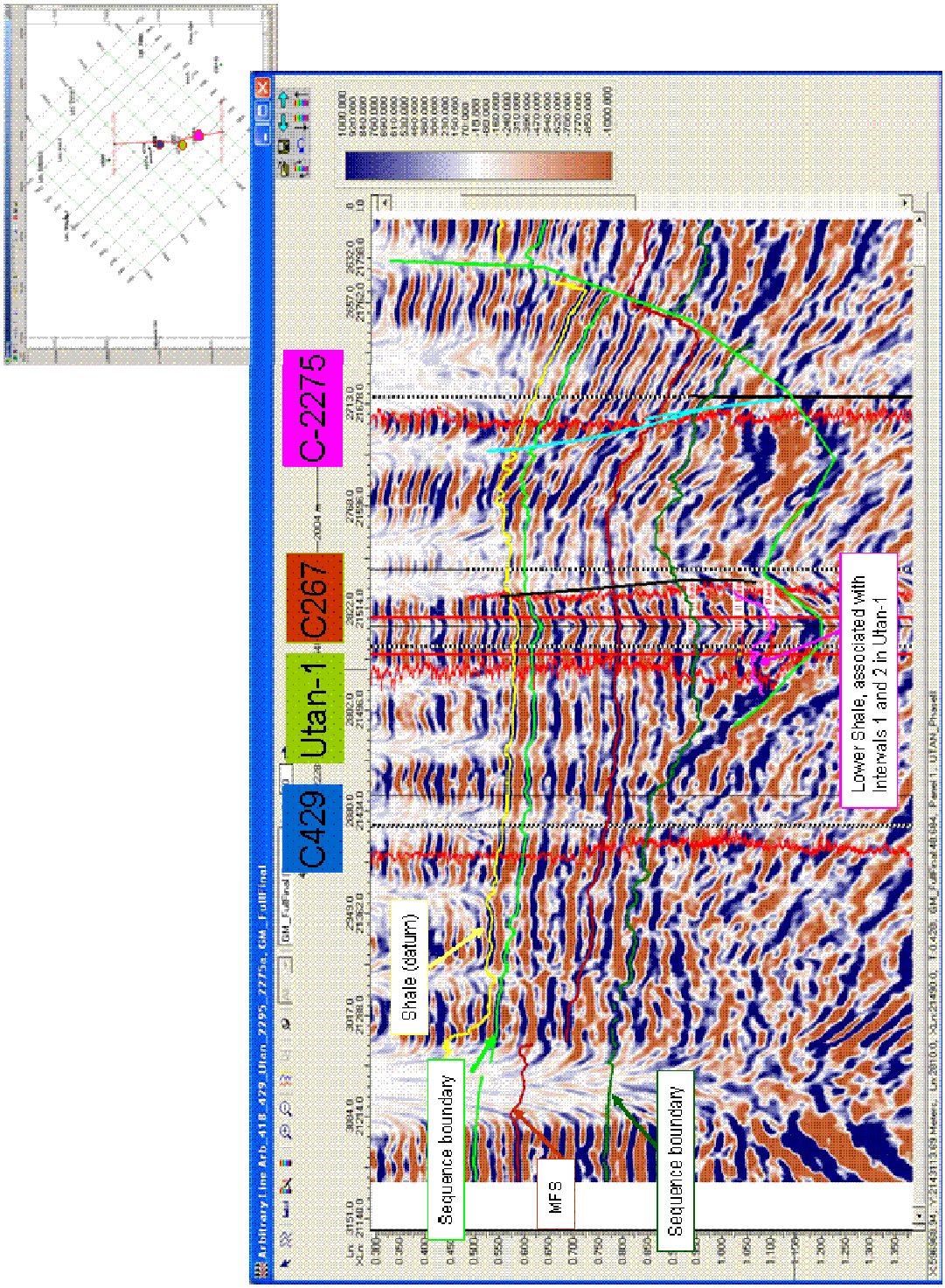


**Figure 7.8: Seismic section crossing the wells C-429, Utan-1, C267 and C2275.**

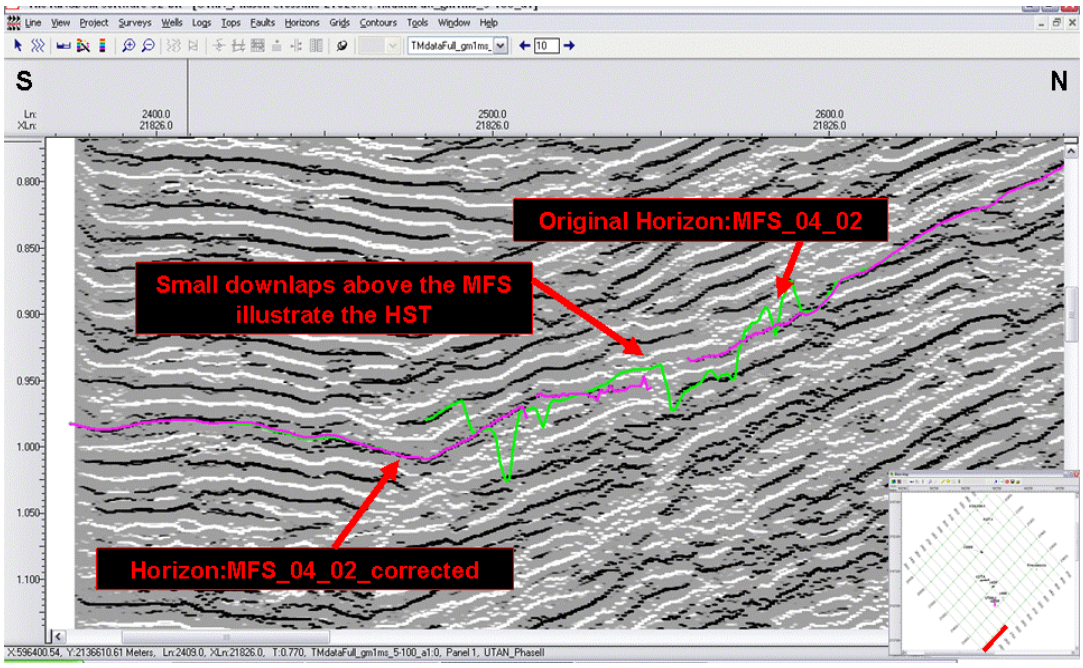


**Figure 7.9: Seismic Inversion for Reflectivity (Thinman), showed good capabilities for seismostratigraphic interpretation by increasing vertical resolution. The attribute was helpful to smooth spiky picked horizons and to guide the interpretation. A MFS surface is corroborated as a downlap surface separating a TST from a HST.**

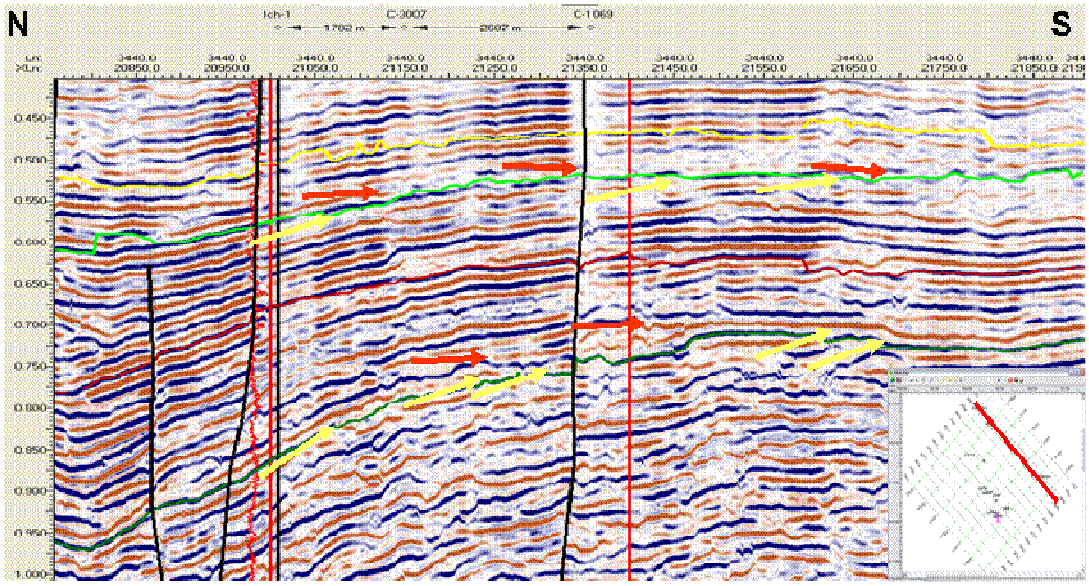


**Figure 7.10: Clear stratigraphic evidence shown by seismic inversion for reflectivity. "Onlap" (red) y "Toplap" (yellow) seismic terminations calibrate and verify the proposed sequence boundaries.**

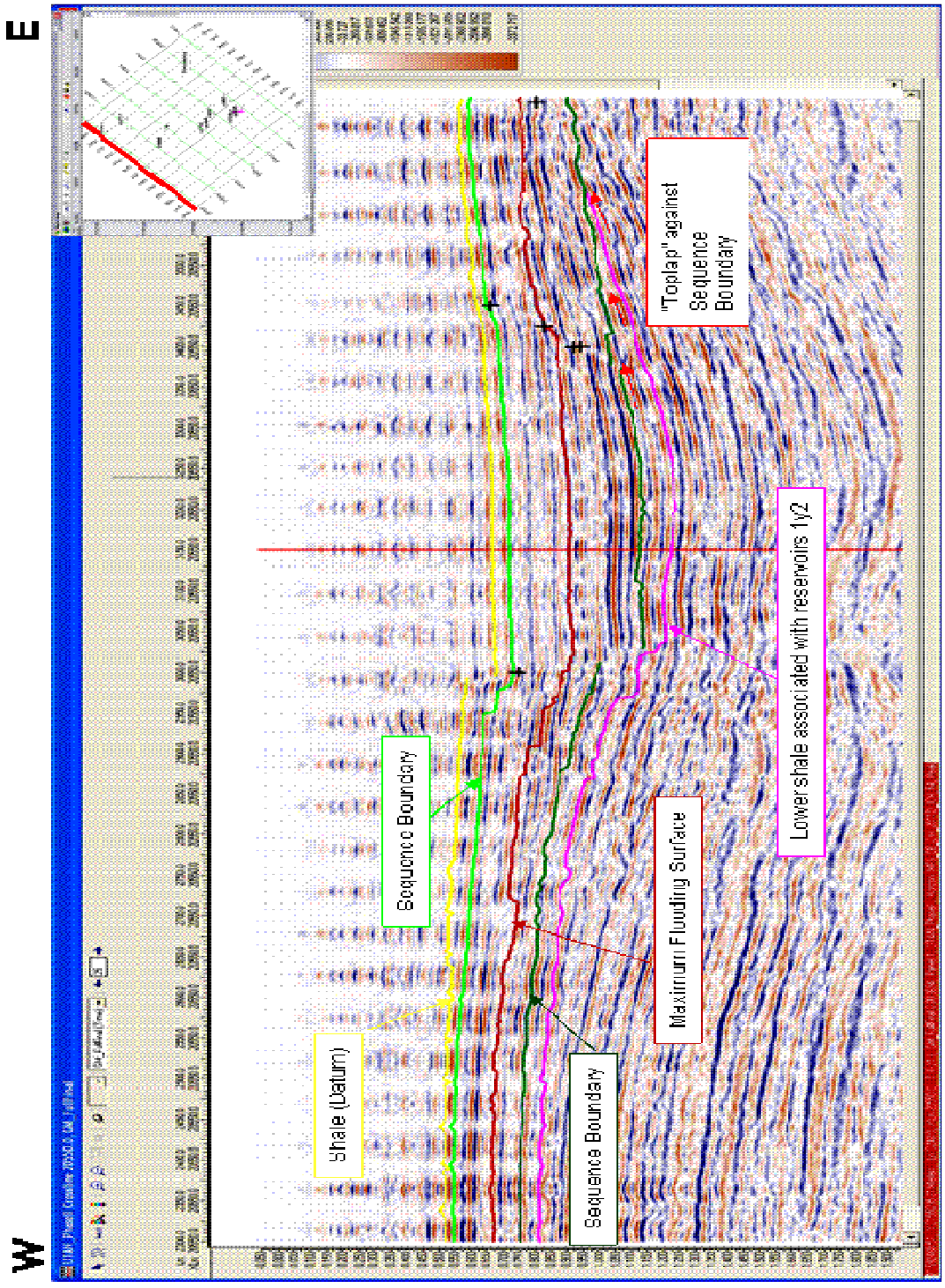


**Figure 7.11: Sequence stratigraphic surfaces interpreted in the study area tied and extrapolated to the seismic data.**

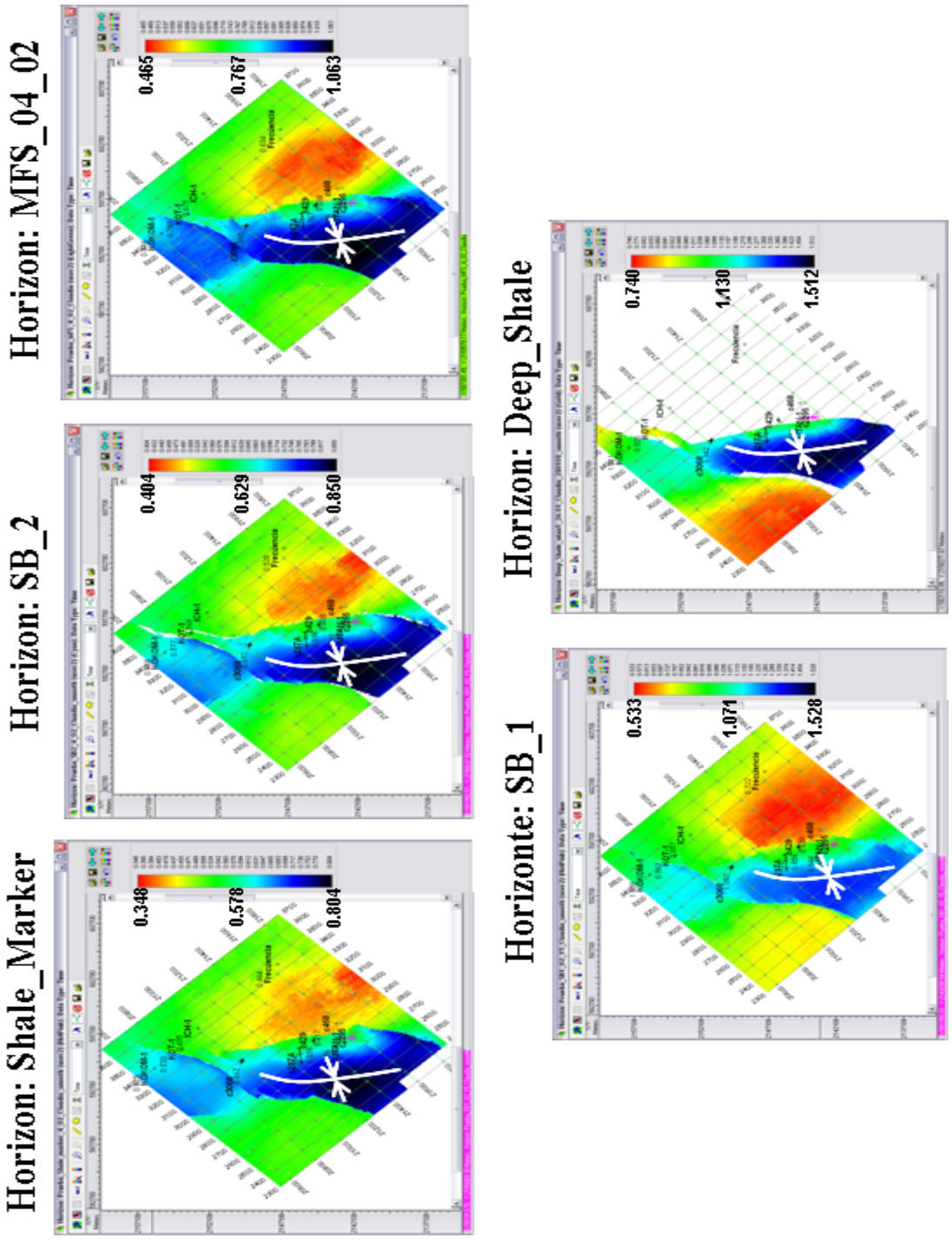


**Figure 7.12: Seismic time contour maps of interpreted key stratigraphic surfaces. The upper part of the scale means shallower times.**

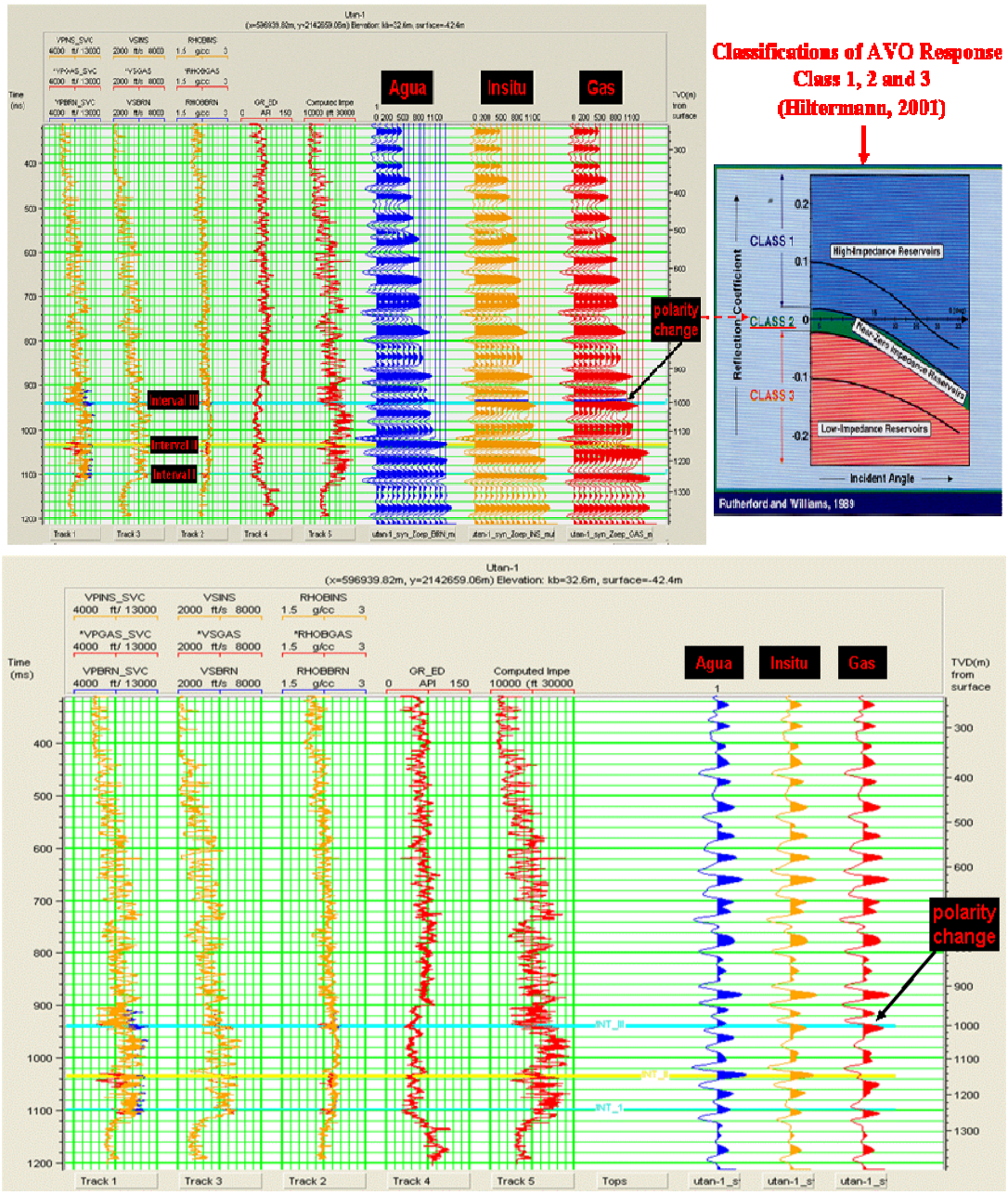


**Figure 7.13: Fluid substitution modeling for the Utan-1 well. A polarity change is associated with a Type-II AVO response for both reservoirs. Top: Modeled-gather at well site; Base: Modeled-stack trace.**

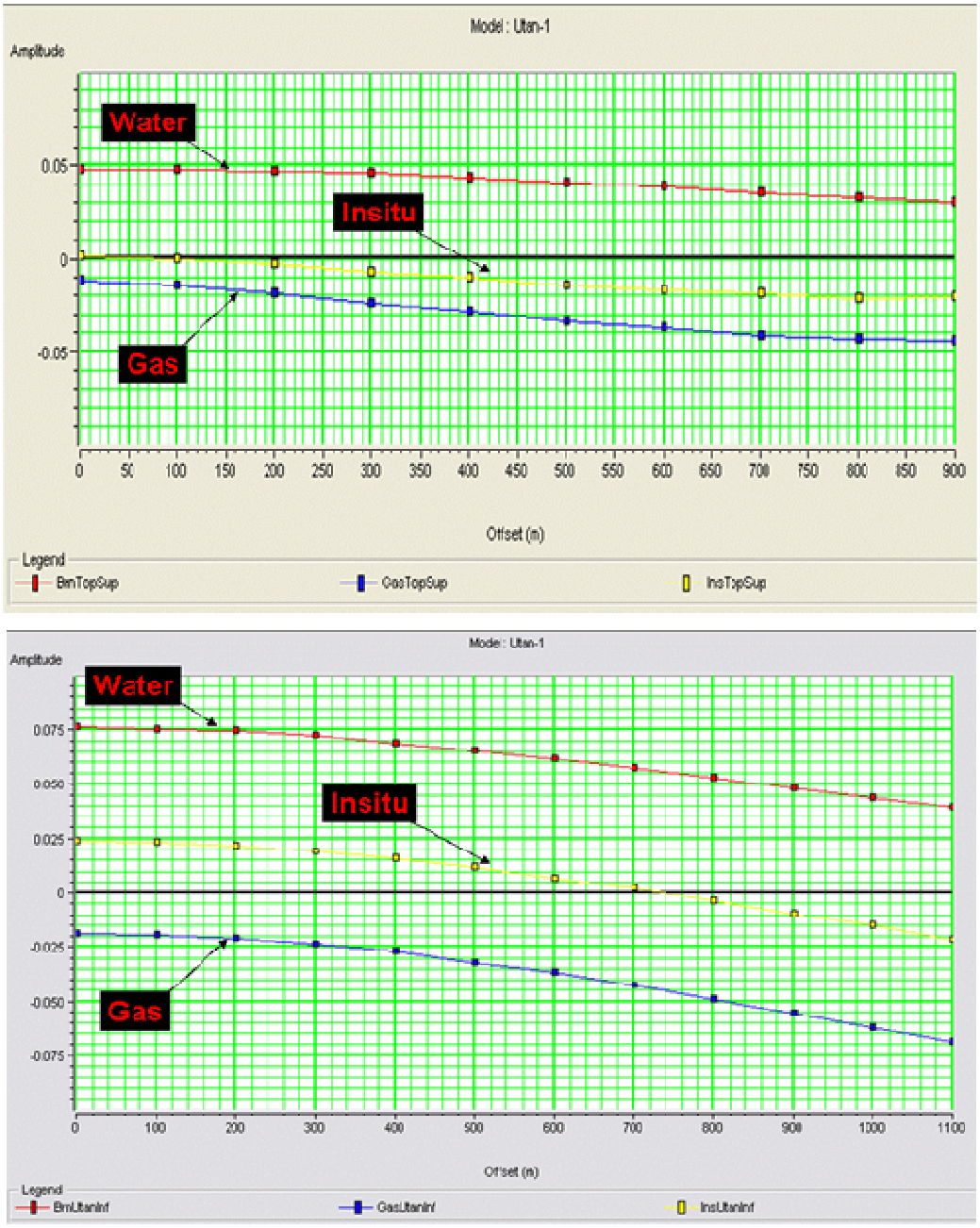


**Figure 7.14: AVO Type-I curves for Utan reservoir intervals. Top: Upper reservoir (labeled as tested interval III); Base: Lower reservoir (labeled as I).**

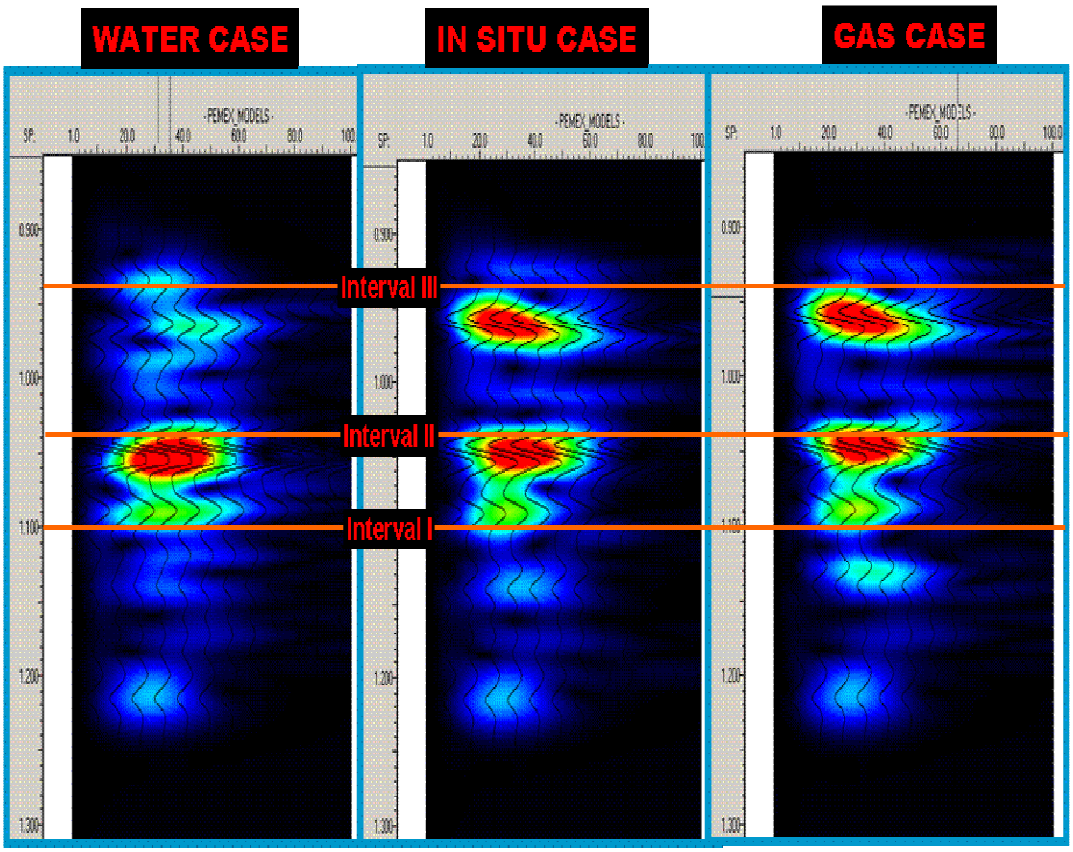


**Figure 7.15: Modeled frequency gathers for the Utan-1 well.**

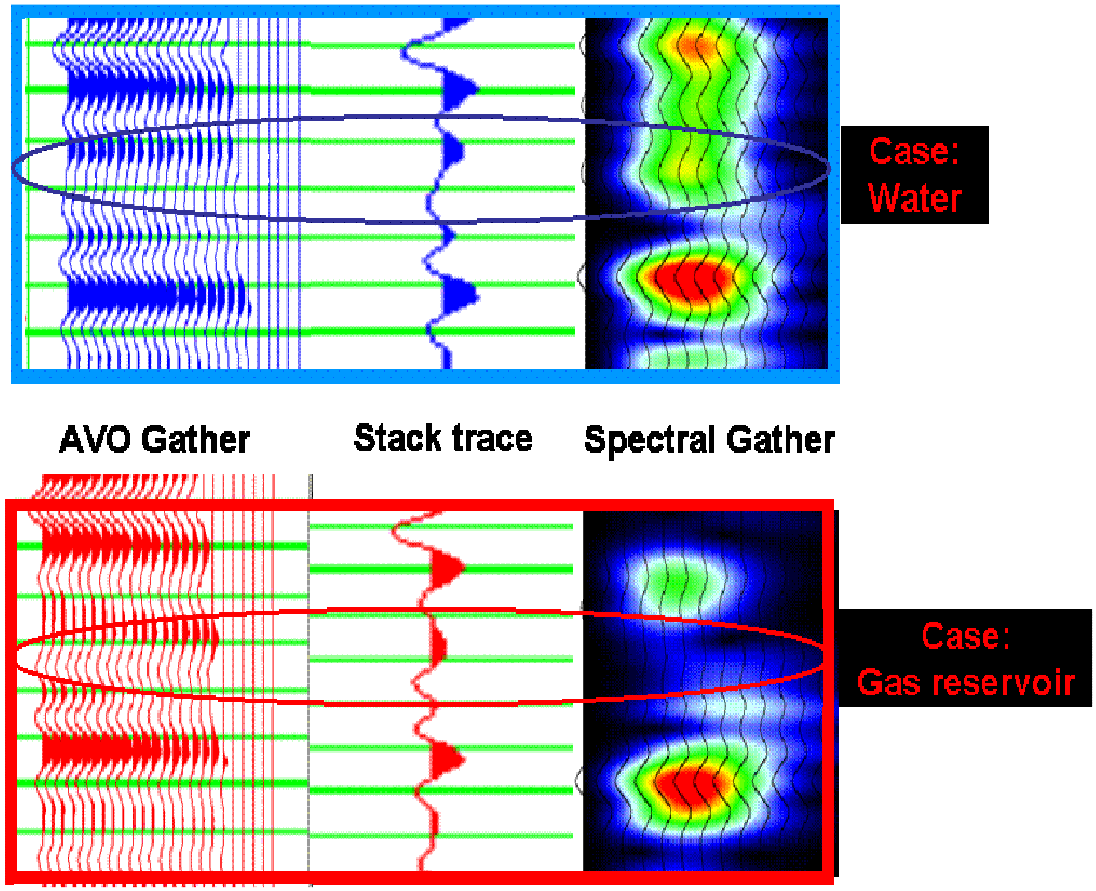


**Figure 7.16: AVO and Spectral Fluid Substitution Modeling for the Utan-1. AVO class II, and a low amplitude/high peak frequency for the spectral response are clear in the presence of gas.**

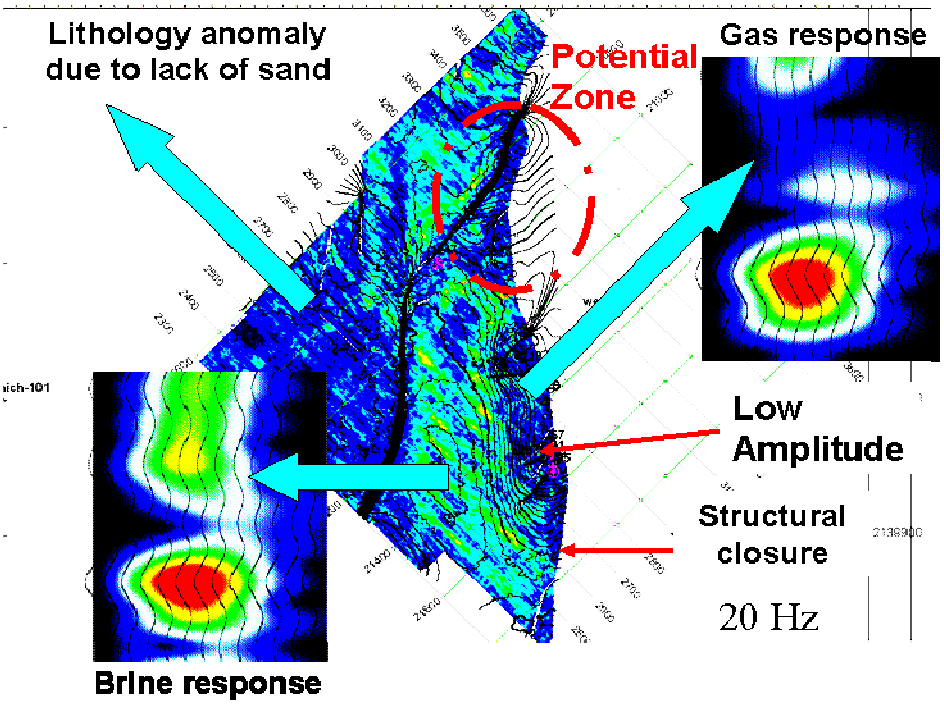


**Figure 7.17: Spectral Decomposition interpretation on top horizon of main reservoir (Mendez et al, 2006).**

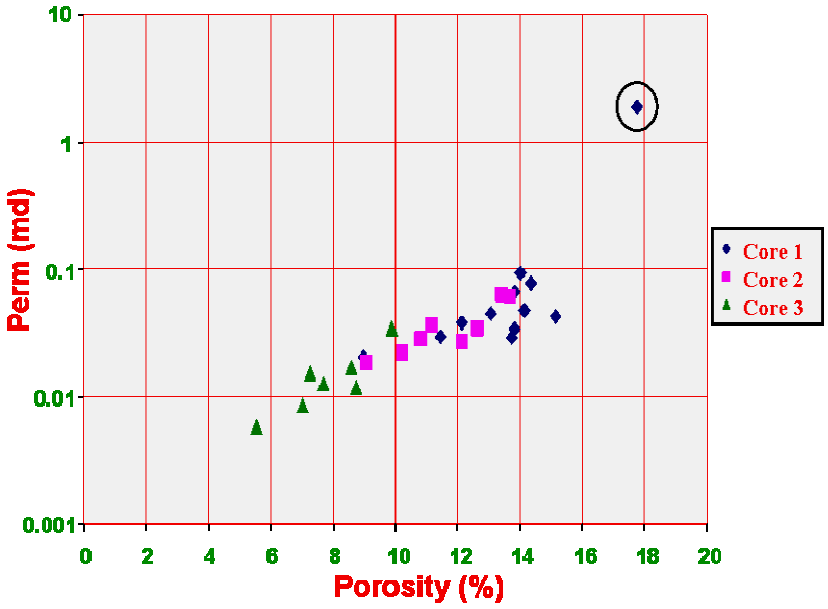


**Figure 7.18: Poro-perm relationship for measured values in cored intervals of Utan-1 well. The sample 1084.17m, corresponding to the base of the upper reservoir with the higher quartz content and the best reservoir conditions, is circled (Mendez et al., 2006).**

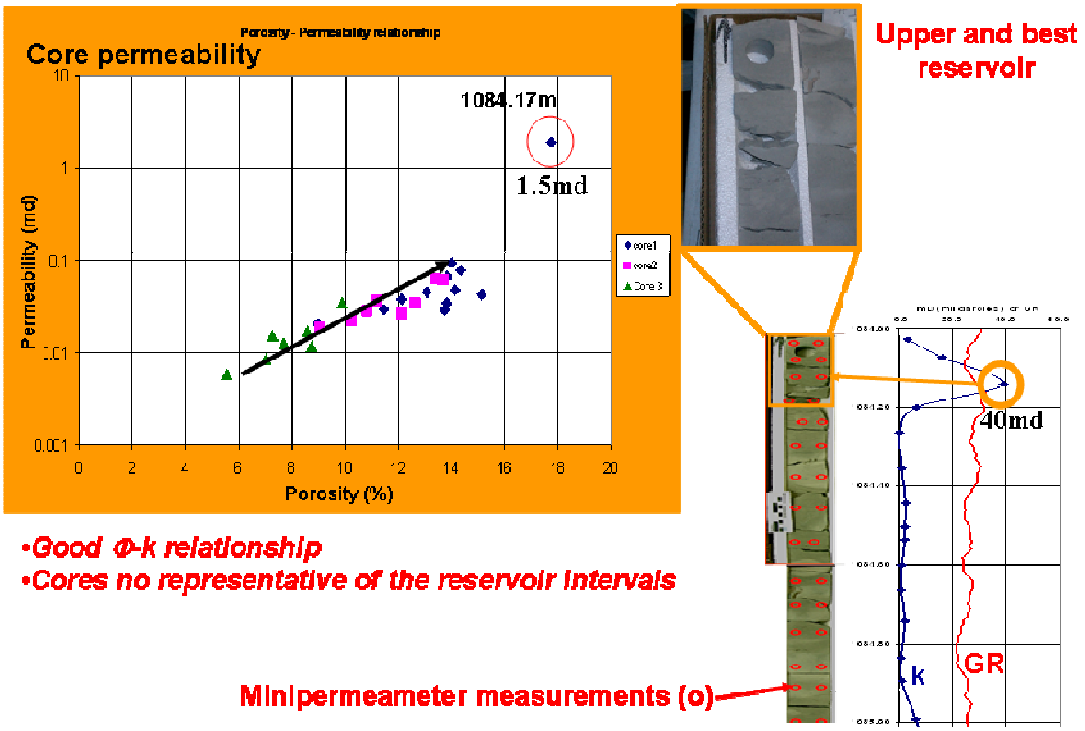


**Figure 7.19: Minipermeameter measurements of the cored interval 1084-1085m (blue curve). Red circles are measurement sites; in red is core gamma ray. The core sample at 1084.17m represents the relatively best reservoir quality zone (core perm=1.5md; miniperm=40md) .**

# CONCLUSIONS AND RECOMMENDATIONS

The information contained in the preceding chapters of this dissertation clearly demonstrates the importance of building a sequence stratigraphic framework for an improved understanding of the depositional model and physical distribution of reservoir properties in the recently discovered Utan gas field of Mexico.

Due to the lack of enough comprehensive well data at Neogene stratigraphic levels in the study area, the Utan-1 well provided the base for extrapolating geological and geophysical conditions away from the well site. Key surfaces for stratigraphic interpretation were age-dated with planktonic foraminiferal biostratigraphy of the Lower-Middle Pliocene section.

Three planktonic foraminiferal biozones were recognized: the Early (Lower) Pliocene *Globorotalia margaritae margaritae*, the Middle Pliocene *Globorotalia miocenica*; and the Late Pliocene *Globorotalia truncalinoides truncalinoides*. Three third order sequence boundaries which bracket two third order depositional sequences, as well as one maximum flooding surface, were interpreted from the well sequence stratigraphy and extrapolated to nearby wells through well log correlation and seismic correlation.

Recognition of the two gas reservoir intervals as retrogradational parasequences sitting atop major sequence boundaries that are mappable both

seismically and from well logs provides an important new play concept in the Utan area.

Reservoir facies were deposited in shallow inner neritic environments. Mineralogically, reservoir quality is driven by the amount of quartz grains within carbonate matrix. As the quartz content increases and the carbonate content decreases the porosity and permeability increase.

Major climatic effects, which could be associated with Milankovitch Cycles during the Middle Pliocene (the warmest climate during the Neogene), may have led to the increase in water depths by transgression. Trangressive seas across a shallow shelf would have provided broader intertidal environments where Utan reservoir facies were deposited.

Seismic data was designed for structurally deeper objectives. Thus, the data had to be conditioned for diminishing shallow noise and acquisition footprint effects in order to leave the seismic database suitable for seismic interpretation and attribute extraction at the Utan stratigraphic level. Vertical seismic resolution was determined to be 25m. In order to accomplish zero-phase requirements for a better stratigraphic interpretation and the later attribute extraction, the seismic data was rotated 70 degrees.

AVO and spectral decomposition provided good indicators of gas presence. A Type-I AVO response and dimmed spectral decomposition amplitudes following structural contours were indicative of gas presence and can be used to delineate reservoirs under the established sequence stratigraphic framework described in this dissertation.

Gas composition is mostly biogenic methane. This fact, plus the thin sheet reservoir geometries and the lack of infrastructure for gas transportation make the commercial exploitation and transportation of this resource economically unattractive. However, it is feasible to reinject the Pliocene gas at Mesozoic levels to improve the recovery efficiency of Cantarell field.

The geological model established here, as well as the nature and physical distribution of reservoir properties, was based on the sparse information available at the time this research was initiated. Therefore, new knowledge should be included and the model has to be regularly updated as new wells are drilled and new G&G data is acquired for Tertiary objectives in this area.

In particular, it is strongly recommended that the design of future seismic surveys in this province take into consideration: (1) the recovery of near-offset signals for proper AVO analysis at shallow levels; (2) adequate field layouts for diminishing acquisition footprint effects which affect signal quality; (3) design of a proper source pattern to increase the vertical resolution through the recovery of higher frequencies, and (4) a wider frequency bandwidth for proper visualization of these subtle stratigraphic traps at shallow levels.

Most of the wells utilized for this research were drilled for deeper objectives. Therefore, most of the well logs required editing due to bad borehole effects. Special planning will require future drilling for shallow targets to maintain good hole conditions. This will increase the level of accuracy in log measurements and

consequently in the derived well log analysis, especially when dealing with gas reservoirs, thin beds and multimineralogic lithologies, as is the case in the Utan field.

The knowledge gained from this research is an important contribution to the petroleum geology of Mexico and the Gulf of Mexico basin, which confirms the petroleum system for this Pliocene play, defines a new play concept, establishes an integrated workflow for reservoir characterization if analogous projects are undertaken in the future, and defines the basis for further research in the study area.

# REFERENCES


1. Adams Jonathan, 1998; "A quick background to the Pliocene", in *Review and Atlas of Palaeovegetation.* Edited by J.M. Adams, Oak Ridge National Laboratory, website: http://www.esd.ornl.gov/projects/qen/pliocene.html.

2. Allen Sharon, Coterill Katrina, Eisner Pablo, Perez-Cruz Guillermo, Wornardt Walter W., and Vail Peter R., 1991; "Micropaleontology, Well Log and Seismic Sequence Stratigraphy of Plio-Pleistocene Depositional Sequences, Offshore Texas", in *Sequence Stratigraphy as an Exploration Tool: Concepts and Practices in the Gulf Coast*. Edited by John M. Armentrout and Bob F. Perkins, Eleventh Annual Conference, Gulf Coast Section, Society of Economic Paleontologists and Mineralogists Foundation. Reprinted with Addenda for the 1991 Midyear Research Conference, p.11-13.

3. Angeles-Aquino F.J., et. al, 1994; "Tectonic Evolution, Structural Styles, and Oil Habitat in Campeche Sound, Mexico", Transactions of The Gulf Coast Association of Geological Societies, Vol. XLIV, p.53-62.

4. Angeles-Aquino, F., and Cantu-Chapa A., 2001; "Subsurface Upper Jurassic stratigraphy in the Campeche Shelf, Gulf of Mexico", in *The western Gulf of Mexico Basin: Tectonics, sedimentary basins, and petroleum systems.* Edited by C. Bartolini, R. T. Buffler, and A. Cantú-Chapa, AAPG Memoir 75, p. 343-352.

5. Angeles-Aquino Francisco, Durán-González Fernando, Muñoz-Bocanegra Verónica, 2003; "Bosquejo sedimentario del Terciario en la Región Marina Suroeste", Revista Ingeniería Petrolera, Boletín de la Asociación de Ingenieros Petroleros de México, Octubre 2003, p. 43-53.

6. Angeles-Aquino Francisco Javier, 2004; "Bosquejo Geológico de la Sonda de Campeche", Ingeniería Petrolera, Boletín de la Asociación de Ingenieros Petroleros de México, Noviembre 2004, p. 48-59.

7. Angeles-Aquino Francisco Javier, 2004b; "Visión Geológica de la Isla de Ciudad del Carmen", non-published presentation held during the Assembly of the Mexican Association of Petroleum Geologists, Ciudad del Carmen Section.

8. Angeles-Aquino Francisco Javier, 2006; "Monografía Petrolera de la Zona Marina", Boletín Especial de la Asociación Mexicana de Geólogos Petroleros, Marzo 2006.

9. Anselmetti Flavio S., Eberli Gregor P. and Bernoulli Daniel, 1997; "Seismic Modeling of a Carbonate Platform Margin (Montagna della Maiella, Italy):

Variations in seismic facies and implications for sequence stratigraphy", in *Carbonate Seismology*. Edited by Ibrahim Palaz and Kurt J. Marfurt, SEG Geophysical Development Series No.6, p. 373-406.

10. Aquino Jose A., Ruiz Jose M., Flores Marcos A., and García Jesús, 2001; "Sihil Field: Another giant below Cantarell, offshore Campeche, Mexico", The Leading Edge, V.20, No.7, July 2001, p.761-762.

11. Armentrout John M., 1987; "Integration of Biostratigraphy and Seismic Stratigraphy: Pliocene-Pleistocene, Gulf of Mexico", in *Innovative Biostratigraphic Approaches to Sequence Analysis: New Exploration Opportunities.* Selected Papers and Illustrated Abstracts: Eighth Annual Research Conference, Gulf Coast Section, Society of Economic Paleontologists and Mineralogists Foundation, p.6-14.

12. Armentrout John M. and Clement J. Fred, 1991; "Biostratigraphic Calibration of Depositional Cycles: A case study in High Island-Galveston-East Breaks Areas, Offshore Texas", in *Sequence Stratigraphy as an Exploration Tool: Concepts and Practices in the Gulf Coast*. Edited by John M. Armentrout and Bob F. Perkins, Eleventh Annual Conference, Gulf Coast Section, Society of Economic Paleontologists and Mineralogists Foundation. Reprinted with Addenda for the 1991 Midyear Research Conference, p.21-49.

13. Asquith George and Daniel Krygowski, 2004; "Basic Well Log Analysis", Second Edition, AAPG Methods in Exploration Series No. 16, 244p.

14. Avseth Per, Mukerji Tapan, and Mavko Gary, 2005; "Quantitative Seismic Interpretation", Cambridge University Press, 359p.

15. Bahamon Velazquez Carlos; 2006; "An integrated sequence stratigraphic framework for geological reservoir characterization and development plan of a gas field in the southern Gulf of Mexico". Master of Science Thesis, The University of Oklahoma, 74p.

16. Baker George, 2001; "Pemex development tracking fiscal, technological strategies", Oil&Gas Journal, May 7, 2001.

17. Barbosa Fabio, 2001; "Mexico´s new government launches major projects to boost oil production", Oil&Gas Journal, May 7, 2001.

18. Bassiouni Z., 1994; "Theory, Measurement and Interpretation of Well Logs". SPE Textbook Series, 363p.

19. Baum Gerald R. and Vail Peter R., 1987; "Sequence Stratigraphy, Allostratigraphy, Isotope Stratigraphy and Biostratigraphy: Putting it all Together in the Atlantic and Gulf Paleogene", in *Innovative Biostratigraphic*

*Approaches to Sequence Analysis: New Exploration Opportunities*. Selected Papers and Illustrated Abstracts: Eighth Annual Research Conference, Gulf Coast Section, Society of Economic Paleontologists and Mineralogists Foundation, p.15-23.

20. Biju-Duval B., 2002; "Sedimentary Geology", Institut Francais du Pétrole Publications, Editions Technip, 642p.

21. Boggs Sam, Jr., 1995; "Principles of Sedimentology and Stratigraphy", Prentice-Hall Inc., 774p.

22. Bowen Bruce E. and Shaffer Bernard L., 1987; "The Holistic Approach to Gulf Coast Plio-Pleistocene Sequence Stratigraphy", in *Innovative Biostratigraphic Approaches to Sequence Analysis: New Exploration Opportunities*. Selected Papers and Illustrated Abstracts: Eighth Annual Research Conference, Gulf Coast Section, Society of Economic Paleontologists and Mineralogists Foundation, p.34-35.

23. Brown Alistair R., 1996; "Interpretation of Three-Dimensional Seismic Data", AAPG Memoir 42, Fourth Edition.

24. Bruns P. and Hass H.C., 1999; "On Sediment Accumulation Rates and their Determination", in *On the Determination of Sediment Accumulation Rates.* Editors: P. Bruns and H.C. Hass, Trans Tech Publications, 244p.

25. Burnett Michael Dean, Castagna John Patrick, Mendez-Hernandez Efrain, Ziga Rodriguez Genaro, Figon Garcia Leonel, Martinez Vazquez Trinidad, Tellez Aviles Mariano and Vila Villaseñor Raul, 2003; "Application of spectral decomposition to gas basins in Mexico", The Leading Edge, November 2003, p.1130-1134.

26. Cantú-Chapa Abelardo and Landeros-Flores Román, 2001; "The Cretaceous-Paleocene Boundary in the Subsurface Campeche Shelf, Southern Gulf of Mexico", in *The western Gulf of Mexico Basin: Tectonics, sedimentary basins, and petroleum systems.* Edited by C. Bartolini, R. T. Buffler, and A. Cantú-Chapa, AAPG Memoir 75, p.389-395.

27. Castagna, J. P., Batzle, M. L., and Kan, T.K., 1993; "Rock physics - The link between rock properties and AVO response", in *Offset-Dependent Reflectivity-Theory and Practice of AVO Analysis.* Edited by J. P. Castagna and M. Backus, Investigations in Geophysics, No. 8, Society of Exploration Geophysicists, p. 135-171.

28. Castagna, J.P., Sun Shengjie and Siegfried R.W., 2003; "Instantaneous spectral analysis: Detection of low-frequency shadows associated with hydrocarbons", The Leading Edge, February 2003.

29. Castagna John P. and Sun Shengjie, 2006; "Comparison of spectral decomposition methods", First Break, V. 24, March 2006, p.75-79.

30. Chernikoff A., Garcia Hernández J., Schatzinger R., 2006; "Mesozoic extensional tectonics: its impact on oil accumulations in Campeche Sound, Gulf of Mexico", The Leading Edge, Octubre-2006, p.1224-1234.

31. Chi Shihong, Wu Jianghui and Torres-Verdin Carlos, 2004; "Invasion Correction of Acoustic Logs in a Gas Reservoir", SEG Expanded Abstracts, V.23.

32. Chinneck John W., 1999; "How to Organize your Thesis", The University of Carleton, Canada, web site: http://www.sce.carleton.ca/faculty/chinneck/thesis.html

33. Chopra Satinder and Marfurt Kurt J., 2005; "Seismic attributes – A historical perspective", Geophysics, Vol. 70, No. 5, p. 3SO-28SO.

34. Chopra Satinder, Castagna John, and Portniaguine Oleg, 2006; "Seismic resolution and thin-bed reflectivity inversion", CSEG RECORDER, January 2006, p. 19-25.

35. Chopra Satinder, Castagna John, and Xu Yong, 2008; "Thin-Bed Reflectivity – An Aid to Seismic Interpretation", Back to Exploration, 2008 CSPG CSEG CWLS Convention, p.738-742.

36. Cita M.B., Rio D. and Sprovieri R., 1999; "The Pliocene Series: chronology of the type Mediterranean record and standard chronostratigraphy", in *The Pliocene: Time of Change.* The American Association of Stratigraphic Palynologists Foundation, p.49-63.

37. Clement Olson Hilary and Thompson Peter R., 2005; "Sequence Biostratigraphy with Examples from the Plio-Pleistocene and Quaternary", in *Applied Stratigraphy*, Topics in Geobiology, V.23. Edited by Eduardo Koutsoukos, Springer 2005, p. 227-247.

38. Coterill Katrina, Allen Sharon, De Tagle Francisco, Soto Arturo, Liu Chingju, Perez-Cruz Guillermo, Wornardt Walter W., and Vail Peter R., 1991; "Well Log/Seismic Sequence Stratigraphy of Miocene-Pleistocene, Depositional Sequences, High Island Area, Offshore Texas AAPG Transect-Phase II", in *Sequence Stratigraphy as an Exploration Tool: Concepts and Practices in the Gulf Coast*. Edited by John M. Armentrout and Bob F. Perkins, Eleventh Annual Conference, Gulf Coast Section, Society of Economic Paleontologists and Mineralogists Foundation. Reprinted with Addenda for the 1991 Midyear Research Conference, p.135-138.

39. Dairymple Robert W., 1992; “Tidal Depositional Systems”, in *Facies Models – Response to Sea Level Change*. Edited by Roger G. Walker and Noel P. James, Geological Association of Canada Publications, p.195-218.

40. Davis Richard A. Jr., 1983; “Depositional Systems”, Prentice-Hall, Inc., 669p.

41. Davis Tom, 1998; Notes from the course GPGN 558: “Seismic Interpretation”, Colorado School of Mines, Spring 1998.

42. Decker Carrie, 2004; “Better Characterization of Unconventional Gas Reservoirs”, GasTips, a publication of Gas Technology Institute, the U.S. Department of Energy and Hart Energy Publishing, V. 10, N.4, Fall 2004, p.10-13.

43. Dickey Parke A., 1986; “Petroleum Development Geology”, 3rd Edition, PennWell Publishing Company, 530p.

44. Doveton John H., 1994; “Geologic Log Analysis Using Computer Methods”. AAPG Computer Applications in Geology, No. 2.

45. Dwan Fa, Griffiths Don, Gil Jose, Portniaguine Oleg, Moreno Carlos, Burnett Mike, Sparkman Gene and Castagna John, 2007; “High-Resolution Geological Visualization Using Spectral Inversion”, OTC18951, Offshore Technology Conference.

46. Emery Dominic and Myers Keith, eds., 1996; “Sequence Stratigraphy”, Blackwell Science Ltd., 297p.

47. Ewing T.E., 1991; “Structural framework”, in *The Gulf of Mexico Basin: Geological Society of America, The Geology of North America*. Edited by Salvador Amos, v. J, p. 31-52.

48. Galloway W.E., Bebout D.G., Fisher W.L., Dunlap J.B. Jr., Cabrera-Castro R., Lugo-Rivera J.E., Scott Thomas M., 1991; “Cenozoic”, in *The Gulf of Mexico Basin: Geological Society of America, The Geology of North America*. Edited by Salvador Amos, v. J, p. 245-324.

49. Garcia-Hernandez Jesus. et al., 2005; “Structural style of the Gulf of Mexico’s Cantarell complex”, The Leading Edge, February 2005, p.136-138.

50. Garcia-Palomo, Macias J.L. and Espindola J.M., 2004; “Strike-slip faults and K-alkaline volcanism at El Chichon volcano, southeastern Mexico”, Journal of Volcanology and Geothermal Research, No. 136 (2004).

51. Gore Pamela J.W., 2005; “Salinity”, webpage: http://facstaff.gpc.edu/~pgore/Earth&Space/GPS/Salinity.html, Georgia Perimeter College, Clarkston, GA.

52. Gornitz Vivien, 2007; “Sea Level Rise, After the Ice Melted and Today”, NASA GISS Portal-Research: http://www.giss.nasa.gov/research/briefs/gornitz_09.

53. Graham Alan, 1999; “Terrestrial Pliocene climates in Northern Latin America”, in *The Pliocene: Time of Change*, The American Association of Stratigraphic Palynologists Foundation, p.209-216.

54. Guzmán, A. E., and Márquez-Domínguez B., 2001; “The Gulf of Mexico Basin south of the border: The Petroleum Province of the Twenty-First Century”, in *Petroleum provinces of the twenty-first century*. Edited by M.W. Downey, J. C. Threet, and W. A. Morgan, AAPG Memoir 74, p. 337-351.

55. Guzman-Speziale M., 2001; “Active seismic deformation in the grabens of northern Central America and its relationship to the relative motion of the North America-Caribbean plate boundary”, Tectonophysics 337 (2001), website: http://www.geo.mtu.edu/volcanoes/06upgrade/Seismicity-Rudiger/Guzman_speziale_deformation_grabens_northern_ca.pdf.

56. Guzman-Vega M.A. and Mello M.R., 1999; “Origin of Oil in the Sureste Basin, Mexico”. AAPG Bulletin, V. 83, No. 7, July 1999, p.1068-1095.

57. Guzman-Vega M.A., Castro-Ortiz Lilia, Roman-Ramos J.R., Medrano-Morales L., Clara-Valdez l., Vazquez-Covarrubias E., Ziga-Rodriguez G., 2001; “Classification and origin of petroleum in the Mexican Gulf Coast Basin: An overview”, in *The western Gulf of Mexico Basin: Tectonics, sedimentary basins, and petroleum systems*. Edited by C. Bartolini, R. T. Buffler, and A. Cantú-Chapa, AAPG Memoir 75, p.127-142.

58. Halbouty Michael T., 2001; “Exploration into The New Millenium”, in *Petroleum provinces of the twenty-first century*. AAPG Memoir 74, p.11-19.

59. Hall Matt, 2006; “Resolution and uncertainty in spectral decomposition”, First Break, V.24, December 2006, p.43-47.

60. Han De-Hua, Batzle Michael, 2002; “Constrained and Simplified Gassmann´s Equations”, Expanded Abstracts, SEG 72nd. Annual Meeting.

61. Haq Bilal U., Hardenbol Jan, and Vail Peter R., 1988; “Mesozoic and Cenozoic Chronostratigraphy and Cycles of Sea-Level Change”, in *Sea Level Changes: An Integrated Approach*. Special Publication No. 42. Society of Economic Paleontologists and Mineralogists (SEPM), p. 71-108.

62. Hardie Lawrence A., 1986; "Introduction: Tidal-Flat Carbonates and comparative sedimentology", in *Carbonate Depositional Environments-Modern and Ancient*, Part 3: Tidal Flats, Colorado School of Mines Press, p.1-2.

63. Hardie Lawrence A., 1986a; "Carbonate Tidal-Flat Deposition: Ten Basic Elements", in *Carbonate Depositional Environments-Modern and Ancient*, Part 3: Tidal Flats, Colorado School of Mines Press, p.3-6.

64. Hilterman F. John, 2001; "Seismic Amplitude Interpretation", 2001 SEG/EAGE Distinguished Instructor Short Course (DISC), Society of Exploration Geophysicists.

65. Hofmann R., Batzle M., Han D., 2000; "Fluid Control on Velocity Dispersion", paper presented in meeting *Petrophysics meets Geophysics*, Paris, France, 6-8 November 2000, website: crusher.mines.edu/pdf/fluidcontrol_paris.pdf

66. Homewood Peter W., Mauriaud Pierre and LaFont Francois, 2001; "Best Practices in Sequence Stratigraphy", Memoir 25, TotalFina ELF, Technip Editions.

67. Horbury, Andrew D., Hall Stephen, González-P. Francisco, D. Rodríguez-F. Dionisio, A. Reyes-F. Armando, Ortiz-G. Patricia, Martínez-M. Martín, and Quintanilla-R. Guillermo, 2003; "Tectonic sequence stratigraphy of the western margin of the Gulf of Mexico in the late Mesozoic and Cenozoic: Less passive than previously imagined", in *The Circum-Gulf of Mexico and the Caribbean: Hydrocarbon habitats, basin formation, and plate tectonics*. Edited by C. Bartolini, R. T., Buffler, and J. Blickwede, AAPG Memoir 79, p.184-245.

68. Hurley Neil and Peeters Max, 1998; Notes from the course PEGN 419A/GPGN532: "Well Log Analysis and Formation Evaluation", Colorado School of Mines, Fall 1998.

69. Jahn Frank, Cook Mark and Graham Mark, 1998; "Hydrocarbon Exploration and Production", Developments in Petroleum Science #46, Elsevier Science B.V., 384p.

70. Jervey M.T., 1988; "Quantitative Geological Modelling of Siliciclastic Rock Sequences and their seismic expression", in *Sea Level Changes: An Integrated Approach*. Special Publication No. 42, Society of Economic Paleontologists and Mineralogists, p. 47-70.

71. Johnson David E. and Pile Kathryne E., 2006; Well Logging in Nontechnical Languaje", 2nd. Edition, PennWell Corporation, 289p.

72. Ketzer J.M., Morad S. and Amorosi A., 2003; "Predictive diagenetic clay-mineral distribution in siliciclastic rocks within a sequence stratigraphic

framework", in *Clay Sandstones*. Special Publication No. 34 of the International Association of Sedimentologists, Blackwell Publishing, p.43-61.

73. Koutsoukos Eduardo A.M., 2005; "Stratigraphy: Evolution of a Concept", in *Applied Stratigraphy*. Edited by Eduardo Koutsoukos. Topics in Geobiology, V. 23, Springer 2005, p. 3-19.

74. Kouzoub Nikolai and Ronquillo-Jarillo Gerardo, 2002; "Application of 1D and 2D Matching Pursuit for estimation of attributes and seismic data processing", Resumenes de la III Reunion Nacional de Ciencias de la Tierra, Revista GEOS, Union Geofisica Mexicana, v.22, No.2, Noviembre 2002.

75. Kupecz Julie A, Gluyas Jon and Bloch Salman, 1997; "Reservoir Quality Prediction in Sandstones and Carbonates: An overview", in *Reservoir quality prediction in sandstones and carbonates*, AAPG Memoir 69, p. vii-xxiv.

76. Larner Ken, 1998; Notes from the course GPGN452: "Methods in Seismic Prospecting", The Colorado School of Mines, Spring 1998.

77. Leroy S.A.G, Wrenn J.H. and Suc J.-P., 1999; "Global setting to comparative charts of regional events", in *The Pliocene: Time of Change*, The American Association of Stratigraphic Palynologists Foundation, p.1-12.

78. Lewis D.W. and McConchie D., 1994; "Practical Sedimentology", published by Chapman&Hall, 213p.

79. Lopez John A., 1991; "Temporal Resolution of Depositional Processes in the Gulf Coast Tertiary", in *Sequence Stratigraphy as an Exploration Tool: Concepts and Practices in the Gulf Coast*. Edited by John M. Armentrout and Bob F. Perkins, Eleventh Annual Conference, Gulf Coast Section, Society of Economic Paleontologists and Mineralogists Foundation. Reprinted with Addenda for the 1991 Midyear Research Conference, p.217-220.

80. Lyon-Caen H., Barrier E., Lasserre C., Franco A., Arzu I., Chiquin L., Chiquin M., Duquesnoy T., Flores O., Galicia O., Luna J., Molina E., Porras O., Requena J., Robles V., Romero J., Wolf R., 2006; "Kinematics of the North America-Caribbean-Cocos plates in Central America from new GPS measurements across the Polochic-Motagua fault system", Geophysical Research Letters, V. 33, L19039. Published by the American Geophysical Union, website: http://www.geo.mtu.edu/volcanoes/06upgrade/Seismicity-Rudiger/lyon_caen_GPS_Polochic.pdf.

81. Mahob Patrice N. and Castagna John P., 2000; "Fluid substitution and shear-wave velocity prediction including dispersion effects: A case study, NW Shelf, Australia". SEG Annual Meeting 2000 Expanded Abstracts.

82. Mann Paul and Rogers Rob, 2005; "Tectonic Origin & History of the Chortis Block: Integration of Onshore Geological and Offshore well and seismic Data from Eastern Honduras", Caribbean Research at UTIG, Institute for Geophysics, The University of Texas at Austin. UTIG Research Projects Archive, website: http://www.ig.utexas.edu/research/projects/chortis/chortis.htm.

83. Marshall Jeffrey S., 2007; "The Geomorphology and Physiographic Provinces of Central America", in *Central America: Geology, Resources and Hazards*. Edited by Bundschuh and Alvarado. Published by Taylor and Francis, website: www.csupomona.edu/~marshall/jsm.pubs/Marshall.06.pdf.

84. Mavko, G., Mukerji, T., and Dvorkin, J., 1998; "The Rock physics handbook: Tools for seismic analysis in porous media", Cambridge University Press, 329p.

85. McGowran Brian, 2005; "Biostratigraphy", Cambridge University Press, 459p.

86. Mendez-Hernandez Efrain and Acuña Catalina, 1999; "Final Report (non-published) on the technical papers: *Quantitative Geological Modeling of Siliciclastic Rock Sequences and their Seismic Expression* (Jervey M.T., 1988); and *Eustatic Controls on Clastic Deposition I* (Posamentier H.W., 1988)", Course Geology 6330: Sequence Stratigraphy and Basin Analysis", The University of Colorado at Boulder, Spring 1999.

87. Mendez-Hernandez Efrain, 2003; "A brief history and recent advances in seismic technology by the petroleum industry in Mexico", The Leading Edge, November 2003.

88. Mendez-Hernandez Efrain, Vila-Villaseñor Raul, Sosa-Patrón Alejandro, De la Vega Felipe, Hernandez Carrera Gustavo, Carrie Decker, Burnett Mike, Eissa Mohamed, O´Meara Dan and John Castagna, 2003; "Advanced seismic technology improves prospect evaluation and reservoir delineation in the mature Macuspana Basin, Mexico", The Leading Edge, November 2003, p.1142-1147.

89. Mendez-Hernandez Efrain, Slatt Roger M., Bahamon-Velazquez Carlos, Garcia-Hernandez Jesus, 2006; "Workflow for Integrated Characterization of Combination Structural-Stratigraphic Traps: Example from the Southern Gulf of Mexico", in *Reservoir Characterization: Integrating Technology and Business Practices*. Transactions of The Gulf Cost Association of Geological Societies, Special Meeting, December 2006, p.1-32.

90. Middleton Gerard V., 1991; "A short historical review of clastic tidal sedimentology", in *Clastic Tidal Sedimentology"*. Edited by Smith.D.G., Reinson G.E., Zaitlin B.A., and Rahmani R.A., Memoir 16, The Canadian Society of Petroleum Geologists, p. ix-xv.

91. Mitchum R.M., Vail P.R. and Thompson S., 1977; "Seismic Stratigraphy and Global Changes of Sea level, Part 2: The Depositional Sequence as a Basic Unit for Stratigraphic Analysis", in *Seismic Stratigraphy – applications to hydrocarbon exploration"*. Edited by Charles E. Payton, AAPG Memoir 26, p.53-62.

92. Mitchum R.M., Vail P.R. and Sangree J.B., 1977; "Seismic Stratigraphy and Global Changes of Sea level, Part 6: Stratigraphic Interpretation of Seismic Reflection Patterns in Depositional Sequences", in *Seismic Stratigraphy – applications to hydrocarbon exploration"*. Edited by Charles E. Payton, AAPG Memoir 26, p.117-134.

93. Mitchum Robert M. Jr. and Van Wagoner John C., 1991(a) ; "High-frequency sequences and their stacking patterns: sequence-stratigraphic evidence of high-frequency eustatic cycles", Sedimentary Geology, No. 70, p.131-160.

94. Mitchum Robert M. Jr. and Van Wagoner John C., 1991(b); "High-frequency sequences and Eustatic Cycles in the Gulf of Mexico Basin", in *Sequence Stratigraphy as an Exploration Tool: Concepts and Practices in the Gulf Coast*. Edited by John M. Armentrout and Bob F. Perkins, Eleventh Annual Conference, Gulf Coast Section, Society of Economic Paleontologists and Mineralogists Foundation. Reprinted with Addenda for the 1991 Midyear Research Conference, p.257-267.

95. Mitchum Robert M. Jr., Sangree John B., Vail Peter R., Wornardt Walter W., 1991; "Sequence Stratigraphy in Late Cenozoic Expanded Sections, Gulf of Mexico, in *Sequence Stratigraphy as an Exploration Tool: Concepts and Practices in the Gulf Coast*. Edited by John M. Armentrout and Bob F. Perkins, Eleventh Annual Conference, Gulf Coast Section, Society of Economic Paleontologists and Mineralogists Foundation. Reprinted with Addenda for the 1991 Midyear Research Conference, p.237-256.

96. Mitchum Robert M., Sangree John B., Vail Peter R., Wornardt Walter W., 1993; "Recognizing Sequences and Systems Tracts from Well Logs, Seismic Data, and Biostratigraphy: Examples from the Late Cenozoic of the Gulf of Mexico", in *Siliciclastic Sequence Stratigraphy*, AAPG Memoir 58, p. 163-197.

97. Mitra Shankar, 1986; "Duplex structures and imbricate thrust systems: Geometry, structural position, and hydrocarbon potential", AAPG Bulletin, V.70, No.9.

98. Mitra Shankar, Duran-Gonzalez Juan, 2005; "Structural Integration of the Cantarell-Sihil and Ek-Balam Structural Complexes, Campeche Bay, Mexico", non-published Pemex internal report.

99. Mitra Shankar, Correa Figueroa Gerardo, Hernandez Garcia Jesus, and Murillo Alvarado Antonio, 2005; "Three-dimensional structural model of the Cantarell

and Sihil structures, Campeche Bay, Mexico", AAPG Bulletin, V.89, No.1, January 2005, p.1-26.

100. Mitra Shankar, Duran Gonzalez Juan A., García Hernandez Jesus, Hernandez Garcia Sergio and Banerjee Subhotosh, 2006; "Structural geometry and evolution of the Ku, Zaap, and Maloob structures, Campeche Bay, Mexico", AAPG Bulletin, V.90, No. 10, p.1565-1584.

101. Monicard R.P., 1980; "Properties of Reservoir Rocks: Core Analysis", Gulf Publishing Company, 168p.

102. Moore Andy, 2008; Class Notes OCEA 101-The Marine Environment: "The Chemistry of Sea Water", Instructional Computing, Web CT Courses, University of California Santa Cruz, website: http://www.ic.ucsc.edu/~ammoore/ocea101/.

103. Moore Andy, 2008a; Class Notes OCEA 101-The Marine Environment: "The Tides", Instructional Computing, Web CT Courses, University of California Santa Cruz, website: http://www.ic.ucsc.edu/~ammoore/ocea101/.

104. Mount Jeffrey, 1985; "Mixed siliciclastic and carbonate sediments: a proposed first-order textural and compositional classification", Sedimentology, V.32, p.435-442.

105. Mulholland J.W., 1998a; "Sequence stratigraphy: Basic elements, concepts, and terminology", in *The Geologic Column*, The Leading Edge, January 1998, p-37-40.

106. Mulholland J.W., 1998b; "Sequence architecture", in *The Geologic Column*, The Leading Edge, June 1998, p.767-771.

107. Mulholland J.W., 1998c; "The parasequence", in *The Geologic Column*, The Leading Edge, October 1998, p.1374-1376.

108. Murillo A. J. Antonio and Figueroa C. Gerardo, 2004; "Modelo de Evolución Tectónica Terciaria en los Campos Cantarell, Ku, Maloob y Zaap", Program with Papers: AAPG International Conference and Exhibition, Cancun Mexico, 2004.

109. NASA GISS, 2008; "First Planning Meeting for Pliocene Climate Model Intercomparison Project", NASA Goddard Institute for Space Studies Portal-Conferences and Proceedings, website: http://www.giss.nasa.gov/meetings/pliocene2008/.

110. Nichols Gary, 1999; "Sedimentology and Stratigraphy", Blackwell Science Ltd., 355p.

111. Nio Swie-Djin and Yang Chang-Shu, 1991; Diagnostic attributes of clastic tidal deposits: a review, in *Clastic Tidal Sedimentology"*. Edited by Smith.D.G., Reinson G.E., Zaitlin B.A., and Rahmani R.A., Memoir 16, Canadian Society of Petroleum Geologists, p.3-27.

112. Oil&Gas Journal editors, 2001; "Gas output to grow further in Mexico´s Burgos basin", Oil&Gas Journal, V.99, No.19, May 7, 2001.

113. Pacheco Gutiérrez Abacuc C., 2002; "Deformación Transpresiva Miocénica y el Desarrollo de Sistemas de Fracturas en la Porción Nororiental de la Sonda de Campeche", Tesis para obtener el grado de Maestría en Ciencias (Geología), Unidad de Ciclos Profesionales y de Posgrado, Colegio de Ciencias y Humanidades, Posgrado en Ciencias de la tierra, Universidad Nacional Autónoma de México, 98p.

114. Pacht Jory A., Bowen Bruce E., Shaffer Bernard L and Pottorf Bill R., 1991; "Sequence Stratigraphy of Plio-Pleistocene Strata in the Offshore Louisiana Gulf Coast: Applications to Hydrocarbon Exploration", in *Sequence Stratigraphy as an Exploration Tool: Concepts and Practices in the Gulf Coast*. Edited by John M. Armentrout and Bob F. Perkins, Eleventh Annual Conference, Gulf Coast Section, Society of Economic Paleontologists and Mineralogists Foundation. Reprinted with Addenda for the 1991 Midyear Research Conference, p.269-285.

115. Padilla y Sanchez Ricardo J., 2007; "Evolución geológica del sureste mexicano desde el Mesozoico al presente en el contexto regional del Golfo de México", Boletín de la Sociedad Geológica Mexicana, Tomo LIX, Núm. 1, p.19-42.

116. Partika Greg, Gridley James and Lopez John, 1999; "Interpretational applications of spectral decomposition in reservoir characterization", The Leading Edge, March 1999, p.353-360.

117. Passey Q.R., Dahlberg K.E., Sullivan K.B., Yin H., Brackett R.A., Xiao Y.H. and Guzman-Garcia A.G., 2006; "Petrophysical Evaluation of Hydrocarbon Pore-Thickness in Thinly Bedded Clastic Reservoirs". AAPG Archie Series, No. 1, 210p.

118. Payton, C. E. ed., 1977; "Seismic Stratigraphy: Applications to Hydrocarbon Exploration", AAPG Memoir 26, 516p.

119. Peeters Ir. M, 1998; "From Pictures to Properties". Paper presented on the inauguration of the Baker Hughes Distinguished Chair of Petrophysics & Borehole Geophysics by its first recipient: Prof. Ir. M. Peeters, Colorado School of Mines.

120. PEMEX´s internal technical reports, 1989-2005; non-published proprietary confidential information.

121. Portniaguine, O. and J. P. Castagna, 2004; “Inverse spectral decomposition”, 74th SEG Meeting Expanded Abstracts, p.1786-1789.

122. Portniaguine, O. and J. P. Castagna, 2005; “Spectral inversion: Lessons from modeling and Boonesville case study”, 75th SEG Meeting Expanded Abstracts, p.1638-1641.

123. Posamentier H.W., Jervey M.T., Vail P.R., 1988; “Eustatic Controls on Clastic Deposition I: Conceptual Framework”, in *Sea Level Changes: An Integrated Approach*, Special Publication No. 42, Society of Economic Paleontologists and Mineralogists, p. 109-124.

124. Rafaelsen Bjarne, 2003; “Seismic resolution and frequency filtering”, Universitetet I Tromso, webpage: www.ibg.uit.no/~bjarne/Rafaelsen 2003.pdf.

125. Rueda-Gaxiola J., 2003; “The origin of the Gulf of Mexico Basin and its petroleum subbasins in Mexico, based on red bed and salt palynostratigraphy”, in *The Circum-Gulf of Mexico and the Caribbean: Hydrocarbon habitats, basin formation, and plate tectonics*. Edited by C. Bartolini, R. T. Buffler, and J. Blickwede. AAPG Memoir 79, p.246-282.

126. Saleh Azzeldeen, 2004; “Correlation of Atoka and adjacent strata within a sequence stratigraphic framework, Arkoma Basin, Oklahoma”. PhD Dissertation, The University of Oklahoma, 181p.

127. Salvador Amos, 1991 (a); “Introduction”, in *The Gulf of Mexico Basin: Geological Society of America, The Geology of North America*. Edited by Salvador Amos, v. J, p.1-12.

128. Salvador Amos, 1991 (b); “Origin and Development of The Gulf of Mexico Basin”, in *The Gulf of Mexico Basin: Geological Society of America, The Geology of North America*. Edited by Salvador Amos, v. J, p.389-494.

129. Salvador Amos, 1991 (c); “Summary; Current knowledge and unanswered questions”, in *The Gulf of Mexico Basin: Geological Society of America, The Geology of North America*. Edited by Salvador Amos, v. J, p.545-549.

130. Sangree John B., Vail Peter R. and Mitchum Robert M. Jr., 1991; “A Summary of Exploration Applications of Sequence Stratigraphy”, in *Sequence Stratigraphy as an Exploration Tool: Concepts and Practices in the Gulf Coast*. Edited by John M. Armentrout and Bob F. Perkins, Eleventh Annual Conference, Gulf Coast Section, Society of Economic Paleontologists and Mineralogists Foundation. Reprinted with Addenda for the 1991 Midyear Research Conference, p.321-327.

131. Santiago Jose and Baro Alfonso, 1992; “Mexico´s Giant Fields, 1978-1988 Decade”, in *Giant Oil & Gas Fields of the Decade 1978-1988*. Edited by Halbouty Michel T., AAPG Memoir 54, p.73-99.

132. Sawyer D., Buffler R. T., and Pilger R. H., 1991; “The crust under the Gulf of Mexico Basin”, in *The Gulf of Mexico Basin: Geological Society of America, The Geology of North America*. Edited by Salvador Amos, v. J, p.53-72.

133. Selley Richard C., 1998; “Elements of Petroleum Geology”, Academic Press, p.470.

134. Shengjie Sun and Castagna John P., 2002; “Examples of wavelet transform time-frequency analysis in direct hydrocarbon detection”, 72nd SEG Annual Meeting Expanded Abstracts.

135. Slatt Roger M., 2005; Notes from the course GEOL 6970: “Introduction to Petroleum Geology of Deepwater Depositional Systems/Turbidite Petroleum Geology”, The University of Oklahoma, Spring 2005.

136. Slatt Roger M., 2005; Notes from the course GEOL 4970/6970: “Introduction to Reservoir Characterization/Geologic Reservoir Characterization”, The University of Oklahoma, Fall 2005.

137. Slatt Roger M., 2006; “Stratigraphic Reservoir Characterization for Petroleum Geologists, Geophysicists, and Engineers”, Handbook of Petroleum Exploration and Production Series No. 6, Elsevier, 478p.

138. Smith Tad M., Sondergeld Carl H., and Rai Chandra S., 2003; “Gassmann fluid substitutions: A tutorial”, Geophysics V. 68, No. 2, p.430-440.

139. Soto-Cuervo Arturo, 2004; “Sonda de Campeche, Mexico”, non-published PowerPoint presentation in *Introduction to the Petroleum Geology of Mexican Basins*, AAPG-AMGP Short Course, AAPG International Conference and Exhibition, October 24-27, 2004, Cancun MEXICO.

140. Stear John, 2002; “Isotopic Sorting and the Noah´s Flood Model”, website: Creation Science and Earth History, The Evolution Education Site Ring, collection of websites owned by John Stear: http://www.geocities.com/earthhistory/iso.htm.

141. Taylor Gilbert, 1991; “Application of Sequence Stratigraphic Techniques to Production in a Portion of the Plio-Pleistocene Basin, High Island Area, Offshore Texas”, in *Sequence Stratigraphy as an Exploration Tool: Concepts and Practices in the Gulf Coast*. Edited by John M. Armentrout and Bob F. Perkins, Eleventh Annual Conference, Gulf Coast Section, Society of

Economic Paleontologists and Mineralogists Foundation. Reprinted with Addenda for the 1991 Midyear Research Conference, p.337-349.

142. Tearpock Daniel J. and Brenneke James C., 2001; "Multidisciplinary teams, integrated software for shared-earth modeling key E&P success", Oil&Gas Journal, December 10, 2001.

143. UN GEMS/Water, 2004; "Analytical Methods", in GEMS/Water Operational Guide, v. 3.1, United Nations Global Environment Monitoring System (GEMS)/Water Programme.

144. Vail P.R., 1987; "Seismic stratigraphy interpretation procedure, in *Atlas of seismic stratigraphy*. Edited by A.W. Bally, AAPG Studies in Geology 27, V.1, p.1-10.

145. Vail Peter R. and Wornardt Walter W., 1991; "Well Log-Seismic Sequence Stratigraphy: An Integrated Tool for the 90´s", in *Sequence Stratigraphy as an Exploration Tool: Concepts and Practices in the Gulf Coast*. Edited by John M. Armentrout and Bob F. Perkins, Eleventh Annual Conference, Gulf Coast Section, Society of Economic Paleontologists and Mineralogists Foundation. Reprinted with Addenda for the 1991 Midyear Research Conference, p.379-388.

146. Van Wagoner J.C., Mitchum R.M. Jr., Posamentier H.W. and Vail P.R., 2002; "Part 2: Key Definitions of Sequence Stratigraphy", in *Atlas of Seismic Stratigraphy.* Edited by A.W. Bally, AAPG Studies in Geology 27, V.1.

147. Van Wagoner J.C., Mitchum R.M., Campion K.M. and Rahmanian V.D., 1990; "Siliciclastic Sequence Stratigraphy in Well Logs, Cores, and Outcrops", AAPG Methods in Exploration Series, No. 7, 55p.

148. Visher Glenn S., 1990; "Exploration Stratigraphy", PennWell Publishing Company, 433p.

149. Wang Zhijing (Zee), 2001; "Fundamentals of seismic rock physics", Geophysics, V. 66, No. 2, p.398-412.

150. Weimer P. and Posamentier H.W., 1993; "Recent Developments and Applications in Siliciclastic Sequence Stratigraphy", in *Siliciclastic Sequence Stratigraphy*, AAPG Memoir 58, p. 3-12.

151. Weimer Paul, 1999; Notes from the course "Geology 6330: Applied Sequence Stratigraphy and Basin Analysis", The University of Colorado at Boulder, Spring 1999.

152. Willis Julie, 2008; "The tides", Online Oceanography Class OCEA101, MiraCosta College (a public California community college), website: www.**miracosta.cc.ca.us**/home/jwillis/online_class.htm.

153. Wood Leslie J., 2004; "Predicting Tidal Sand Reservoir Architecture Using Data from Modern and Ancient Depositional Systems", in *Integration of outcrop and modern analogs in reservoir modeling*, AAPG Memoir 80.

154. Worden R.H. and Morad S., 2003; "Clay minerals in sandstones: controls on formation, distribution and evolution", in *Clay Sandstones*, Special Publication No. 34 of the International Association of Sedimentologists, published by Blackwell Publishingy of Shelf and Slope Sediments in the Gulf of Mexico", p. 3-41.

155. Wornardt Walter W., Vail Peter R., 1991; "Revision of the Plio-Pleistocene Cycles and their Applications to Sequence Stratigraphy of Shelf and Slope Sediments in the Gulf of Mexico", in *Sequence Stratigraphy as an Exploration Tool: Concepts and Practices in the Gulf Coast*. Edited by John M. Armentrout and Bob F. Perkins, Eleventh Annual Conference, Gulf Coast Section, Society of Economic Paleontologists and Mineralogists Foundation. Reprinted with Addenda for the 1991 Midyear Research Conference, p.391-397.

156. Wornardt, W.W., B.L. Shaffer, and P.R. Vail, 2002; "Late Miocene–Pleistocene Sequence Chronostratigraphy Chart for Gulf of Mexico", website: http://www.micro-strat.com/Wornardt2002.html.

157. Worthington Paul F., 2003; "Effect of clay content upon some physical properties of sandstone reservoirs", in *Clay Sandstones*, Special Publication No. 34 of the International Association of Sedimentologists, Blackwell Publishing, p. 191-211.

158. Wynn Jones Robert, 1996; "Micropaleontology in Petroleum Exploration". Oxford Science Publications, 432p.

159. Wrenn J.H., Suc J.-P. and Leroy S.A.G., with other contributors, 1999; "Comparative Regional Charts of Pliocene Events", in *The Pliocene: Time of Change*, The American Association of Stratigraphic Palynologists Foundation, p.13-47.

160. Yilmaz Ozdogan, 1987; "Seismic Data Processing", Investigations in Geophysics, V. 2, Society of Exploration Geophysicists, 526p.

161. Younis Shahbaz, 2006; "Well logging – The Bore Hole", in *World of Teaching*, Category: Geography and Geology, Free Powerpoint presentations, website: http://www.worldofteaching.com/geographypowerpoints.html.